DEVELOPMENT OF RADIONUCLIDE GENERATORS FOR BIOMEDICAL APPLICATIONS

By

RUBEL CHAKRAVARTY

Bhabha Atomic Research Centre

A thesis submitted to the

Board of Studies in Chemical Sciences

In partial fulfillment of requirements

For the degree of

DOCTOR OF PHILOSOPHY

of

HOMI BHABHA NATIONAL INSTITUTE

June 2011

Homi Bhabha National Institute

Recommendations of the Viva Voce Board

As members of the Viva Voce Board, we certify that we have read the dissertation prepared by **Shri Rubel Chakravarty** entitled **"Development of Radionuclide Generators for Biomedical Applications"** and recommend that it may be accepted as fulfilling the dissertation requirement for the Degree of Doctor of Philosophy.

_____ **Date:**

Chairman – Prof. K. L. Ramakumar

_____ **Date:**

Guide / Convener – Prof. Meera Venkatesh

_____ **Date:**

External Examiner – Prof. Satya Prakash

_____ **Date:**

Member 1 – Prof. Ashutosh Dash (Technology Advisor)

_____ **Date:**

Member 2 – Prof. A. K. Tyagi

_____ **Date:**

Member 3 – Prof. Sharmila Banerjee

Final approval and acceptance of this dissertation is contingent upon the candidate's submission of the final copies of the dissertation to HBNI.

I hereby certify that I have read this dissertation prepared under my direction and recommend that it may be accepted as fulfilling the dissertation requirement.

_____ **Date:**

Guide: Prof. Meera Venkatesh

Place: Mumbai

STATEMENT BY AUTHOR

This dissertation has been submitted in partial fulfillment of requirements for an advanced degree at Homi Bhabha National Institute (HBNI) and is deposited in the Library to be made available to borrowers under rules of the HBNI.

Brief quotations from this dissertation are allowable without special permission, provided that accurate acknowledgement of source is made. Requests for permission for extended quotation from or reproduction of this manuscript in whole or in part may be granted by the Competent Authority of HBNI when in his or her judgment the proposed use of the material is in the interests of scholarship. In all other instances, however, permission must be obtained from the author.

(Rubel Chakravarty)

DECLARATION

I, hereby declare that the investigation presented in the thesis has been carried out by me. The work is original and has not been submitted earlier as a whole or in part for a degree / diploma at this or any other Institution / University.

(Rubel Chakravarty)

Dedicated to my Parents

ACKNOWLEDGEMENTS

First and foremost, I would like to take this opportunity to place on record my deep sense of gratitude and indebtedness to my mentor and Ph.D. supervisor **Prof. Meera Venkatesh,** Former Head, Radiopharmaceuticals Division, Bhabha Atomic Research Centre and presently Director, Division of Physical and Chemical Sciences, IAEA, Vienna for her unstinted inspiration, invaluable guidance, profound advice, persistent encouragement, keen interest, good wishes and valuable suggestions throughout my entire research tenure.

I would like to express my gratitude to **Prof. Ashutosh Dash,** Head, Therapeutic and Reference Sources Section, who is my immediate superior, for guiding me through the work, helping me in crucial experiments, monitoring the progress of the work on a day to day basis, teaching me the preparation of scientific manuscripts which enabled me to publish a number of research papers which form part of this thesis. It is his extreme support that made this work a reality.

The guidance and constant encouragement received from **Prof. M.R.A. Pillai,** currently, Head, Radiopharmaceuticals Division during the entire course of the work is gratefully acknowledged. The work on the electrochemical $^{90}Sr/^{90}Y$ generator was initiated based on the suggestion given by him while working at IAEA, which subsequently led to the development of other generators such as $^{188}W/^{188}Re$ and $^{99}Mo/^{99m}Tc$ generators, based on electrochemistry.

I am extremely grateful to **Prof. A.Q. Contractor**, Department of Chemistry, Indian Institute of Technology, Mumbai and **Prof. S.K. Sengupta,** Department of Chemistry, Banaras Hindu University, Varanasi for their valuable guidance in electrochemistry because of which the work on electrochemical generators could be initiated. The initial studies on the electrochemical generators carried out in this dissertation would not have been possible without the access to the facility at the Indian Institute of Technology, Mumbai.

I sincerely and gratefully acknowledge the valuable guidance received from **Prof. A.K. Tyagi,** Chemistry Division on synthesis and structural characterization of nanomaterials, presentation of scientific data and

preparation of scientific manuscripts. His research group has been a source of friendship as well as good advice and collaboration.

I owe sincere thanks to **Prof. V. Venugopal**, Director, Radiochemistry and Isotope Group for providing me an opportunity to work in the Isotope Programme and for his administrative support during the course of the work.

No thesis can be complete without being reviewed by a Doctoral Committee. The Doctoral Committee of this dissertation guided me through all these years. I want to take this opportunity to record my sincere thanks to the Chairman (**Prof. K.L. Ramakumar**) and members (**Prof. Ashutosh Dash, Prof. A.K. Tyagi** and **Prof. Sharmila Banerjee**) of the Doctoral Committee for the critical review of the work reported in the thesis and for their accessibility, interest, academic support, insightful questions, valuable discussions and helpful comments during progress reviews and pre-synopsis viva-voce. I am grateful to **Prof. S.K. Ghosh**, Dean, Chemical Sciences, HBNI for his support and encouragement during the course of the work.

My sincere thanks are due to **Dr. Tapas Das** for his valuable guidance and help in carrying out the radiolabeling experiments described in this thesis. It is my pleasant duty to acknowledge the valuable help received from my colleague **Shri Ramu Ram** in carrying out some of the radiochemical studies described in this thesis. I am thankful to **Shri Rakesh Shukla**, Chemistry Division for his valuable help in carrying out the structural characterization of nanomaterials.

I express my thanks to **Dr. S.V. Thakare** and **Shri K.C. Jagdeesan** for their help in coordinating the irradiations at the Dhruva Reactor. I sincerely thank **Shri P.V. Joshi**, Head, Radiochemicals Section and the staff members of his section for providing ^{99}Mo, for generator work.

I express my thanks to **Shri Pritam Bansode** for making the drawings used in the thesis. Special mention deserves to be made of the help and cooperation provided by Group Facility workshop and glass blowing unit of RPhD in making various apparatus that I needed to perform my experiments. Special thanks to due to **Shri B.J. Avhad** and **Shri S. Moorthy** for their timely help, in this regard.

I acknowledge the friendly cooperation and valuable suggestions received from my colleagues **Shri Anupam Mathur, Dr. Sudipta Chakraborty,**

Shri Suresh Subramaniam, Shri Viju Chirayil, Shri S.K. Saxena, Dr. Usha Pandey, Shri J. Udhayakumar, Shri Madhav Mallia, Dr. R.B. Manolkar, Shri A.R. Mathakar, Shri Yogendra Yadav, Smt. Yugandhara Yadav and ***Shri Manoj Kumar*** during the course of the work. I wish to thank my friends ***Dr. Prabhat Kumar Singh*** and ***Dr. Arnab Sarkar*** for their moral support and diversified help during the course of the work.

I thank ***Shri M.S. Tikka, Shri B.J. Jadhav*** and ***Late Shri G.S. Kolge*** for the help received during the execution of the work.

The last, and surely the most, I express my sincere gratitude to my parents (***Prof. Bimalendu Bikash Chakravarty*** and ***Smt. Runa Chakravarty***) who have been a continuous source of inspiration for me. I gratefully acknowledge the sincere encouragement received from my brother ***Snehel*** and all other family members during the course of the work. Finally, I would like to thank the ***God,*** the Almighty for His blessings which helped me in fulfilling this ambition of my life.

Trombay, Mumbai ***(Rubel Chakravarty)***

June, 2011

CONTENTS

SYNOPSIS OF THE THESIS

"It is the lone worker who makes the first advance in a subject; the details may be worked out by a team, but the prime idea is due to enterprise, thought, and perception of an individual."

ALEXANDER FLEMING

The discovery of radioactivity by Henri Becquerel in 1896 and the subsequent discoveries of radioactive elements by Marie Curie and Pierre Curie had a profound effect on understanding of the biological effects of radiation. One of the consequences was the dawn of medical applications of radionuclides and radiation. Nuclear Medicine is a clinical discipline in which radiopharmaceuticals (molecules labeled with radionuclides) are used for diagnosis or therapy [1]. Production of radioisotopes is an important aspect in the field of Nuclear Medicine and there has always been considerable interest in the standardization of easy and economically viable processes for obtaining promising radionuclides. The invention of cyclotron in 1930s and the building of nuclear reactors in 1940s paved the way for production of artificial radioisotopes. A wide variety of medically useful radioisotopes such as ^{3}H, ^{14}C, ^{35}S, ^{32}P, ^{51}Cr, ^{60}Co, ^{125}I, ^{131}I, ^{197}Hg and ^{198}Au [2] were produced in the early years and commercially supplied for medical applications. But Nuclear Medicine witnessed a major upswing after the development of $^{99}Mo/^{99m}Tc$ generator by Walter Tucker and Margaret Greene at Brookhaven National Laboratory in 1950s [3]. ^{99m}Tc, an ideal diagnostic radionuclide occupied a dominant position in modern Nuclear Medicine and a variety of ^{99m}Tc based radiopharmaceuticals became available commercially, for imaging nearly all organs/systems of the human body. ^{99m}Tc is hence referred to as the 'work horse of Nuclear Medicine' [3] and is currently being used in ~80% of the diagnostic Nuclear Medicine procedures world-wide [4].

Today, radioisotopes used for Nuclear Medicine are produced either in cyclotrons or nuclear reactors or obtained directly at the hospital radiopharmacies from the radionuclide generators. The availability of short-lived radioisotopes from radionuclide generators is an inexpensive and convenient alternative to 'in-house' radioisotope production facilities like reactors or cyclotrons. Radionuclide generators can be conveniently transported to institutions far from the site of reactors or cyclotrons. A generator is developed on the

principle of decay-growth relationship between a long-lived parent and its short-lived daughter, existing in a state of radioactive equilibrium. It involves an effective radiochemical separation of the daughter radionuclide from the decaying parent, by taking advantage of their difference in chemical properties, such that the daughter activity is obtained with high radionuclidic, radiochemical and chemical purities. Owing to the fact that the daughter and parent are different radioelements, the daughter activity is availed in a 'no-carrier-added' (NCA) form with highest specific activity. Radionuclide generators are historically called 'cows' since the daughter activity is 'milked' (i.e. separated) from its precursor (parent) and the parent then generates a fresh supply of the daughter. The increasing use of generator-produced short-lived radionuclides for biomedical applications has fostered the need for development of radionuclide generators.

In a radionuclide generator, as a result of the decay of the parent radioisotope, the daughter activity grows and reaches the state of transient or secular equilibrium (depending on the relative half-lives of parent-daughter pairs) within 4-5 half-lives of the daughter. After it reaches the state of equilibrium, the daughter activity appears to decay with the same half-life as that of the parent. At this stage, the daughter activity is separated from the parent. The daughter activity again starts to grow in the generator, until equilibrium is reached in the manner described above. Thus, the daughter radioisotope can be repeatedly separated from the parent. Since generator produced radioisotopes are intended for clinical applications, it is imperative that the radionuclide generators undergo strict quality control procedures before being handed over to the Nuclear Medicine physicians for patient applications. Quality control procedures involve specific tests and measurements that ensure the elution efficiency of the generator, product identity, purity and radioactive concentration of the daughter radionuclide, biological safety and labeling efficacy of the radionuclide for the preparation of radiopharmaceuticals.

The shelf-life of the radionuclide generator is the period for which the generator can be safely used for the designated clinical applications. The loss in efficacy of a typical radionuclide generator over a period of time is determined by the physical half-life of the parent radioisotope, yield, radioactive concentration and the purity of the daughter radioisotope. The overall economy of production of short-lived radioisotopes via a radionuclide generator is decided by the shelf-life of the generator, which in turn determines the cost of treatment using radiopharmaceuticals based on generator produced radionuclides. To a great extent, the shelf-life of a radionuclide generator is influenced by the procedure adopted for the separation of the parent-daughter pairs belonging to the adjacent group of elements. The separation technique is usually selected based on the technical, economic and logistic reasons, with emphasis on one or other of these factors depending on the circumstances. Additionally, the radionuclide generators developed for biomedical applications must be simple in design, efficient and easy to operate.

The development of radionuclide generators for biomedical applications presents many challenges owing to the stringent requirements for such applications [5]. These requirements can only be met with advances in separation chemistry. Various techniques, like column chromatography, solvent extraction and sublimation have been reported for the preparation of radionuclide generators [6]. Conversion of the parent radionuclide into an insoluble 'gel-based' matrix and its use as the column matrix from which the daughter radionuclide can be eluted is yet another strategy that has been reported [7]. Of these, column chromatography and solvent extraction are the most commonly used methods for the preparation of radionuclide generators for biomedical applications. The column chromatography method relies upon the separation of the daughter activity from the parent, by virtue of the difference in their retention affinity in the column matrix. The generators developed by adopting this approach are simple to operate and demonstrate excellent elution

characteristics. However, the limited radiation and chemical stability of the sorbent in certain cases [8,9], is a major cause of concern in adopting this approach. This leads to the breakthrough of the longer lived parent radioisotope and addition of chemical impurities in the daughter eluate, thereby rendering it unsuitable for clinical applications. Additionally, owing to the limited sorption capacity of the column matrix, the parent radioisotope must be available with very high specific activity in order to elute the daughter with appreciably high radioactive concentration. This restriction on the specific activity of the parent radioisotope could be overcome to a great extent by the solvent extraction approach [6], which is based on the relative solubility of the parent and the daughter radionuclides in two immiscible liquids, usually water and an organic solvent. The major limitation of this approach is the cumbersome multi-step separation process involving complicated apparatus. Therefore, it requires highly trained personnel for successful operation. Moreover, the detrimental effect of radiolysis in lowering the extraction efficiency of the organic solvent and addition of organic residues in the daughter product cannot be ignored [6]. Further, the radiation dose to the personnel in a solvent extraction set up is generally a concern. The other less commonly adopted procedures like sublimation and 'gel-based' systems also have their inherent limitations for clinical use [6,7]. In view of these limitations, development of alternate viable processes for the preparation of radionuclide generators for biomedical applications still remains an interesting challenge.

In this thesis, development of radionuclide generators based on two novel approaches has been described. While the first approach involves the use of electrochemical separation technique, the second involves the use of sorbents based on nanomaterials for use as column chromatography matrices for the preparation of radionuclide generators. Electrochemical method provides a simple and convenient approach of performing a wide variety of metal ion separations. A mixture of metal ions having adequate difference in their formal potential

values in an electrolytic medium can be mutually separated by selective electrodeposition of one metal on an electrode surface under the influence of controlled applied potential. In-situ electrochemical deposition of a daughter radionuclide is an attractive route to develop radionuclide generators. The major advantage of this approach is that the daughter radioisotope can be obtained with very high radionuclidic purity and radioactive concentration, irrespective of the specific activity of the parent radioisotope. The second approach based on the use of nanomaterials based sorbents as column matrices for the preparation of generators relies on the unique morphological features, pore structure, high surface areas and high surface charge of nanomaterials. Such sorbents demonstrate much higher sorption capacity and selectivity for sorption of the parent radioisotope compared to their bulk counterparts. The daughter activity can be obtained with appreciably high radioactive concentration and purity suitable for biomedical applications.

Adopting these novel approaches, radionuclide generators have been developed both for diagnostic applications (^{99}Mo/^{99m}Tc and ^{68}Ge/^{68}Ga) as well as therapeutic applications (^{90}Sr/^{90}Y and ^{188}W/^{188}Re). The suitability of these generators for biomedical applications has been evaluated. The thesis is divided into six chapters. A brief summary of the contents of each chapter is given below.

Chapter 1: Introduction

The introductory chapter begins with a general overview of the field of Nuclear Medicine and discusses the importance of radioisotopes and radiopharmaceuticals in Nuclear Medicine. The categorization of radioisotopes based on their application (diagnostic and therapeutic) and the essential characteristics of each type are described in detail. A list of commonly used diagnostic and therapeutic radionuclides along with their decay characteristics is also included. Different routes for the production of radionuclides along with their relative advantages and disadvantages are described with a special emphasis on

production of radionuclides using radionuclide generators. The chapter briefs about the concept of radioactive equilibrium between the parent and daughter radioisotopes in a generator and deals with the mathematical equations involved in the decay and growth of the parent and daughter radioisotopes. The commonly used methods for the development of radionuclide generators are described along with the relevant quality control procedures. The relative advantages and disadvantages of these conventional methods are discussed and the need for development of alternate methods for the preparation of radionuclide generators is highlighted. To a large extent, progress in the development of radionuclide generator systems and in the medical application of radioisotopes in general, is dependent on improvements in separation technology. The widespread interest of the medical community in the diagnostic and therapeutic use of generator produced radioisotopes has led to the development of alternate methods by which the separation can be effected. The alternate approaches employing electrochemical separation and column chromatography using nanomaterial based sorbents are introduced and their advantages over the conventional methods are briefly discussed. Finally, the chapter presents a broad outline of the scope of the work carried out by the author.

Chapter 2: Synthesis and structural characterization of nanomaterial based sorbents

In recent times, use of nanoparticles have become one of the most exciting subject of investigation and have played important roles in the forefront areas of Physics, Chemistry, Engineering, Biology and Medical Science [10]. Nanomaterials hold promise for providing many breakthroughs in the near future that is expected to change the direction of technological advances in a wide range of applications. Nanoparticles are objects of the size in the range of nanometer (1-100 nm). The science of nanometer scale objects is called nanoscience and it aims at achieving the capability to manipulate matter in a desired fashion,

atom by atom. In the nanometer scale, the properties of materials are markedly different from the bulk materials which make such materials scientifically fascinating [10].

Apart from various other uses, nanomaterials have the potential to provide unprecedented opportunities in developing a new class of sorbents for chromatographic applications. One of the important aspects of nanomaterials is the high percentage of the atoms residing on the surface. These surface atoms are unsaturated, exhibit intrinsic surface reactivity and have a tendency to chemisorb charged species in aqueous solution in order to achieve surface stabilization. Moreover, nanocrystalline materials are more tolerant towards radiation than their bulk counterparts with larger grain sizes [11]. The prospective of such nanomaterials as a new generation of sorbents in the chromatographic separation of metal ions has been exploited [12,13]. In order to explore the potential of nanomaterials as sorbents in the relatively unexplored field of radionuclide generators, four nanomaterial based sorbents, namely, polymer embedded nanocrystalline titania (TiP), tetragonal nano-zirconia (t-ZrO_2), mixed phase nano-zirconia (nano-ZrO_2) and nano-ceria-polyacrylonitrile composite (CeO_2-PAN) were synthesized for the preparation of radionuclide generators, namely, $^{99}Mo/^{99m}Tc$, $^{68}Ge/^{68}Ga$ and $^{188}W/^{188}Re$ generators.

The chapter begins with a brief discussion on the importance of nanomaterial based sorbents in the preparation of radionuclide generators. Further, the different methods of synthesis of nanoparticles are briefly described. The advantages of the chemical methods of syntheses of nanoparticles in terms of the relative ease of synthesis and the potential to be scaled up are discussed. The synthetic methodologies for preparation of the nanomaterial based sorbents are described in detail. The structural characterization of these nanomaterials was carried out by various analytical techniques like X-ray diffraction, surface area and pore size determination, infrared spectroscopy and transmission electron microscopy. In order to understand the sorption behavior of these sorbents, their zeta-potentials were determined at

different pH environments. The suitability of these nanomaterials for use as column matrices in chromatographic radionuclide generators was evaluated in this chapter, in terms of (a) granularity and chemical stability of the materials and (b) reliability, reproducibility and ease of synthesis. The more specific parameters such as the retention capacity of the sorbents, selectivity and efficiency of separation, and performance on prolonged use, were evaluated prior to the development of each of the radionuclide generators and are described in the subsequent chapters. The synthesis and characterization of each nanomaterial based sorbent constitutes a separate section of this chapter.

Chapter 3: Development of ^{99}Mo/^{99m}Tc generators

A variety of ^{99m}Tc/^{99}Mo generator systems have been thoroughly investigated during the last 50 years, due to the ever-lasting demand for ^{99m}Tc, the most commonly used diagnostic radioisotope in Nuclear Medicine [4]. The column chromatographic generator using a bed of acidic alumina has emerged as the most popular generator system [4,14]. The capacity of alumina for taking up molybdate ions is limited (2-20 mg Mo per g of alumina) [15] necessitating the use of ^{99}Mo of the highest specific activity available, generally possible only in ^{99}Mo produced through fission route. However, the production of fission ^{99}Mo has several inherent complexities [6]. The current global production of fission ^{99}Mo is inadequate to meet the demand and this has adversely affected patient services in many countries [16]. In order to reduce the reliance on fission ^{99}Mo, two novel approaches for the development of ^{99}Mo/^{99m}Tc generator, using ^{99}Mo produced through neutron activation of ^{98}Mo, have been described in this chapter. In the first approach, the feasibility of separation of ^{99m}Tc from ^{99}Mo by controlled application of electrode potential is demonstrated. Adopting the second approach, ^{99}Mo/^{99m}Tc generators were developed using two nanomaterial based sorbents (TiP and t-ZrO_2). The development of ^{99}Mo/^{99m}Tc generators using these novel approaches are described in two different sections of this chapter.

Electrochemical $^{99}Mo/^{99m}Tc$ generator: In the beginning of this section, the reason for choosing electrochemical separation method for the preparation of $^{99}Mo/^{99m}Tc$ generator is briefly explained. The electrochemical principle and the reactions involved in the separation of ^{99m}Tc from ^{99}Mo are described. The electrochemical set up used and the optimization of the experimental parameters for the efficient electrochemical separation of ^{99m}Tc from ^{99}Mo are described in detail. The development of a 9.25 GBq $^{99}Mo/^{99m}Tc$ generator and its performance evaluation for 10 days are described. The quality control measures adopted to ensure the suitability of ^{99m}Tc for biomedical applications have been detailed and the performance of the generator over its shelf-life of 10 days with respect to these quality control parameters is also enumerated. Finally, the major advantages of this generator are highlighted.

$^{99}Mo/^{99m}Tc$ generators using nanomaterials as sorbents: This section begins with a brief discussion on the limitations of the conventional inorganic sorbents in the preparation of $^{99}Mo/^{99m}Tc$ generators and proposes the utilization of two nanomaterial based sorbents, TiP and t-ZrO_2 for such applications. The optimization of experimental parameters for achieving maximum sorption of ^{99}Mo on these sorbents and efficient elution of ^{99m}Tc is described in detail. The mechanism of Mo-sorption by the nanomaterials was established by correlating the distribution ratio (K_d) values of Mo and Tc ions with the zeta potential of the sorbents. The sorption capacities of these sorbents were determined under both static as well as dynamic conditions, and the sorption capacity values were compared with that of the conventionally used alumina. The development of $^{99}Mo/^{99m}Tc$ generators, one each based on the two sorbents, is described. The evaluation of the elution performance of the generators for a period of 10 days is discussed. The quality control studies carried out to ensure the suitability of ^{99m}Tc for clinical applications and the performance of these two generators with

respect to these quality control parameters are described. In the end, the advantages of this approach for the preparation of $^{99}Mo/^{99m}Tc$ generator are enlisted.

Chapter 4: Development of $^{68}Ge/^{68}Ga$ generators

^{68}Ga is an excellent positron emitting radioisotope suitable for clinical applications in Nuclear Medicine using positron emission tomography (PET). The cyclotron independent availability of ^{68}Ga from a $^{68}Ge/^{68}Ga$ generator at a reasonable cost makes it an attractive and realistic option for countries with limited or no cyclotron facilities. Though several $^{68}Ge/^{68}Ga$ generators have been reported [8] in the past, their direct application in a clinical context could not be accomplished, primarily due to non-availability of suitable sorbent materials. The ^{68}Ga solution eluted from these generators was contaminated with residues of matrix materials (such as TiO_2, SnO_2, Ti and Sn ions) and other cations (such as Fe, Mn etc.) [8]. The presence of these impurities in the ^{68}Ga solution was a major obstacle in labeling receptor-specific biomolecules [8]. Further, ^{68}Ga was eluted from these generators with low radioactive concentration and contained significant amounts of long-lived ^{68}Ge ($t_{½}$= 279 d) as a radionuclidic impurity [8]. The ^{68}Ga eluate from these generators could only be used for radiopharmaceutical applications after tedious multiple post-elution processing steps [8].

In view of these drawbacks of the conventional $^{68}Ge/^{68}Ga$ generators, development of generators devoid of such shortcomings would be relevant and meaningful. Development and evaluation of two novel $^{68}Ge/^{68}Ga$ column chromatographic generators using t-ZrO_2 and CeO_2-PAN as sorbents is described in this chapter. The chapter discusses the important characteristics of these nanomaterials which make them suitable for the preparation of $^{68}Ge/^{68}Ga$ generators. The optimization of the experimental parameters for the chromatographic separation of ^{68}Ga from ^{68}Ge is described in detail. The Ge-sorption capacities of these sorbents were determined under both static and dynamic conditions. The mechanism of sorption of ^{68}Ge and elution of ^{68}Ga has been explained on the basis of the pH-

dependent surface charge on the nanosized metal oxides. A detailed description of the development of two $^{68}Ge/^{68}Ga$ generators (each of 740 MBq activity) using these sorbents is provided. The quality control procedures adopted to evaluate the suitability of ^{68}Ga for biomedical applications are described. The elution performance of these generators and the quality control parameters over a period of 1 year is illustrated and discussed. Finally, the chapter discusses the major advantages of using t-ZrO_2 and CeO_2-PAN sorbents for the preparation of clinical grade $^{68}Ge/^{68}Ga$ generators.

Chapter 5: Development of $^{90}Sr/^{90}Y$ generator

^{90}Y is a therapeutic radioisotope of enormous interest, and several established radiopharmaceuticals with this isotope are currently in use in radiotherapy [17]. For targeted therapy, ^{90}Y of very high purity and specific activity is required. A radionuclide generator system based on the secular equilibrium of ^{90}Sr decaying to ^{90}Y is the most suitable method to avail high specific activity ^{90}Y. Although a variety of separation technologies for the preparation of $^{90}Sr/^{90}Y$ generators have been developed, the feasibility of installation of a generator system for operation in a Nuclear Medicine department is still an unrealistic proposition [17]. Most of the current separation techniques involve multiple steps such as solvent extraction, ion exchange, extraction chromatography either alone or in combination. The possible degradation of the organic solvent or the column matrix by the intense β^- radiation of ^{90}Y reduces the useful life of such generators. Additionally, the possibility of unacceptable levels of ^{90}Sr impurity in ^{90}Y is an issue of concern, as ^{90}Sr localizes in the skeleton and thus has a very low maximum permissible body burden of 74 kBq (2 μCi) [18]. Considering that a patient can receive not more than 74 kBq ^{90}Sr through the life-time and that often in-vivo radiotherapy using ^{90}Y-radiopharmaceuticals will need to be administered in large quantities and several times, the limit for ^{90}Sr acceptable in ^{90}Y becomes extremely low. Although there is no clear consensus on the ^{90}Sr levels acceptable in ^{90}Y, currently 74

kBq ^{90}Sr in 37 GBq ^{90}Y is the limit that is followed. Currently, ^{90}Y is separated by industrial manufacturers and supplied as a radiochemical in inorganic form to the radiopharmacies. The cost of ^{90}Y is high and the availability is limited due to logistics issues related to distribution. Hence, the benefits of targeted therapy using ^{90}Y based radiopharmaceuticals at present are available to a small number of patients in 3-4 of the most developed countries.

In order to circumvent these problems, a simple ^{90}Sr/^{90}Y generator based on electrochemical separation technique was developed and this is described in this chapter. The chapter discusses the principle involved in the electrochemical separation of ^{90}Y from ^{90}Sr and attempts to provide a mechanism for the separation. The electrochemical set up used for the separation is described in detail. The optimization studies carried out to achieve selective electrodeposition of ^{90}Y from ^{90}Sr/^{90}Y mixture is elaborated. A detailed description of the development of a 1.85 GBq (50 mCi) ^{90}Sr/^{90}Y generator is provided and the precautions to be adopted are mentioned. The issues regarding the maintenance of the ^{90}Sr feed solution, are discussed. The various quality control studies carried out to ensure the suitability of ^{90}Y for clinical applications are described. The consistency in the performance of the generator over a period of 2 years is demonstrated. The experiments carried out using Sr/Y mixtures simulated to represent 37 GBq (1 Ci) of ^{90}Sr are described and the relevance of this study for scaling up of the ^{90}Sr/^{90}Y generator to higher level of activity has been explained. Finally, the major advantages of the electrochemical ^{90}Sr/^{90}Y generator are discussed at the end of this chapter.

Chapter 6: Development of ^{188}W/^{188}Re generators

^{188}Re is one of the useful radioisotopes which has been explored and demonstrated for a wide variety of therapeutic applications in Nuclear Medicine [17]. The attractive physical properties of ^{188}Re and its availability in a NCA form, from a ^{188}W/^{188}Re generator with an adequate shelf-life, makes it an interesting option for clinical use. The ^{188}W parent

radionuclide is available in relatively low specific activity (111-185 GBq g^{-1} (3-5 Ci g^{-1}) of W) even when produced using high flux reactors such as the High Flux Isotope Reactor (HFIR) in Oak Ridge National Laboratory, USA or SM Reactor in Dmitrovgrad, Russian Federation [19]. The commercially available $^{188}W/^{188}Re$ generators are akin to the $^{99}Mo/^{99m}Tc$ generators using alumina columns, which have limited W-sorption capacity (maximum 80 mg W g^{-1}) [20]. Depending on the specific activity of the available ^{188}W, the currently available generators yield ^{188}Re of low specific volume (activity mL^{-1}) and consequently often require an additional concentration step [19]. Hence, it is pertinent to develop $^{188}W/^{188}Re$ generators where the concentration step can be avoided and even low specific activity ^{188}W prepared in medium flux research reactors can be used.

This chapter describes the development of two novel approaches for the preparation of $^{188}W/^{188}Re$ generators suitable for biomedical applications. The first approach is based on the selective electrodeposition of ^{188}Re from a feed solution of ^{188}W by controlled application of electrode potential. In the second approach, nanomaterial based sorbents (TiP and nano-ZrO_2) were utilized for the preparation of the $^{188}W/^{188}Re$ column chromatographic generators. Additionally, in order to concentrate ^{188}Re obtained from the conventional alumina based $^{188}W/^{188}Re$ generator, a simple electrochemical approach for the post-elution of ^{188}Re has been developed and described.

Electrochemical $^{188}W/^{188}Re$ generator: The reason for adopting the electrochemical approach for preparation of $^{188}W/^{188}Re$ generator is briefly explained in the beginning of this section. Subsequently, the principle and major electrochemical reactions involved in the separation of ^{188}Re from ^{188}W are discussed. The electrochemical set up used and the experiments carried out to optimize the electrolysis parameters to achieve effective electrochemical separation of ^{188}Re from ^{188}W are discussed. The development of a 1.11 GBq (30 mCi) $^{188}W/^{188}Re$ generator is described in detail along with its performance evaluation.

The quality control measures adopted to demonstrate the suitability of ^{188}Re for biomedical applications are mentioned. Finally, the attractive features of this generator are highlighted.

***Post-elution concentration of ^{188}Re by electrochemical metho*d:** This section describes an electrochemical approach to concentrate $Na^{188}ReO_4$ obtained from alumina based ^{188}W/^{188}Re generator. The development of an alumina based ^{188}W/^{188}Re generator of 1.85 GBq is described. The electrochemical assembly used for concentration of ^{188}Re is described along with the optimization of the electrochemical parameters to achieve maximum yield of ^{188}Re. The effect of volume of ^{188}Re solution on the electrodeposition yield of ^{188}Re is discussed. The quality control measures adopted to demonstrate the suitability of the concentrated ^{188}Re for clinical use are described. In the end, the advantages of the electrochemical concentration procedure are discussed.

^{188}W/^{188}Re generators using nanomaterials as sorbents: This section describes the development of ^{188}W/^{188}Re generators using TiP and nano-ZrO_2 as sorbents. The effect of pH of the solution on the K_d values of ^{188}W and ^{188}Re ions were studied to optimize the experimental conditions necessary for satisfactory loading of ^{188}W feed in the column as well as easy elution of ^{188}Re. The mechanism of uptake of ^{188}W by these sorbents is proposed by correlating the K_d values of W ions with the zeta potential of the sorbents. The sorption capacities of these sorbents were determined under both static and dynamic conditions and compared with the values reported for alumina. The procedure for the development of two ^{188}W/^{188}Re generators (of 1.85 GBq each), using TiP and nano-ZrO_2 as sorbents, respectively, and evaluation of their elution performance for 6 months are described. The quality control procedures adopted to demonstrate the suitability of ^{188}Re for clinical use are discussed. The chapter ends with a mention of the advantages of using this class of sorbents for the preparation of ^{188}W/^{188}Re generators.

References

[1] Rayudu GVS. Production of radionuclides for medicine. Sem Nucl Med 1990; 20: 100-110.

[2] Adelstein SJ, Manning FJ (editors) Isotopes for Medicine and the Life Sciences. National Academy Press, Washington D.C., USA, 1995.

[3] Richards P, Tucker WD, Srivastava SC. Technetium-99m: An historical perspective. Int J Appl Radiat Isot 1982; 33: 793-799.

[4] Eckelman WC. Unparalleled contribution of technetium-99m to medicine over 5 decades. J Am Coll Cardiol Img 2009; 2: 364-368.

[5] Mirzadeh S, Knapp Jr FF. Biomedical radioisotope generator systems. J Radioanal Nucl Chem 1996; 203: 471-488.

[6] Boyd RE. Technetium-99m generators- The available options. Int J Appl Radiat Isot 1982; 33: 801-809.

[7] Boyd RE. The gel generator: a viable alternative source of ^{99m}Tc for nuclear medicine. Appl Radiat Isot 1997; 48: 1027-1033.

[8] Roesch F, Riss PJ. The renaissance of the ^{68}Ge/^{68}Ga radionuclide generator initiates new developments in ^{68}Ga radiopharmaceutical chemistry. Curr Top Med Chem 2010; 10: 1633-1668.

[9] Mushtaq A. Inorganic ion-exchangers: Their role in chromatographic radionuclide generators for the decade 1993-2002. J Radioanal Nucl Chem 2004; 262: 797-810.

[10] Pradeep T. Nano: The essentials Understanding Nanoscience and Nanotechnology. First edition. Tata McGraw Hill Publishing Company Limited, New Delhi, India, 2008.

[11] Bai XM, Voter AF, Hoagland RG, Nastasi M, Uberuaga BP. Efficient annealing of radiation damage near grain boundaries via interstitial emission. Science 2010; 327: 1631-1634.

[12] Cumbal L, Greenleaf J, Leun D, Sengupta AK. Polymer supported inorganic nanoparticles: characterization and environmental applications. React Funct Polym 2003; 54: 167–180.

[13] Okuyama K, Lenggoro IW. Preparation of nanoparticles via spray route. Chem Eng Sci 2003; 8: 537–547.

[14] Bremer K. Large-Scale production and distribution of Tc-99m generators for medical use. Radiochim Acta 1987; 41: 73-81.

[15] Molinsky VJ. A review of ^{99m}Tc generator technology. Int J Appl Radiat Isot 1982; 33: 811-819.

[16] Cecchin D, Zucchetta P, Faggin P, Bolla E, Bui F. ^{99}Mo/^{99m}Tc generator shortage. J Nucl Med 2010; 51: 14N-15N.

[17] Therapeutic Radionuclide Generators: ^{90}Sr/^{90}Y and ^{188}W/^{188}Re generators. IAEA Technical Report Series No. 470 (2009).

[18] Maximum permissible body burden and maximum permissible concentrations of radionuclides in air and water for occupational exposure. National Bureau of Standards Handbook. 69, U.S. Department of Commerce, AFP 160-67; p. 38 (1959).

[19] Guhlke S, Beets AL, Oetjen K, Mirzadeh S, Biersack HJ, Knapp Jr. FF. Simple new method for effective concentration of ^{188}Re solution from an alumina based ^{188}W-^{188}Re generator. J Nucl Med 2000; 41: 1271-1278.

[20] Perego R, Wierczinski B, Zhernosekov K, Henkelmann R, Türler A, Nikula T, Buck O. Development of an improved 130 GBq ^{188}W/^{188}Re generator. Eur J Nucl Med Mol Imaging 2007; 34: S210.

LIST OF FIGURES

LIST OF TABLES

CHAPTER 1

INTRODUCTION

"Research is to see what everybody else has seen and to think what nobody else has thought"

ALBERT SZENT-GYORGYI

1.1 The evolution of Nuclear Medicine

The discovery of X-rays by Wilhelm Conrad Rontgen in 1895 and of radioactivity by Henri Becquerel in 1896 opened up a vast avenue for a number of phenomenal discoveries to follow in the next few decades and thus laid the foundation of the 'nuclear era' [1]. Marie and Pierre Curies investigated extensively the phenomenon of radioactivity, discovered by Henri Becquerel. It was Marie Curie who coined the term 'radioactivity'. By 1898, foresight and further work by the Curies led to the discovery of two new elements, namely, polonium and radium. The Curies rightly pointed out that radioactive decay is a phenomenon of spontaneous emission of particles or electromagnetic radiation from an atomic nucleus due to its instability. The emanations from radioactive substances were found to have components like alpha (α), beta (β) or gamma (γ) radiations and sometimes neutron, proton or other heavy particles resulting in the transformation of the nucleus. With the discovery of artificial radioactivity by Irene Curie and Frederic Joliot in 1934 and the discovery of nuclear fission by Otto Hahn and Fritz Strassmann in 1938, many new radionuclides could be produced, which could be utilized for variety of applications in diverse fields such as healthcare, industry, food and agriculture benefitting the mankind [2]. One of the most important applications of radionuclides is in the field of healthcare and this branch of medicine is known as 'Nuclear Medicine'.

Nuclear Medicine is the medical specialty that involves the use of radioisotopes in the diagnosis and treatment of diseases [3]. In other words, it employs the nuclear properties of radioisotopes to evaluate metabolic, physiologic and pathologic conditions of the human body. Today, Nuclear Medicine offers procedures that are immensely helpful to a broad span of medical specialties ranging from oncology and cardiology to psychiatry bringing solace to millions of patients all over the world annually. Nuclear Medicine has a multifaceted heritage. Soon after its discovery by Pierre and Marie Curies, radium began to be used for

treatment of disease conditions and was considered 'cure all' till the 1920s [4]. An important breakthrough took place in the year 1923, when George de Hevesy, one of the pioneers of Nuclear Medicine, introduced the concept of 'tracer' wherein a radioisotope could be used to trace the path of radiolabeled molecule in a biological system [4]. He demonstrated that with just a miniscule quantity of radioactive element, amazingly large number of body functions could be studied without altering the biochemical make-up or the physiological function of the organ being studied. The invention of the cyclotron by E.O. Lawrence in the 1930's paved the way for production of number of radioisotopes in small quantities (mCi levels) by 'charged particle acceleration' [5]. The first clinical application of artificial radioactivity was probably carried out in the year 1938, when a 29 year old chronic myelogenous leukemia patient was treated with ^{32}P at the University of California, Berkeley, USA [4]. Even today, ^{32}P is extensively used as one of the most important therapeutic radioisotopes [6]. The production of ^{131}I by Livingood and Seaborg in accelerator led to its use in thyroid cancer therapy [4]. A landmark event of Nuclear Medicine occurred in 1949 when Professor David Smithers of Royal Marsden Hospital of London performed the first successful radioiodine treatment on a 20 year old woman suffering from inoperable neck tumor [7]. After the mastery over the controlled chain reaction of nuclear fission in the 1940s and the subsequent commissioning of nuclear reactors, production of medically useful radioisotopes became feasible in the nuclear reactors [3]. In the early 1950s, reactor produced radioisotopes on a large scale such as ^{3}H, ^{14}C, ^{35}S, ^{32}P and ^{125}I became available commercially in large quantities. Soon after, ^{131}I could be produced in large quantities (Curie levels) in the nuclear reactors and sealed sources containing ^{60}Co became extensively available for use in teletherapy for the treatment of cancers.

Towards the end of 1950's the in-vitro technique, Radioimmunoassay, based on the competitive binding between natural and labeled antigen to an antibody [8] was invented by

Solomon Berson and Rosalyn Yalow for measurement of very low concentrations of hormones in human samples such as serum. This Nobel Prize winning technology was a turning point in the world of clinical diagnosis and paved the way for quick, simple and sensitive measurement of hundreds of biologically important molecules such as hormones, drugs etc. in human samples.

These significant developments in the medical applications of radioisotopes and radiation have been considered by many as the dawn of Nuclear Medicine. However, the widespread clinical use of Nuclear Medicine was witnessed after the advent of ^{99m}Tc in 1960s. Though ^{99m}Tc was discovered by Seaborg and Emilio Segre in 1937 [9,10], the potential of this excellent radioisotope for diagnostic Nuclear Medicine could not be unearthed until the development of ^{99}Mo/^{99m}Tc generator by Walter Tucker and Margaret Greene at Brookhaven National Laboratory in 1957 [11]. The practice of Nuclear Medicine got a giant momentum after the development of the ^{99}Mo/^{99m}Tc generator. Soon, ^{99m}Tc occupied a dominant position among the diagnostic tools in modern Nuclear Medicine and a variety of ^{99m}Tc based radiopharmaceuticals became available commercially. This radioisotope is referred to as the 'work horse of Nuclear Medicine' [11] and is currently being used in ~80% of the diagnostic Nuclear Medicine procedures world-wide [12]. The introduction of radionuclide generators was a catalyst in the growth of Nuclear Medicine, as short-lived radioisotopes could easily be availed at Nuclear Medicine departments far away from the reactors or cyclotrons. Subsequently, owing to the tremendous advancement in the Nuclear Medicine technology and instrumentation after 1965, Nuclear Medicine registered a phenomenal growth as a specialty discipline. By the end of seventies it was possible to visualize almost all the major organs by employing Nuclear Medicine techniques. With the development of single photon emission tomography in 1980s, it was possible to obtain three dimensional images of the heart, which helped in the critical diagnosis of various heart

diseases. The introduction of the concept of computed tomography (CT) and associated reconstruction techniques led to the development of Single Photon Emission Computed Tomography (SPECT). The advent of Positron Emission Tomography (PET), wherein positron emitting radionuclides are employed to obtain tomographic images of the organs, helped Nuclear Medicine to become one of the most exciting diagnostic specialties in healthcare [13]. This field continues to grow and is now extensively used in conjunction with computed tomography, magnetic resonance imaging, ultrasonography etc. to gain maximum information.

1.2 Radiopharmaceuticals

Nuclear Medicine procedures are mostly carried out by administration of very small amounts of radiochemical preparations known as 'Radiopharmaceuticals'. Radiopharmaceuticals are defined as a special class of radiochemical formulation having high purity, sterility and apyrogenicity, suitable for administration to human patients either orally or intravenously, either for diagnosis or therapy [13]. Radiopharmaceuticals could be simple ions such as $^{32}PO_4^{3-}$, $^{89}Sr^{2+}$, $^{131}I^-$ which localize in the organs of interest owing to their biochemical action [13]. However, such examples are very few and generally, a radiopharmaceutical can be considered to be a two component system consisting of a radionuclide attached to a carrier moiety. The carrier moiety is the biologically active part which directs the radiopharmaceutical to the desired target while the role of the radionuclide is to either aid imaging (diagnosis) or irradiate the cell to cause killing (therapy). While designing a radiopharmaceutical for a particular application, a suitable carrier molecule is chosen to achieve preferential localization in the organ of interest or emulation of physiological functions of the organ of interest and a radionuclide with appropriate decay characteristics is chosen to achieve diagnostic or therapeutic efficacy.

1.3 Classifications of the radionuclides based on their application: Diagnostic and therapeutic radionuclides

The radioisotopes that are used for the preparation of radiopharmaceuticals can be broadly classified into two types, namely diagnostic radionuclides and therapeutic radionuclides, depending on their specific applications [14].

1.3.1 Diagnostic radionuclides

Diagnostic radionuclides are used in the preparation of radiolabeled molecules that are aimed at getting information regarding the internals of the body, in a non-invasive manner. Most diagnostic procedures using radiopharmaceuticals are for imaging organs such as heart, brain, liver, lungs, etc. in order to identify any abnormalities at the early stage of the disease as well as to determine the functioning of organs and to delineate abnormal growths such as tumors. The essential criteria for using a radionuclide for diagnostic purpose are discussed below.

a) Absence of particulate emission: Since the main objective of using a diagnostic radionuclide is to visualize its location non-invasively, the radiation emitted must be capable of passing through the tissues without depositing the energy within the tissue. Thus, it is desirable that the radionuclide used for diagnostic purposes emits only γ-rays. Consequently, the radionuclide should decay purely either by electron capture (EC) or by isomeric transition (IT) without any internal conversion (IC). Further, emission of a single energy photon/γ-ray is even more desirable, as this would allow tomographic 3-dimensional images of the body internals to be registered. Such "Single Photon Emission Computed Tomography" (SPECT) images are far better for delineating lesions for diagnostic purposes and are hence preferred over simple 2-dimensional images. Radionuclides emitting particles, such as α and β^- particles are not suitable due to their short range of penetration and high linear energy transfer (LET). These particulate radiations get completely absorbed in the tissues rendering a

high radiation dose to the patient without aiding diagnosis. However, positron (β^+) emitting radionuclides can be used for diagnostic applications, as annihilation of the positron with an electron leads to emission of two 511 keV γ-rays, which aid in diagnosis. In the case of positrons, the images obtained using "Positron Emission Tomography" (PET) cameras have far better resolutions than the SPECT images, due to the far lower background noise achievable with coincidence counting.

b) Emission of suitable energy γ-photons with high yield: In addition to the emission of photons that can permeate tissues, the emitted γ-radiations should be in the optimal energy range for diagnostic imaging. The gamma cameras used for SPECT as well as rectilinear imaging of gamma emissions employ NaI(Tl) detectors, and gamma emissions in the range of 80-300 keV are ideally suited for use in such cameras. Below 35 keV, the γ-photons are attenuated inside the patient's body and hence not detected by the detector. To be useful for imaging, the γ-photons must have at least 80 keV energy [13]. On the other hand, γ-photons of more than 300 keV energy, cannot be properly collimated and therefore, sub-optimal image with poor sensitivity and low resolution is obtained in SPECT imaging [13]. However, in PET imaging, the two 511 keV γ-photons which emanate on annihilation of positron are detected in coincidence, using suitable detectors such as Bismuth Germanate. A high yield of γ-photons is desired as this would allow reduction in activity to be administered and time requirement for imaging.

c) Suitable half-life: A radionuclide having a short physical half-life is generally suitable for the preparation of diagnostic radiopharmaceuticals, as it is desirable that it decays after the procedure is completed. However, the half-life should be adequately long for completion of the preparation and quality control of the radiopharmaceutical, transport of the radiopharmaceutical to the desired site and subsequent imaging studies with the available instrumentation. Apart from the physical half-life, the biological half-life of the

radiopharmaceutical has a bearing on its residence time in the body, and this depends on the nature of the carrier molecule used.

d) Ease of production of the radionuclide: The radionuclide must be easily available and its production route must be cost effective.

e) High specific activity and purity: The radionuclide of interest must be available with high specific activity and very high radionuclidic, radiochemical and chemical purity. High specific activity ensures that the desired activity of the radiopharmaceuticals to be injected can be acquired with minimum amount of carrier molecule. High radionuclidic purity of the radionuclide reduces the undesired dose to the patient from the radionuclidic impurities while high radiochemical and chemical purity ensure its suitability for labeling various ligands and biomolecules for the preparation of the radiopharmaceuticals.

f) Favorable chemistry: The radionuclide chosen should have versatile chemistry amenable for manipulation into various chemical forms with the desired biological behavior. In case of the metallic radionuclides, the complexation chemistry of the radio-element should be favorable for the preparation of a wide variety of radiopharmaceuticals.

Based on the imaging modalities for which diagnostic radionuclides are used, they may be further categorized into two types, namely, the radionuclides used for SPECT imaging and the ones used for PET imaging [14].

i) Radionuclides used for SPECT imaging: SPECT, as mentioned earlier, is a technique to obtain 3D images of the organs, by processing the data when a single energy γ-ray emitting radionuclide is used. The most common SPECT systems consist of a gamma camera with one to three NaI(Tl) detector heads mounted on a gantry, an online computer for acquisition and processing of data and a display system [13]. The detector head rotates along the long axis of the patient at small angular increments (3º-10º) for 180º or 360º angle sampling and the information is typically presented as cross-sectional slices, which can be freely reformatted or

manipulated as required to obtain transverse, saggital or coronal images [13]. ^{99m}Tc is the most common radioisotope used for SPECT imaging. Apart from ^{99m}Tc, several other radionuclides such as ^{67}Ga, ^{111}In, ^{123}I and ^{201}Tl also enable SPECT imaging. The physical characteristics of the commonly used radionuclides for SPECT imaging are given in **Table 1.1**.

Table 1.1: Physical characteristics of radionuclides used for SPECT imaging

Radionuclide	**Half-life** [15]	**Mode of decay**[@]	**Principal γ-component E in keV (% abundance)** [16]
^{99m}Tc	6.0 h	IT	140.5 (88.9)
^{123}I#	13.3 h	EC	159.0 (82.8)
^{67}Ga	3.3 d	EC	93.3 (38.3)
^{111}In	2.8 d	EC	245.4 (94.2)
^{201}Tl	72.9 h	EC	167.4 (10.0)

[@]*Only principal decay mode is mentioned; EC indicates decay by electron capture; IT indicates decay by isomeric transition; E indicates energy*

It may be mentioned that, ^{131}I is also an important diagnostic radionuclide, widely used for thyroid imaging, owing to the highly specific accumulation of iodide ions in the thyroid. However, due to the emission of multiple γ-rays and the strong β- rays, SPECT imaging is not possible using ^{131}I. The easy availability and lower cost of ^{131}I make it the preferred isotope despite the existence of another iodine isotope ^{123}I which enables SPECT imaging.

ii) Radionuclides used for PET imaging: PET imaging, as indicated earlier, is based on the detection of two 511 keV photons emitted in opposite directions after annihilation of a positron (β^+) with an electron. The two emerging photons are detected by two detectors placed at 180° in coincidence, and the data collected around the body axis of the patient are used to reconstruct the activity distribution [13]. In modern PET systems, multiple detectors are distributed in two to eight circumferential arrays arranged in circles, hexagons or

octagons around the patient, wherein, each detector is connected to the opposite detector by a coincidence circuit [13], enabling quick imaging.

PET, as compared to SPECT has the ability to record images with superior sensitivity and high spatial resolution, owing to the much reduced background noise. PET can be very helpful in detecting very small lesions, which may be missed in SPECT imaging using ^{99m}Tc based radiopharmaceuticals. ^{18}F ($t_{½}$ = 110 min), the most important PET radionuclide, is used as a metabolic tracer in the form of ^{18}F-FDG (^{18}F-fluoro deoxy glucose), for the diagnosis of a variety of conditions, most importantly in cancer detection and staging. The exponential growth of PET imaging using ^{18}F-FDG in the past two decades, has aptly resulted in it being called the 'molecule of the millennium' [1,17,18]. ^{18}F-FDG accounts for about 10% of all imaging done presently in Nuclear Medicine [1]. Other radioisotopes that are used for PET imaging include, ^{11}C, ^{13}N, ^{15}O, ^{68}Ga, ^{82}Rb etc. The physical characteristics of commonly used radionuclides for PET imaging are given in **Table 1.2**.

Table 1.2: Physical characteristics of radionuclides used for PET imaging

Radionuclide	**Half-life** [15]	**Mode of decay**[@]	**Principal γ-component E in keV (% abundance)** [16]
^{18}F	109.8 min	β^+	511 (200.0)
^{68}Ga	68.3 min	β^+, EC	511 (176.0)
^{11}C	20.4 min	β^+	511 (199.5)
^{13}N	9.9 min	β^+	511 (199.6)
^{15}O	122.2 s	β^+	511 (199.8)
^{82}Rb	1.2 min	β^+, EC	511 (192.0)

[@] *Only principal decay mode is mentioned; E indicates energy*

Among these, ^{68}Ga ($t_{½}$ = 67.7 min) has gained considerable interest in the recent times, mainly because it can be availed from a radionuclidic generator, obviating the need to have a

cyclotron at the vicinity of the Nuclear Medicine center [19].

1.3.2 Therapeutic radionuclides

Therapeutic radionuclides are utilized for the preparation of radiolabeled molecules, which are designed to deliver therapeutic dose of ionizing radiation to specific disease sites with high specificity in the body. An ideal therapeutic radionuclide should have the following characteristics.

a) Emission of high linear energy transfer (LET) radiations: The radionuclides used for therapy should emit high LET particulate radiations such as α, β^- or Auger electrons. These particles (α, β^- or Auger electrons), depending on their energy and mass have different penetration ranges in tissue. These radiations are effective in delivering localized cytotoxic doses of radiation, resulting in target cell death. Although α-rays have high LET, unless they are targeted very precisely to the diseased site, they can result in unnecessary radiation dose to the healthy tissues. In the case of Auger or conversion electrons, these rays carry very small energy and dissipate all the energy within a very short range of the order of nm. Thus, it is essential that the radiopharmaceutical is targeted inside the cancer cell, preferably the DNA. On the other hand the β^- rays have a range of few μm to mm, depending on their energy and a large variety of β^- emitting metallic radionuclides are feasible to be produced in reactors. Hence, generally, the β^- emitting radionuclides are preferred for therapeutic applications [20].

b) Emission of imageable γ-photons with low abundance: Apart from the particulate radiation required for therapeutic effectiveness, emission of γ-rays of energy suitable for imaging (80-300 keV), is desirable in a therapeutic radionuclide. Imaging the in-vivo distribution of the radiopharmaceutical will enable the physician to ascertain the proper localization as well as to determine the dosimetry in patients. [21,22]. However, as γ-radiations irradiate the non-target tissues also, resulting in increase of radiation dose burden

to the patients as well as increase in personnel exposure, emission of suitable energy photons in low abundance is preferred for minimum increase in dose burden of the patient.

c) Suitable half-life: The physical half-life of the radionuclide is an important consideration in the design of radiotherapeutic agents. In order to maximize the therapeutic ratio, the physical half-life of the radionuclide should match well with the in-vivo localization and the pharmacokinetics of the radiolabeled drugs [21,22]. Depending on the nature for which it is utilized, a suitable therapeutic radionuclide should be judiciously chosen based on the half-life.

Apart from these, just like an ideal diagnostic radionuclide, a therapeutic radionuclide should be available at a reasonable cost with specific activity and purity suitable for radiopharmaceutical application. Moreover, its chemistry should be amenable for preparation of a wide variety of radiopharmaceuticals. Both therapeutic as well as diagnostic radionuclide should form a strong and irreversible bonding with the carrier molecule resulting in the formation of a highly stable radiolabeled molecule. A list of commonly used therapeutic radionuclides along with their physical characteristics is shown in **Table 1.3**.

Table 1.3: Physical characteristics of some therapeutic radionuclides

Radionuclide	**Half-life** [15]	**Mode of decay**[@]	**Energy (keV)**[#]	**Principal γ-component E in keV (% abundance)** [16]
^{32}P	14.3 d	β^-	1710.6	Nil
^{47}Sc	3.3 d	β^-, γ	600.1	159.4 (68.0)
^{67}Cu	61.8 h	β^-, γ	577.0	184.6 (48.7)
^{77}As	38.8 h	β^-, γ	682.9	239.0 (1.6)
^{89}Sr	50.5 d	β^-	1496.6	Nil
^{90}Y	64.1 h	β^-	2282.0	Nil

Continued in the next page

Radionuclide	Half-life [15]	Mode of decay[@]	Energy (keV)[#]	Principal γ-component E in keV (% abundance) [16]
^{105}Rh	35.4 h	β^-, γ	567.0	318.9 (19.2)
^{109}Pd	13.7 h	β^-, γ	1115.9	88.0 (3.6)
^{111}Ag	7.4 d	β^-, γ	1036.8	342.1 (6.7)
^{131}I	8.0 d	β^-, γ	970.8	364.5 (81.2)
^{133}Xe	5.2 d	β^-, γ	427.4	81.0 (37.1)
^{142}Pr	19.1 h	β^-, γ	2162.3	1575.6 (3.7)
^{149}Pm	53.1 h	β^-, γ	1071.0	285.9 (2.8)
^{153}Sm	46.3 h	β^-, γ	808.4	103.2 (28.3)
^{159}Gd	18.5 h	β^-, γ	970.6	58.0 (26.2)
^{165}Dy	2.3 h	β^-, γ	1286.2	94.7 (3.6)
^{166}Ho	26.8 h	β^-, γ	1854.5	80.6 (6.2)
^{169}Er	9.4 d	β^-, γ	351.2	Nil
^{175}Yb	4.2 d	β^-, γ	470.0	396.3 (6.5)
^{177}Lu	6.7 d	β^-, γ	498.2	208.4 (11.0)
^{186}Re	90.6 h	β^-, γ	1069.5	137.2 (8.6)
^{188}Re	16.9 h	β^-, γ	2120.4	155.0 (14.9)
^{194}Ir	19.3 h	β^-, γ	2246.9	328.4 (13.0)
^{198}Au	2.7 d	β^-, γ	1372.5	411.8 (95.5)
^{199}Au	3.1 d	β^-, γ	452.6	158.4 (36.9)
^{211}At	7.2 h	α, γ	5982.4	687.0 (0.3)
^{212}Bi	60.6 min	α, γ	6207.1	727.2 (11.8)
^{213}Bi	45.6 min	α, γ	5982.0	439.7 (27.3)
^{223}Ra	11.4 d	α, γ	5979.3	269.4 (13.6)
^{225}Ac	10.0 d	α, γ	5935.1	99.7 (3.5)

[@]Only principal decay mode is mentioned; [#]For β^- particles maximum β^- energy is mentioned

1.4 Production of radionuclides for Nuclear Medicine applications

The radionuclides used in Nuclear Medicine are mostly artificially produced, either in a cyclotron or a nuclear reactor [3,23]. Various factors influence the nuclear reaction and the product radionuclide that ensues, both in nuclear reactors as well as cyclotrons. Among these, the nature of the target atom and the type and energy of the projectiles influence the reactions significantly. Other factors such as the purity of the target material, the nuclidic abundance of the target nuclide, the irradiation duration etc. have a bearing on the kinds and extent of radionuclidic impurities in the desired product as well as the amounts and specific activity of the product radionuclide [3,23]. One convenient route of radioisotope production, especially for the short-lived radioisotopes, is the use of radionuclide generator systems wherein high-specific activity radionuclides can be produced in a no-carrier-added (NCA) form and can readily be obtained at the desired site [24-26]. However, the parent radionuclides used in these generators are either produced in a nuclear reactor or a cyclotron. The three different methodologies for the production of medically useful radionuclides are discussed below, with special emphasis on generator produced radionuclides.

1.4.1 Cyclotron produced radionuclides

In a cyclotron, targets of stable elements are bombarded with a high energy beam of charged particles generated by accelerating the charged particles, such as p, d, α, ^{3}He etc., by means of an electromagnetic field. A wide variety of radionuclides can be produced in a cyclotron by varying the type of target and the energy of the charged particle in the cyclotron [3,23,27]. Generally, the radionuclides produced in cyclotron are neutron deficient and hence decay either by electron capture or β^{+} or both, followed by γ-emission in certain cases. In a cyclotron, the radioisotopes produced are with atomic numbers different from those of the target isotopes, and hence it is necessary to separate the radioisotope from the target after the irradiation. This can be accomplished by techniques such as ion-exchange chromatography,

solvent extraction, precipitation, electrochemical separation, distillation, simple filtration, paper chromatography, etc., and the radioisotopes can be availed in NCA form [28,29]. The target material for the production of radionuclides must be pure and preferably mono-isotopic or at least isotopically enriched to avoid the production of extraneous radionuclides. Additionally, the energy and the type of particles used for bombardment must be carefully chosen so that contamination with undesirable radionuclides from extraneous nuclear reactions can be avoided or minimized. The irradiation of a target in a cyclotron may require external beam irradiation or internal beam irradiation depending on the situation and requirements [3]. High flux delivering modern charged particle accelerators generate excess heat (higher than 1000 ºC) within the target. This requires fast removal of heat by circulating cold deionized water around the targets and using highly stable target materials as metal foils, electroplated metals, metal powders, metal oxides and salts melted on duralmin plate [3]. Sometimes, the targets are irradiated at a lower current in order to overcome the heating problems.

Cyclotron produced radionuclides such as ^{67}Ga, ^{111}In, ^{123}I and ^{201}Tl which decay by electron capture, are used for SPECT imaging while β^+ emitting radionuclides such as, ^{11}C, ^{13}N, ^{15}O, and ^{18}F are useful in PET studies. **Table 1.4** lists some of the commonly used cyclotron produced radionuclides along with their half-lives, principal decay modes and commonly used production routes.

Table 1.4: Physical characteristics of some cyclotron produced radionuclides

Radionuclide	**Half-life** [15]	**Mode of decay**[*]	**Common production route**[@]	**Natural abundance of target (%)**[#]
^{11}C	20.4 min	β^+	$^{14}N(p,\alpha)^{11}C$	99.6
^{13}N	9.9 min	β^+	$^{16}O(p,\alpha)^{13}N$	99.8
^{15}O	122.2 s	β^+	$^{14}N(d,n)$ / $^{15}N(p,n)^{15}O$	99.6/0.4
^{18}F	109.8 min	β^+	$^{18}O(p,n)^{18}F$	0.2
^{19}Ne	17.3 s	β^+	$^{19}F(p,n)$ / $^{16}O(\alpha,n)^{19}Ne$	100.0 / 99.8
^{21}Na	23 s	β^+	$^{20}Ne(d,n)$	90.5
^{28}Mg	21.2 h	β^-	$^{26}Mg(\alpha,2p)^{28}Mg$	11.0
^{47}Sc	3.3 d	β^-,γ	$^{48}Ti(p,2p)^{47}Sc$	73.8
^{57}Ni	36.0 h	β^+,EC	$^{56}Fe(^3He,2n)^{57}Ni$	91.7
^{64}Cu	12.8 h	β^-,β^+,EC	$^{64}Ni(p,n)^{64}Cu$	0.9
^{67}Cu	61.8 h	β^-,γ	$^{68}Zn(p,2p)^{67}Cu$	18.8
^{67}Ga	3.2 d	EC	$^{68}Zn(p,2n)^{67}Ga$	18.0
^{68}Ge	271.0 d	EC	$^{69}Ga(p,2n)^{68}Ge$	60.0
^{74}As	17.9 d	β^-,β^+,EC	$^{71}Ga\ (\alpha,n)^{74}As$	40.0
^{77}As	38.8 h	β^-,γ	$^{80}Se(p,\alpha)^{77}As$	49.6
^{77}Br	57.0 h	EC	$^{75}As(\alpha,2n)^{77}Br$	100.0
^{86}Y	14.7 h	β^+	$^{86}Sr(p,n)\ ^{86}Y$	9.8
^{103}Pd	16.9 d	EC	$^{103}Rh(p,n)^{103}Pd$	100.0
^{111}In	2.8 d	EC	$^{111}Cd(p,n)^{111}In$	12.8
^{117m}Sn	13.6 d	CE	$^{121}Sb(p,2p,3n)^{117m}Sn$	57.4
^{123}I	13.3 h	EC	$^{121}Sb(\alpha,2n)^{123}I$	57.4

Continued in the next page

Radionuclide	Half-life [15]	Mode of decay*	Common production route@	Natural abundance of target (%)#
^{127}Xe	36.4 d	EC	^{127}I(p,n)^{127}Xe	100.0
^{165}Er	10.3 h	EC	^{165}Ho(p,n)^{165}Er	100.0
^{197}Hg	64.1 h	EC	^{197}Au(p,n)^{197}Hg	100.0
^{201}Tl	72.9 h	EC	^{203}Tl(p,3n)^{201}Tl	29.5
^{211}At	7.2 h	α, γ	^{209}Bi(α,2n)^{211}At	100.0

**Only principal decay mode is mentioned; @Other routes of production also exists; EC indicates decay by electron capture; CE indicates decay by emission of conversion electrons*

1.4.2 Reactor produced radionuclides

A large number of radionuclides used in Nuclear Medicine are produced in the nuclear reactors [3,23]. A nuclear reactor is an assembly in which fission chain reaction takes place in a controlled manner, generally, for the production of energy. A nuclear reactor is constructed with fuel rods made up of fissile materials such as ^{235}U or ^{239}Pu. The nuclear fission reactions, apart from producing enormous amounts of energy, also result in copious amounts of neutrons. These neutrons are essential for sustaining the nuclear fission chain reaction and can undergo further nuclear reactions. In addition, they are also used for artificial production of radioisotopes. Since, neutrons emitted from fission reactions have very high energies and consequently very high velocities; the probability of their interaction with other nuclides is very low. Hence, these neutrons are slowed down in nuclear reactors to the thermal region with energy in the range of 0.025 eV by using moderators. Thermal neutrons have comparatively higher probability of interaction with the nucleus of atoms and are extremely important for the production of radioisotopes [30]. Though, many countries in the world have nuclear reactors suitable for the production of radioisotopes, very few of them have nuclear reactors which have fluxes high enough to produce radioisotopes with adequate specific activities and amounts required for applications in Nuclear Medicine [31,32]. In

India, the radioisotope production and application was among the important mandates from the beginning of the "Atomic Energy" program in the late 1940s and early 1950s. Till recently, three research reactors, namely, Apsara, CIRUS and Dhruva were operational at Bhabha Atomic Research Centre in Mumbai, to cater to the need of radioisotope production in India. However, the Apsara reactor has been temporarily shut down for refurbishment while the CIRUS reactor has been decommissioned in December, 2010. The maximum neutron flux available in Apsara and CIRUS reactors were 5×10^{12} and 6×10^{13} n cm^{-2} s^{-1}. Presently, the Dhruva reactor with a maximum thermal neutron flux of 1.8×10^{14} n cm^{-2} s^{-1} is used for the production of radioisotopes. The different types of neutron induced reactions commonly used for the production of radioisotopes are briefly discussed below.

1.4.2.1 Radiative neutron capture or (n,γ) reaction

In a radiative neutron capture reaction, the target nucleus captures one thermal neutron and emits γ-rays to produce an isotope of the same element. Often the isotope formed is unstable, and hence is radioactive. Generally, the radioisotope formed is neutron rich and decays by β^- emission with relatively long half-life. The radioisotope cannot be separated from the target as they are the same elements and therefore its specific activity is low. Specific activity is also limited by the available neutron flux and cross section. Various medically useful radionuclides such as ^{60}Co, ^{99}Mo, ^{24}Na, ^{192}Ir, ^{198}Au and ^{82}Br are produced by this method. (n,γ) reactions are useful to produce radioisotopes which decay to either stable isotopes or longer-lived radioisotopes, which would find an application. Very rarely, two consecutive (n,γ) reactions are used for production of a radioisotope. Such a production route would understandably require very high neutron flux, high neutron capture cross-sections for both reactions as well as high isotopic abundance of the target nuclide.

Most often, (n,γ) reactions lead to β^- emitting isotopes, which may further yield another β^- emitter. However, in some elements with large number of stable isotopes, (n,γ)

reactions could result in neutron deficient isotope which may decay either by 'electron capture' mode or rarely by 'β^+' mode. Such reactions, wherein (n,γ) is followed by another transmutation, lead to radioisotopes of another element which are of interest for medical applications, as the final product radionuclide can be separated from the original target element. The major advantage of this mode is that the radionuclide can be produced with very high specific activity in a NCA form.

1.4.2.1.1 Neutron capture (n,γ) followed by β⁻ decay

Many (n,γ) reactions produce short lived radioisotopes which decay by β^- emission to another β^- emitting radioisotope having a longer half-life. The most widely used isotope produced by this route is ^{131}I. ^{130}Te on (n,γ) reaction, yields ^{131}Te ($t_{½}$ = 25 min), which decays to ^{131}I, which is then separated and used. Another example is ^{176}Yb which undergoes (n,γ) reaction to produce ^{177}Yb ($t_{½}$ = 1.9 h) which subsequently decays by β^- decay to produce ^{177}Lu ($t_{½}$ = 6.7 d). The radionuclide ^{177}Lu can then be separated from the irradiated Yb target.

1.4.2.1.2 Neutron capture (n,γ) followed by EC/β⁺ decay

Target nuclides which have room to accommodate a few more neutrons in their nucleus when bombarded with neutrons may yield higher stable isotopes of the same element or a radioisotope of the same element, which is not neutron rich. This product nuclide transmutes by EC (or rarely β^+) mode to an isotope of neighboring element which could also be a neutron deficient isotope decaying by EC mode. Such a situation arises in elements which have large number of stable isotopes, such as Xe. A good example is ^{124}Xe, which on (n,γ) reaction yields ^{125}Xe ($t_{½}$ = 16.89 h), which decays by EC to ^{125}I ($t_{½}$ = 60 d). ^{125}I is a very useful medical isotope produced by irradiation of Xe gas through the above route.

1.4.2.2 Neutron capture with particle emission: (n,p) and (n,α) reactions

In some cases, neutron capture leads to emission of charged particles such as proton or α-particle from the compound nucleus, if sufficient excitation energy is available for such

a reaction. The typical examples of such reactions are ^{32}S (n,p) ^{32}P and ^{27}Al (n,α) ^{24}Na. In these cases also, the product radionuclide is non-isotopic with the target radionuclide and hence can be obtained in NCA form after its separation from the target.

1.4.2.3 Neutron capture with fission or (n,f) reaction

The neutron induced fission of ^{235}U or ^{239}Pu during normal reactor operation produces a wide variety of radioisotopes. The peak fission yield of 6% corresponds to isotopes with mass numbers 95-100 and 135-140 [30]. Among these, there are several radioisotopes which have potential for use in medical as well as other applications. However, since a large number of radioactive and stable isotopes are produced in fission, isolation of a particular radioisotope of interest with adequate radionuclidic purity requires elaborate and extensive processing facilities. The fission produced radionuclides normally possess very high specific activity, as other isotopes of the same element also formed during fission would be in low amounts. One good example of a medically useful isotope availed through the (n,f) route is ^{99}Mo, which is formed in very high specific activities, containing small amounts of other stable Mo isotopes like ^{100}Mo.

A list of some reactor produced radionuclides is given in **Table 1.5** along with their half-lives, principal decay modes, commonly used production routes, natural abundance of target materials, and the cross-section of the nuclear reaction by which the radionuclide is produced.

Table 1.5: Physical characteristics of some reactor produced radionuclides

Radionuclide	Half-life [15]	Mode of decay*	Common production route	Natural abundance (%) [15]	Cross-section (b) [15]
			(n,γ) reaction		
^{24}Na	15.0 h	β^-	$^{23}Na(n,\gamma)^{24}Na$	100.0	0.53
^{32}P	14.3 d	β^-	$^{31}P(n,\gamma)^{32}P$	100.0	0.18
^{35}S	87.5 d	β^-	$^{34}S(n,\gamma)^{35}S$	4.2	0.29
^{51}Cr	27.7 d	EC	$^{50}Cr(n,\gamma)^{51}Cr$	4.4	15.9
^{59}Fe	44.5 d	β^-,γ	$^{58}Fe(n,\gamma)^{59}Fe$	0.3	0.0013
^{60}Co	5.3 y	β^-,γ	$^{59}Co(n,\gamma)^{60}Co$	100.0	37.18
^{75}Se	119.8 d	EC	$^{74}Se(n,\gamma)^{75}Se$	0.9	51.8
^{99}Mo	67.0 h	β^-,γ	$^{98}Mo(n,\gamma)^{99}Mo$	24.1	0.13
^{109}Pd	13.7 h	β^-,γ	$^{108}Pd(n,\gamma)^{109}Pd$	26.5	8.3
^{142}Pr	19.1 h	β^-,γ	$^{141}Pr(n,\gamma)^{142}Pr$	100.0	11.5
^{153}Sm	46.3 h	β^-,γ	$^{152}Sm(n,\gamma)^{153}Sm$	26.7	206
^{159}Gd	18.5 h	β^-,γ	$^{158}Gd(n,\gamma)^{159}Gd$	24.8	2.2
^{165}Dy	2.3 h	β^-,γ	$^{164}Dy(n,\gamma)^{165}Dy$	28.2	1610
^{166}Ho	26.8 h	β^-,γ	$^{165}Ho(n,\gamma)^{166}Ho$	100.0	66
^{169}Er	9.4 d	β^-,γ	$^{168}Er(n,\gamma)^{169}Er$	26.8	2.74
^{175}Yb	4.2 d	β^-,γ	$^{174}Yb(n,\gamma)^{175}Yb$	31.8	69
^{177}Lu	6.7 d	β^-,γ	$^{176}Lu(n,\gamma)^{177}Lu$	2.6	2100
^{186}Re	90.6d	β^-,γ	$^{185}Re(n,\gamma)^{186}Re$	37.4	106
^{192}Ir	73.8 d	β^-,γ	$^{191}Ir(n,\gamma)^{192}Ir$	37.3	645
^{194}Ir	19.2 h	β^-,γ	$^{193}Ir(n,\gamma)^{194}Ir$	62.7	111
^{198}Au	2.7 d	β^-,γ	$^{197}Au(n,\gamma)^{198}Au$	100.0	98.65

Continued in the next page

Radionuclide	Half-life [15]	Mode of decay*	Common production route	Natural abundance (%) [15]	Cross-section (b) [15]
			Sequential neutron capture		
^{166}Dy	81.5 h	β^-	^{164}Dy(n,γ)^{165}Dy(n,γ)^{166}Dy	28.2	2700; 3500
^{188}W	69.0 d	β^-,γ	^{186}W(n,γ)^{187}W(n,γ)^{188}W	28.6	36; 70
			(n, γ) followed by β⁻ decay		
^{77}As	1.6 d	β^-,γ	^{76}Ge(n,γ,β^-)^{77}As	7.7	0.092
^{105}Rh	35.3 h	β^-,γ	^{104}Ru(n,γ,β^-)^{105}Rh	18.6	145
^{111}Ag	7. 5 d	β^-,γ	^{110}Pd(n,γ,β^-)^{111}Ag	11.7	0.37
^{131}I	8.0 d	β^-,γ	^{130}Te(n,γ,β^-)^{131}I	33.8	0.27
^{149}Pm	53.1 h	β^-,γ	^{148}Nd(n,γ,β^-)^{149}Pm	5.8	2.50
^{177}Lu	6.7 d	β^-,γ	^{176}Yb(n,γ,β^-)^{177}Lu	12.7	2.40
^{199}Au	3.1d	β^-,γ	^{198}Pt(n,γ,β^-)^{199}Au	7.2	3.66
			(n,p) and (n,α) reaction		
^{3}H	12.3 y	β^-	^{6}Li(n,α)^{3}H	7.5	940
^{14}C	5730 y	β^-	^{14}N(n,p)^{14}C	99.6	1.83
^{32}P	14.3 d	β^-	^{32}S(n,p)^{32}P	95.0	0.07
^{67}Cu	2.4 d	β^-,γ	^{67}Zn(n,p)^{67}Cu	4.1	0.0012
^{89}Sr	50.5 d	β^-	^{89}Y(n,p)^{89}Sr	100.0	0.0003
			(n, fission)		
^{90}Sr	28.6 y	β^-	^{235}U(n,f)^{90}Sr	0.7	Y=5.89%
^{99}Mo	67.0 h	β^-,γ	^{235}U(n,f)^{99}Mo	0.7	Y=6.14%
^{131}I	8.0 d	β^-,γ	^{235}U(n,f)^{131}I	0.7	Y=2.84%

**Only principal decay mode is mentioned; EC indicates decay by electron capture, 'b' refers to barn (1 b = 10^{-24} cm^2), 'Y' indicates the fission yield*

1.4.3 Generator produced radionuclides

A radionuclide generator is a device wherein a parent nuclide decays to a radioactive daughter nuclide, which can be separated from the parent and used. One important obvious requirement for availing a radionuclide through generator system is that the parent nuclide should have a longer half-life than the daughter nuclide. Thus, although there are several radionuclides produced in reactors or cyclotrons which decay to radioactive daughters, not all of them are eligible to be used in a generator system. In the past few decades, the use of short lived radioisotopes has grown considerably in both diagnostic as well as therapeutic Nuclear Medicine, because large doses of these radionuclides can be administered with only minimum radiation dose to the patients and excellent quality images can be obtained [24-26,33]. The increasing application of these short lived radioisotopes has led to the development of radionuclide generators which serve as a convenient means of their production [24-26,33-35]. The availability of the short-lived radioisotopes from radionuclide generators serves as an inexpensive and convenient alternative to 'in-house' radioisotope production facilities like reactors or cyclotrons. The radionuclide generators can be conveniently transported to institutions far from the site of reactors or cyclotrons. A generator is developed on the principle of decay-growth relationship between a long-lived parent and its short-lived daughter, existing in a state of radioactive equilibrium. It involves an effective radiochemical separation of the decaying parent and daughter radionuclides, by taking advantage of their difference in chemical properties, so that the daughter activity is obtained with high radionuclidic, radiochemical and chemical purities. Owing to the fact that the daughter and parent are different elements, the daughter activity is availed in a NCA form. A list of some medically important radionuclide generator systems is given in **Table 1.6**, along with the decay characteristics of the parent and daughter radionuclides.

Table 1.6: Some medically important radionuclide generator systems

Daughter radionuclide					Parent radionuclide		
Radio-nuclide	**Half-life** [15]	**Mode of decay***	**β^-, α energy in keV** [15]	**Principal γ energy in keV (% abundance)** [16]	**Radio-nuclide**	**Half-life** [15]	**Mode of decay***
^{44}Sc	3.9 h	EC, β^+	-	511.0 (188.0)	^{44}Ti	46 y	EC
^{62}Cu	9.7 min	β^+	-	511.0 (194.9)	^{62}Zn	9.2 h	EC, β^+
^{66}Cu	5.1 min	β^-, γ	2642.4	1039.2 (8.0)	^{66}Ni	54.6 h	β^-
^{68}Ga	67.6 min	β^+	-	511.0 (178.2)	^{68}Ge	270.8 d	EC
^{72}As	26.0 h	β^+	-	511.0 (150.0)	^{72}Se	8.4 d	EC
^{82}Rb	1.3 min	β^+	-	511.0 (190.6)	^{82}Sr	25.6 d	EC
^{87m}Sr	2.8 h	IT	-	388.0 (80.0)	^{87}Y	3.3 d	EC, β^+
^{90}Y	64.1 h	β^-	2282.0	Nil	^{90}Sr	28.8 y	β^-
^{99m}Tc	6.0 h	IT	-	140.5 (88.9)	^{99}Mo	65.9 h	β^-, γ
^{103m}Rh	65.1 min	IT	-	39.7 (0.07)	^{103}Ru	39.4 d	β^-, γ
^{109m}Ag	39.8 s	IT	-	88 (3.7)	^{109}Cd	453.0 d	EC
^{112}Ag	3.1 h	β^-, γ	3956.0	616.8 (42.9)	^{112}Pd	21.0 h	β^-, γ
^{113m}In	1.7 h	IT	-	391.7 (64.9)	^{113}Sn	115.1 d	EC
^{132}I	2.3 h	β^-, γ	2118.1	667.7 (98.7)	^{132}Te	3.3 d	β^-
^{137m}Ba	2.6 min	IT	-	661.6 (89.9)	^{137}Cs	30.1 y	β^-
^{140}La	1.7 d	β^-, γ	3761.9	1596.2 (95.4)	^{140}Ba	12.7 d	β^-, γ
^{166}Ho	26.8 h	β^-, γ	1854.5	80.6 (6.2)	^{166}Dy	81.6 h	β^-, γ
^{178}Ta	9.3 min	EC	1910.0	325.8 (84.7)	^{178}W	21.6 d	EC
^{188}Re	16.9 h	β^-, γ	2120.4	155.0 (14.9)	^{188}W	69.4 d	β^-, γ
^{194}Ir	19.2 h	β^-, γ	2246.9	328.4 (13.0)	^{194}Os	6.0 y	β^-, γ
^{195m}Au	30.6 s	IT	-	261.7 (68.0)	^{195m}Hg	40.0 h	EC, γ

Continued in the next page

Daughter radionuclide					Parent radionuclide		
Radio-nuclide	**Half-life** [15]	**Mode of decay***	**β^-, α energy in keV** [15]	**Principal γ energy in keV (% abundance)** [16]	**Radio-nuclide**	**Half-life** [15]	**Mode of decay***
^{212}Bi	60.6 min	α, β^-, γ	6207.1 (α) 2254.02 (β)	727.2 (11.8)	^{212}Pb	10.6 h	β^-, γ
^{213}Bi	45.9 min	α, γ	5982.0	439.7 (27.3)	^{225}Ac	10.0 d	α, γ
^{225}Ac	10.0 d	α, γ	5935.1	99.7 (3.5)	^{229}Th	7430 y	α, γ

**Only principal decay mode is mentioned; EC indicates decay by electron capture; IT indicates isomeric transition*

1.5 The development of Radionuclide Generators: A Historical Perspective

The development of radionuclide generators over the past five decades was primarily motivated by the increasing gamut of applications of short-lived radionuclides and their compounds in Nuclear Medicine [24-26,33-35]. This has resulted in significant progress in the production of radionuclides to be used as parent nuclide in generators and development of sophisticated radiochemical separations and reliable technical designs of the generator systems [24-26,33-35]. The first radionuclide generator for biomedical applications was developed by Fallia in 1920 [36,37], by the use of the ^{226}Rd ($t_{½}$= 1620 y) $\rightarrow$ ^{222}Rn ($t_{½}$= 3.8 d) parent-daughter pair to obtain ^{222}Rn seeds for radiation therapy. However, the real practical importance of radionuclide generators was realized only in 1951 with the development of the ^{132}Te ($t_{½}$ = 78 h)/^{132}I ($t_{½}$ = 2.29 h) generator at the Brookhaven National Laboratory (BNL) in USA [38]. A simplified version of this generator was developed in BNL by the mid-1950s [38]. The similarities between the ^{132}Te/^{132}I and ^{99}Mo/^{99m}Tc parent-daughter pairs led to the pioneering development of ^{99}Mo/^{99m}Tc generator system in 1957 at BNL by Walter Tucker and Margaret Greene [11]. Subsequently, several other radionuclide generator systems were

also developed, some of which have significant practical applications [24-26,36].

1.6 The mathematical equations of radioactive decay and growth

In a radionuclide generator, a 'parent' radionuclide (A) decays to a 'daughter' radionuclide (B) which further decays to stable/nearly stable 'grand-daughter' nuclide (C). This decay scheme can usually be represented as in **Fig. 1.1** for two successive radionuclides. In this decay scheme λ_1 is the decay constant for A having N_1^0 initial number of atoms and λ_2 the decay constant for B. For the sake of simplicity, it is generally assumed that $N_2(t=0) = N_2^0 = 0$ and $N_3(t=0) = N_3^0 = 0$ and the grand-daughter product C, as a stable nuclide characterized by $\lambda_3 = 0$.

Then at any given time t, one can write the following differential equations [39]:

$$dN_1(t) = -\lambda_1 N_1(t)dt \quad \text{or} \quad \frac{dN_1(t)}{dt} = A_1(t) = -\lambda_1 N_1(t) \quad \ldots\ldots\ldots\ldots\ldots\ldots (1)$$

$$dN_2(t) = +\lambda_1 N_1(t)dt - \lambda_2 N_2(t)dt \quad \text{or} \quad \frac{dN_2(t)}{dt} = \lambda_1 N_1(t) - \lambda_2 N_2(t) \ldots\ldots (2)$$

and $$dN_3(t) = +\lambda_2 N_2(t)dt \quad \text{or} \quad \frac{dN_3(t)}{dt} = +\lambda_2 N_2(t) \ldots\ldots\ldots\ldots\ldots\ldots\ldots\ldots\ldots\ldots (3)$$

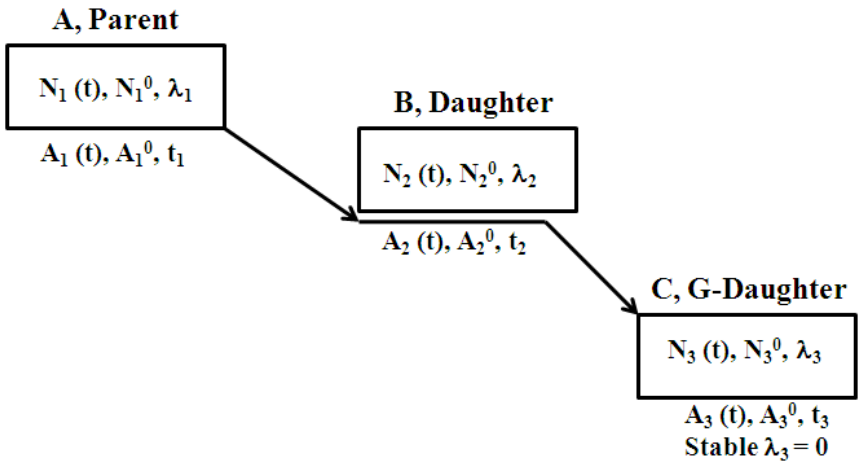

Fig. 1.1: The decay scheme of a parent-daughter pair in a radionuclide generator

Equation 1 describes the rate of change of number of atoms of type A, supposing that the only source of these atoms is from the initial supply N_1^0 at $t = 0$. Equation 2 describes the rate

of change of the number of atoms of type B which is equal to the supply by the decay of atoms A corrected for the loss through its own decay. Equation 3 describes the rate of change of the number of atoms of type C fed by only the decay of atoms B (being stable, C is continuously accumulated). The solution of equation 1 leads to the well known decay equation of a single radionuclide i.e.:

$$N_1(t) = N_1^0 e^{-\lambda_1 t} \text{ and } A_1(t) = \lambda_1 N_1^0 e^{-\lambda_1 t} = A_1^0 \, e^{-\lambda_1 t} \quad \ldots\ldots\ldots\ldots (4)$$

The solution of equation 2 leads to the following expression (assuming $N_2(0) = N_2^0 = 0$):

$$N_2(t) = N_1^0 \frac{\lambda_1}{\lambda_2 - \lambda_1}\left(e^{-\lambda_1 t} - e^{-\lambda_2 t} \right) \quad \ldots\ldots\ldots\ldots\ldots\ldots\ldots\ldots\ldots (5)$$

Here, the activity $A_2(t)$ is given by the general definition of the activity. Therefore,

$$A_2(t) = \lambda_2 N_2(t) = N_1^0 \frac{\lambda_1 \lambda_2}{\lambda_2 - \lambda_1}\left(e^{-\lambda_1 t} - e^{-\lambda_2 t} \right) \ldots\ldots\ldots\ldots\ldots\ldots\ldots\ldots (6)$$

$$\text{or } A_2(t) = A_1^0 \frac{\lambda_2}{\lambda_2 - \lambda_1}\left(e^{-\lambda_1 t} - e^{-\lambda_2 t} \right) \quad \ldots\ldots\ldots\ldots\ldots\ldots (7)$$

where, $A_1^0 = \lambda_1 N_1^0$.

1.6.1 Time taken by the daughter radioisotope to attain maximum radioactivity

The radioactivity of the daughter isotope reaches maxima when the feeding of the daughter atoms (B) exactly compensates their decay:

$$\text{i.e. when } A_1(t) = A_2(t) \quad \text{or} \quad \lambda_1 N_1(t) = \lambda_2 N_2(t)$$
$$\text{or when } \frac{dA_2(t)}{dt} = \frac{dN_2(t)}{dt} = 0 \qquad \ldots\ldots\ldots\ldots\ldots\ldots\ldots\ldots (8)$$

Then one can write:

$$t_{max} = \frac{\ln(\lambda_2 / \lambda_1)}{\lambda_2 - \lambda_1} = \left(\frac{1.44 t_1 t_2}{t_1 - t_2} \right) \ln\left(\frac{t_1}{t_2} \right) \ldots\ldots\ldots\ldots\ldots\ldots\ldots\ldots\ldots\ldots (9)$$

where, t_1 and t_2 are the half-lives of the parent and daughter radionuclides, respectively and t_{max} is the time taken by the daughter radioisotope to attain maximum radioactivity.

1.7 Radioactive Equilibrium

When the 'daughter' radionuclide decays at the same rate at which it is being produced, it is said to have reached the state of 'radioactive equilibrium'. Radionuclide generators can be categorized on the basis of the ratio of the half-life of the parent to that of the daughter radionuclide and two principal situations are considered: (1) If the ratio of λ_1:λ_2 is ~0.1, the parent-daughter system is said to exist in a state of transient equilibrium (2) If λ_1 is very much smaller than λ_2 (and t_1 is much greater than t_2) the system is said to exist in secular equilibrium [39]. Both the cases are discussed briefly, with suitable examples.

Case 1: Transient equilibrium

In this case, $\lambda_1<\lambda_2$ or $t_1>t_2$ with t_1/t_2 ~10. The most suitable example for this case is the ^{99}Mo/^{99m}Tc radionuclide pair.

$$^{99}_{42}Mo \xrightarrow{\beta^-(t_1 = 65.94h)} {}^{99m}_{43}Tc \xrightarrow{\gamma(t_2 = 6.01h)} {}^{99}_{43}Tc \text{ (ground state)}$$

In this case, the transient equilibrium is reached at:

$$t_{\max} = \left(\frac{1.44 t_1 t_2}{t_1 - t_2}\right) \ln \frac{t_1}{t_2} = 22.79 \text{ hours}$$

After this period of time, the daughter activity (^{99m}Tc) comes in equilibrium with the parent activity (^{99}Mo) and then it follows the same half-life as that of its parent. This is illustrated in **Fig. 1.2**. Few other radionuclide pairs which exist in a state of transient equilibrium are ^{81}Rb/^{81m}Kr, ^{82}Sr/^{82m}Rb, ^{87}Y/^{87m}Sr, ^{113}Sn/^{113m}In and ^{191}Os/^{191m}Ir.

Case 2: Secular equilibrium

In this case, λ_1 is far less than λ_2 or t_1 is much greater than t_2. Some well known examples of this case are ^{90}Sr/^{90}Y, ^{137}Cs/^{137m}Ba parent-daughter systems.

$$^{137}_{55}Cs \xrightarrow{\beta(t_1 = 30.07\,y)} {}^{137m}_{56}Ba \xrightarrow{\beta(t_2 = 2.55m)} {}^{137}_{56}Ba$$

$$\text{or } {}^{90}_{38}Sr \xrightarrow{\beta(t_1 = 28.8\,y)} {}^{90}_{39}Y \xrightarrow{\beta(t_2 = 2.55m)} {}^{90}_{40}Zr$$

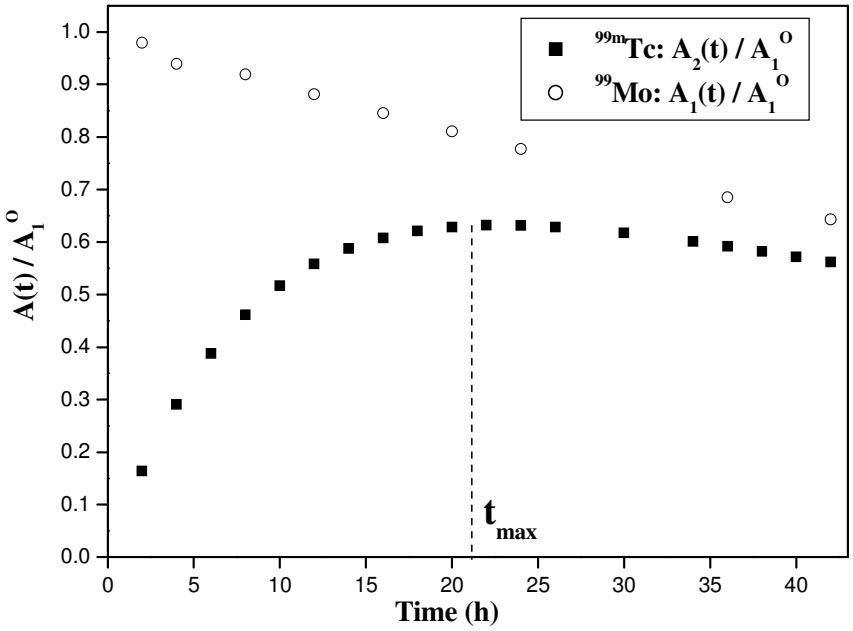

Fig. 1.2: Activity profile of the ^{99}Mo/^{99m}Tc transient equilibrium system

For practical purposes, these situations could be considered to correspond to $\lambda_1 \to 0$ or $t_1 \to \infty$. Thus $A_1(t) \approx \lambda_1 N_1^0 = A_1^0$ and $N_1(t) = N_1^0$ due to the fact that $e^{-\lambda_1 t} \approx (1-\lambda_1 t) \approx 1$. Consequently, with respect to the decay of the daughter activity, the radioactivity of the parent appears to be constant. The equation for the radioactivity of the daughter radioisotope becomes:

$$A_2(t) = A_1^0 \frac{\lambda_2}{\lambda_2 - \lambda_1}\left(e^{-\lambda_1 t} - e^{-\lambda_2 t}\right) \approx A_1^0\left(1 - e^{-\lambda_2 t}\right) \quad \text{..... (10)}$$

Under this condition, the total radioactivity of the parent and daughter reaches the maximum and does not decrease appreciably for several half-lives of the daughter product. The activity profile of the ^{137}Cs/^{137m}Ba system is illustrated in **Fig. 1.3**.

1.8. Separation of the daughter product from the parent in a radionuclide generator

A radionuclide generator generally consists of a closed system housing parent and daughter radionuclides in a state of radioactive equilibrium and the daughter activity can be

separated from the parent by exploiting their differences in their chemical properties, using suitable separation techniques.

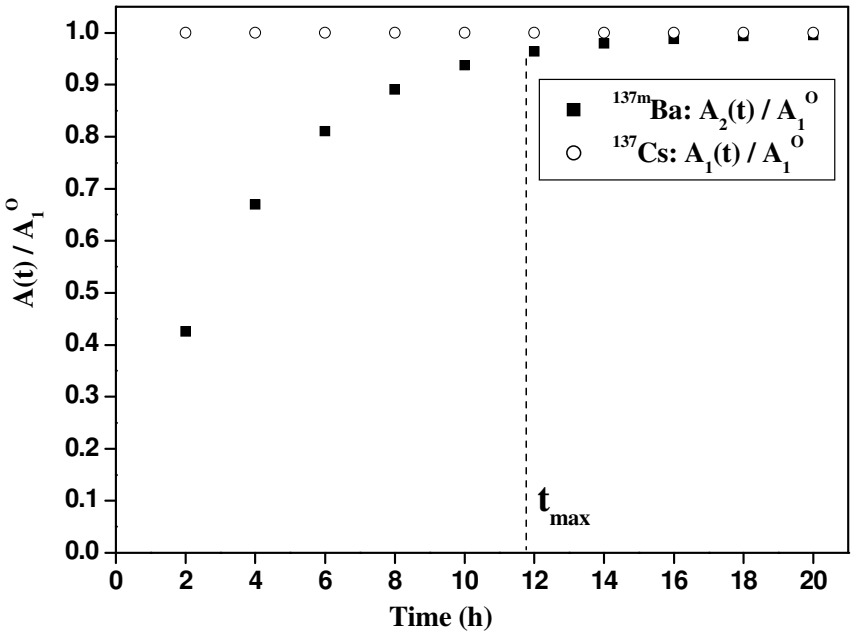

Fig. 1.3: Activity profile of the ^{137}Cs/^{137m}Ba secular equilibrium system

The activity of the daughter radionuclide grows as a result of the decay of the parent until either a transient or secular equilibrium is reached within several half-lives of the daughter (as determined by t_{max}, defined in section 1.6.1), after which the daughter appears to decay with the same half-life as that of the parent. At this stage, the daughter activity is separated from the parent. After separation, the parent regenerates a fresh supply of the daughter. Theoretically, the elution of the daughter activity from the generator can be made repeatedly. **Fig. 1.4** illustrates the multiple growth and elution of the daughter activity. Radionuclide generators are historically called 'cows' since the daughter activity is 'milked' (i.e. separated) from its parent (precursor) and the parent then generates a fresh supply of the daughter.

1.9 The available options for the preparation of radionuclide generators

The separation of the parent-daughter pairs belonging to the adjacent group of elements is one of the most challenging aspects of research in the field of radionuclide generators. Sometimes separation is complicated by the multiple oxidation states of the pair and its tendency to form a variety of complexes [26]. Moreover, the requirement of the daughter radionuclide in a form suitable for clinical applications, further places stringent requirements on the separation chemistry. This requires selection of the suitable separation procedure, providing high yield of the daughter radionuclide in minimum volumes (high radioactive concentration) and highest purity.

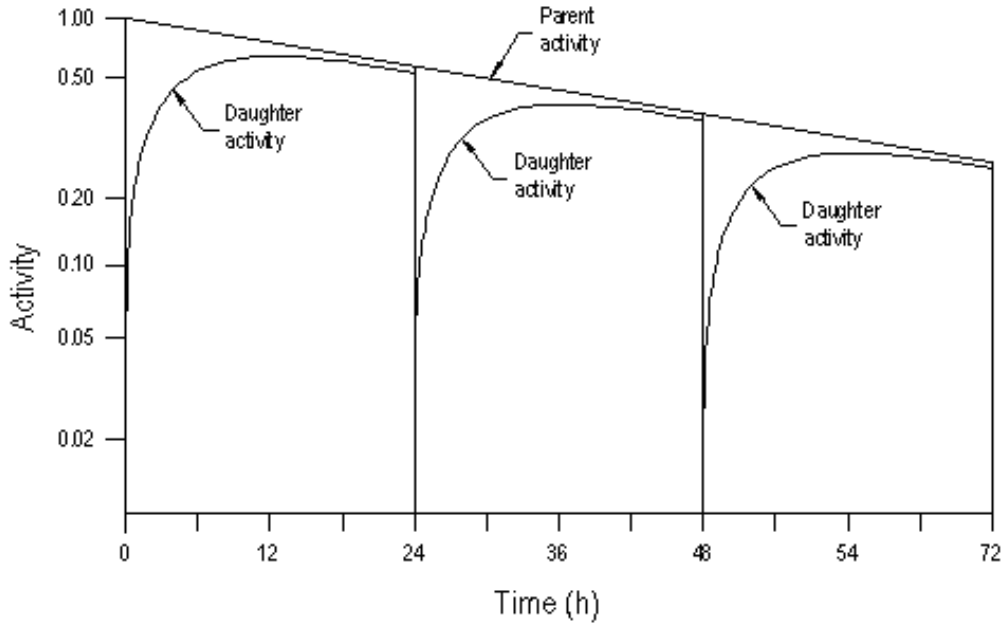

Fig. 1.4: Multiple growth and elution of daughter activity in a radionuclide generator

Preferably, the daughter activity should be obtained in a form that is amenable for direct use in the preparation of radiopharmaceuticals. In the case of metallic radionuclides, uncomplexed form is the most desirable. Additionally, the radionuclide generators for biomedical applications must be simple in design, efficient and easy to operate. Various techniques, such as column chromatography, solvent extraction and sublimation have been reported for the preparation of radionuclide generators [40-43]. Conversion of the parent

radionuclide into an insoluble 'gel' and its use as the column matrix from which the daughter radionuclide can be eluted is yet another strategy that has been reported [25,44]. Out of these, column chromatography and solvent extraction are the most commonly used methods for the preparation of radionuclide generators for biomedical applications. The choice of a particular technique is usually made for technical, economic and logistic reasons, with emphasis on one or other of these factors depending on the circumstances. The relative advantages and disadvantages of each of these techniques are discussed below.

1.9.1 Column chromatography: This is the most commonly used method for the preparation of radionuclide generators, primarily due to its simplicity of operation. This method relies upon the chromatographic separation of the daughter radioisotope from the parent, by the virtue of their difference in their retention affinity in the column [45,46]. Generally, the column matrix has very high retention affinity for the parent radionuclide while the affinity for the daughter radionuclide is substantially low. The long-lived parent is adsorbed on a solid support and the daughter activity is selectively and periodically eluted using suitable eluents. Both inorganic and organic sorbents have been evaluated as chromatographic supports for radionuclide generators [45]. However, the radiation damage to the organic matrix deteriorates the performance of the generator with respect to the elution yield and parent breakthrough, on prolonged use. Moreover, the radiolytic fragments of the organic matrix may come along with the daughter activity in the eluate as undesirable chemical impurities. The limited resistance of these organic resins to radiation also limits the radioactivity of the parent that can be loaded onto the generator column. The inorganic sorbents, on the other hand, possess appreciably high radiation resistance and good ion-exchange properties which make them suitable for the preparation of radionuclide generators. Typically, hydrated metal oxides (such as Al_2O_3, ZrO_2, SnO_2, TiO_2 etc.) are used as inorganic sorbents for the preparation of radionuclide generators [45]. A cause of concern with such

sorbents is the solubility of metal oxides in aqueous solutions. In certain cases, the solubility of metal oxide increases with successive elutions over a prolonged period of time [45,19]. This in turn adds chemical impurities in the daughter product, rendering it unsuitable for the preparation of radiopharmaceuticals [19].

Another major limitation of the chromatographic approach is the limited sorption capacity of the column matrices. The required volume of the eluent for the quantitative elution of the daughter radioisotope from a chromatographic generator depends on the size of the column which in turn is inversely proportional to the specific activity of the parent radioisotope [40]. Consequently, high specific activity parents are required in order to reduce the size of the column. If the specific activity of the parent radioisotope is low, the daughter activity can only be availed with low-radioactive concentration from such systems, thereby requiring post-elution concentration of the daughter activity prior to the preparation of radiopharmaceuticals [25]. The requirement for the multiple-step post-elution concentration procedure results in a fairly complex system, introduction of chemical impurities in the daughter eluate and overall low reliability. Sometimes, the column chromatographic generators exhibit degrading performance on repeated elution, over a prolonged period of time [19]. For certain cases, it is reported that the yield of the daughter activity decreases and the breakthrough of the parent increases with time [19]. This in turn reduces the shelf-life of the generator and makes it cost-ineffective.

1.9.2 Solvent Extraction: Solvent extraction is another approach which has been widely exploited for the preparation of radionuclide generators [40-43,47,48]. This method is based on the relative solubility of the parent and the daughter radioelements in two immiscible liquids, usually water and an organic solvent [49]. The solvent extraction generators have some economic and technical advantages. Unlike in column chromatographic approach, here, low specific activity parent can be used for the preparation of radionuclide generators and the

daughter activity is obtained with high radioactive concentration with low levels of radionuclidic impurities. However, solvent extraction involves a cumbersome multi-step separation process using complicated apparatus. Therefore, it requires highly trained personnel for successful operation. The handling of large volumes of organic extractant may pose possible fire hazard due to the volatile organic vapors. Moreover, the organic solvent may undergo radiolysis and introduce organic residues in the daughter product, which may interfere in the subsequent radiolabeling reactions and bring undesirable changes in the biological properties of the radiopharmaceutical. The detrimental effect of radiolysis may also lower the extraction efficiency of the organic solvent.

1.9.3 Sublimation: This approach has a very limited scope as it can be used for the separation of daughter radionuclide from the parent, only if there is a sufficient difference between their volatilities at an elevated temperature. Till date, this approach has been restricted only to the $^{99}Mo/^{99m}Tc$ generator system. The fundamental work in the sublimation of ^{99m}Tc from ^{99}Mo was carried out at the Australian Atomic Energy Commission, to provide a source of medically acceptable ^{99m}Tc [40-43,50]. For this, irradiated molybdenum trioxide was heated at 850 ºC in a stream of oxygen, in a specially designed apparatus. Under these conditions, the oxide of technetium (Tc_2O_7) sublimed, thus separating from the molten molybdenum oxide. The major advantage of this approach is that low specific activity parent (^{99}Mo) can be used for the preparation of the generator [40]. Moreover, irradiated target (MoO_3) can directly be used without any chemical processing and the daughter radionuclide (^{99m}Tc) can be obtained with very high radioactive concentration and radionuclidic purity [40]. However, there are numerous disadvantages of this approach. Firstly, the separation process is very complicated and a gadget suitable for use in small Nuclear Medicine laboratory has not been developed. Secondly, the separation efficiency was poor (~25-40%) and it reduced further after first separation. Thirdly, there are chances of leakage of radioactivity in gaseous form

and therefore the entire process requires dedicated facility and very skilled working personnel. Therefore, despite its ability to produce ^{99m}Tc of very high quality, this process has very limited acceptability.

1.9.4 'Gel-based' system: Here, the parent radionuclide is used as the column matrix by converting it into a suitable insoluble compound. The use of the term 'gel' is owing to the initial work with ^{99}Mo, wherein the matrix resembled gels, while strictly these matrices may not be 'gels'. However, since the term has come to stay in the world of radionuclide generators, it is continued. The 'gel' based system is an useful alternative to the chromatographic generator wherein low specific activity parent can be used [44]. It retains the simplicity of the chromatographic systems and can be conveniently operated in a hospital radiopharmacy. This approach has been exploited for the preparation of ^{99}Mo/^{99m}Tc and ^{188}W/^{188}Re generators [44,51-53]. For this, the neutron irradiated ^{99}Mo as molybdate or ^{188}W as tungstate can be incorporated into insoluble precipitates of zirconium or titanium [44,51-54]. The content of Mo or W inside the gel matrix is ~25-30% and it is possible to use medium specific activity ^{99}Mo or ^{188}W for preparation of the gel [54]. Though the 'gel generator' is simple to operate, the preparation of the gel itself is quite complicated and pose several challenges. The properties of these generators depend essentially upon their preparation conditions [44,51-55]. Consequently, the factors such as the pH of ^{99}Mo-molybdate or ^{188}W-tungstate, the molar ratios of X:Mo or X:W (X = Zr, Ti etc.), the concentrations of the reagents, the order of reactive addition, the drying temperature of the final product etc. influence the elution of ^{99m}Tc or ^{188}Re from the gel. Thus it is important to have strict "Standard Operating Procedures" (SOP) for preparation of these gel generators. Even if the 'gel generator' is prepared under the most optimum conditions, the specific concentration of ^{99m}Tc or ^{188}Re may be too low for clinical use [25].

1.10 Quality control of the generator produced radioisotopes

Since generator produced radioisotopes are intended for clinical applications, it is imperative that the radionuclide generators undergo strict quality control procedures before being handed over to the Nuclear Medicine physicians for patient applications. Quality control involves specific tests and measurements that ensure the elution efficiency of the generator, product identity, purity and radioactive concentration of the daughter radionuclide, biological safety and the efficacy of the radionuclide for the preparation of radiopharmaceuticals. These methods are briefly described below.

a) Elution efficiency of the radionuclide generator: The elution efficiency of the radionuclide generator is defined as the proportion of the daughter radioisotope present in the generator system that is separated during the elution process. Theoretically, the activity (A_2) of the daughter radioisotope present in the generator system at the time of elution is given by the equation (7). In practice, the activity of the daughter radioisotope eluted is less than that predicted by the theory. If the measured activity of the separated daughter radioisotope after allowing time 't' for its growth, is denoted by A_s, then the elution efficiency can be defined by the equation:

$$\%\,Elution\ efficiency = \frac{A_s}{A_2} \times 100 \quad \text{..... (11)}$$

For a radionuclide generator to be cost-effective, it is essential that its elution efficiency should be fairly high (>80%) and it should remain constant during the stipulated period of utilization (or the useful shelf life) of the generator.

b) Radionuclidic purity of the separated daughter radioisotope: Radionuclidic purity is defined as the fraction of the total radioactivity in the form of the desired radionuclide [56]. In the separated daughter radioisotope obtained from the radionuclide generator, the primary radionuclidic impurity that may be expected is the long-lived parent radioisotope. Sometimes, the parent radioisotope may be associated with other radionuclidic impurities which may also

come in the separated daughter activity. Understandably, radionuclidic impurities are undesirable in the daughter product, as these can have various implications for its use in Nuclear Medicine, such as interference in the reaction for preparation of the radiopharmaceutical leading to poor yields or unwanted compounds, increase in the unwanted radiation exposure to the patient, obscure scintigraphic images, and possible radio-toxicity. Hence the radionuclidic purity of the intended radionuclide needs to be determined and the impurities ascertained to be well within the stipulated limits [56]. Determination of radionuclidic impurities in the separated daughter radioisotope is mostly done by γ-ray spectrometry using HPGe detector coupled with a multi-channel analyzer [56]. This technique can be used for both qualitative as well as quantitative estimation of radionuclidic impurities in the daughter product obtained from the radionuclide generator. However, in case of generator systems where both parent and daughter radioisotopes are pure β^- emitters (as in the case of $^{90}Sr/^{90}Y$ generator) and no γ-emissions are available to permit γ-spectrometric analysis, β^- counting has to be done after a quality control test wherein the parent radionuclidic impurity is unambiguously separated from the daughter product [57-59]. In such cases, the radionuclidic purity may also be checked and determined by β-spectrometry using a liquid scintillation counter [59].

c) Radiochemical purity of the separated daughter radioisotope: The radiochemical purity of a generator produced radionuclide may be defined as the fraction of the total radioactivity present in the desired chemical form [56]. Radiochemical impurities may arise in the daughter radionuclide during its separation from the parent or its subsequent storage due to several factors such as the action of the solvent and the effect of radiolysis, change in temperature or pH, presence of oxidizing or reducing agents. The radiochemical impurities present in the daughter radionuclide may not be suitable for labeling with ligands and biomolecules. This may also affect the biological behavior of the radiopharmaceutical as the

agent may not be selectively taken up by the target organ [56]. The presence of radiochemical impurities in generator produced radioisotopes can be detected and determined by various analytical methods. These include, paper chromatography, thin layer chromatography, paper electrophoresis, high performance liquid chromatography, gel filtration, gel chromatography, ion exchange chromatography, solvent extraction, inverse dilution and precipitation [56]. In this thesis, paper chromatography and thin layer chromatography techniques have been used for determining the radiochemical purity of the generator derived radioisotopes.

d) Chemical purity: Any unwanted chemical species (organic or inorganic) present in the daughter product is considered as chemical impurity. The presence of these chemical impurities may affect the chemistry of the radionuclide for the preparation of radiopharmaceuticals. The chemical impurities may be introduced in the daughter radionuclide by a variety of ways. This includes the use of impure chemicals and use of radioactive parent solutions containing undesired chemicals introduced during its radiochemical processing. Also, in case of column chromatographic and solvent extraction based generators, the radiolytic or chemical degradation of the column matrix or the solvent may lead to the addition of chemical impurities to the daughter radionuclide. The presence of these chemical impurities can be avoided by the use of highly pure chemicals and adoption of appropriate separation methodology. The level of these chemical impurities may be detected and determined by various analytical techniques like colorimetry, spot-tests, spectrophotometry, inductively coupled plasma atomic emission spectroscopy (ICP-AES) etc. [56]. Of these techniques, ICP-AES has been utilized in this thesis for the determination of the chemical purity of the generator produced radionuclides. If required, the chemical impurities present in the radionuclide may be removed by applying simple separation techniques, such as, precipitation, solvent extraction, ion-exchange and distillation [56].

e) Labeling efficacy: Generally, generator produced radionuclides are used for clinical application, only after radiolabeling a suitable ligand or a biomolecule with it. The suitability of a generator produced radionuclide for radiopharmaceutical applications can be demonstrated by its efficacy to prepare standard radiolabeled agents. This is also an indirect test of the chemical purity of the radionuclide as high chemical purity is required for the preparation of the radiolabeled agent with the no-carrier-added radionuclide.

f) Biological tests: Biological quality control tests are carried out to examine the sterility and apyrogenicity of the generator-produced radionuclide before the preparation of radiopharmaceuticals. Sterility indicates the absence of any viable bacteria or microorganism in a radiochemical. It is essential to avail the daughter radionuclide from the generator in sterile form in order to prepare clinical grade radiopharmaceuticals. Administration of non-sterile radiopharmaceutical can cause a wide variety of infections leading to several physiological problems including death [56]. Steam or high temperature sterilization and sterilization by filtration through microfilters are the commonly used procedures for sterilizing the radiochemicals. Generally, in order to obtain the generator produced radionuclide in a sterile form it is filtered through commercially available Millipore filters [56], which are membrane filters made of cellulose esters, available in various pore sizes and disposable units.

Pyrogens are either polysaccharides or proteins produced by metabolism of microorganisms and if present in a radiopharmaceutical can cause a wide variety of physiological problems, such as, fever, chills, malaise, leucopenia, flushing, sweating, headache and pain in joints [56]. It is mandatory that all products intended for injection into the humans, including radiopharmaceuticals should have pyrogens below the stipulated limits. Pyrogen free radionuclides can be obtained from the generator without much difficulty

using high quality chemicals and taking particular care during the preparation and storage of the generator.

Numerous methods are reported for testing the sterility and apyrogenicity of a radiochemical [56]. However, since all these methods are time consuming, the sterility and apyrogenicity tests for short-lived generator produced radionuclides are done post-facto. However, in order to reach this level of confidence on the product, several batches have to be produced, tested and repeatedly shown to be complying with the quality requirements, before actual use in humans. The daughter radionuclide obtained from the generator is used for radiopharmaceutical preparation, provided the manufacturer has already established its sterility and apyrogenicity before the generator is commercialized.

1.11 Shelf-life of a radionuclide generator

The shelf-life of a radionuclide generator is the period for which the generator can safely be used for the designated clinical applications. The shelf-life of a typical radionuclide generator is influenced by the physical half-life of the parent radioisotope as well as the generator performance which are gauged by measuring the elution yield, radioactive concentration and the purity of the daughter radioisotope. The parent radioisotopes having longer physical half-lives are generally expected to have longer shelf-life. However, the shelf-life of a radionuclide generator is also influenced by the procedure adopted for the separation of the parent-daughter pairs. The suitability of a separation procedure to withstand the effects of radiolysis and chemical degradation over a prolonged period of time enhances the shelf-life of the generator. Overall, the economics of production of short-lived radioisotopes via a radionuclide generator is decided by the shelf-life of the generator which in turn determines the cost of treatment using radiopharmaceuticals based on generator produced radionuclides.

1.12 Motivation for the work carried out in this thesis

Radionuclide generators play an important role in providing short-lived radioisotopes in a no-carrier-added form, for use in Nuclear Medicine. To a great extent, progress in the development of new radionuclide generator systems and medical applications of generator-produced radioisotopes, is dependent on improvements in separation technology. As discussed earlier (Section 1.9), the currently available options for the preparation of radionuclide generators have several limitations which have an impact on their widespread acceptability and adaptability in a clinical scenario. In view of these limitations, development of alternate viable processes for the preparation of radionuclide generators for biomedical applications still remains an interesting challenge.

In this thesis, development of radionuclide generators based on two novel approaches has been described. The first approach involves the use of electrochemical separation technique and the second involves the use of nanomaterials based sorbents for the preparation of radionuclide generators. Electrochemical method provides a simple and convenient approach of performing a wide variety of metal ion separations. A mixture of metal ions having adequate difference in their formal potential values in an electrolytic medium can be mutually separated by selective electrodeposition of one metal on an electrode surface under the influence of controlled applied potential [60]. In-situ electrochemical deposition of a daughter radionuclide is an attractive route to develop radionuclide generators. The major advantage of this approach is that the daughter radioisotope can be obtained with very high radionuclidic purity and radioactive concentration, irrespective of the specific activity of the parent radioisotope. The second approach based on the use of nanomaterials based sorbents for the preparation of generators relies on the unique morphological features, pore structure, high surface areas and high surface charge of nanomaterials. Such sorbents demonstrate much higher sorption capacity and selectivity for the sorption of the parent radioisotope

compared to their bulk counterparts. The daughter activity can be availed with appreciably high radioactive concentration and purity suitable for biomedical applications.

1.13 Scope of the present thesis

The work carried out in this thesis pertains to the development of some of the most important radionuclide generators for biomedical applications, adopting the novel approaches described above. Radionuclide generators have been developed for both diagnostic applications (^{99}Mo/^{99m}Tc and ^{68}Ge/^{68}Ga generators) as well as therapeutic applications (^{90}Sr/^{90}Y and ^{188}W/^{188}Re generators). The development of each of these radionuclide generators is described as separate chapters in this thesis (Chapters 3-6). The synthesis and structural characterization of four nanomaterial based sorbents, namely, polymer embedded nanocrystalline titania (TiP), mixed phase nano-zirconia (nano-ZrO_2), tetragonal nano-zirconia (t-ZrO_2) and nano-ceria-polyacrylonitrile composite (CeO_2-PAN) which are of common relevance for the preparation of ^{99}Mo/^{99m}Tc, ^{68}Ge/^{68}Ga and ^{188}W/^{188}Re generators has been described in Chapter 2.

CHAPTER 2

SYNTHESIS AND STRUCTURAL CHARACTERIZATION OF NANOMATERIAL BASED SORBENTS

"All truths are easy to understand once they are discovered; the point is to discover them."

GALILEO GALILEI

2.1 Introduction

2.1.1 Nano – The Beginning

In the recent times, nanoparticles, or objects of size in the range of nanometer (1-100 nm) have become one of the most exciting objects of investigation and have played important roles in the forefront areas of Physics, Chemistry, Engineering, Biology and Medical Science [61,62]. Such materials show great promise in providing many breakthroughs in the near future that may change the direction of technological advances in a wide range of applications [61]. Nanoscience or the science of nanoparticles refers to the control and manipulation of matter at nanometer dimension, which includes synthesis, characterization, exploration, and application of nanostructured and nanosized materials. While the word 'nanoscience' is relatively new, the applications of nanomaterials can be historically traced back to even before the generation of modern science and technology. Nature makes nanometer sized objects of varying kind. Several structures of nanometer dimensions have probably existed on earth ever since the inception of life on it [61]. The abalone, a mollusk, constructs very strong shells having iridescent inner surfaces by utilizing calcium carbonate as strong 'nanostructured bricks' held together by 'glue' made of carbohydrate-protein mix. Cracks initiated on the outside are unable to move through the shell because of the nanostructured bricks. The shells represent a natural demonstration that a structure fabricated from nanoparticles can be much stronger than that made with bulk materials. Another example is that of the bacteria, 'Magnetosperillum magnetotacticum', which makes nanometer sized magnetite (Fe_3O_4) particles of specific morphology [61]. The magnetism caused by such particles helps the bacteria in finding a direction favorable for its growth. There are several other bacteria like the familiar 'Lactobacillus' which can take up metal ions added into butter milk, and reduce them inside the cell and make nanoparticles [61].

It is not clear when humans first began to take advantage of the nanosized materials. It is known that in the 4th century A.D., Roman glassmakers were fabricating glasses containing nanosized metals [61]. In the ancient Indian medical system called Ayurveda, nanosized gold particles were used in several medicinal preparations [61]. Over 5000 years ago, the Egyptians also used nanosized gold particles in dentistry [61]. Photography, now an advanced and mature technology was developed in the eighteenth and nineteenth centuries based on production of silver nanoparticles sensitive to light. However, the science of nanometer scale objects was not discussed until much later. In 1959, the Nobel Prize winning physicist, Richard Feynman presented a visionary and prophetic lecture at a meeting of the American Physical Society, entitled "There is plenty of room at the bottom", where he speculated on the possibility and potential of nanosized materials [61,63]. But, it was not until the 1990s with the emergence of appropriate methods of fabrication of nanostructures that a notable increase in research activity occurred, and a number of significant developments resulted. This period was also marked by the phenomenal success in developing important tools for viewing, characterizing and for atomic manipulation of the nanostructures. Several sophisticated instruments for characterization and manipulation such as scanning electron microscopy, transmission electron microscopy and scanning probe microscopy became available for researchers to explore the nanoworld.

Owing to their unique properties, nanomaterials are now used in various diverse fields like nanophotonics, lasers, nanoelectronics, solar cells, resonators, high sensitivity sensors, catalysis, functional coatings, energy storage, drug delivery and biomedicines [61,62,64]. Today, nanomaterials are revolutionizing social and economic development by offering innovative and viable solutions to some of the most pressing problems of the world community. However, these are only a limited part of the fast developing applications of nanomaterials and numerous other applications of these materials are yet to be unfolded.

2.1.2 Nanomaterials as sorbents for radionuclide generators

Nanomaterials are expected to provide unprecedented opportunities in developing a new class of sorbents for chromatographic applications due to their unique surface and morphological features. While the structural features of such materials are in between of those of atoms and the bulk materials, the properties of materials with nanometer dimensions are significantly different from those of atoms and bulks materials. Due to their small dimensions, nanomaterials have extremely large surface area to volume ratio, which makes a large fraction of atoms of the materials to be the surface or interfacial atoms, resulting in more 'surface-dependent' material properties. These surface atoms are unsaturated, exhibit intrinsic surface reactivity and have a tendency to chemisorb charged species in aqueous solution in order to achieve surface stabilization. Moreover, the small size of nanomaterials either renders them free of internal structural imperfections or impurities present cannot multiply sufficiently in them to cause mechanical failure [65,66]. The imperfections within the nano dimension are highly energetic and will migrate to the surface to relax themselves under annealing, thereby leaving pure and perfect material structures inside the nanomaterials. This phenomenon of increased materials perfection affects the properties of nanomaterials. For example, the chemical stability for certain nanomaterials may be enhanced and the mechanical properties of nanomaterials will be better than the corresponding bulk materials [65,66]. Further, it is reported that nanocrystalline materials are more radiation resistant than their bulk counterparts with larger grain sizes [67,68].

There are few reports available in the literature on the exploitation of nanomaterial based sorbents in the chromatographic separation of metal ions [69,70]. However, the potential of using such materials as column matrices in radionuclide generators for biomedical applications is yet to be explored. Owing to their high surface area and intrinsic surface reactivity, nanomaterial based sorbents have much higher sorption capacity and

selectivity compared to the conventional sorbents. Consequently, parent radioisotopes obtained from medium flux reactors with low specific activity can also be used for the preparation of radionuclide generators and the daughter activity can be availed with appreciably high radioactive concentration and purity. The enhanced mechanical and chemical stability of such sorbents ensure that the column matrix does not dissolve even after multiple elutions and prolonged use of the generator, thereby preventing the addition of chemical impurities in the eluate. Further, owing to the high radiation stability, nanomaterials can withstand the radiation environment and demonstrate consistently good performance over a prolonged period of time.

2.1.3 Synthesis of nanomaterials

The synthesis of nanoparticles forms an essential component of nanoscience and requires strict control over size, shape and crystalline nature, in order to utilize them for the desired applications [62]. Several methods of synthesis of nanoparticles have been reported in the literature, which include high energy milling, sputtering, laser ablation, utilization of plasma generated by radiofrequency heating coils, thermolysis, combustion, chemical-vapor deposition, electrodeposition, sol-gel and chemical solution methods [62,71,72]. Of these, the chemical solution method is probably the most useful method of synthesis of nanomaterial based sorbents for radionuclide generators. This is primarily due to the suitability of this method to be scaled up for the routine synthesis of large quantities of nanomaterials using inexpensive and less complicated apparatus [62]. Moreover, chemical methods have proved to be much more effective than other methods, as they provide better size-control, homogeneity and enable different shapes and functionalization [62,71].

Chemical synthesis of nanomaterials has been reviewed by many authors [65,71-74], and innumerable improvements and better methods are being reported continually. In accomplishing the synthesis and manipulation of nanomaterials using this approach, a variety

of reagents and strategies have been employed, besides, a wide spectrum of reaction conditions. It must be mentioned here that there is no general strategy to make nanoparticles with narrow size distribution, tailored properties, and desired morphologies, which could be universally applied to different materials. It is believed that the formation of nanoparticle using chemical method follows the classic LaMer mechanism, which suggests a short burst of nucleation followed by slow diffusive growth, favoring formation of monodisperse crystalline nanoparticles [75]. In this thesis, chemical solution method has been used for the syntheses of various nanomaterial based sorbents for use in radionuclide generators.

2.1.4 Characterization of nanomaterials and understanding their properties

The characterization of nanomaterials is generally done with a probe which may consist of photons, electrons, neutrons, atoms, ions or even atomically sharp pins [61,62,65]. For nanomaterials, the probing light or particle often has varying frequencies, ranging from gamma to infrared rays or beyond in the case of photons or hyperthermal (<100 keV) to relativistic energies in case of particles. The resulting information can be processed to yield images or spectra which reveal the topographic, geometric, structural, chemical or physical details of the material. Several techniques are available under the broad umbrella of characterization of materials [61,62,65] and a systematic application of one or more techniques leads to a complete understanding of the nanomaterial. In this thesis, techniques like Brunauer-Emmett-Teller (BET) surface area analysis, Fourier Transform Infrared Spectroscopy (FTIR), powder X-Ray Diffraction (XRD), Transmission Electron Microscopy (TEM) and zeta-potential analysis were used for the characterization of the materials and understanding their properties. The chemical stability of the nanomaterial based sorbents in different medium was determined using Inductively Coupled Plasma Atomic Emission Spectroscopy (ICP-AES). These techniques are briefly described below.

2.1.4.1 BET Surface Area Analysis

Gas sorption (both adsorption and desorption) on the clean surface of dry solid powders is the most popular method for determining the surface area and pore size distribution of nanomaterials [76]. In a gas sorption experiment, the material is heated and degassed by vacuum force or inert gas purging to remove adsorbed foreign molecules. Controlled doses of an inert gas, such as nitrogen, krypton, or argon, are introduced and the gas is adsorbed, and later, withdrawn and desorbed. This cycle of adsorption and desorption is carried out several times. The sample material is placed in a vacuum chamber at a constant and very low temperature, usually at the temperature of liquid nitrogen (77.4 K), and subjected to a wide range of pressures, to generate adsorption and desorption isotherms. The amounts of gas molecules adsorbed or desorbed are determined by the pressure variations due to the adsorption or desorption of the gas molecules by the material (the adsorbent). Various amounts of gas molecules will be adsorbed or desorbed at different doses of the gas (the adsorbate). Knowing the area occupied by one adsorbate molecule, (for example, 16.2 $Å^2$ for nitrogen), and using an adsorption model, the total surface area of the material can be determined. The specific surface area that can be determined by gas sorption ranges from 0.01 to over 2000 $m^2 g^{-1}$. Determination of pore size and pore size distribution of porous materials can also be made from the adsorption/desorption isotherm using an assessment model, suitable for the shape and structure of the pores [76]. The range of pore sizes that can be measured using gas sorption is from a few Angstroms up to about half a micron.

2.1.4.2 FTIR Spectroscopy

Molecules and crystals can be thought of as systems of balls (atoms or ions) connected by springs (chemical bonds) [77]. These systems can be set into vibration, and they vibrate with frequencies determined by the mass of the balls (atomic weight) and by the stiffness of the springs (bond strengths). The molecular and crystal vibrations are at very high

frequencies ranging from 10^{12} – 10^{14} Hz (3-300 μm wavelength), which are in the infrared (IR) region of the electromagnetic spectrum. The oscillations induced by certain vibrational frequencies provide a means for matter to couple with an impinging beam of infrared electromagnetic radiation and to exchange energy with it when the frequencies are in resonance. These absorption frequencies represent excitation of vibration of the chemical bonds and are thus specific to the type of bonds and group of atoms involved in the vibration. In the infrared spectroscopy, the intensity of a beam of infrared radiation is measured before and after it interacts with the sample as a function of light frequency. A plot of relative intensity versus frequency is the infrared spectrum. The term 'FTIR' refers to Fourier Transform Infrared Spectroscopy, when the intensity-time output of the interferometer is subjected to a Fourier Transformation to convert it into the familiar infrared spectrum (intensity versus frequency). The identities, surrounding environments and atomic arrangements, and concentration of chemical bonds that are present in the sample can be determined.

2.1.4.3 Powder X-Ray Diffraction

X-Ray Diffraction (XRD) is a very important technique that has long been used to address numerous issues related to the crystal structures of solids, including lattice constants and geometry, identification of unknown materials, orientation of single crystals, preferred orientation of polycrystals, defects, stresses etc. In XRD, a collimated beam of X-rays with a wavelength typically ranging from 0.7 to 2 Å, is incident on a specimen and is diffracted by the crystalline phases in the specimen according to Bragg's Law [78]:

$$n\lambda = 2d \sin \theta$$

where, n is the order of diffraction, d is the spacing between atomic planes in the crystalline phase and λ is the X-ray wavelength. The intensity of the diffracted X-rays is measured as a function of diffraction angle 2θ and the specimen's orientation. The diffraction pattern is used

to measure the specimen's crystalline phases and measure its structural properties. The most commonly used X-ray diffraction technique is the powder diffraction [78]. Powder XRD can be used to determine the average crystallite size of a nanocrystalline material [78]. If the average crystallite size in a powder is below a certain limit (~2000 Å diameter), additional broadening of diffracted X-ray beams occurs. From measurement of this extra broadening an average crystallite size can be obtained. However, a normal diffraction line might also have a finite width due to several reasons: the radiation is not absolutely monochromatic, the Kα line has finite breadth due to Heisenberg Uncertainty Principle and the focusing geometry of the instrument may not be perfect for a variety of reasons. In order to correct for the peak broadening which is caused by the diffractometer due to the aforementioned reasons, the peak broadening due a sample is always measured in comparison with that of a standard material. The crystallite size, D, might be estimated from the peak width using the Scherrer's formula:

$$D = \frac{0.9\lambda}{B\cos\theta}$$

where, λ is the X-ray wavelength and θ is the Bragg angle. B is the line broadening, indicating the extra peak width of the sample in comparison to the standard, derived using the Warren formula, $B^2 = B_M^2 - B_S^2$, where M and S refer to specimen and the standard. B_M and B_S are measured in radians at half the peak height (full width at half maxima, FWHM). The sample and standard must have peaks close to each other. With good experimental techniques, crystallite sizes up to 200 nm can be measured by using the Scherrer formula. In the range of 5-50 nm, the broadening is easy to determine. At larger particle sizes, the difference between the sample and standard is small and at small particle sizes, the peak is difficult to distinguish from the background. For smaller particles, low angle peaks are used for size determination as they are less broad as compared to the large angle peaks.

2.1.4.4 Transmission electron microscopy

Transmission Electron Microscopy (TEM) is a well known technique for imaging

solid materials at atomic resolution. Structural information can be acquired both by (high resolution) imaging as well as by electron diffraction [65]. Additional detectors allow for elemental and chemical analysis down to sub-nanometer scale. The greatest advantages that TEM offers are the high magnification ranging from 50 to 10^6 and its ability to provide both image and diffraction information from a single sample. TEM instruments with resolving powers in the vicinity of 1 Å are now common and have become one of the most essential tools for the characterization of nanomaterials. In TEM, the electrons from a source such as an electron gun (W or LaB_6) enter the sample, are scattered as they pass through it, are focused by the objective lens, are amplified by the magnifying projector lens, and finally produce the desired image. The transmitted electrons are used to create the image of a sample. Scattering occurs when an electron beam interacts with matter. Elastic scattering involves no energy loss and give rise to diffraction patterns. Inelastic interactions between primary electrons and the sample electrons at heterogeneities such as grain boundaries, dislocations, second phase particles, defects, density variations etc., can cause complex absorption and scattering effects, leading to a spatial variation in the intensity of the transmitted electrons. In TEM, one can switch between imaging the sample and viewing its diffraction pattern by changing the strength of the intermediate lens.

The higher the operating voltage of a TEM instrument, the greater is the lateral spatial resolution. High voltage TEM instruments (e.g. with 400 kV) have resolutions better than 0.2 nm. High voltage TEM instruments have additional advantage of greater electron penetration, because high energy electrons interact less strongly with matter than low energy electrons. So it is possible to work with thicker samples using a high voltage TEM. However, the chances of irradiation damages are more at higher acceleration voltages.

2.1.4.5 Zeta potential of nanomaterial based sorbents

The zeta potential (ζ) of a nanomaterial based sorbent is commonly used to describe

the charge developed on the surface of the nanoparticles when they interact with their surroundings and is a very useful tool in the interpretation of their sorption behavior. The development of positive or negative charge at the surface of the nanoparticle affects the distribution of ions in the surrounding interfacial region, resulting in an increased concentration of counter ions (ions of charge opposite to that of the particle) close to the surface. Thus an electrical double layer exists round each particle [79,80]. The liquid layer surrounding the particle exists as two parts; an inner region (Stern plane) where the ions are strongly bound and an outer (diffuse) region where they are less firmly associated. Within the diffuse layer there is a notional boundary inside which the ions and particles form a stable entity. When a particle moves (e.g. due to gravity), ions within the boundary also move with it. Those ions beyond the boundary stay with the bulk dispersant. The potential at this boundary (surface of hydrodynamic shear) is the zeta potential (ζ).The pH of the solution in which the nanomaterial is dispersed is one of the most important factors that affect its zeta potential. A zeta potential value on its own without defining the solution conditions is virtually a meaningless number. Generally, the zeta potential values change with change in pH of the solution. Sometimes, at a particular pH, the zeta potential of a nanoparticle is zero. This point is called as 'isoelectric point' (IEP) of the sample.

When nanoparticles are dispersed in the electrolyte of interest and an electric field is applied across the electrolyte, the charged nanoparticles suspended in the electrolyte are attracted towards the electrode of opposite charge due to electrostatic attraction. Viscous forces acting on the particles tend to oppose this movement. When equilibrium is reached between these two opposing forces, the particles move with constant velocity. The velocity is dependent on the strength of electric field or voltage gradient, the dielectric constant of the medium, the viscosity of the medium and the zeta potential. The velocity of a particle in a

unit electric field is referred to as its electrophoretic mobility. Zeta potential is related to the electrophoretic mobility by the Henry equation:-

$$U_E = \frac{2\varepsilon\zeta f(\kappa a)}{3\eta}$$

where U_E = electrophoretic mobility, ζ = zeta potential, ε = dielectric constant, η = viscosity and $f(\kappa a)$ = Henry's function which depends on the ratio of the particle radius to electrical double layer thickness. For aqueous electrolyte of moderate concentration, $f(\kappa a)$ is taken as 1.5, and this is referred to as the Smoluchowski approximation.

The zeta potential of a sample is measured by an instrument known as 'Zetasizer', which uses a combination of laser Doppler velocimetry and phase analysis light scattering (PALS) [81]. A laser is used to provide a light source to illuminate the particles within the sample. This light source is split to provide an incident and reference beam. The incident laser beam passes through the centre of the sample cell, and the scattered light is detected. When an electric field is applied to the cell, any particles moving through the measurement volume will cause the intensity of light detected to fluctuate with a frequency proportional to the particle speed (electrophoretic mobility) and this information is passed to a digital signal processor and then to a computer. The zetasizer has a software which produces a frequency spectrum from which the electrophoretic mobility and hence zeta potential is calculated.

2.1.4.6 Inductively coupled plasma atomic emission spectroscopy (ICP-AES)

ICP-AES is a spectral method used to determine very precisely the presence of metal analyte and the elemental concentration thereof. There are numerous reports on utilization of this technique for analysis of nanoparticles [82-85]. ICP-AES analysis requires a sample to be in solution. It works by the emission of photons from analytes that are brought to an excited state by the use of high-energy plasma. The plasma source is induced when passing argon gas through an alternating electric field that is created by an inductively couple coil. A peristaltic pump delivers the sample into a nebulizer where it is atomized and introduced directly inside

the plasma flame. When the analyte is excited, the electrons try to dissipate the induced energy by moving to a ground state of lower energy and in doing this they emit the excess energy in the form of light. The wavelength of light emitted depends on the energy gap between the excited energy level and the ground state and is thus specific to the element. In this way, the wavelength of light can be used to determine what elements are present by detection of the light at specific wavelengths. In order to determine the concentration of elements present, a calibration curve is developed using analyte solutions of known concentrations, whereby the intensity of the signal changes as a function of the concentration of the material that is present. When measuring the intensity from a sample of unknown concentration, the intensity from this sample can be compared with the calibration curve to determine the concentration of the analytes within the sample.

2.1.5 The present work

This chapter describes the synthesis and characterization of four nanomaterial based sorbents, namely, polymer embedded nanocrystalline titania (TiP), mixed phase nano-zirconia (nano-ZrO_2), tetragonal nano-zirconia (t-ZrO_2) and nano-ceria-polyacrylonitrile composite (CeO_2-PAN) for use in the preparation of radionuclide generators.

2.2 Materials

2.2.1 Chemicals

Reagents such as hydrochloric acid, ammonium hydroxide, oxalic acid, cerium (III) nitrate etc. were of analytical grade and were procured from S.D. Fine Chemicals, Mumbai, India. Zirconyl chloride ($ZrOCl_2.8H_2O$), titanium tetrachloride and isopropyl alcohol (A.R. grade) were obtained from E. Merck, Darmstadt, Germany. Polyacrylonitrile (PAN) beads (+99.9%, A.R. grade) were procured from Aldrich, England.

2.2.2 Instruments

X-ray diffraction

X-ray diffraction data were collected on the powder sample for the phase identification and crystallite size estimation, using monochromatized Cu-Kα radiation on a PANalytical X-ray diffractometer (X'pert PRO). The instrument was operated at 40 kV and 30 mA. Silicon was used as an external standard for the correction due to instrumental line broadening. The nano powder was ground and loaded in the groove of the perspex sample holder. XRD pattern was recorded in the 2θ range of 10-90^{o} for 1 h with a scan step size of 0.02^{o}.

Surface area measurement

The surface area and the pore size analysis were carried out by nitrogen adsorption (BET) technique at 77 K using Quantachrome, Autosorb-1 analyzer (Quantachrome Instruments, FL 33426 USA). The nanomaterial was first preheated in vacuum at 300^{o} C for 1 h to activate the sample.

Transmission electron microscopy

TEM data were recorded using TEM, JEOL FX microscope (Jeol Ltd., Tokyo, Japan) on the powder sample. The preparation of samples for TEM analysis involved sonication in ethanol for 5 minutes and deposition on a carbon coated copper grid. The accelerating voltage of the electron beam was 200 kV.

Zeta potential analysis

The zeta potential of the nanomaterials was measured using a zeta potential analyzer (Zetasizer Nano ZS/ZEN3600, Malvern Instruments Ltd., UK). The preparation of samples for zeta potential analysis involved dispersion of ~5 mg of the nanomaterial in 50 mL of de-ionized water, followed by sonication for 5 min. The pH of the suspension was adjusted using

$HClO_4$ and NaOH solution, and a small volume of the suspension was injected into the electrolytic cell. All measurements were carried out at 25 ºC in triplicate.

ICP-AES analysis

The chemical analysis for the determination of trace levels of metal ion contaminants in solution was done using ICP-AES (ICP-AES Model JY-238, Emission Horiba Group, France). The calibration curve for the metal ions was obtained by using standard solutions having known concentration of these ions.

2.3 Synthesis and characterization of TiP

2.3.1 Synthesis of TiP

Titanium tetrachloride was drop-wise added to isopropyl alcohol with vigorous stirring. The ratio of the two reactants, titanium tetrachloride : isopropyl alcohol was maintained at 2:1 (v/v). The viscosity of the reaction mixture increased gradually with time and after 4-6 h, a semisolid mass was formed which was difficult to stir. The reaction between isopropyl alcohol and titanium tetrachloride was very slow. The semisolid mass was kept for 5 days to complete the reaction and subsequently dried under an infrared lamp at a temperature of 80^{o}-90^{o} C for nearly 2 days to remove the generated HCl fumes and excess unreacted isopropyl alcohol. The reaction time and the drying time were very important for the preparation of the desired quality sorbent. With decrease in reaction time, the product obtained was not homogeneous and crumbled into fine powder. The material obtained after this initial stage of drying was water soluble. To render the water soluble precursor as an insoluble sorbent, it was heated for 2 h at a temperature of 160 $^{\circ}$C in a furnace. The solid mass obtained was subjected to repeated washings with distilled water to remove traces of remaining HCl and isopropyl alcohol. The residue was dried, ground in a porcelain mortar and sieved using a sieve of 50-100 mesh (149 – 297 μm). After drying and sieving, the

product obtained was granular and exhibited free flow characteristics for use in a column. It was insoluble in water and most of the mineral acids and alkalis.

2.3.2 Chemical stability of TiP

The chemical stability of the TiP was assessed in several mineral acids and bases, such as HCl, HNO_3, NaOH and NH_4OH of concentration up to 5 N. A weighed amount of TiP (1 g) was placed in 50 mL solvent of interest and kept for 24 h with continuous shaking at room temperature. It was clear that only a negligible amount of sorbent dissolved even after 24 h of shaking, as there was no turbidity in the solvent. Subsequently, it was filtered and the level of Ti metal ions in the filtrate, as determined by ICP-AES analysis was <0.1 ppm. This characteristic shows that the sorbent can safely be used for generator preparation.

2.3.3 Structural characterization of TiP

The structural characteristics of TiP were investigated by various analytical techniques like FTIR spectroscopy, BET surface area analysis, XRD and TEM.

2.3.3.1 FTIR spectroscopy

The FTIR spectrum of TiP is shown in **Fig. 2.1**. The sample as such showed a broad absorption peak in the range 3600-3000 cm^{-1}, which was due to the sum of the contributions of hydroxyl groups and water molecules. Absorption peak at 1614 cm^{-1} was due to the bending mode of OH^- group attached to the matrix. The continuous absorption peak appearing at <1000 cm^{-1} was due to titanium-oxygen bonds [86].

2.3.3.2 BET surface area analysis

The surface area measurement by standard BET technique was carried out on the prepared sample. The surface area of TiP was found to be 30 $m^2\ g^{-1}$. The surface area was also measured after decomposing the polymer matrix and it was found to be 38 $m^2\ g^{-1}$. The increase in surface area might be due to the decomposition of the sorbent accompanied by

evolution of gases, which makes the product more porous. The average pore size of the powder was found to be ~4 Å.

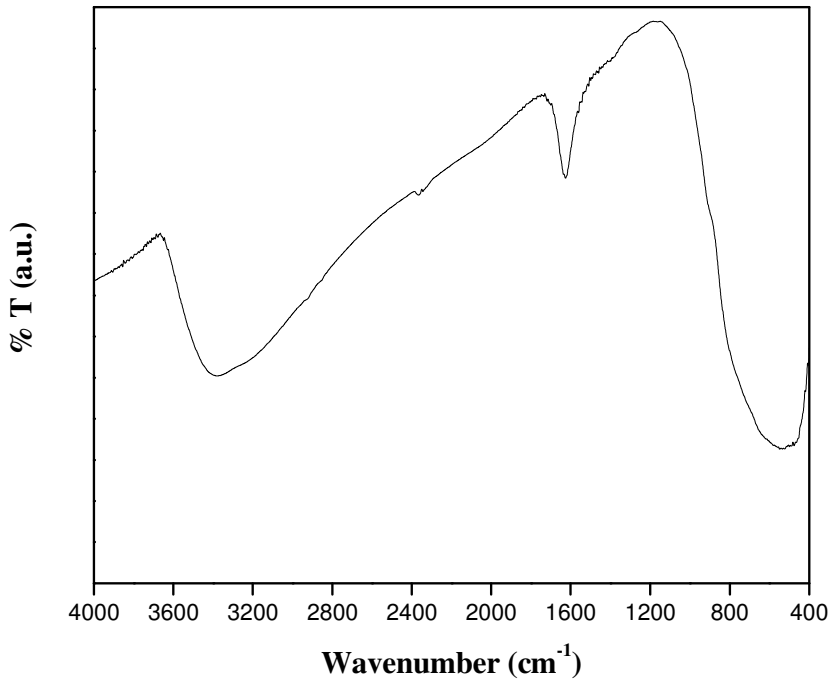

Fig. 2.1: FTIR spectrum of TiP

2.3.3.3 XRD studies

The XRD pattern of TiP is shown in **Fig. 2.2** and it matches well with the rutile modification of TiO_2. The average crystallite size of TiO_2 was calculated using Scherrer's formula and was found to be 5.2 ± 0.6 nm (n=5).

2.3.3.4 TEM studies

The TEM micrograph of TiP is shown in **Fig. 2.3** and it reveals the network of polymer with dispersed titania phase. The crystallite size of TiP as observed from the TEM micrograph ranged between 4-6 nm, which was in accordance with the result obtained from XRD studies. Excess time exposure of the electron beam to the sample caused degradation of the polymer. This led us to the inference that in TiP, TiO_2 nanoparticles are embedded in the polymer matrix.

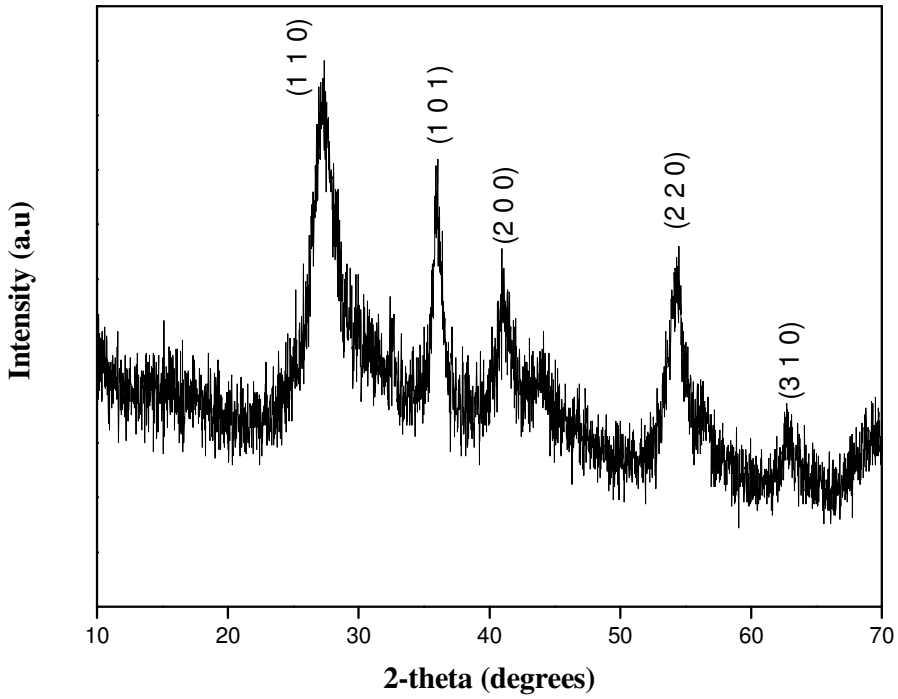

Fig. 2.2: XRD pattern of TiP

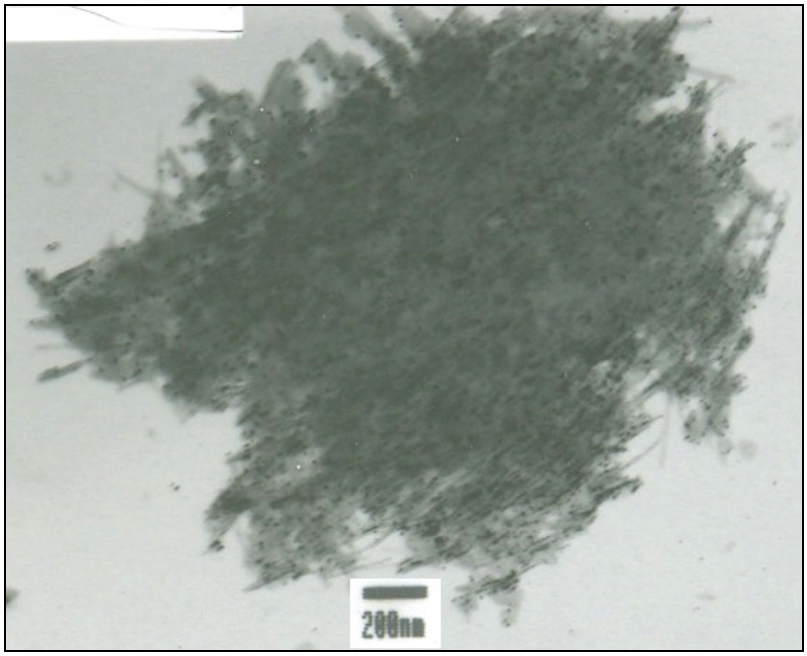

Fig. 2.3: TEM micrograph of TiP

2.3.4 Zeta potential of TiP at different pH environments

The variation of zeta potential of TiP with pH is illustrated in **Fig. 2.4**. The zeta potential values are positive in the pH range 1-6 and have a maximum at ~pH 2.

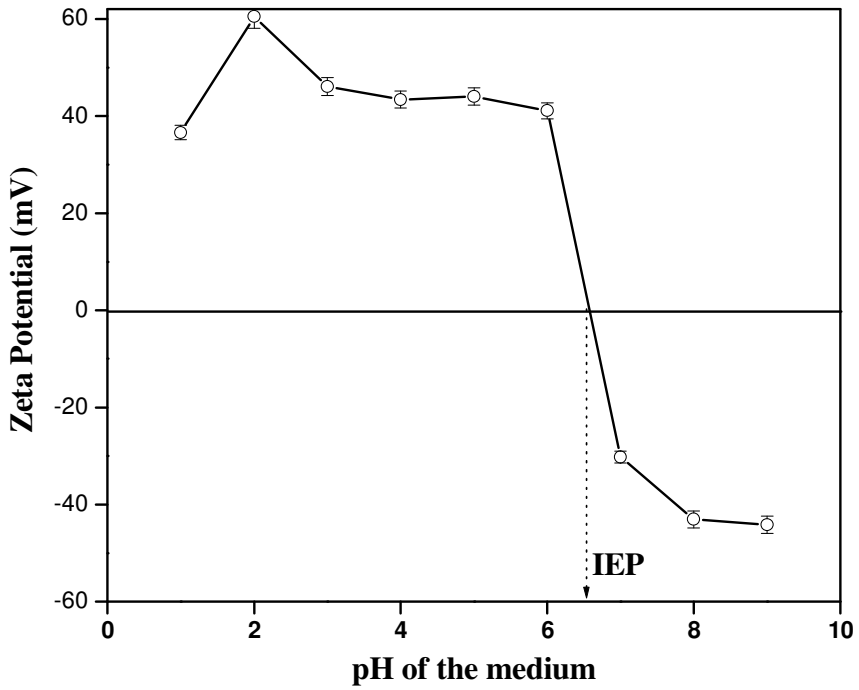

Fig 2.4: Variation in zeta potential of TiP with variation in pH of the medium

This indicates that in this pH range, coulombic attraction can readily take place, in conjunction with specific chemical adsorption, between the sorbent and negatively charged ions. On further increase in pH, the zeta potential of TiP decreases and passes through isoelectric point (IEP) at pH between 6 and 7. Under alkaline conditions, the zeta potential of TiP was negative. The material was synthesized in 10 different batches and the structural characteristics and properties of the material remained unchanged in all the batches.

2.4 Synthesis and characterization of nano-ZrO_2

2.4.1 Synthesis of nano-ZrO_2

nano-ZrO_2 was synthesized by controlled hydrolysis of zirconium oxychloride in isopropyl alcohol medium. Zirconium oxychloride was dissolved in 80% isopropyl alcohol

and 20% ammonia solution in isopropyl alcohol medium was added drop-wise to it with vigorous stirring. The stirring of the reaction mixture was essential in order to prevent agglomeration and obtain nanocrystalline zirconia. The ammonia solution was added until complete formation of the white precipitate. However, the pH of the reaction medium was maintained at ~4 during the course of the reaction. The precipitate was subsequently refluxed for 12 hours at ~96 ^{o}C, maintaining pH at ~4, to facilitate the stabilization of the nano-zirconia particles. The precipitate obtained was washed with distilled water, dried at 100 $^{\circ}$C and calcined at 600 $^{\circ}$C for 2 h. The material produced was sieved to obtain particles of 50-100 mesh size (149 – 297 μm). The product obtained was granular with adequate mechanical strength for reliable fixed-bed column operation.

2.4.2 Chemical stability of nano-ZrO_2

The chemical stability of the nano-ZrO_2 was assessed in several mineral acids and bases, such as HCl, HNO_3, NaOH and NH_4OH of concentration up to 5 N. A weighed amount of nano-ZrO_2 (1 g) was placed in 50 mL solvent of interest and kept for 24 h with continuous shaking at room temperature. It was clear that no appreciable amount of dissolution took place and the sorbent was fairly stable in most of the dilute mineral acids and alkalis. There was no turbidity when the sorbent was suspended in dilute mineral acids and alkalis for 24 hours. Subsequently, it was filtered and the level of Zr metal ions in the filtrate, as determined by ICP-AES was <0.1 ppm. This characteristic shows that the sorbent can safely be used for generator preparation.

2.4.3 Structural characterization of nano-ZrO_2

In order to obtain information on the structure of nano-ZrO_2, it was subjected to FTIR spectroscopy, BET surface area analysis, XRD and TEM.

2.4.3.1 FTIR spectroscopy

The FTIR spectrum of nano-ZrO_2 is shown in **Fig. 2.5**. The spectrum shows a broad

absorption peak in the range 3600-3000 cm^{-1}, which can be attributed to the sum of the contributions of hydroxyl groups and water molecules.

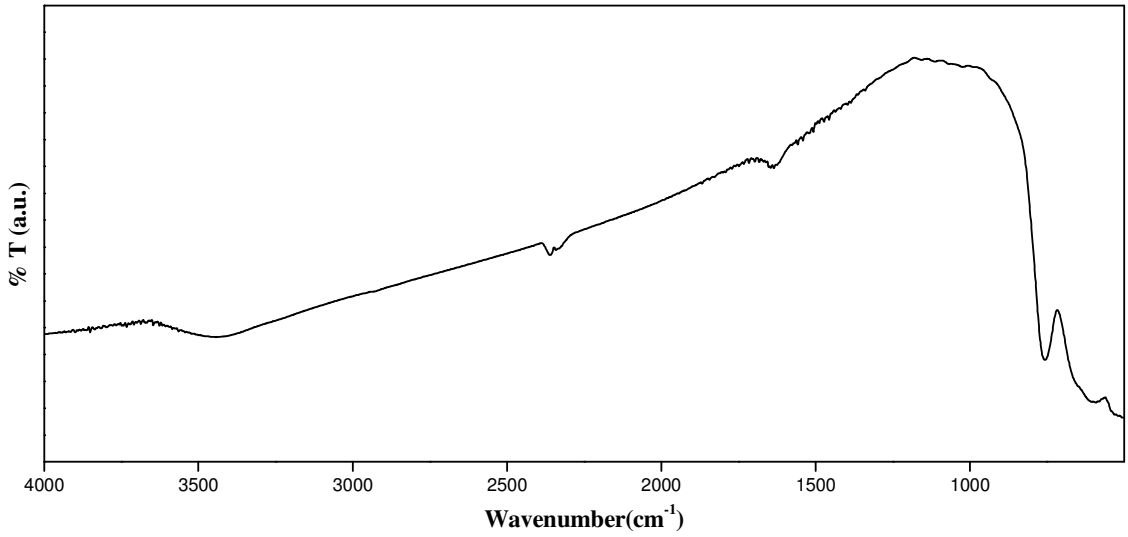

Fig. 2.5: FTIR spectrum of nano-ZrO_2

The absorption band centred at around ~1614 cm^{-1} can be attributed to the bending mode of OH^- group attached to the matrix. The band at 490-501 cm^{-1} is attributed to Zr-O-Zr bond [87]. The presence of a small peak at ~2300 cm^{-1} may be due to carbon dioxide trapped inside the bulk structure of the nano oxide.

2.4.3.2 BET surface area analysis

The surface area measurement and the pore size distribution of the sorbent were carried out by standard BET technique. The surface area of nano-ZrO_2 was found to be ~45 $m^2\ g^{-1}$. The average pore size was determined to be ~4 Å. It was observed that the pore sizes were quite uniform.

2.4.3.3 XRD studies

The XRD pattern of nano-ZrO_2 is shown in **Fig. 2.6**. It shows that nanocrystalline zirconia prepared by this method consists of two phases, of which the major crystalline phase is monoclinic zirconia. The minor phase is tetragonal zirconia.

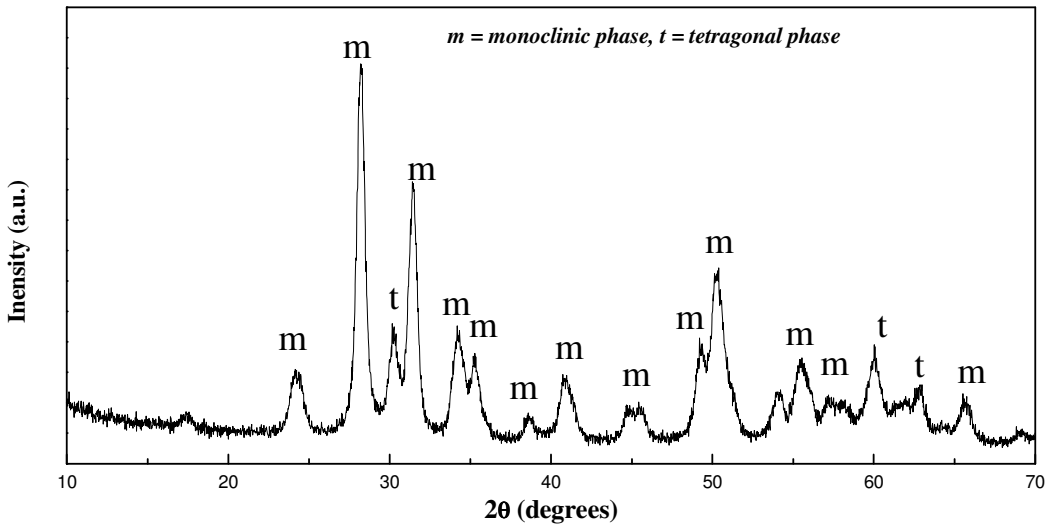

Fig. 2.6: XRD pattern of nano-ZrO_2

This tetragonal modification could be stabilized due to the excess surface energy possessed by the nanosized material. The average crystallite size of nano-ZrO_2 as determined from the XRD pattern using Scherrer's formula was ~15 nm.

2.4.3.4 TEM studies

The TEM micrograph indicated that the nanocrystalline zirconia prepared was crystalline and agglomerated (**Fig. 2.7**). It was also observed from the TEM that the particles are quite uniform in size and shape. The average particle size of nano-ZrO_2 as determined by TEM measurement was found to be in the range of 15-20 nm which was in accordance with the results obtained from XRD studies.

2.4.4 Zeta potential of nano-ZrO_2

The zeta potential of the sorbent was investigated at pH 1-8 and the results are shown in **Fig. 2.8**. This study clearly shows that the surface charge of the sorbent varies at different pH values. The surface charge of nano-ZrO_2 is positive at pH <4 and becomes increasingly negative with rise in pH. The isoelectric point (IEP) of the sorbent surface was reached at pH ~4.5, in this particular ionic system.

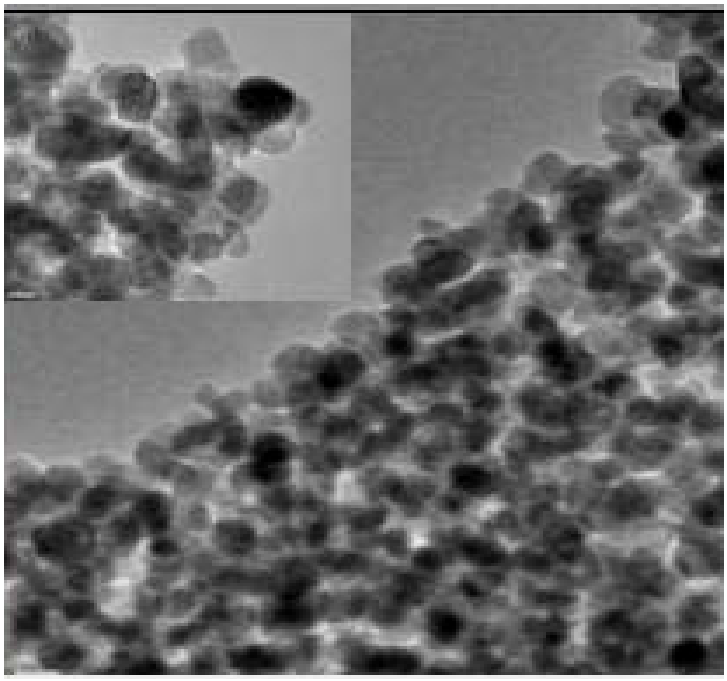

Fig. 2.7: TEM micrograph of nano-ZrO_2

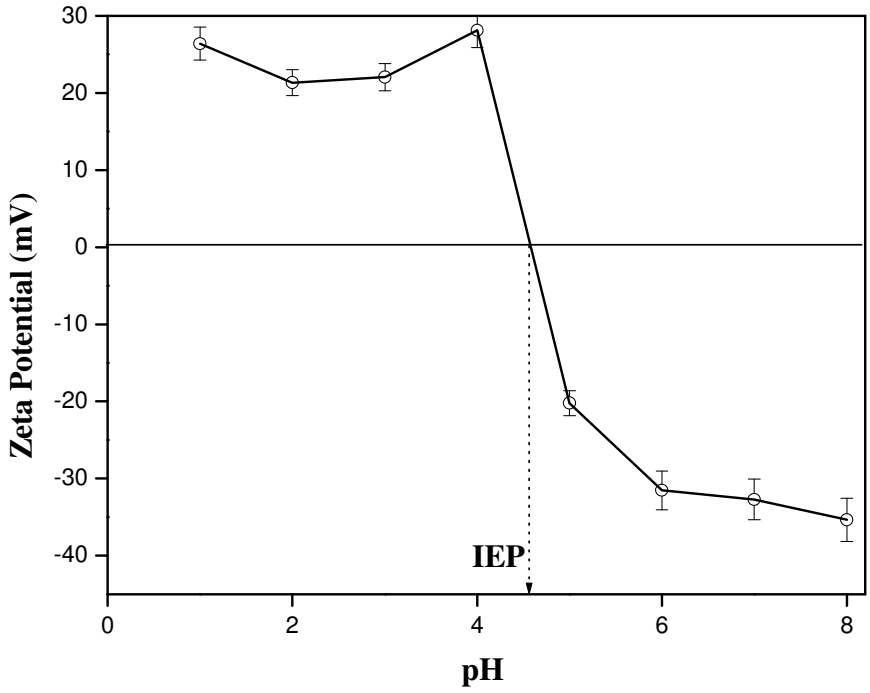

Fig. 2.8: Variation in zeta potential of nano-ZrO_2 with variation in pH of the medium

Several batches of nano-ZrO_2 were synthesized and reproducible results were obtained in all the batches.

2.5 Synthesis and characterization of t-ZrO_2

2.5.1 Synthesis of t-ZrO_2

t-ZrO_2 was synthesized by controlled hydrolysis of zirconyl chloride in ammonical medium as per the procedure reported by Yin et al [88]. Zirconyl chloride solution (0.17 M) was added drop-wise into a round bottom flask containing 2.5 M ammonia solution, with careful control of pH (9-11) and with vigorous stirring. This order of addition of reagents is important as formation of zirconia precipitate in alkaline environment helps in stabilization of the precursor to t-ZrO_2 nanoparticles [89,90]. The vigorous stirring of the reaction mixture prevents agglomeration of the precipitate and hence facilitates the formation of the nanoparticles. The resultant hydrogel was washed with de-ionized water until free of chloride ions. The hydrogel was then digested under reflux at 96 ^oC for 24 h in a 1 L round bottom flask that contained aqueous solution of ammonia (pH ~12). The reflux digestion of the basic solution in the glass vessel leads to stabilization of nanometer-sized tetragonal crystals [88]. Subsequently, the digested gel was washed extensively with de-ionized water. The washed gel was dried at 100 ^oC overnight. The dried gel was calcined at 600 ^oC for 5 h and used for structural studies. Further, it was ground in a porcelain mortar and sieved to get particles of 50-100 mesh (149 – 297 μm). The product obtained was granular in texture with adequate mechanical strength and exhibited free flowing characteristics in fixed-bed column operation.

2.5.2 Chemical stability of t-ZrO_2

The chemical stability of the t-ZrO_2 was assessed in several mineral acids and bases, such as HCl, HNO_3, NaOH and NH_4OH of concentration up to 5 N. A weighed amount of t-ZrO_2 (1 g) was placed in 50 mL solvent of interest and kept for 24 h with continuous shaking at room temperature. The solvent used was clear and no turbidity was observed in it even after 24 h of shaking with t-ZrO_2 suspended in it. Subsequently, it was filtered and the level of Zr metal ions in the filtrate as determined by ICP-AES analysis, was <0.1 ppm. This shows

that t-ZrO_2 is insoluble in water, dilute mineral acids and alkalis and can safely be used as a sorbent in a radionuclide generator.

2.5.3 Structural characterization of t-ZrO_2

The structural characterization of t-ZrO_2 was carried out by various analytical techniques such as FTIR spectroscopy, BET surface area and pore size analysis, XRD and TEM.

2.5.3.1 FTIR spectroscopy

The FTIR spectrum of t-ZrO_2 is shown in **Fig. 2.9**. The sample as such showed a broad absorption peak in the range 3600-3000 cm^{-1}, which is due to the sum of the contributions of hydroxyl groups and water molecules. Absorption peak at 1614 cm^{-1} was due to the bending mode of OH^- group attached to the matrix. The bands at 1000 cm^{-1}, 490-501 cm^{-1} are attributed to the Zr-O-Zr bond [87].

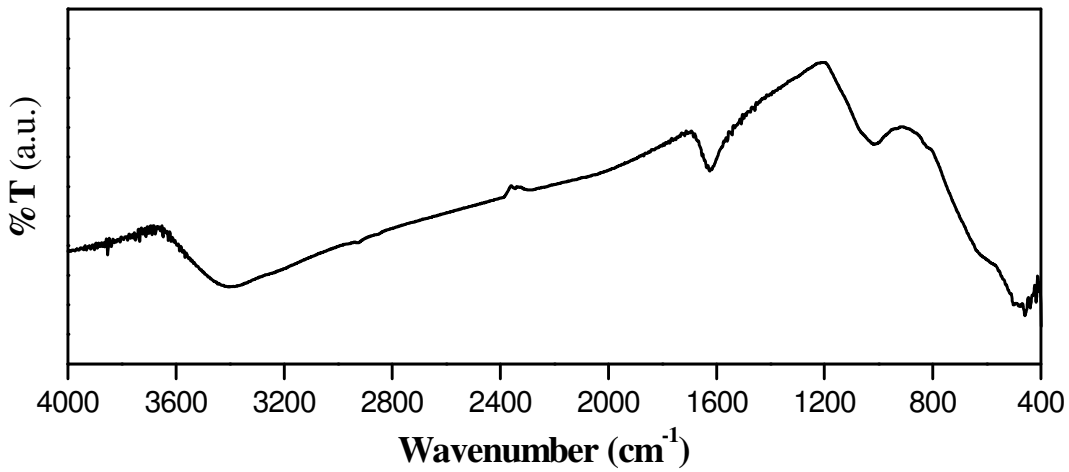

Fig. 2.9: FTIR spectrum of t-ZrO_2

2.5.3.2 BET surface area analysis

The surface area measurements and the pore size distribution of the sorbents were carried out by standard BET technique. The surface area of t-ZrO_2 was found to be as high as

~340 m^2 g^{-1}. The average pore size of the material was determined to be ~4 Å. It was observed that pores sizes are uniform which facilitate permeation of liquid.

2.5.3.3 XRD studies

The XRD pattern of t-ZrO_2 is shown in **Fig. 2.10**. The results indicate that the nano-zirconia prepared by this method, is present purely in tetragonal phase. The tetragonal phase was perhaps stabilized due to the excess surface energy possessed by the nanosized material. The average crystallite size of t-ZrO_2 determined by Scherrer's method was found to be ~7 nm.

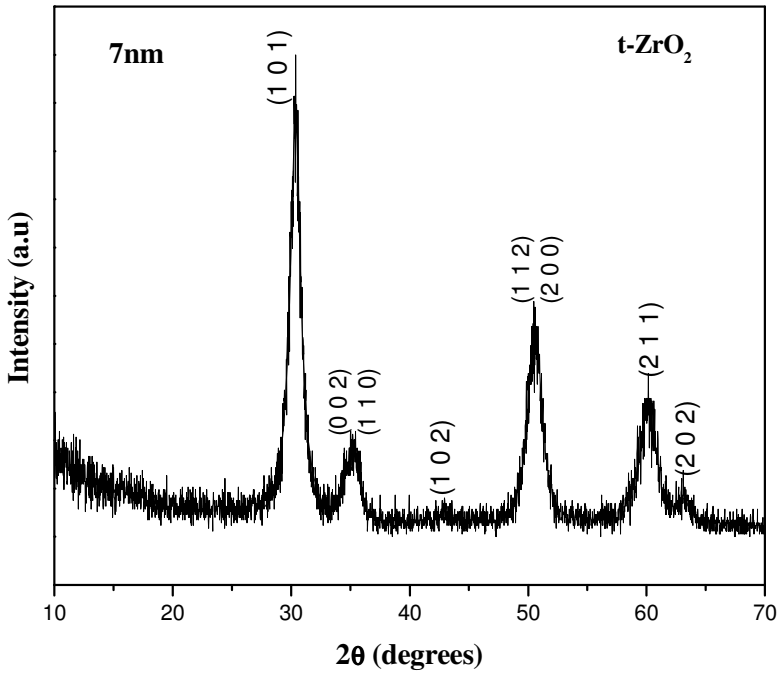

Fig. 2.10: XRD pattern of t-ZrO_2

2.5.3.4 TEM studies

The TEM micrograph (**Fig. 2.11**) indicated that the t-ZrO_2 was highly agglomerated and the particles are quite uniform in size and shape. The average crystallite size of t-ZrO_2 as determined by the TEM measurements was found to be in the range of 6-10 nm, which was in accordance with the results obtained from the XRD method. The nano-sized crystallites have

high surface energy. It is an established observation that in order to stabilize themselves, the nano-sized crystallites get agglomerated to form micron sized granules (comprising of large number of primary particles). The agglomeration of the crystallites and the subsequent crushing and sieving of the agglomerates renders free flowing granular particles of t-ZrO_2 suitable for use in column operations.

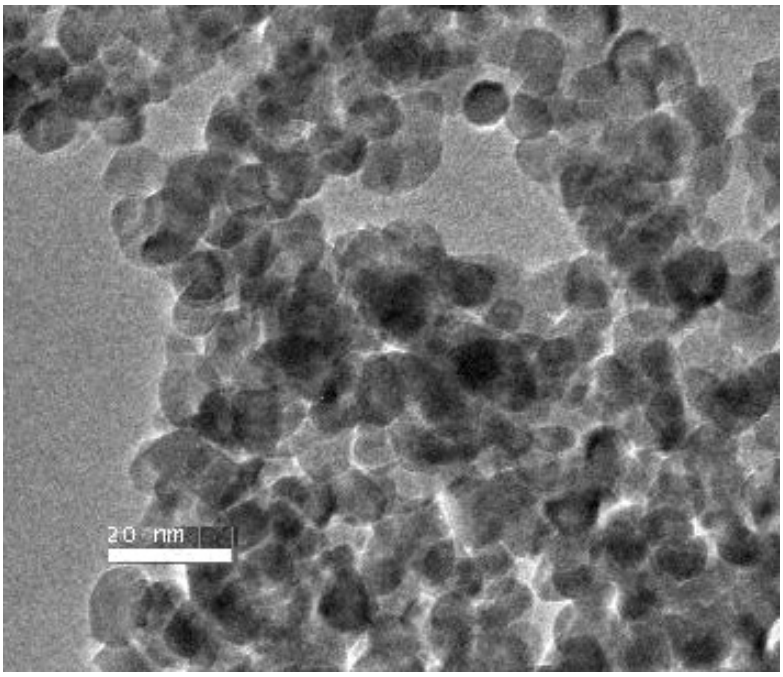

Fig. 2.11: TEM micrograph of t-ZrO_2

2.5.4 Zeta potential of t-ZrO_2

The zeta potential of t-ZrO_2 sorbent was determined at different pH environments. The effect of pH on zeta potential of t-ZrO_2 in aqueous solution is shown in **Fig. 2.12**. It is clearly evident from the figure that interaction of t-ZrO_2 particles with aqueous solutions imparts a pH-dependent surface charge. The zeta potential value is positive in the pH range 1-4. On further increase of pH, the zeta potential value passes through zero (isoelectric point) and then it develops negative zeta potential. The IEP, as determined from the figure, occurs at pH ~4.5. On further increase in pH, the zeta potential of the material was found to be negative.

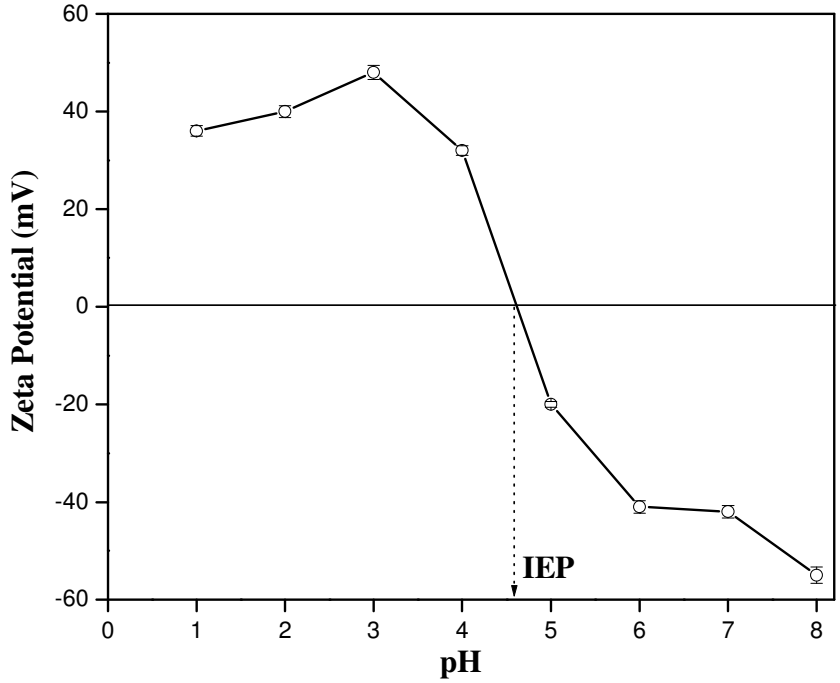

Fig. 2.12: Variation in zeta potential of t-ZrO_2 with variation in pH of the medium

Several batches of t-ZrO_2 were synthesized and the properties of the material remained unchanged in all the batches.

2.6 Synthesis and characterization of CeO_2-PAN

2.6.1 Synthesis of CeO_2-PAN

For the synthesis of nanocrystalline ceria, indirect precipitation technique was adopted in which cerium oxalate was precipitated by drop-wise addition of 1 N oxalic acid solution to 0.6 N cerium (III) nitrate solution in iso-propyl alcohol - deionized water medium (4:1 v/v). The precipitate was thoroughly washed with deionized water and dried under an infrared (IR) lamp for 1 h. The residue obtained was directly introduced in the furnace at 500 °C and calcined for 30 min in static air. The cerium oxalate precipitate decomposed at 500 °C to form nanocrystalline CeO_2. The thermal decomposition of the oxalate material accompanied by evolution of gases increased the porosity of the material.

The material obtained consisted of fine powder and hence was not amenable for use as a column matrix owing to low permeability to aqueous solutions. In order to use nano ceria for column applications, a suitable binding agent was required, which would improve the granulometric properties and flow characteristics of the sorbent material [91-93]. Polyacrlonitrile (PAN) was selected for this purpose due to its favorable features such as strong adhesive force with inorganic materials, high hydrophilicity, excellent chemical stability in acidic and radiation environments [91-94]. PAN has been shown to effectively immobilize ion-exchange materials into granular forms, without altering the sorption behavior of these materials [91-93]. The PAN granules obtained by dispersing PAN solution in water are highly porous [91-93,95]. The pores of these granules are mainly (>99.9%) composed of macropores (pore size >0.05 μm) along with a minor portion (<0.1%) of mesopores (pore size between 0.002 μm and 0.05 μm) [95]. When the ion-exchanger is mixed with the PAN solution and dispersed in water, the resultant PAN granules obtained can accommodate very high loadings of the ion-exchange material (up to 90% by weight) into the PAN matrix [91-95]. These porous PAN granules exhibit numerous advantages over other sorbents such as improved kinetics, enhanced sorption capacity owing to the increased availability of the sorbent material, easy modification of physicochemical properties (hydrophilicity, porosity, and mechanical strength) and simplified production [91-93]. The granular material obtained from this method is suitable for column chromatographic applications due to the presence of hard agglomerates and high surface area.

For the preparation of the nano ceria-PAN composite, a weighed amount (1 g) of PAN was dissolved in 25 mL of 10 M HNO_3 with mild heating (~70° C) and continuous stirring, till a viscous solution was obtained. An equal amount (1 g) of calcined cerium oxide (in 1:1 mass ratio) was added to the PAN solution with vigorous stirring to obtain homogeneous suspension of the composite. The homogeneous suspension thus formed was

poured into a water bath containing 1 L of deionized water, resulting in the formation of a lump. The lump obtained was washed several times with deionized water and dried for 12 h at 70° C in a furnace. The dried lump was crushed mechanically and sieved to obtain the particles of 50-100 mesh size (149 – 297 μm).

2.6.2 Chemical stability of CeO_2-PAN

The chemical stability of CeO_2-PAN was assessed in mineral acids such as HCl, HNO_3 and H_2SO_4 up to concentration of 5 M. The dried material (1 g) was immersed in 50 mL solution in a stoppered conical flask for 24 h at room temperature, under continuous shaking using a wrist action shaking machine. Subsequently the solution was filtered and the level of Ce ions in the filtrate was determined by ICP-AES. Negligible amount of Ce ions (<0.1 ppm) were detected in the filtrate and therefore CeO_2-PAN was stable in these solutions.

2.6.3 Structural characterization of CeO_2-PAN

2.6.3.1 FTIR spectroscopy

The FTIR spectrum of CeO_2-PAN is shown in **Fig. 2.13**. The sample showed a broad absorption peak in the range 3600-3000 cm^{-1}, which was due to the sum of the contributions of hydroxyl groups and adsorbed water molecules. The sharp absorption peak at 2237 cm^{-1} was due to CN stretching [96]. Absorption peak at 1624 cm^{-1} was due to the bending mode of OH^- group attached to the matrix. The peak at 1449 cm^{-1} was due to the bending mode of the CH_2 group in the polymer matrix [96]. The intense peak at 1381 cm^{-1} was assigned to the bending mode of NO_2 group. The peaks observed at 1038 cm^{-1} and 800 cm^{-1} were attributed due to the combination of stretching and bending modes of C-CN bonds [96]. The absorption peak at 735 cm^{-1} was due to the bending mode of NO_3 group [96,97]. The absorption peak at 580 cm^{-1} (shown in inset) was attributed to Ce-O bond [98]. The small crystallite size of

CeO_2 nanoparticles results in shortening of the bond length of Ce-O bond and therefore the absorption peak was observed at such high energy or low wavenumber [98].

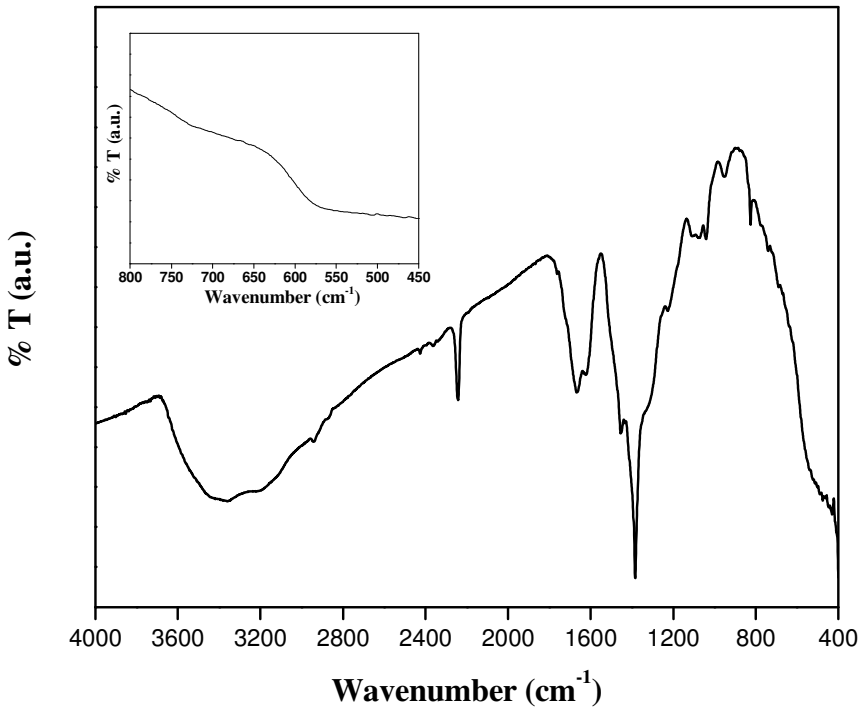

Fig. 2.13: FTIR spectrum of CeO_2-PAN

2.6.3.2 BET surface area analysis

The surface area measurements and the pore size distribution of CeO_2-PAN were carried out by standard BET technique. The surface area of CeO_2-PAN was found to be ~72 $m^2 g^{-1}$. The average pore size was determined to be ~3.6 Å. It was observed that pores sizes are uniform which facilitate permeation of liquid.

2.6.3.3 XRD studies

The XRD pattern of CeO_2 is shown in **Fig. 2.14** and it reveals that the material is nanocrystalline. The average crystallite size of CeO_2, as calculated using Scherrer's equation, was ~10 nm. The XRD pattern of nano ceria remained unchanged on binding with PAN.

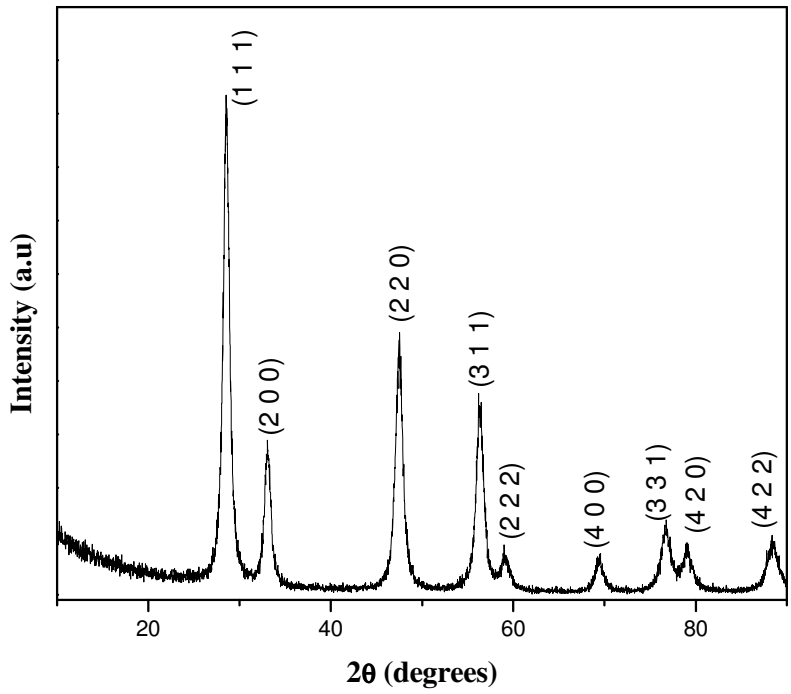

Fig. 2.14: XRD pattern of nano-CeO_2

2.6.3.4 TEM studies

The TEM micrograph indicated that CeO_2-PAN was nanocrystalline and highly agglomerated (**Fig. 2.15**). The average crystallite size of nanocrystalline ceria as determined from the TEM micrograph was found to be in the range of 8-10 nm which was in good agreement with the results obtained from XRD.

2.6.4 Zeta potential of CeO_2-PAN

The zeta potentials of nano ceria and CeO_2-PAN were determined at different pH environments and the results are illustrated in **Fig. 2.16**. It is clear from the figure that the surface-charge of these nanomaterials varies with variation in pH. The zeta potentials of both nano ceria as well nano ceria coated with PAN (CeO_2-PAN) were positive up to pH ~6 and became increasingly negative with further increase in pH. The isoelectric point (IEP) of these nanomaterials in this particular ionic system was reached at pH between 6 and 7. On further increase in pH, the zeta potential of these materials became increasingly negative.

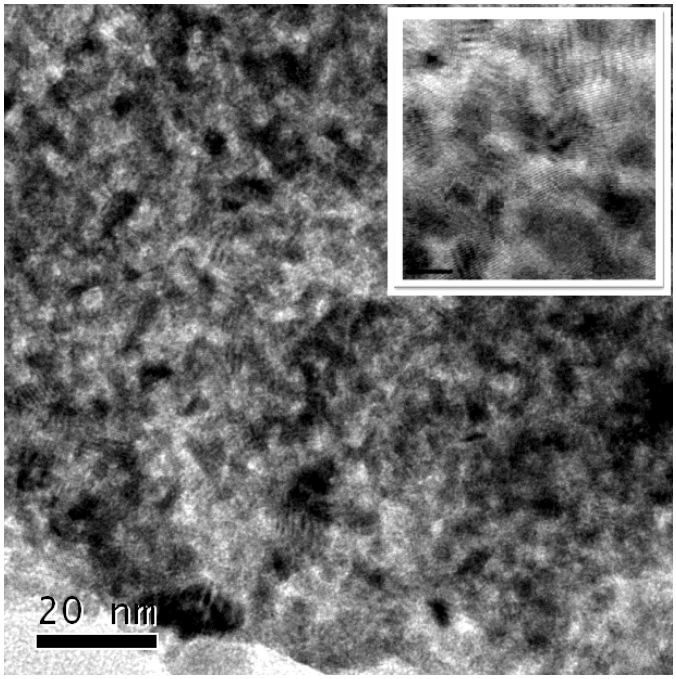

Fig. 2.15: TEM micrograph of CeO_2-PAN

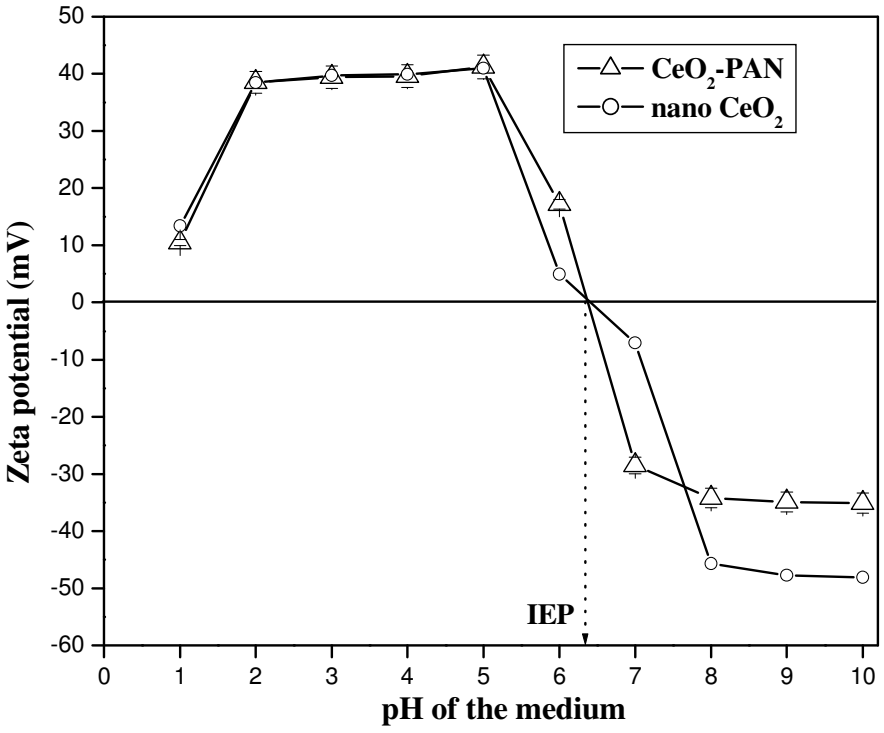

Fig. 2.16: Variation in zeta potential of (a) nano-CeO_2 and (b) CeO_2-PAN with variation in pH of the medium

It can be seen from the figure that the zeta potential of nano ceria, under acidic conditions, did not change significantly on coating with PAN. Therefore, it could be concluded that the sorption characteristics of nano ceria remained unaltered on preparation of the composite sorbent (CeO_2-PAN).

2.7 Conclusions

Potential pathways to rationally synthesize nanomaterial based sorbents for use as column matrices in radionuclide generators have been established. The materials synthesized were nanocrystalline and possessed appreciably high chemical stability and surface area. Owing to their granular strength and free flow characteristics, the materials are suitable for column operations. The efficacy of these sorbent materials for the development of radionuclide generators are described in the subsequent chapters. It is envisioned that nanomaterials can become critical components of radionuclide generators in the near future and shall open up many new opportunities in synthesis and application of novel nanomaterial based sorbents.

CHAPTER 3

DEVELOPMENT OF $^{99}Mo/^{99m}Tc$ GENERATORS

"A scientific truth does not triumph by convincing its opponents and making them see the light, but rather because its opponents eventually die and a new generation grows up that is familiar with it."

MAX PLANCK

3.1 Introduction

3.1.1. Technetium-99m (^{99m}Tc): The work-horse of Nuclear Medicine

The important role that ^{99m}Tc has played in shaping the field of diagnostic Nuclear Medicine has been clearly established and remains undisputed, till date [12,25,41,43,99]. The early realization by the Brookhaven group that ^{99m}Tc possess ideal nuclear decay characteristics for organ imaging set forth a chain of events that ensured the widespread acceptance of nuclear techniques in medical diagnosis [11]. Inspite of the greatly increased availability of other radioisotopes in the present times, ^{99m}Tc still remains the 'work-horse' of diagnostic Nuclear Medicine and is used in approximately 20-25 million procedures annually, comprising ~80% of all diagnostic Nuclear Medicine procedures worldwide [12]. In fact, it would not be an exaggeration to state that Nuclear Medicine, to a large extent, owes its emergence and existence to ^{99m}Tc. This preferred use of ^{99m}Tc radiopharmaceuticals reflects the ideal nuclear properties of the radioisotope. ^{99m}Tc emits a 140 keV γ-ray with 89% abundance [15], which is nearly optimal for imaging with commercial gamma cameras. The absence of particulate emission allows the injection of activities of more than 1.11 GBq (30 mCi) with low radiation exposure to the patient. The 6 h half-life of ^{99m}Tc allows for centralized preparation of radiopharmaceuticals in radiopharmacies, distribution to hospitals, administration time for accumulation in the target tissue, and collection of the image while still ensuring minimal radiation dose to the patient. Additionally, the chemistry of technetium is amenable for the preparation of a wide variety of radiopharmaceuticals.

3.1.2 Availability of ^{99m}Tc from ^{99}Mo

The preeminence of ^{99m}Tc as a medically useful radioisotope is directly attributable to the conception and development of the ^{99}Mo/^{99m}Tc generators in the late 1950s [11,12,25,41,43,99]. Without this development, the ready availability of the short-lived ^{99m}Tc ($t_{½}$ = 6 h) would not have become a reality. The availability of ^{99m}Tc from its relatively long-

lived parent Molybdenum-99 (^{99}Mo, $t_{½}$ = 66 h) enables this radionuclide to be used at places far away from the site of production. The simplified decay scheme of ^{99}Mo is shown in **Fig. 3.1**.

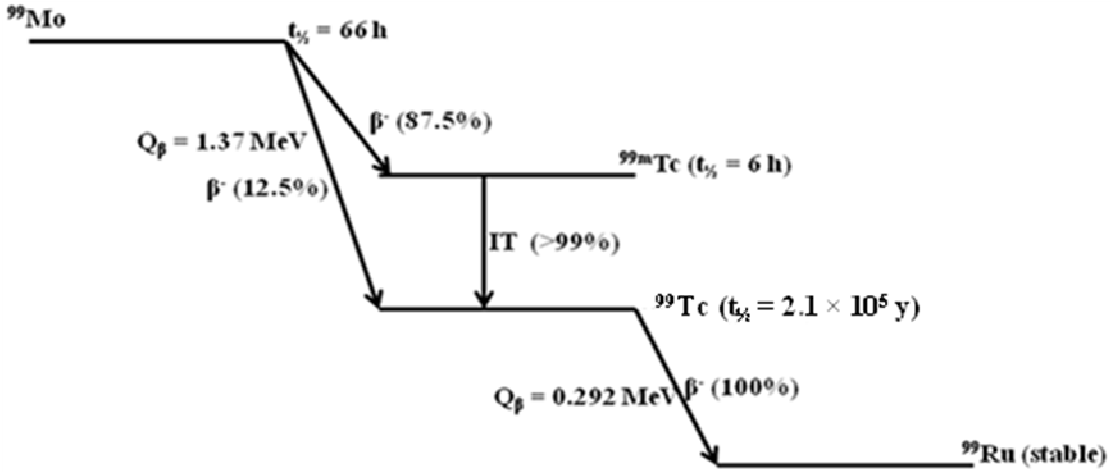

Fig. 3.1: Simplified decay scheme of ^{99}Mo (energy levels not drawn to scale)

The medical benefits of ^{99m}Tc are dependent on a reliable and continuous supply chain of ^{99}Mo. More than 90% of the world's supply of ^{99}Mo is derived from the fission of highly enriched uranium (HEU) at the 5 nuclear reactors, namely, NRU at Chalk River in Canada, HFR at Petten in Netherlands, BR-2 at Fleurus in Belgium, OSIRIS at Saclay in France and SAFARI-1 at Pelindaba in South Africa [100,101]. Most of these reactors are aged (42-51 y), nearing the time of their decommissioning and need extensive routine maintenance [100,102]. This is a deep concern for a reliable and consistent supply of the most important medical radioisotope, ^{99}Mo [100-105]. Moreover, nuclear non-proliferation and security concerns have led to advanced discussions around the world about restricting and eventually abolishing the use of HEU, both as reactor fuel as well as targets for producing fission products such as ^{99}Mo [100-105]. Thus, the global production of fission ^{99}Mo is inadequate to meet the demand of this radioisotope, and therefore adversely affects

patient services in many countries. This not only highlights the fragile nature of fission ^{99}Mo supplies but also raises concerns over its dependency [106].

Owing to the unavailability of the production technology and the non-proliferation concerns [100], it is not possible for most of the countries in the world to produce fission ^{99}Mo to meet their own internal needs. The separation and purification of fission ^{99}Mo, involves an elaborate and complex processing technology which is expensive and results in huge quantities of radioactive wastes. Alternative options for long term production of ^{99}Mo include processing of the liquid fuel in aqueous homogeneous reactors (AHR) [107], charged particle acceleration in high-power accelerators and photo fission of ^{238}U [108], all of which are still in the conceptual stage. Although such approaches hold promise, considerable research and huge resources are required to develop, test and deploy the technology. The economics of these routes still remains debatable, and these approaches are not likely to materialize in the near future. In view of the complex problems, the most successful solution rarely involves uncertain investments. A more prudent approach to shoring up the tenuous supply chain of ^{99}Mo would be to reduce reliance on fission-produced ^{99}Mo and implementing the use of (n,γ)^{99}Mo. This alternative approach needs to be emphasized as a back-up measure and to supplement ^{99m}Tc accessibility to meet the continually growing demand for ^{99m}Tc in Nuclear Medicine. However, the specific activity of (n,γ) ^{99}Mo (~300-1000 mCi g^{-1}) produced by irradiation of natural Mo target is much lower than that of fission ^{99}Mo (~10^4 Ci g^{-1}) [109].

3.1.3 Separation of ^{99m}Tc from ^{99}Mo

Over the past 50 years, several versions [40-44,48,50,110-115] of the ^{99}Mo/^{99m}Tc generator have been developed, the most common being the original alumina based chromatographic generator system. The ease of operation, high elution efficiency, high radionuclidic purity and radioactive concentration of ^{99m}Tc eluate are the attractive features of

these generator systems. The capacity of alumina for taking up molybdate ions is limited (2-20 mg Mo g^{-1} of alumina) [42] necessitating the use of ^{99}Mo of the highest specific activity available, generally possible only in ^{99}Mo produced through fission route. However, the key challenge in the use of this technique is the current global shortage of fission ^{99}Mo, attributable to the reasons discussed above.

In order to minimize the dependence on the fission produced ^{99}Mo, several alternative approaches like 'batch' solvent extraction and dry distillation of ^{99m}Tc from $(n,\gamma)^{99}MoO_3$ target were reported for accessing ^{99m}Tc from $(n,\gamma)^{99}$Mo [40,42,48,50,111]. The need for strict adherence to the operational protocol, good laboratory practices from both pharmaceutical and radiological safety angles and the requirement for well-trained, skilled operator are the major limitations of these techniques. The need for a simple user-friendly column based generator that uses $(n,\gamma)^{99}$Mo, prompted researchers to explore the 'gel generator' route [44,51,52]. However, the developments over the last two decades have shown that it has inherent disadvantages which limit its wide applicability. Attempts to develop systems with primary alumina column generator containing $(n,\gamma)^{99}$Mo, in tandem with a device to concentrate large volume of eluate to an acceptable small volume of <5 mL [116,117], have also been tried with limited success. There has also been widespread interest in the development of ^{99}Mo/^{99m}Tc generators from $(n,\gamma)^{99}$Mo using alternate sorbents having higher sorption capacity compared to alumina [118-120]. Masakazu et al. [120] developed a ^{99}Mo/^{99m}Tc generator using polymeric zirconium compound (PZC) which showed high sorption capacity for ^{99}Mo (~200 mg Mo g^{-1}). However, the slow kinetics of sorption and appreciably high ^{99}Mo breakthrough [120] are the significant drawbacks that limit its applicability in a clinical context. The commonly available options for the preparation of ^{99}Mo/^{99m}Tc generators and their advantages and limitations are summarized in **Table 3.1.**

Table 3.1: The commonly available options for the preparation of $^{99}Mo/^{99m}Tc$ generators

Method	^{99}Mo source	Efficiency of separation of ^{99m}Tc	Advantages	Limitations
Chromatography (alumina)	$(n,f)^{99}Mo$	80-85%	Simple, portable, high radioactive concentration and high purity of ^{99m}Tc	Global shortage of fission ^{99}Mo, complex ^{99}Mo production technology
Chromatography (alumina)	$(n,\gamma)^{99}Mo$	80-85%	Simple, portable, high purity of ^{99m}Tc	Low radioactive concentration of ^{99m}Tc
Solvent extraction (MEK)	$(n,\gamma)^{99}Mo$	>80%	Low specific activity ^{99}Mo can be used, high radioactive concentration of ^{99m}Tc	Complex and cumbersome process, possible fire hazard
Sublimation	$(n,\gamma)^{99}Mo$	<50%	Low specific activity ^{99}Mo can be used, high radioactive concentration and high radionuclidic purity of ^{99m}Tc	Complex and cumbersome process, low separation yield

Continued in the next page

Method	^{99}Mo source	Efficiency of separation of ^{99m}Tc	Advantages	Limitations
Gel based	(n,γ)^{99}Mo	>70%	Simple to operate	Low radioactive concentration of ^{99m}Tc, complicated gel production method
Chromatography (PZC)	(n,γ)^{99}Mo	>70%	Simple to operate	Slow kinetics of ^{99}Mo sorption, ^{99}Mo breakthrough

3.1.4 The present work

This chapter describes the development of two novel approaches for the development of ^{99}Mo/^{99m}Tc generator using (n,γ)^{99}Mo. In the first approach the feasibility of electrochemical separation of ^{99m}Tc from ^{99}Mo by controlled application of electrode potential is demonstrated. In the second approach two kinds of ^{99}Mo/^{99m}Tc generators were developed using two nanomaterial based sorbents (TiP and t-ZrO_2). The overall process concept, scientific basis and the development of ^{99}Mo/^{99m}Tc generators using these novel approaches have been described and the suitability of these approaches for availing ^{99m}Tc for regular use, in terms of yield and purity of ^{99m}Tc has been evaluated.

3.2 The electrochemical $^{99}Mo/^{99m}Tc$ generator

A mixture of metal ions having adequate difference in their formal potential values in an electrolytic medium can be mutually separated by selective electrodeposition of one metal on an electrode surface under the influence of controlled applied potential [121-127]. The separation of long-lived ^{99}Tc from nuclear waste by electrodeposition from its aqueous acidic solutions has been reported [128,129]. Details on the electrodeposition methods employed for the isolation of milligram amounts of ^{99}Tc from neutron irradiated Mo metal, using a copper cathode was described in 1960 [130]. But, this procedure is unsuitable for the preparation of $^{99}Mo/^{99m}Tc$ generators as the deposited Tc appeared to be metallic, firmly bound to the substrate and difficult to leach out from the cathode surface. An alternative electrochemical pathway, based on use of an alkaline electrolyte solution to deposit ^{99m}Tc as a loose adhesion on an inert metal cathode from a mixture of ^{99}Mo and ^{99m}Tc, would be ideal for radiopharmaceutical application and hence investigated. The feasibility of the method, both in terms of yield and the purity of the ^{99m}Tc for preparation of radiopharmaceuticals, has been demonstrated and evaluated.

3.2.1 Materials

^{99}Mo produced by (n,γ) route with a specific activity of 12.9 GBq (350 mCi) g^{-1} as sodium (^{99}Mo) molybdate was available in the Radiopharmaceuticals Division, BARC. Reagents such as hydrochloric acid, oxalic acid, ammonium hydroxide, etc. were of analytical grade and were procured from S.D. Fine Chemicals, Mumbai. Acidic Al_2O_3 for column chromatography was obtained from Fluka, Germany. Standard cold kits for the preparation of ^{99m}Tc labeled Dimercaptosuccinic acid (DMSA) and Ethylene dicysteine (EC) were obtained from the BRIT, India. Platinum metal wires of high purity were procured from M/s Hindustan Platinum Ltd, Mumbai, India. Paper chromatography strips were obtained

from M/s. Whatman, UK. Flexible silica gel plates (coating thickness 0.25 mm) were from J.T. Baker Chemical Company, USA.

A HPGe detector (Canberra Eurisys, France) coupled to a multichannel analyzer was used for analysis of ^{99m}Tc in the presence of ^{99}Mo. A D.C. power supply with 100 V compliance, a maximum current of 2 A, 1.2 nA current resolution and $>10^{13}$ Ohms input impedance was used for electrochemical studies. The chemical analysis for the trace level of Al^{3+} ions was done using Inductively Coupled Plasma-Atomic Emission Spectroscopy (ICP-ES JY-238, Emission Horiba Group, France).

3.2.2 Electrochemical separation of ^{99m}Tc from ^{99}Mo

3.2.2.1 Principle of separation of ^{99m}Tc from a mixture of ^{99}Mo and ^{99m}Tc

The separation of ^{99m}Tc from a mixture of ^{99}Mo and ^{99m}Tc is based on the selective electrodeposition of ^{99m}Tc on a platinum electrode. This is attributed to the difference in standard electrode potential of MoO_4^{2-} and TcO_4^- ions in alkaline media. The electrochemical reactions involved and their standard reduction potentials are as follows [131]:

$$MoO_4^{2-} + 4H_2O + 6e \rightarrow Mo + 8OH^- \quad E_0 = -1.05 \text{ V}$$

$$TcO_4^- + 4H^+ + 3e \rightarrow TcO_2 + 2H_2O \quad E_0 = +0.738 \text{ V}$$

^{99m}Tc can be selectively electrodeposited by careful control of the applied potential. The electrodeposition of long-lived ^{99}Tc ($t_{½} = 2.2 \times 10^5$ y) has been well reported in the literature [128-130]. However, Mo metal can never be electrodeposited from its aqueous solution [132]. This is because of the low hydrogen overvoltage and the high discharge overpotential of the MoO_4^{2-} ions in aqueous medium [132]. At present, Mo coatings are electrodeposited almost exclusively from their molten salts [132]. Owing to these properties, ^{99m}Tc could be electrochemically separated from ^{99}Mo, in aqueous medium. Since ^{99m}Tc is continuously produced in the electrolyte as a result of the radioactive decay of ^{99}Mo, repeated electrodeposition is a feasible means to avail ^{99m}Tc from the same electrolyte solution.

3.2.2.2 The electrochemical set-up

A schematic diagram of the electrochemical cell is shown in **Fig. 3.2** and is briefly described as follows. The electrochemical cell consisted of a quartz vial (24 × 40 mm, 20 mm ID) and a teflon cap with a small hole (~2.5 mm) for venting off any gases. The electrodes used were made of high purity platinum wires (60 mm length, 1.5 mm diameter), which were fitted on the mouth of the glass vial, parallel to each other, 5 mm apart and connected to the power supply. In the electrochemical cell, platinum was used as the electrode material as it is inert and hence suitable for repeated effective removal of the deposited ^{99m}Tc without addition of chemical impurities. The electrolysis was carried out in a single 'electrolysis cell', in order to reduce the radiation exposure and to maintain the inventory of ^{99}Mo. In order to minimize the radiation exposure to the operating personnel, the whole system was housed in a 100 mm lead container.

3.2.2.3 Optimization of parameters for the electrochemical separation of ^{99m}Tc from ^{99}Mo

A number of factors were observed to have marked effect on the selective deposition of ^{99m}Tc, both in terms of yield and quality. In order to obtain consistent deposition of ^{99m}Tc with minimal contamination of ^{99}Mo, thorough optimization of electrolysis parameters was found to be essential and hence pursued. 37 MBq (1 mCi) of ^{99}Mo/^{99m}Tc was used for the optimization experiments. The electrolytic separation of ^{99m}Tc from ^{99}Mo was tried in different electrolytes over a period of 1 week. The electrodeposition yield of ^{99m}Tc and the percentage of ^{99}Mo impurity associated in the deposits were monitored in each case. Various parameters such as the nature of the electrolyte, pH of the electrolyte, applied potential and electrodeposition time were optimized to obtain the maximum yield of ^{99m}Tc.

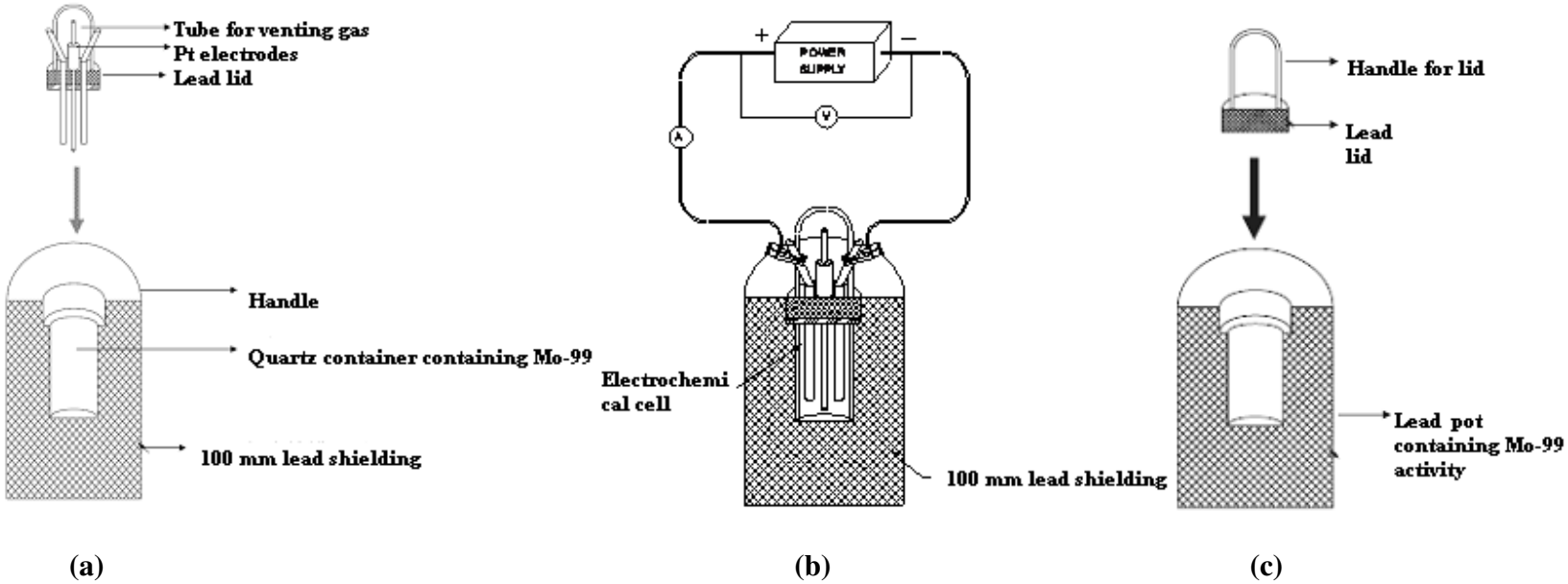

Fig. 3.2: Schematic diagram of the electrochemical $^{99}Mo/^{99m}Tc$ generator (a) Assembly of electrochemical set-up (b) Electrochemical cell in a lead shielded container (c) Storage of $^{99}Mo/^{99m}Tc$ solution

3.2.2.3.1 Choice of the electrolyte

Since the target MoO_3 can be dissolved either in acidic or alkaline medium, it was important to initially assess the electrodeposition of ^{99m}Tc in various electrolyte media, for deciding the medium to be used in the further optimization process. The results are summarized in **Table 3.2**. Electrodeposition of ^{99m}Tc in nitric acid medium was not pursued owing to the consumption of cell current by the nitrate ions [129].

Table 3.2: Performance of electrochemical separation of ^{99m}Tc in different media

Medium	Time of electrodeposition (min)	^{99m}Tc deposition yield (%)	^{99}Mo impurity (%)	Performance over a period of 1 week
0.1 M HCl	150	>90%	2.9%	Consistent
0.1 M H_2SO_4	90	>90%	2.3%	Consistent
0.1 M oxalic acid	20	>99%	5.1%	Low ^{99m}Tc yield after first separation
0.5 M NaOH	60	>93%	0.1%	Consistent

(n = 3)

Although the electrodeposition of ^{99m}Tc was feasible in other mineral acids such as HCl and H_2SO_4, they seemed unsuitable for this purpose as the deposited ^{99m}Tc was associated with significant amounts of ^{99}Mo impurity and longer deposition time was needed to achieve satisfactory yields. Hence, further investigations in these media were discontinued. Use of oxalic acid solution was tried since it is reported that oxalate ions favor electrodeposition of Re from ReO_4^- solution [133]. The electrochemical behavior of Re and Tc ions are expected to be similar. However, this approach was unsuccessful as this resulted in significant amount of ^{99}Mo deposition along with ^{99m}Tc. Among the electrolytic media studied, the most suitable medium for separation of ^{99m}Tc from ^{99}Mo was found to be NaOH solution, wherein ^{99}Mo exists as sodium molybdate. ^{99m}Tc could be selectively electrodeposited with >92% yield and

the level of ^{99}Mo impurity present in it was only ~0.1%. However, in order to further optimize the extent of alkalinity to be used, the effect of pH of the electrolyte in the alkaline range was studied.

3.2.2.3.2 Effect of the pH of the electrolyte

The pH of the electrolytic solution was varied from neutral (pH 7) to an alkalinity of 1 N NaOH (pH 14) to gauge if the role of alkalinity is crucial in determining the efficiency of ^{99m}Tc electrodeposition. The results are summarized in **Table 3.3**.

Table 3.3: Effect of pH on the electrodeposition yield of ^{99m}Tc

pH of the electrolyte	Yield of ^{99m}Tc (%)	Associated ^{99}Mo impurity in ^{99m}Tc (%)
7	59±5	5±1
8	62±3	3.1±0.5
9	67±2	1.3±0.2
10	72±3	0.8±0.1
11	79±2	0.6±0.1
12	88±1	0.15±0.08
13	92±1	<0.1
14	93±2	<0.1

(n = 3, '±' indicates standard deviation)

In pH range 7-12, the yield of ^{99m}Tc gradually increased from a low value with increase in pH and reached a maximum at pH 13, remaining almost the same till pH 14. Further, it was observed that, if the electrodeposition was carried out at pH <13, the electrodeposition yield of ^{99m}Tc from the same feed solution decreased significantly after the first electrolysis and some fine black particles were observed in the electrolyte. The black particles were probably reduced molybdenum oxide species in which ^{99m}Tc got trapped and hence could not be electrodeposited. From these studies, it could be inferred that pH <13 was not suitable for

electrochemical separation of ^{99m}Tc from ^{99}Mo and hence it was essential to adjust the pH of the electrolytic solution to ~13-14 prior to every electrolysis step. It was decided to keep the pH at 13 in further optimization experiments, in order to handle the alkali at the minimum concentration possible.

3.2.2.3.3 Effect of the applied potential

The effect of applied potential on electrodeposition of ^{99m}Tc from 0.1 N NaOH solution at room temperature is shown in **Table 3.4**.

Table 3.4: Effect of applied potential on the electrodeposition yield of ^{99m}Tc

Potential (V)	**Current (mA)**	**^{99m}Tc deposition yield (%)**
1	10	4±1
2	40	11±2
3	140	29±4
4	250	40±3
5	500	94±2
6	750	>99
7	900	>99

(n = 3, '±' indicates standard deviation)

The percentage of ^{99m}Tc deposited increased with increasing potential and approached the maximum value at ~5 V, and therefore this potential was adapted in all subsequent experiments. At a potential higher than 5 V, although the electrodeposition yield of ^{99m}Tc increased marginally, black particles were observed in the electrolyte solution and the yield of ^{99m}Tc decreased drastically on subsequent electrolysis when the same ^{99}Mo feed solution was used, after allowing time for in-growth of ^{99m}Tc.

3.2.2.3.4 Effect of the time of electrodeposition

The effect of time on the electrodeposition yield of ^{99m}Tc is shown in **Fig. 3.3**. As seen from the figure, the ^{99m}Tc deposition yield increases with time, reaching a maximum value at ~45 min. Hence, electrolysis was carried out for 45 min in all subsequent experiments.

3.2.2.4 Effect of Mo concentration on the separation efficiency

Several experiments were carried out to evaluate the efficiency of the method to separate ^{99m}Tc using range of ^{99}Mo solutions of different specific activity. The simulated ^{99}Mo solutions of different specific activities were prepared by dissolving non-radioactive sodium molybdate in 100 mL of 0.5 N NaOH.

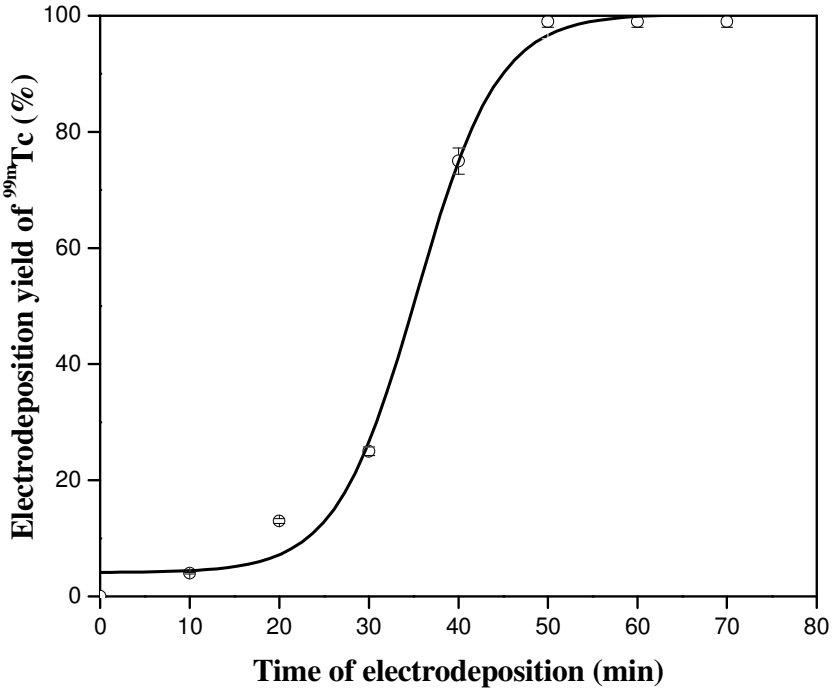

Fig. 3.3: Effect of time on the electrodeposition yield of ^{99m}Tc

The resulting solutions were each spiked with 185 MBq (5 mCi) of ^{99}Mo. The electrolysis was carried out under the optimized conditions and the deposition yield and radionuclidic purity of ^{99m}Tc was monitored. The results **(Table 3.5)** demonstrate that the efficiency of

separation and purity of ^{99m}Tc is independent of the specific activity of ^{99}Mo used. The process could be used for the separation of ^{99m}Tc from ^{99}Mo of specific activity as low as 1.85 GBq (50 mCi) g^{-1}. The level of ^{99}Mo impurity present in ^{99m}Tc was always ~0.1% and could easily be removed by a purification step using a column of alumina.

Table 3.5: Effect of specific activity of ^{99}Mo on the selective electrodeposition of ^{99m}Tc

Specific activity of ^{99}Mo (GBq g^{-1})	Yield of ^{99m}Tc (%)	^{99}Mo impurity in ^{99m}Tc (%)
18.5	92±1	0.09±0.01
14.8	93±2	0.08±0.03
11.1	93±3	0.12±0.02
7.4	91±1	0.18±0.04
3.7	90±1	0.14±0.02
1.85	94±3	0.11±0.06

(n = 3, '±' indicates standard deviation)

For electrodeposition of ^{99m}Tc from its aqueous solution, the applied potential must be set to a value more cathodic than the redox half-cell potential of Tc. In order to achieve quantitative deposition of ^{99m}Tc within a reasonable period of time, a potential much higher than the standard reduction potential (E_o) was required for depositing ^{99m}Tc. The evolution of hydrogen gas at that high potential facilitates a non-adherent deposit of ^{99m}Tc on the electrode surface. The deposited ^{99m}Tc is expected to be a mixture of Tc(0) and oxide/hydroxide of Tc(IV) [134], which could be easily detached from the electrode surface for radiopharmaceutical applications. The ^{99m}Tc deposit was electrochemically dissolved into saline solution in $^{99m}TcO_4^-$ form, by application of reverse potential.

3.2.3 Process demonstration: Development of ^{99}Mo/^{99m}Tc generator

After optimization of electrodeposition parameters, further experiments were carried out using 9.25 GBq (250 mCi) of ^{99}Mo activity as 5 mL of $Na_2{}^{99}MoO_4$ solution. The

electrochemical cell (**Fig. 3.2**) was placed in a lead shielded assembly. In order to examine the efficiency of the electrochemical separation, the process demonstration run was performed over 5 batches. Prior to every electrolysis, the alkalinity of the electrolyte solution was checked and adjusted to pH ~13 by adding 0.5 N NaOH solution if required. Electrolysis was performed by applying a constant potential of 5 V (current 450 mA, current density 328 mA cm^{-2}), for 50 min. After the electrolysis, the electrodes were moved up from the cell along with the lead cap while maintaining the potential and turned off after removal. An identical lead cap with acrylic lining but without electrodes was placed on the quartz cell for radiation shielding (**Fig. 3.2**). The electrodeposited ^{99m}Tc could be brought into saline (0.9% NaCl) solution by placing the electrode in a narrow (1 mL) glass vial (0.5 cm diameter) containing 500 μL of saline solution. A new Pt electrode was also dipped in the solution and the polarity of the cathode was reversed. A high voltage (10 V) was applied for ~20 s and both the electrodes were taken out from the solution after switching off the current. The $^{99m}TcO_4^-$ solution obtained above was passed through a small column (10 mm × 2 mm) containing 200 mg of alumina, preconditioned with normal 0.9% saline to remove any traces of ^{99}Mo that might be present. The yield of ^{99m}Tc after the first electrolysis step was 96±3%. However, it was associated with trace amounts of ^{99}Mo contamination (~0.1%), which could be removed by passing the solution through the alumina column. The trace level of ^{99}Mo was retained by the alumina column and the bulk of the ^{99m}Tc activity that eluted out was a colorless solution at pH ~7. The ^{99}Mo level in this solution was <0.001%. The purification step reduced the overall yield of ^{99m}Tc by about 3-5%. The performance of a typical batch is illustrated in **Table 3.6**. The overall performance of the ^{99}Mo/^{99m}Tc generator remained nearly consistent over a period of 10 days, which is normally the shelf-life of a ^{99}Mo/^{99m}Tc generator, with marginal tendency to dip towards the end of the life.

Table 3.6: Performance of the electrochemical $^{99}Mo/^{99m}Tc$ generator in a typical batch

S. No.	Activity of ^{99}Mo (GBq)	Time of growth (h)	Theoretical activity of ^{99m}Tc (GBq)	Activity of ^{99m}Tc obtained (GBq)		Overall efficiency of the generator (%)
				After first step	After purification	
1	9.25	24	5.84	5.46	5.28	90.4
2	7.19	24	4.54	4.34	4.16	91.6
3	5.58	24	3.52	3.24	3.16	89.8
4	4.34	24	2.73	2.62	2.51	91.9
5	3.37	24	2.12	1.99	1.90	89.6
6	2.62	24	1.65	1.59	1.50	90.9
7	2.04	48	1.08	0.92	0.88	81.5
8	1.23	24	0.78	0.72	0.69	88.4
9	0.96	24	0.61	0.55	0.52	85.2

3.2.4 Maintenance of the ^{99}Mo feed solution and the electrodes after each electrolysis

The inventory of ^{99}Mo was carefully maintained during the shelf-life of the $^{99}Mo/^{99m}Tc$ generator. During the course of electrolysis, the pH of the $Na_2{}^{99}MoO_4$ solution decreased slightly. It was essential to maintain the pH of the electrolyte at ~13, after the end of electrolysis. If the pH of the solution was not maintained at ~13, black particles were observed in the electrolyte and the electrodeposition yield of ^{99m}Tc decreased substantially in the subsequent electrolysis. Therefore, 1 mL of 0.5 N NaOH solution was added to the ^{99}Mo electrolyte solution, after every electrolysis.

After each batch of electrolysis, in order to make the electrodes ready for subsequent experiments, they were washed with 3 M HNO_3 and subjected to electrolytic cleaning by applying a positive potential of 10 V for 15 min. The platinum electrodes were then washed

with water followed by washing with acetone. The cleaning of the electrodes was essential in order to get reproducible results. It was observed that if the platinum cathodes were not cleaned after 2-3 batches, the electrodeposition yield of ^{99m}Tc was very low (<40%) from the subsequent batches. This was probably due to the passivation of the platinum plates during electrolysis. The washing of the electrodes with nitric acid solution removed the trace level of metal ions deposited on the surface of the electrode. Further, the electrolytic cleaning of the electrodes removed all the ions which could not be removed by dissolution in acid. Moreover, it also removed the adsorbed hydrogen gas and thus activated the electrodes.

3.2.5 Quality control of ^{99m}Tc

3.2.5.1 Radionuclidic purity

In order to utilize ^{99m}Tc availed from the generator for medical applications, the presence of radionuclidic impurities in the form of the parent radioisotope (^{99}Mo) must be within the prescribed limits of $<10^{-2}$ % [135]. The level of ^{99}Mo impurity in the ^{99m}Tc eluate was studied by several means. In order to rapidly estimate the ^{99}Mo impurity in ^{99m}Tc immediately after its separation, a lead container of 4 mm wall thickness was used, wherein the 140 keV photon of ^{99m}Tc got nearly completely cut off (the half-value thickness for ^{99m}Tc is 0.3 mm of lead and 4 mm thick lead would attenuate the radiation flux by a factor of ~10000) and the level of ^{99}Mo impurity could be determined as per the reported procedure [136]. The rapid analysis of ^{99m}Tc by lead shielding method revealed that the amount of ^{99}Mo impurity present in it was <0.1% [136]. The ^{99m}Tc activity was allowed to decay for 1 day, during which its activity was measured using a NaI (Tl) detector. The decay profile of ^{99m}Tc is shown in **Fig. 3.4**. The half life of ^{99m}Tc derived from this data was 6.1 ± 0.3 h (n =5), which agrees well with the literature value of 6.02 h.

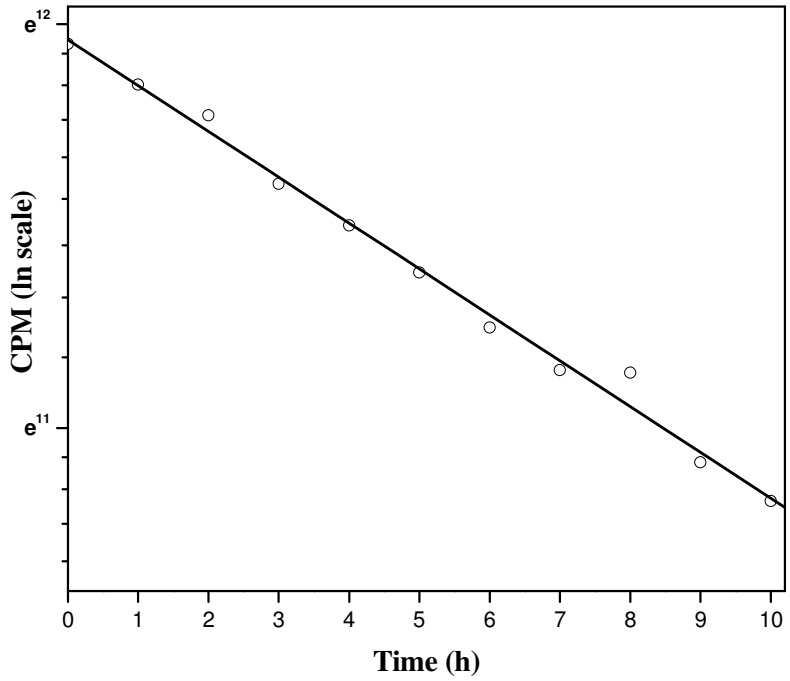

Fig. 3.4: Decay profile of ^{99m}Tc

^{99m}Tc eluted from the generator was examined in a HPGe detector to see the presence of any γ-rays peaks corresponding to ^{99}Mo. The γ-spectrum of ^{99m}Tc as illustrated in **Fig. 3.5**, did not show the presence of such peaks, thereby confirming the absence of ^{99}Mo in the eluted ^{99m}Tc. The analysis of the decayed samples of ^{99m}Tc by γ-spectroscopic technique revealed that the level of ^{99}Mo present in the eluate was $<10^{-3}$ % in all the batches of ^{99m}Tc, which was well within the stipulated limits [135].

3.2.5.2 Radiochemical purity

The radiochemical purity of $^{99m}TcO_4^-$ was determined by paper chromatographic technique. 5 μL of the activity was applied on a paper chromatographic strip (Whatman 12 cm ×1 cm) at 1.5 cm from the lower end. The strip was developed in 0.9% NaCl solution. After the chromatography, the paper strip was dried, and cut into 1 cm pieces and counted in a NaI(Tl) counter. The paper chromatographic pattern **(Fig. 3.6)** of ^{99m}Tc in 0.9% NaCl

solution reveals that >99% of ^{99m}Tc was present as $^{99m}TcO_4^-$, which was well above the prescribed limits of ≥95% as per the Pharmacopoeias [135].

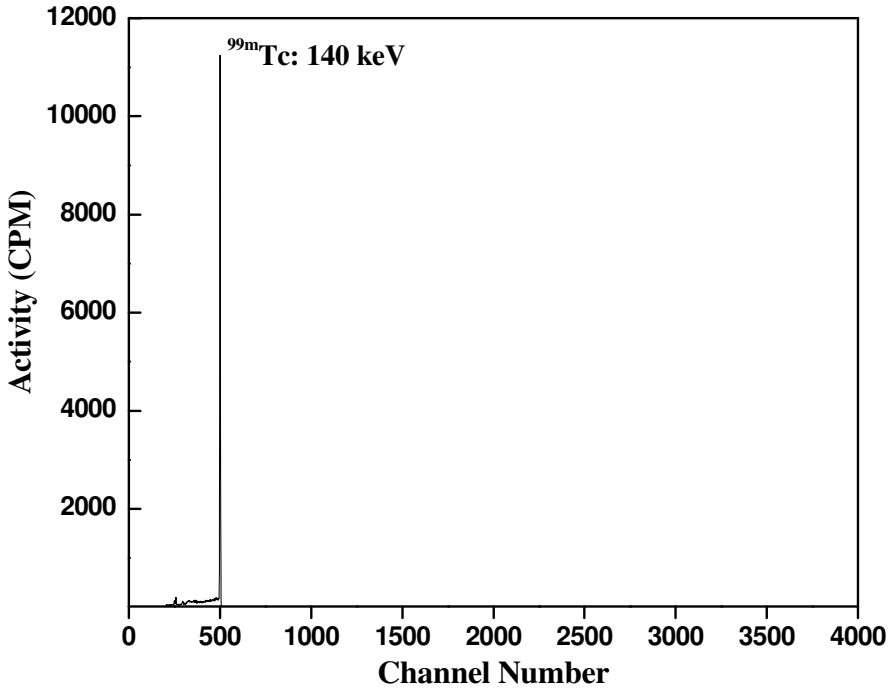

Fig. 3.5: Gamma spectrum of ^{99m}Tc

3.2.5.3 Chemical purity

In order to determine the presence of Al^{3+} ions contaminating the ^{99m}Tc product, the ^{99m}Tc samples were allowed to decay for 20 days. The trace levels of Al^{3+} ion contamination in the decayed samples were determined by ICP-AES. The limit for $A1^{3+}$ in ^{99m}Tc obtained from alumina column generator is stipulated to be 20 μg of Al mL^{-1} (20 ppm) [135]. ICP-AES analysis of the decayed samples of ^{99m}Tc solutions indicated less than <0.1 ppm of Al^{3+} ions, which was far below the permissible level.

3.2.6. Labeling efficacy of ^{99m}Tc

In order to examine the suitability of $^{99m}TcO_4^-$ obtained from the generators, for radiolabeling studies, it was complexed with commonly available ligands like DMSA and EC using standard kits.

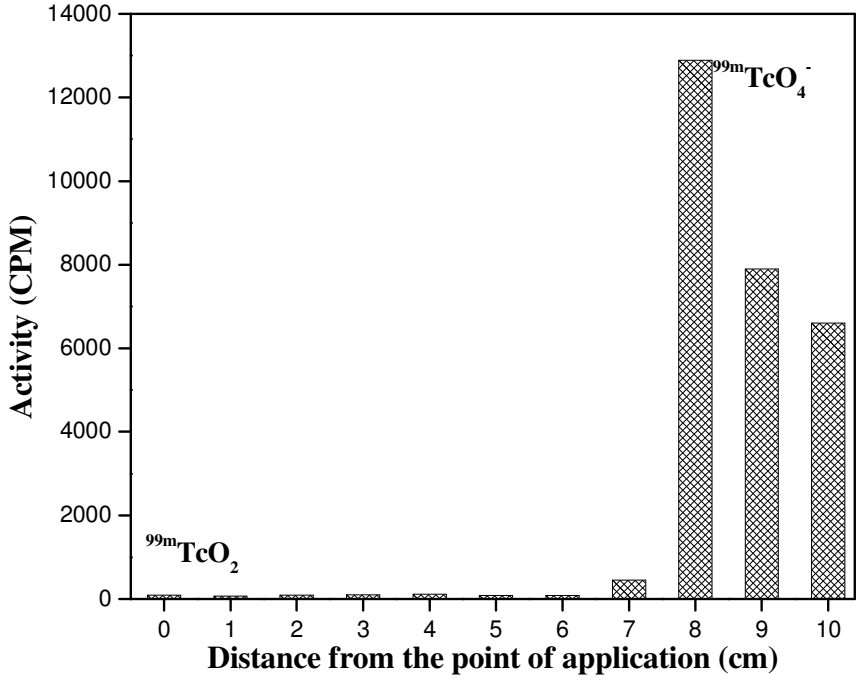

Fig. 3.6: Paper chromatography pattern of ^{99m}Tc in 0.9% NaCl solution

The paper chromatography patterns for ^{99m}Tc-EC and ^{99m}Tc-DMSA are shown in **Fig. 3.7.** In TLC using acetone as solvent, the complexes remained at the point of application. Under identical conditions, $^{99m}TcO_4^-$ moved towards the solvent front. However, if reduced hydrolyzed technetium ($^{99m}TcO_2$) is present, it will also remain at the origin and hence an additional quality control procedure was essential to estimate the radiochemical impurity of reduced hydrolyzed technetium in the complex. In paper chromatography, using 50% acetonitrile in water as eluting solvent for ^{99m}Tc-EC and 0.9% NaCl solution for ^{99m}Tc-DMSA, both free $^{99m}TcO_4^-$ as well as the complexes migrated towards the solvent front, whereas reduced hydrolyzed technetium remained at the origin. By combining the results of both the paper chromatography patterns, the complexation yield was estimated to be >98% in both the cases. These results justify the suitability of ^{99m}Tc obtained from the generator for preparation of radiopharmaceuticals.

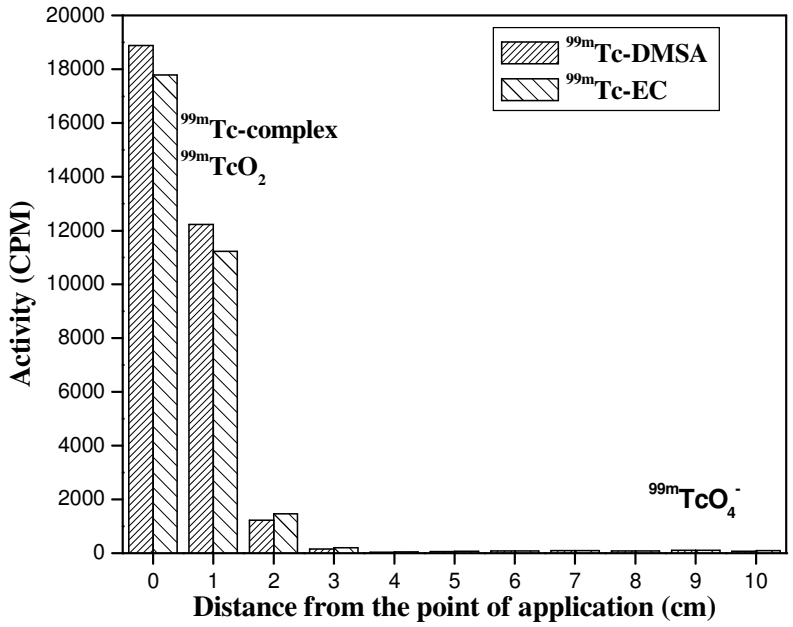

(a)

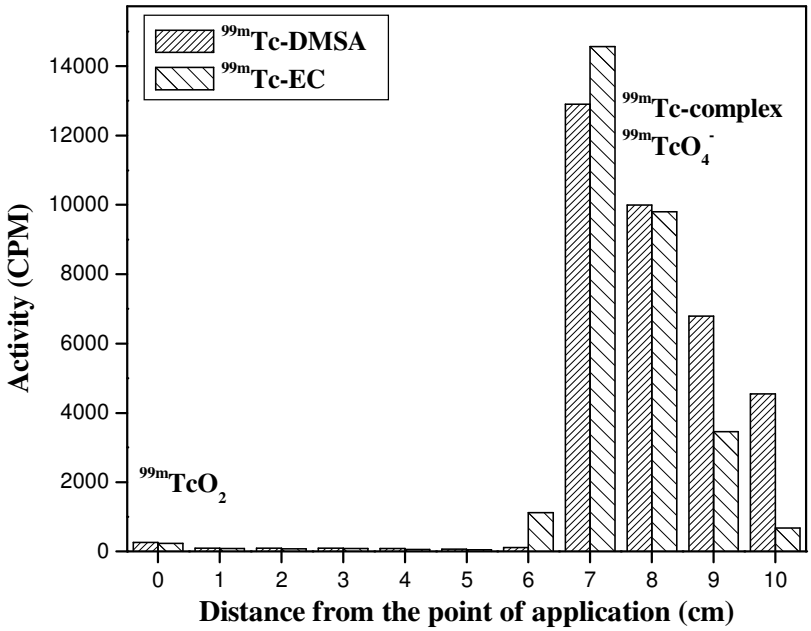

(b)

Fig. 3.7: Paper chromatographic patterns of ^{99m}Tc-DMSA and ^{99m}Tc-EC complexes developed in (a) acetone and (b) 50% acetonitrile in water (v/v) for ^{99m}Tc-EC and 0.9% NaCl solution for ^{99m}Tc-DMSA

3.2.7 Advantages of the electrochemical $^{99}Mo/^{99m}Tc$ generator

The major advantage of this technique is that there is no restriction on the specific activity of ^{99}Mo that can be used. Even while using medium to low specific activity $(n,\gamma)^{99}Mo$, ^{99m}Tc can be obtained with acceptable radioactive concentration and purity for clinical applications. The purity of ^{99m}Tc was comparable to that obtained from the standard alumina column generators containing fission ^{99}Mo. The same electrodes were used for repeated separations during 1 year time period without any sign of physical or chemical deterioration. Further, the separation process involves simple electrochemistry and is therefore, amenable for automation. The adaptation of this technique extends the shelf-life life of a $^{99}Mo/^{99m}Tc$ generator to a considerable extent and is therefore economical. The prospects of using the electrochemical $^{99}Mo/^{99m}Tc$ generator system in a centralized radiopharmacy appear promising. The proposed route could be one of the prospective options to avail ^{99m}Tc without using fission ^{99}Mo and thus might contribute to the regional needs.

3.2.8 Conclusions

The potential utility of electrochemical method for the preparation of $^{99}Mo/^{99m}Tc$ generator using (n,γ) ^{99}Mo was demonstrated. The electrodeposition process is simple, highly efficient and could be carried out at room temperature. It uses relatively inexpensive equipments, and the deposited ^{99m}Tc could be easily recovered with >90% yield and high radionuclidic and radiochemical purity. The compatibility of the product in the preparation of ^{99m}Tc labeled formulations was evaluated and found to be satisfactory. In this separation technique, there is no restriction on specific activity of ^{99}Mo that could be used and no requirement for post-elution concentration of ^{99m}Tc. In order to demonstrate the accomplishments, additional work is being conducted in the Radiopharmaceuticals Division, BARC to test the system at higher level of activity. This new generator allows for a non-fission based method of producing and recovering ^{99m}Tc. Though, this alternative strategy

may not be enough to fill the shortage of fission ^{99}Mo, it can serve as an option for accessing ^{99m}Tc, particularly in countries with medium flux research reactors for radioisotope production.

3.3 The $^{99}Mo/^{99m}Tc$ generators using nanomaterials as sorbents

The conventional inorganic sorbents like alumina have low sorption capacity due to the limited number of active sites and relatively low accessible surface area. Owing to the low specific activity of ^{99}Mo produced by (n,γ) method, chromatographic generators prepared using such sorbents would require much larger size columns, which in turn would necessitate larger shields. ^{99m}Tc availed from these generators have very low radioactive concentration and hence unsuitable for radiopharmaceutical applications. Moreover, distribution of such bulky generators to hospital sites is not a feasible or economical proposition. Hence, such sorbents cannot be used for the preparation of $^{99}Mo/^{99m}Tc$ generators utilizing low specific activity $(n,\gamma)^{99}Mo$. One of the effective approaches to increase their accessible surface area and active sites is to nanoengineer the bulk particles. The surface atoms of nanoparticulate metal oxides are unsaturated, exhibit intrinsic surface reactivity and can be used in the chromatographic separation of metal ions [69,70,137,138]. In this section, the feasibility of using nanomaterials as potential new generation sorbents for the preparation of $^{99}Mo/^{99m}Tc$ generator has been evaluated. Two novel $^{99}Mo/^{99m}Tc$ generators were developed using polymer embedded nanocrystalline titania (TiP) and tetragonal nano-zirconia (t-ZrO_2) as the sorbents. TiP and t-ZrO_2 were selected for this purpose mainly because of the effectiveness of hydrous titania and zirconia as ion-exchangers for the separation of metal ions [70,137,138]. The effectiveness of these sorbents in the development of $^{99}Mo/^{99m}Tc$ generator and suitability of ^{99m}Tc for radiopharmaceutical applications was demonstrated and is detailed here.

3.3.1 Materials

Reagents such as hydrochloric acid, ammonium hydroxide, isopropyl alcohol etc. were of analytical grade and were procured from S.D. Fine Chemicals, Mumbai, India. $ZrOCl_2.8H_2O$ (99.9%) and $TiCl_4$ (99.9%) was obtained from E. Merck, Darmstadt, Germany.

Dimercaptosuccinic acid (DMSA) and Ethylene Dicysteine (EC) kits were obtained from the Board of Radiation and Isotope Technology, Navi Mumbai, India. Paper chromatography strips were purchased from Whatman International Limited, Maidstone, England. Molybdenum-99 (specific activity 11.1-18.5 GBq (300-500 mCi g^{-1}) as Sodium (^{99}Mo) Molybdate was available in the Radiopharmaceuticals Division, BARC. For the determination of the distribution ratio of ^{99}Mo in t-ZrO_2, lower specific activity ^{99}Mo (~11.1 GBq g^{-1}) was used while for the preparation of the ^{99}Mo/^{99m}Tc generator, freshly produced ^{99}Mo of higher specific activity (~18.5 GBq g^{-1}) was used.

Gamma activity of ^{99m}Tc was assayed using a NaI (Tl) scintillation counter (100-160 keV). HPGe detector coupled with a multichannel analyzer (MCA) (Canberra Eurisys, France) with a 1.5 keV resolution at 1333 keV and range from 1.8 keV to 2 MeV was used for the analysis of ^{99}Mo in the presence of ^{99m}Tc and also for quantitative estimation. The radioisotope levels were determined by quantification of the photo peaks corresponding to ^{99m}Tc [140 keV (88.97%)] and ^{99}Mo [181 keV (6%) and 740 keV (12.2%)].

3.3.2 Separation of ^{99m}Tc from ^{99}Mo

3.3.2.1 Synthesis of TiP and t-ZrO_2

The synthesis of TiP and t-ZrO_2 sorbents was carried out as per the procedure described in Chapter 2. Owing to the simple and reliable synthesis procedure using commercially available chemicals, large scale preparation of these materials could be achieved in the laboratory. The salient features of the adapted synthesis procedures were (i) nano-sized oxides (<10 nm) could be prepared at low temperatures, (ii) the products were homogeneous and had high surface area, (iii) the particles were porous and exhibited excellent flow characteristics. An important property of these materials is their extremely low solubility in dilute mineral acids and alkalis, which is crucial for chromatographic applications. The materials are capable of preserving its physicochemical and sorption

properties over long use. Subsequent investigations were directed towards the selection of the optimal experimental conditions necessary to separate ^{99m}Tc from ^{99}Mo.

3.3.2.2 Determination of distribution ratios (K_d) of $^{99}MoO_4^{2-}$ and $^{99m}TcO_4^-$ ions

The distribution ratios (K_d) of $^{99}MoO_4^{-2}$ and $^{99m}TcO_4^-$ ions at different pH were evaluated in order to predict the experimental conditions necessary for the optimal loading of ^{99}Mo as well as efficient elution of ^{99m}Tc. Distribution ratios of MoO_4^{2-} and TcO_4^- ions for both the sorbents were determined at different pH, using ^{99}Mo and ^{99m}Tc radiotracers. For estimation of K_d values for ^{99}Mo, ^{99}Mo/^{99m}Tc mixture was used, while for ^{99m}Tc, pure ^{99m}Tc was used. In each experiment, 200 mg of sorbent was suspended in 20 mL solution containing the radioactive metal ions, in a 50 mL stoppered conical flask. The flasks were shaken in a wrist arm mechanical shaker for 1 h at 25 °C and then filtered. The activities of the solution before and after equilibration were measured in a HPGe counter using an appropriate γ-ray peak (140 keV for ^{99m}Tc and 181 keV for ^{99}Mo). The distribution ratios were calculated using the following expression:

$$K_d = \frac{(A_i - A_{eq})V}{A_{eq}\, m}$$

where, A_i is the initial total radioactivity of 1 mL the solution, A_{eq} is the unadsorbed activity in 1 mL of the solution at equilibrium, V is the solution volume (mL) and m is the mass (g) of the sorbent. The distribution ratio (K_d) results for $^{99}MoO_4^{2-}$ and $^{99m}TcO_4^-$ ions in TiP and t-ZrO_2 at different pH conditions are summarized in **Table 3.7** and **Table 3.8**, respectively. It is apparent from the respective tables that in both the sorbents, the K_d values for MoO_4^{2-} and TcO_4^- ions attained the maximum value at ~pH 3 and hence this medium is suitable for sorption of ^{99}Mo. For both the sorbents, in 0.9% NaCl solution, the high K_d values for ^{99}Mo clearly indicate that it can be efficiently retained by the sorbent, while the low K_d values for ^{99m}Tc indicate that it shall not be retained and hence eluted out easily.

Table 3.7: Distribution ratios (K_d) of $^{99}MoO_4^{2-}$ and $^{99m}TcO_4^-$ ions in TiP

Medium (pH)	K_d	
	$^{99}MoO_4^{2-}$	$^{99m}TcO_4^-$
1	146±5	3±1
2	188±4	14±2
3	489±12	41±6
4	362±5	33±2
5	225±6	3.2±0.9
6	74±2	0.3±0.1
7	14±4	0.2±0.1
8	11±2	0.5±0.1
0.9% NaCl	216±7	0.3±0.2

n = 3, '±' indicates standard deviation

In order to get a better insight about the sorption behavior of polymolybdate anions on TiP and t-ZrO_2, it was felt necessary to compare the K_d values of ^{99}Mo and ^{99m}Tc ions with the zeta potential of the sorbents determined at various pH values. The effect of pH on zeta potential of TiP and t-ZrO_2 in aqueous solution were shown in **Fig. 2.4** and **Fig. 2.12**, respectively. It is clearly evident from the figures that interaction of TiP and t-ZrO_2 particles with aqueous solutions imparts a pH-dependent charge on surface of the nanomaterials. In case of TiP, the zeta potential values were positive in the pH range 1-6, whereas in the case of t-ZrO_2, the values were positive in the pH range 1-4. On further increase in pH of the solution, the zeta potential of the sorbents became zero (isoelectric point, IEP) and then the sorbents developed negative zeta potentials. It could be inferred that the pH value of the ^{99}Mo feed solution must be less than the pH corresponding to the IEP of the sorbents (pH value of ~6.5 for TiP and ~4.5 for t-ZrO_2), under which condition the sorbents possess positive

charges, facilitating the sorption of anionic polymolybdate species. These observations were in agreement with the K_d values, in case of both the sorbents.

Table 3.8: Distribution ratios (K_d) of $^{99}MoO_4^{2-}$ and $^{99m}TcO_4^-$ ions in t-ZrO_2

Medium (pH)	K_d	
	$^{99}MoO_4^{2-}$	$^{99m}TcO_4^-$
1	129±7	3±2
2	295±18	14±3
3	611±22	35±1
4	560±17	29±4
5	525±9	2.7±0.8
6	174±8	0.3±0.1
7	34±2	0.1±0.1
8	10±1	0.6±0.2
0.9% NaCl	270±5	0.2±0.1

n = 3, '±' indicates standard deviation

The dependence of zeta potential of the nanomaterials on the pH of the external solution, helps in investigating the sorption mechanism. In aqueous systems, TiP and t-ZrO_2 particles are hydrated, and ≡M-OH (M = Ti or Zr) groups cover their surface completely. These amphoteric hydroxyl groups on the surface of the nanomaterials can undergo reaction with either H^+ or OH^- and develop positive or negative charges on the surface depending on the pH [139]. In weakly acidic solution, molybdate polymerizes as follows [140]:

$$7\,MoO_4^{2-} + 8\,H^+ \rightleftharpoons Mo_7O_{24}^{6-} + 4H_2O$$

There is a strong attractive interaction between the positively charged TiP and t-ZrO_2 surfaces and the negatively charged species from the liquid solution. The mechanism of ^{99}Mo

uptake therefore may be considered to take place in two steps. The first one may be the exchange of polymolybdate anions for hydroxyl ions on the surfaces of the particles. Subsequently, it may form a stable complex of the type $[MMo_6O_{24}]^{8-}$ (M = Ti or Zr), similar to that reported with alumina [141]. The decay of ^{99}Mo to ^{99m}Tc is not accompanied by any serious disruption of chemical bonds. As these polymolybdate ions start transforming into pertechnetate ion, which has only -1 charge, the binding would get weaker. Moreover, saline solution used for elution of ^{99m}Tc has pH ~7 and in case of both the sorbents the zeta potential values are negative at that pH. Owing to electrostatic repulsion, $^{99m}TcO_4^-$ gets easily eluted with normal 0.9% saline. However, in order to predict the exact mechanism of ^{99}Mo uptake, further studies are warranted which is beyond the scope of this work.

3.3.2.3 Determination of the time of equilibration

The time durations required for the complete sorption of the ^{99}Mo onto TiP and t-ZrO_2 sorbents were studied by following the distribution ratio (K_d) at different time intervals. The K_d values (mean of three experiments) were taken as an indication of the progress of the sorption process. The distribution ratio (K_d) of $^{99}MoO_4^{2-}$ ions in 0.001 M HNO_3 solution was determined at different time intervals (5-60 min), as described above. The time when K_d remained unchanged, was taken as the indication of the attainment of equilibrium. For TiP, the plot of K_d versus time is shown in **Fig. 3.8**. As inferred from the curve, a contact period 35 minutes was maintained for all equilibrium experiments. In case of t-ZrO_2, it was observed that the K_d values remained almost constant (~600) after all the time intervals, which indicated that the equilibrium was reached within 5 minutes.

3.3.2.4 Determination of sorption capacity of TiP and t-ZrO_2

3.3.2.4.1 Static sorption capacity

The static sorption capacity of the respective sorbents for Mo ions was determined by batch equilibration method. 0.5 g aliquots of accurately weighed sorbent were taken in a

stoppered conical flask and equilibrated with 50 mL of sodium molybdate solution (10 mg of Mo mL^{-1}) spiked with ~3.7 MBq (100 μCi) of ^{99}Mo for 30 min at room temperature.

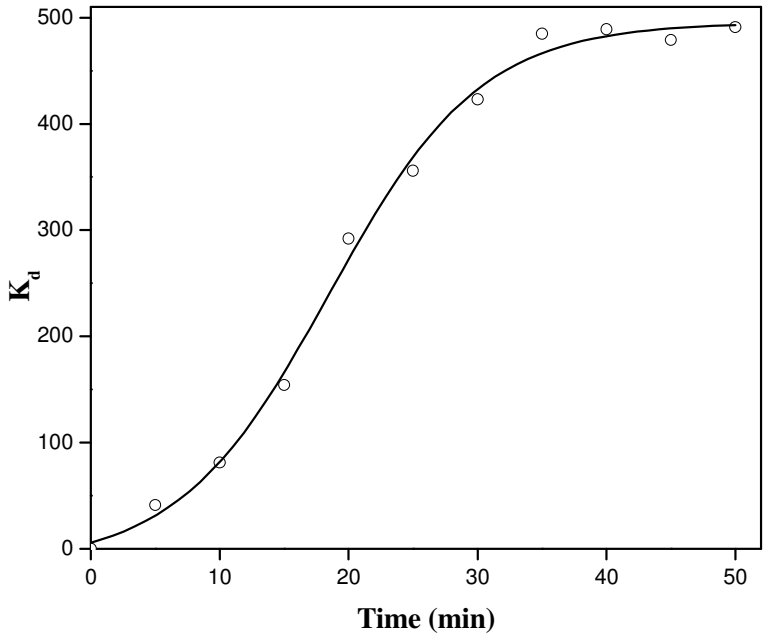

Fig. 3.8: Variation in K_d values of $^{99}MoO_4^{2-}$ ions with time using TiP as sorbent

At the end, the contents were filtered through a Whatman filter paper (No. 542). The activities of ^{99}Mo in the solution before and after absorption were estimated by using HPGe detector coupled to a multichannel analyzer, by measuring the counts at 181 keV peak corresponding to ^{99}Mo in 1 mL aliquots. All measurements were carried out at 25° C in triplicate. The sorption capacity was calculated using the following expression:

$$\text{Capacity} = \frac{(A_o - A_e)V.C_o}{A_o\, m}$$

where A_o and A_e represented the radioactivity of ^{99}Mo in 1 mL of supernatant solution before and after sorption, respectively, C_o was the total Mo content (10 mg) in 1 mL of solution before sorption, V was the volume of solution and m was the mass (g) of the sorbent. The values of the static sorption capacities were 108±6 mg Mo g^{-1} for TiP and 250±10 mg Mo g^{-1}

for t-ZrO_2 (n = 10) These results clearly illustrate the superiority of these materials over alumina which has a sorption capacity of only 2-20 mg Mo g^{-1} [42].

3.3.2.4.2 Dynamic sorption capacity

In order to estimate the Mo sorption capacity under dynamic conditions, two borosilicate glass columns of dimension 15 cm (l) × 0.4 cm (i.d.) with sintered disc (G_0) at the bottom were packed with 0.5 g of the respective sorbents. Each column was conditioned with 0.001 M HNO_3 solution. Subsequently, sodium molybdate solution (10 mg Mo mL^{-1}), spiked with ^{99}Mo tracer [370 kBq (10 μCi)] was allowed to pass through each column at a flow rate of 0.25 mL min^{-1}. 0.5 mL of the above solution was kept as reference. The effluent was collected in fractions of 0.5 mL aliquots. The radioactivity of ^{99}Mo in the reference and effluent fractions were determined by measuring the 181 keV γ-ray peak of ^{99}Mo in a HPGe detector. The ratio of the count rate 'C' of each 0.5 mL effluent to the count rate 'C_o' of 0.5 mL of the original feed Mo solution was taken as the parameter to follow the sorption pattern. Under dynamic conditions, the sorption behavior of TiP and t-ZrO_2 for Mo are depicted in **Fig. 3.9** and **Fig. 3.10,** respectively. It can be noted from the figures that the breakthrough capacity in case of TiP is ~75 mg Mo g^{-1}, while in case of t-ZrO_2 is ~80 mg Mo g^{-1}. In case of both the sorbents, the value of the breakthrough capacity is much higher than that of alumina (~2-20 mg Mo g^{-1} of alumina) [42]. In both the sorbents, it was seen that the sorption capacity under dynamic conditions was much less than that under equilibrium (static) conditions. This might be attributed to mass transfer limitations, such as incomplete external film diffusion and/or intra-particle transfer and slow kinetics of sorption.

However, the protocol for preparing chromatographic column using sorbent matrix preloaded with ^{99}Mo under static conditions is not recommended owing to difficulties in handling of radioactive material. This will not only cause associated radioactive contamination problem but also increase the radiation exposure to the personnel involved.

Furthermore, even if the column is prepared, the operating performance thereof is likely to deteriorate. Therefore, post loading of ^{99}Mo activity protocol was followed despite the lower sorption capacity that could be achieved.

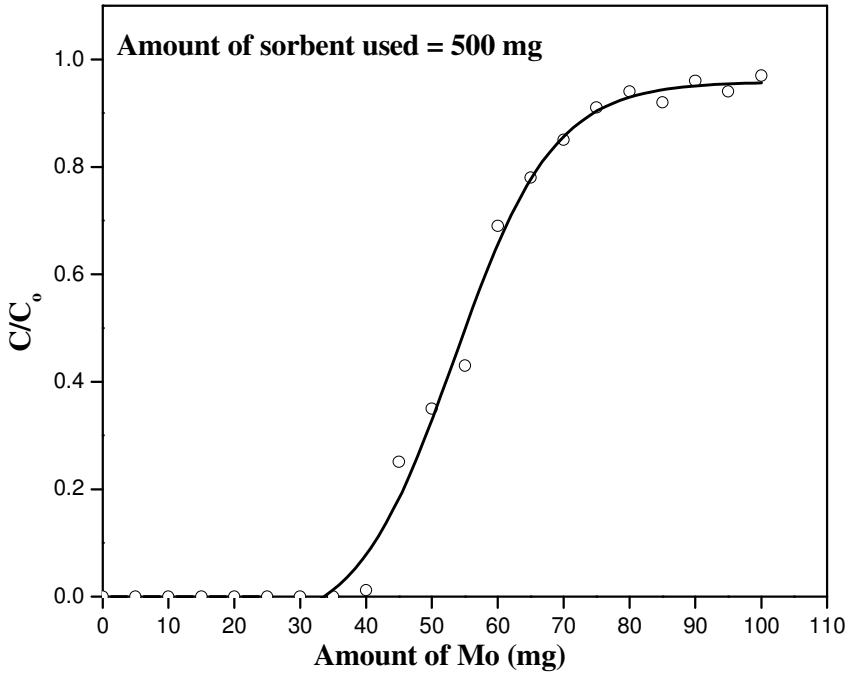

Fig. 3.9 Breakthrough profile of MoO_4^{2-} ions on passing Mo (10 mg Mo mL^{-1}) solution through a 500 mg TiP column at a flow rate of 0.25 mL min^{-1}

3.3.2.4.3 Practical sorption capacity

In order to determine the maximum sorption capacity of TiP and t-ZrO_2 sorbents, under final practical conditions, two borosilicate glass columns of dimension 30 cm (l) × 0.4 cm (i.d.) with sintered disc (G_0) the bottom were packed with 1 g of the respective sorbents. After the columns were conditioned with 0.001 M HNO_3, 20 mL of sodium molybdate solution (10 mg Mo mL^{-1}, pH 3), spiked with ^{99}Mo tracer (370 kBq) was added into the columns and allowed to stand under static conditions for 1 h. 1 mL of the above solution was kept as reference.

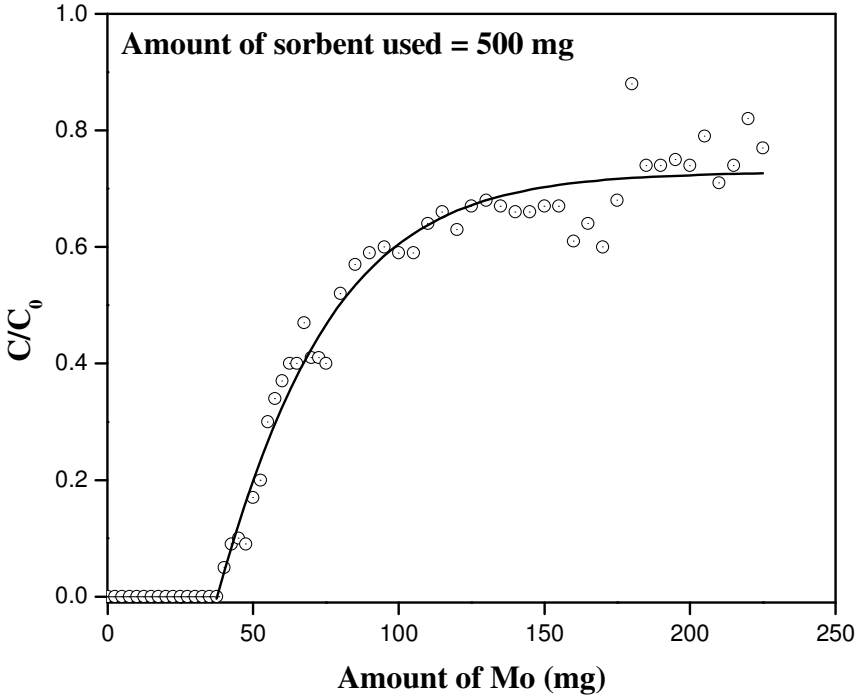

Fig. 3.10 Breakthrough profile of MoO_4^{2-} ions on passing Mo (10 mg Mo mL^{-1}) solution through a 500 mg t-ZrO_2 column at a flow rate of 0.25 mL min^{-1}

Subsequently, the solution was allowed to pass through each column at a flow rate of 0.25 mL min^{-1}. The columns were then washed with 50 mL of 0.9% NaCl solution. For each column, the effluents were pooled together and the activity was determined. The sorption capacity was determined by comparing the ^{99}Mo activity in the effluent with that added into the column (influent). Under these conditions the sorption capacities of TiP and t-ZrO_2 were determined to be 88±4 mg Mo g^{-1} and 155±12 mg Mo g^{-1} (n = 10), respectively.

3.3.3 Development of ^{99}Mo/^{99m}Tc generators

The separation processes could be demonstrated by developing two ^{99}Mo/^{99m}Tc generators using TiP and t-ZrO_2 as the sorbent matrices. For the preparation of each generator, a borosilicate glass column of dimension 12 cm (l) × 0.8 cm (i.d.) with sintered disc (G_0) at the bottom was packed with 4 g of the respective sorbent in a lead shield. A

schematic diagram of the $^{99}Mo/^{99m}Tc$ generator system is shown in **Fig. 3.11**. All the operations were carried out in the closed cycle system using connecting tubes.

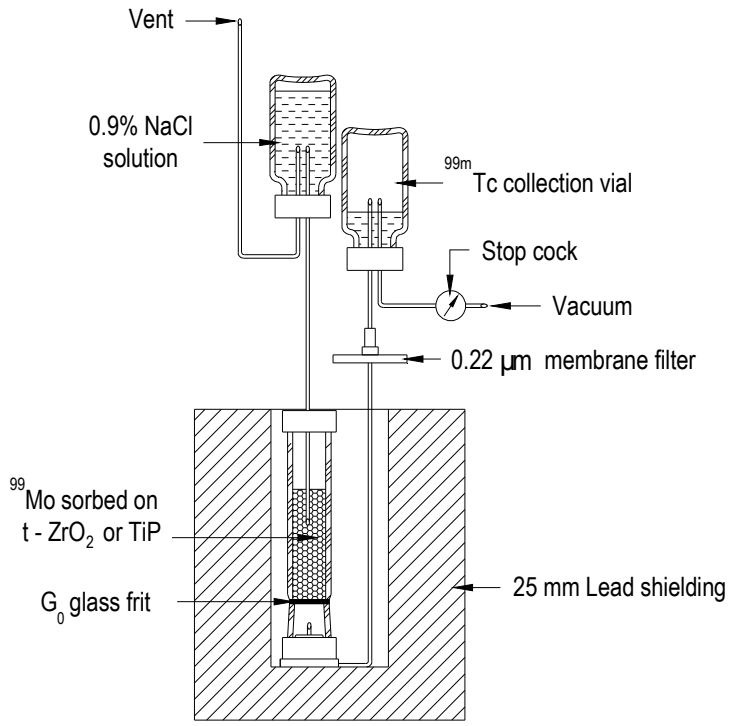

Fig. 3.11: Schematic diagram of $^{99}Mo/^{99m}Tc$ generator system

Input/output connections were made with standard teflon tubings of 1 mm inner diameter and connectors. The generator column, connectors and connection tubings were integrated within a small portable lead shielded unit throughout experimental use for radioprotection purpose. Only the elution vial and output vial were accessible externally. A disposable 0.22 µm membrane filter was attached to the generator column output by teflon tubing. The generator column was preconditioned with 0.001 N nitric acid solution and then $Na_2{}^{99}MoO_4$ (specific activity 17.8 GBq g^{-1}) solution maintained at pH 3 was added into the column and allowed to stand under static conditions for 1 h. Subsequently, the ^{99}Mo solution was passed through the column at a flow rate of 0.25 mL min^{-1}, by applying suction using a peristaltic pump. Since the practical sorption capacity of TiP is less than that of t-ZrO_2, 3.74 GBq (100 mCi) of ^{99}Mo was passed through TiP column while 9.25 GBq (250 mCi) of ^{99}Mo was passed through t-ZrO_2 column. The respective columns were then washed with 100 mL of 0.9% NaCl solution.

In case of both the sorbents, >99% of ^{99}Mo was retained in the respective columns and on washing with 0.9% NaCl solution, <0.3% of ^{99}Mo came out. The generators were eluted on every working day with 4 mL of 0.9% NaCl solution for 10 days.

3.3.4 Elution profile of the ^{99}Mo/^{99m}Tc generators

In order to optimize the minimum volume of eluent required for elution of ^{99m}Tc with maximum yield, the elution profile of the generators were studied. The generators were eluted with 0.9% NaCl solution at a flow rate of 1 mL min^{-1}. The eluate was collected in a series of 1 mL aliquots and the activity of each fraction was measured. The elution profiles of the TiP and t-ZrO_2 based ^{99}Mo/^{99m}Tc generators are illustrated in **Fig. 3.12** and **Fig. 3.13**. All runs were performed at room temperature. It can be seen from the figures that in both the cases, >80% of $^{99m}TcO_4^-$ available in the generator was eluted within the first 3-4 mL volume of 0.9% NaCl solution. Thus, ^{99m}Tc could be eluted from these generators with appreciably high radioactive concentration.

3.3.5 Quality control of ^{99m}Tc

The suitability of ^{99m}Tc obtained from TiP and t-ZrO_2 based ^{99}Mo/^{99m}Tc generators were determined by adopting the quality control procedures described for the electrochemical ^{99}Mo/^{99m}Tc generator (Section 3.2.3). The levels of ^{99}Mo impurity, as determined by the γ-ray spectrometry of the decayed ^{99m}Tc samples, were <10^{-4}%. The radiochemical purity of ^{99m}Tc as $^{99m}TcO_4^-$ was >99%. The level of Ti and Zr ions in the ^{99m}Tc eluate was determined by ICP-AES analysis of the decayed ^{99m}Tc samples and was found to be <0.1 ppm. The level of radionuclidic, radiochemical and chemical impurities in ^{99m}Tc obtained from both the generators were well within the acceptable limits prescribed in the Pharmacopoeias [135].

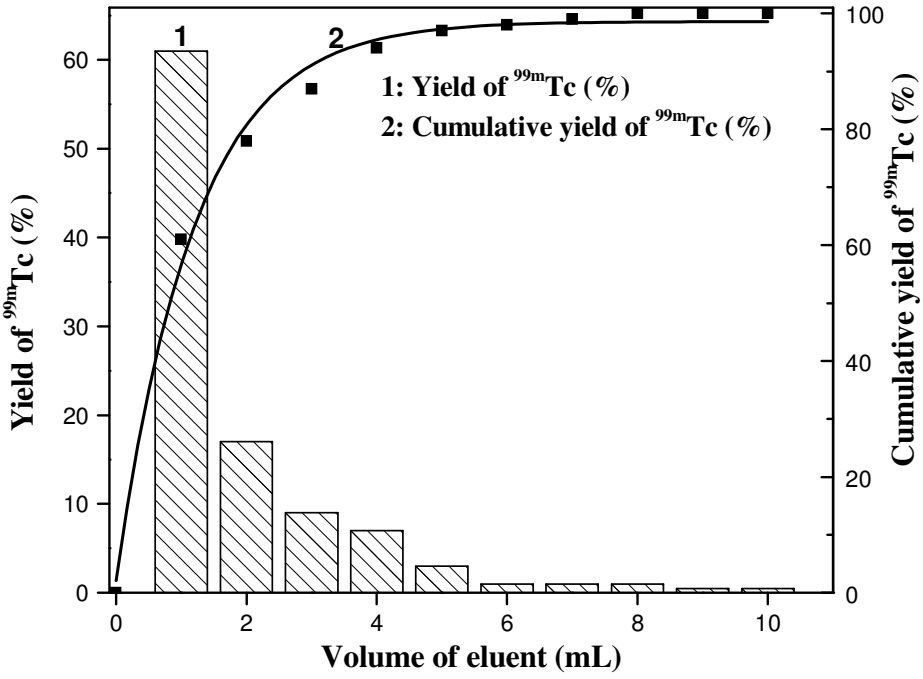

Fig. 3.12: Elution profile of the TiP based ^{99}Mo/^{99m}Tc generator

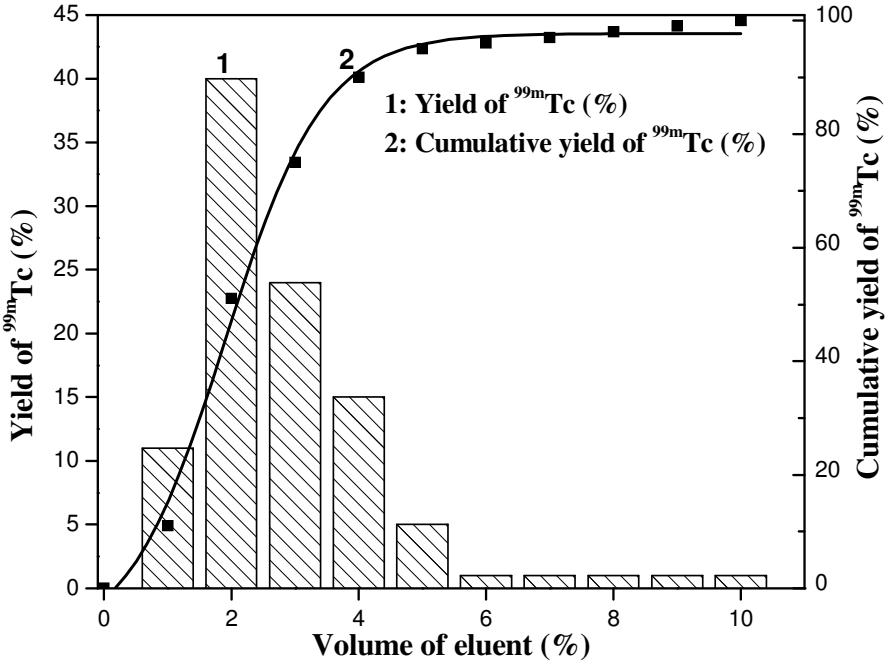

Fig. 3.13: Elution profile of the t-ZrO_2 based ^{99}Mo/^{99m}Tc generator

3.3.6 Labeling efficacy of ^{99m}Tc

In order to examine the suitability of $^{99m}TcO_4^-$ obtained from the generators for radiolabeling studies, it was complexed with DMSA and EC, as per the procedure described earlier (Section 3.2.4). The complexation yield of ^{99m}Tc-EC and ^{99m}Tc-DMSA was always >98%, demonstrating the suitability of ^{99m}Tc obtained from the TiP and t-ZrO_2 based generators for biomedical applications.

3.3.7 Elution performance of the ^{99}Mo/^{99m}Tc generators over a period of 10 days

The TiP and t-ZrO_2 based ^{99}Mo/^{99m}Tc generators were eluted on every working day over a period of 10 days. **Table 3.9** and **Table 3.10** summarize the results of operation of the TiP and t-ZrO_2 based ^{99}Mo/^{99m}Tc generators over a period of 10 days.

Table 3.9: Elution performance of the TiP based ^{99}Mo/^{99m}Tc generator

Elution no.	^{99}Mo activity GBq (mCi)	^{99m}Tc growth period (h)	Expected ^{99m}Tc activity GBq (mCi)	^{99m}Tc recovered GBq (mCi)	^{99m}Tc recovered (%)	^{99}Mo impurity in ^{99m}Tc (%)
1	3.7 (100.0)	24	2.5 (68.8)	2.2 (58.7)	85	8×10^{-4}
2	2.9 (77.7)	24	2.0 (53.4)	1.7 (47.1)	88	3×10^{-4}
3	2.2 (60.4)	24	1.5 (41.5)	1.3 (36.3)	87	1×10^{-4}
4	1.7 (46.9)	24	1.2 (32.2)	1.0 (28.1)	87	2×10^{-4}
5	1.3 (36.4)	24	0.9 (25.0)	0.8 (21.7)	87	1×10^{-4}
6	1.0 (28.3)	24	0.7 (19.5)	0.6 (16.2)	83	2×10^{-4}
7	0.8 (21.9)	48	0.5 (12.7)	0.4 (10.9)	86	6×10^{-4}
8	0.5 (13.2)	24	0.3 (9.1)	0.3 (7.7)	85	1×10^{-4}
9	0.4 (10.2)	24	0.26 (7.0)	0.2 (5.9)	84	3×10^{-4}

Table 3.10: Elution performance of the t-ZrO_2 based $^{99}Mo/^{99m}Tc$ generator

Elution no.	^{99}Mo activity GBq (mCi)	^{99m}Tc growth period (h)	Expected ^{99m}Tc activity GBq (mCi)	^{99m}Tc recovered GBq (mCi)	^{99m}Tc recovered (%)	^{99}Mo impurity in ^{99m}Tc (%)
1	9.3 (250.1)	24	5.8 (157.2)	5.3 (143.0)	91	3×10^{-4}
2	7.2 (194.3)	24	4.5 (122.7)	4.2 (112.9)	92	2×10^{-4}
3	5.5 (150.1)	24	3.5 (94.7)	3.1 (84.3)	89	5×10^{-4}
4	4.3 (116.6)	24	2.7 (73.6)	2.4 (66.24)	90	1×10^{-4}
5	3.3 (90.6)	24	2.1 (57.2)	1.8 (49.7)	87	4×10^{-4}
6	2.6 (70.4)	24	1.6 (44.5)	1.4 (39.1)	88	3×10^{-4}
7	1.6 (44.5)	48	0.9 (23.6)	0.7 (19.3)	82	7×10^{-4}
8	1.0 (26.8)	24	0.6 (16.9)	0.5 (14.2)	84	2×10^{-4}
9	0.8 (20.8)	24	0.5 (13.2)	0.4 (11.2)	85	3×10^{-4}

It can be seen from the tables that for both the generators, the elution yield of ^{99m}Tc was always >85%. The level of ^{99}Mo impurity in ^{99m}Tc was always $<10^{-3}$%. The performance of the generators remained consistent over the period of 10 days, which is the normally expected shelf-life of a $^{99}Mo/^{99m}Tc$ generator.

3.3.8 Recovery of enriched ^{99}Mo from the spent generator columns and their regeneration

Although the generators developed based on the nanomaterials could use the ^{99}Mo obtained by (n,γ) route using natural Mo, irradiation of enriched ^{98}Mo would greatly enhance the maximum activity that can be loaded, because natural Mo has only ~24% of ^{98}Mo. If expensive enriched ^{98}Mo target are irradiated for the preparation of a clinical scale $^{99}Mo/^{99m}Tc$ generator, this process would be economically more viable if the ^{98}Mo adsorbed

on the TiP and t-ZrO_2 matrices could be recovered and reused in many cycles of operation. Moreover, since TiP and t-ZrO_2 are not available commercially, it is also desirable to regenerate the used generator columns after the expiry of their shelf-lives. Therefore, attempts were made to remove the absorbed ^{99}Mo from the generator column after expiry of the shelf-life of the generator. The spent generator columns were washed with saline, and the Mo was desorbed with 5 M NaOH solution containing H_2O_2 (15 mL of 5 M NaOH solution + 1 mL of 30% H_2O_2). The flow rate of the eluent was ~1 mL min^{-1}. The eluates were collected in a series of 1 mL aliquots throughout the elution, and each sample was then subjected to γ-ray spectrometry. The elution behavior of Mo from the TiP and t-ZrO_2 columns is illustrated in **Fig. 3.14** and **Fig. 3.15**, respectively.

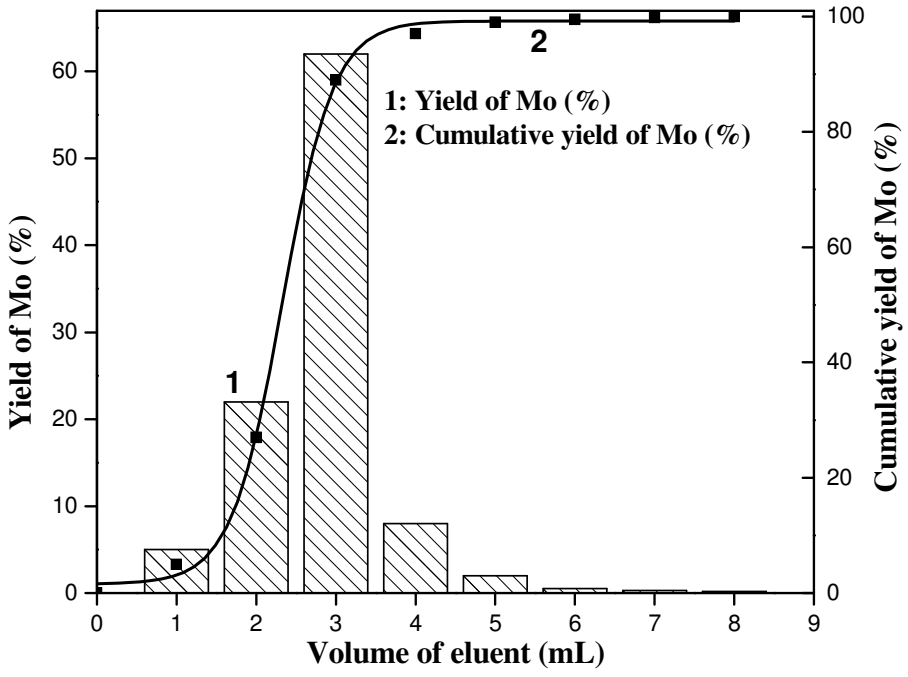

Fig. 3.14: Recovery of Mo from the used TiP column by passing NaOH-H_2O_2 mixture at a flow rate of 0.5 mL min^{-1}

It can be readily seen from the figures that both in case of TiP as well as t-ZrO_2 columns, the recovery of Mo were quite fast and the adsorbed Mo could be eluted out in the

first 3-4 mL of the eluent. Subsequently, all the eluate fractions were mixed together and the total activity of ^{99}Mo eluted was determined. By passing 5 M NaOH solution, >95% of Mo was desorbed from both the columns. Each column was further washed with deionized water and then conditioned with nitric acid solution at pH 3. ^{99}Mo activity was re-loaded in the respective column and ^{99m}Tc could be eluted out under the same conditions as mentioned earlier.

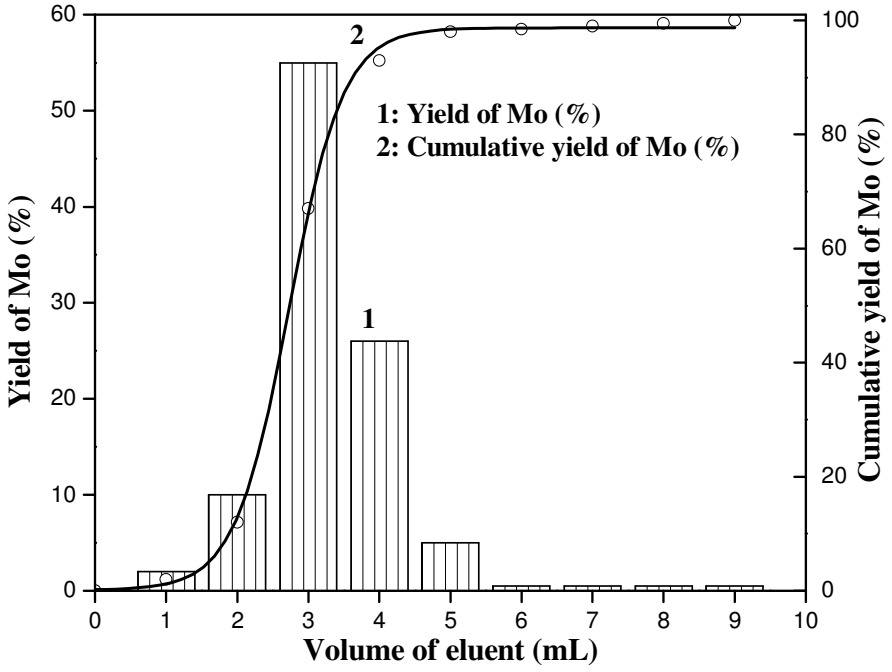

Fig. 3.15: Recovery of Mo from the used t-ZrO_2 column by passing NaOH-H_2O_2 mixture at a flow rate of 0.5 mL min^{-1}

The mechanism of desorption of Mo from the spent TiP and t-ZrO_2 columns could be explained as follows. The zeta-potential of the sorbents is negative under alkaline conditions. As the pH of the external solution rises, depolymerisation of polymolybdate anionic species sorbed in the column takes place and they exist as MoO_4^{2-} under alkaline conditions. Owing to electrostatic repulsion, the negatively charged MoO_4^{2-} ions get desorbed from the column by passing NaOH solution.

3.3.9 Advantages of the TiP and t-ZrO_2 based $^{99}Mo/^{99m}Tc$ generators

The major advantages of the nanomaterial based sorbents are the high sorption capacity, excellent selectivity and appreciable radiation and chemical stability. The procedure for the synthesis of these sorbents is simple and economical and can be easily scaled up. Medium specific activity $(n,\gamma)^{99}Mo$ indigenously produced in the Dhruva reactor of our institution could be utilized for the preparation of the $^{99}Mo/^{99m}Tc$ generators. This approach retains the simplicity of the alumina based chromatographic $^{99}Mo/^{99m}Tc$ generators and is therefore amenable for automation. Unlike the other non-conventional $^{99}Mo/^{99m}Tc$ generators, these nanomaterial based column chromatographic $^{99}Mo/^{99m}Tc$ generators are expected to be more acceptable to the hospital radiopharmacies, as the adaptation of this approach would not require the radiopharmacies to change their operating strategies or increase their personnel resources.

3.3.10 Conclusions

The present study amply demonstrates that TiP and t-ZrO_2 are potential sorbent materials for the preparation of clinical grade $^{99}Mo/^{99m}Tc$ generators of moderate strength, using medium specific activity $(n,\gamma)^{99}Mo$. ^{99m}Tc could be availed from the generators with >85% yields and high radionuclidic, radiochemical and chemical purity and appreciably high radioactive concentration. The compatibility of the product in the preparation of ^{99m}Tc labeled formulations was evaluated and found to be satisfactory. The sorbents are stable to radiation and the $^{99}Mo/^{99m}Tc$ generators demonstrate satisfactory performance for >10 days, which is normally the shelf-life of $^{99}Mo/^{99m}Tc$ generators. The present concept would provide unequivocal support to the Nuclear Medicine industry, especially in developing countries like India, which currently do not have the technology/facility to produce high specific activity ^{99}Mo.

CHAPTER 4

DEVELOPMENT OF $^{68}Ge/^{68}Ga$ GENERATORS

"The important thing in science is not so much to obtain new facts as to discover new ways of thinking about them."

WILLIAM LAWRENCE BRAGG

4.1 Introduction

4.1.1 Gallium-68 (^{68}Ga): An excellent radioisotope for Positron Emission Tomography

^{68}Ga is an excellent positron emitting radioisotope suitable for clinical positron emission tomography (PET) applications in Nuclear Medicine [19,142]. It emits positrons with 89% positron branching accompanied by 1,077 keV photon emission of low (3.22%) abundance [15]. The relatively short half-life of ^{68}Ga ($t_{½}$ = 67.71 min) permits PET application with suitable ^{68}Ga radiotracers, while maintaining an acceptable radiation dose to the patient. Moreover, the half-life of ^{68}Ga matches the pharmacokinetics of many peptides and other small molecules due to rapid diffusion, localization at the target and fast blood clearance [143].The efficacies of ^{68}Ga-based tracers are comparable to that of ^{18}F-based agents and have stimulated researchers to investigate the potential of ^{68}Ga based PET imaging agents [19,142,144]. Apart from being a PET radionuclide that enables imaging with better resolution, $^{68}Ga^{3+}$ has more amenable chemistry attributes for labeling than ^{99m}Tc, a versatile SPECT radionuclide as well as ^{18}F, the most widely used PET radionuclide. Numerous ^{68}Ga based radiopharmaceuticals have been found useful in clinical studies [19,145-153]. $^{68}Ga^{3+}$ is stable and forms complexes with the cyclic ligand DOTA with high affinity and is thus suitable for preparation of high specific activity ^{68}Ga-labeled peptides or other biomolecules conjugated to DOTA [19,145]. ^{68}Ga-labelling of DOTA-coupled peptides can be performed in a very short time, allowing excellent imaging of neuroendocrine and neuroectodermal tumors [19,143,145]. Particularly, DOTA-TOC (DOTA-D-Phe^{1}-Tyr^{3}-octreotide) labeled with ^{68}Ga have shown high binding affinity for human somatostatin receptors and possess excellent tumor imaging capabilities [152,153].

4.1.2 Availability of ^{68}Ga from ^{68}Ge/^{68}Ga generator

The ^{68}Ge/^{68}Ga generator system is an excellent source to avail ready-to-use ^{68}Ga for clinical positron emission tomography (PET) applications, allowing PET imaging at facilities

without an on-site cyclotron [19,142,154]. The cyclotron independent availability of ^{68}Ga from a ^{68}Ge/^{68}Ga generator at a reasonable cost makes it an attractive and realistic option for countries with limited or no cyclotron facilities. The relatively long-lived ^{68}Ge ($t_{½}$ 270.95 d, electron capture (EC) 100%) produces short-lived ^{68}Ga ($t_{½}$ 67.71 min), which subsequently decays to stable ^{68}Zn [15,19]. The simplified decay scheme of ^{68}Ge is illustrated in **Fig. 4.1**.

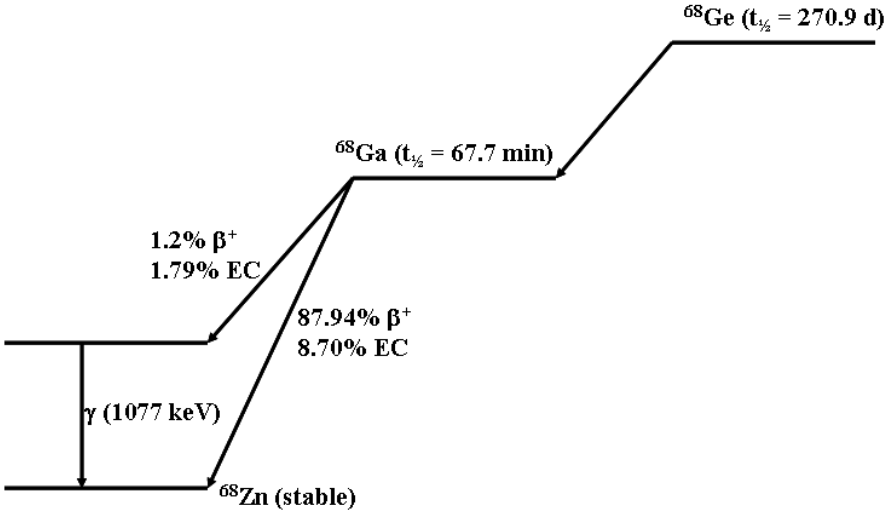

Fig. 4.1: Simplified decay scheme of ^{68}Ge (energy levels not drawn to scale)

The long half-life of the parent radionuclide ^{68}Ge ensures the cost-effective availability of ^{68}Ga within the PET facility for long periods of time. The parent radioisotope, ^{68}Ge can be produced in a small cyclotron through various reactions, such as, ^{69}Ga (p,2n), ^{69}Ga (d,3n), ^{66}Zn (α,2n) etc. involving varied targets and charged particles [19,155]. The processes amenable for the production of ^{68}Ge are listed in **Table 4.1**. It can be seen from the table that though the yield of the ^{69}Ga (p,2n) reaction using Ga_2O_3 film is almost comparable to that of Ge (p,xn) reaction, higher energy protons are required for the latter reaction. The Ge (p,xn) reaction is not preferred because the specific activity of ^{68}Ge produced is significantly lower than that from ^{69}Ga (p,2n) reaction. Moreover, radioarsenic isotopes are also formed in the Ge (p,xn) processes. The yields for the ^{69}Ga (d,3n), Zn (α,xn) and ^{66}Zn (α,2n) reactions are much smaller than for ^{69}Ga (p,2n) and Ge (p,xn) reactions.

Table 4.1: The relevant nuclear reactions yielding ^{68}Ge

Nuclear reaction	Target form			Projectile		Yield	Reference
	Chemical	Physical	Thickness	Energy (MeV)	Current (μA)	(μCi μA^{-1} h^{-1})	
^{69}Ga (p,2n)	$^{nat.}Ga_4Ni$	disk	3 mm	19.5-0	2-3	9.2	[156]
^{69}Ga (p,2n)	$^{nat.}Ga_2O_3$	film	-	55-13	2	45	[157]
^{69}Ga (p,2n)	Ga	solid	-	22	50	15	[158]
$^{nat.}$Ge (p,xn)	Ge	foil	107 mg cm^{-2}	64-28	1	48	[159]
^{69}Ga (d,3n)	Ga_2O_3	disk	0.5 mm	30	10	1.7	[160]
$^{nat.}$Zn (α,xn)	Zn	foil	13 mg cm^{-2}	40-20	0.5	1	[161]
^{66}Zn (α,2n)	Zn	film	-	40-20	0.5	1-2	[162]

'nat.' indicates natural target

Therefore, out of these, the ^{69}Ga (p,2n) reaction is most suitable for routine production of carrier free ^{68}Ge using a compact medical cyclotron [19,155], owing to the energetics of the reaction as well as the purity of the product that can be obtained.

Though the ^{68}Ge/^{68}Ga radionuclide generators have been the object of development and investigation for almost 50 years [19,154], their proper and relevant clinical use has started only recently [144,163,164], due to lack of proper sorbents, as one of the reasons. Undoubtedly, the major impetus for the development of ^{68}Ge/^{68}Ga generator stems from the recognized potential of PET technique and ^{68}Ga-based radiopharmaceuticals, which demand instant, in-house availability of ^{68}Ga suitable for clinical use [165-167]. Several ^{68}Ge/^{68}Ga generator systems have been proposed over the past 50 years in an attempt to provide a reliable source of the positron-emitter ^{68}Ga, that can readily be converted into radiopharmaceuticals for PET [19,155,168-182]. Of these systems, the column chromatographic ^{68}Ge/^{68}Ga generator has emerged as an effective, efficient, and the most popular generator system, owing to its simplicity and convenience to use in a hospital radiopharmacy.

In the early attempts towards the preparation of column chromatographic ^{68}Ge/^{68}Ga generators, inorganic oxides such as Al_2O_3 or ZrO_2 were used as sorbent materials [19,168]. For the preparation of these generators, carrier-free ^{68}Ge was absorbed onto the column and ^{68}Ga could be eluted with EDTA solution. The elution yields of such generators were appreciably high (~70-80%). Since these early generator systems provided ^{68}Ga in a chelated form, destruction of the EDTA complex was necessary, which rendered the preparation of the radiopharmaceutical tedious, time-consuming, and with a reduced overall yield. Thus, further development was focused on generator systems yielding $^{68}Ga^{3+}$ in its hydrated ionic form. Though there are several reports on the preparation of ^{68}Ge/^{68}Ga generators using metal oxides or hydroxides (like Al_2O_3, $Fe(OH)_3$, SiO_2, Sb_2O_5, SnO_2 and TiO_2) as sorbents [19,168-

178], from which ^{68}Ga could be eluted in an ionic form, their clinical use failed because of the presence of these metal oxides or the corresponding metal ions in the ^{68}Ga eluate [19,168]. A very low breakthrough of the column packing material and the parent radioisotope were reported for a CeO_2 based ^{68}Ge/^{68}Ga generator [177]. However, this approach was not taken further as the yield of ^{68}Ga from the CeO_2 based generator was low (~56%) [177]. Alternatively, a macroporous styrene-divinylbenzene copolymer with *N*-methylglucamine groups was used as the sorbent matrix for the preparation of ^{68}Ge/^{68}Ga generator. ^{68}Ga was eluted from this generator with the low affinity chelator, sodium citrate, in good yields (~80%), and the ^{68}Ge breakthrough was <0.0004% [181,182]. Another complementary approach was the use of a pyrogallol-formaldehyde resin with high affinity for Ge (IV), where ^{68}Ga was obtained as $^{68}GaCl_4^-$ using 5.5 M HCl as eluent [173]. The $[^{68}GaCl_4]^-$ complex was then adsorbed on a small anion exchange column to remove low levels of ^{68}Ge breakthrough (<1 ppm). Elution with small volume of water resulted in the decomposition of the chloro complexes, and concentrated solutions of $^{68}Ga^{3+}$ in 0.5 M HCl were finally obtained. However, the performance of both these organic sorbents for the preparation of ^{68}Ge/^{68}Ga generator has been demonstrated only with tracer level of activity (~370 kBq of ^{68}Ge/^{68}Ga) [173,181,182]. Therefore, further investigations on the radiation stability and performance of the organic sorbents at higher level of activity are needed before clinical applications are undertaken.

Nowadays, the most commonly available commercial ^{68}Ge/^{68}Ga generator systems are based on 'modified' TiO_2 or SnO_2 sorbents [19,167,183], from which ionic $^{68}Ga^{3+}$ can be availed in 0.1-1 N HCl medium. The major limitation of these commercially available generators is that the ^{68}Ga obtained from the primary column is not optimally suited for the routine synthesis of ^{68}Ga-labeled radiopharmaceuticals [19,167,183]. The ^{68}Ga-eluates from most of the commercial generators have low specific volume of ^{68}Ga and may contain

different trace elements owing to the solubility of metal oxide sorbent. The presence of these competing metal ions in the eluate is a major obstacle in the complexation chemistry of ^{68}Ga [19,166,167,183] and therefore necessitates the inclusion of multiple post-elution processing steps [19,165-167,184,185]. Moreover, there is a drastic decrease in the elution yield of ^{68}Ga and increase in the ^{68}Ge breakthrough with passage of time or increasing number of elutions [19,166].

In view of the above described drawbacks, development of alternate sorbents with high sorption capacity and selectivity for ^{68}Ge along with appreciable radiation resistance and chemical stability in acidic medium, is of considerable importance and deserves a serious consideration. Use of such sorbents would not only facilitate the elution of ^{68}Ga with high radioactive concentration and avoid the need of additional concentration step, but also render ^{68}Ga of acceptable radionuclidic and chemical purity.

4.1.3 The present work

The availability of a reliable, simple-to-handle ^{68}Ge/^{68}Ga generator would facilitate more research on new diagnostic radiopharmaceuticals with ^{68}Ga. In this chapter, the attention is focused on exploring the potential of nanomaterials as promising sorbents for the preparation of ^{68}Ge/^{68}Ga generators. The potential of nanomaterial based sorbents in the preparation of clinically useful ^{99}Mo/^{99m}Tc generators was described in the earlier chapter. It is expected that use of such materials can minimize the number of steps involved in obtaining clinical grade ^{68}Ga from ^{68}Ge. Several favorable characteristics, such as high surface area, availability of reactive surface sites and pore structure make nanoparticles excellent sorbent for generator preparation. This chapter describes the development of two novel ^{68}Ge/^{68}Ga generators using tetragonal nano-zirconia (t-ZrO_2) and nano-ceria-polyacrylonitrile composite (CeO_2-PAN) as the sorbent matrices. The feasibility of each of these methods, in terms performance of the generators with respect to ^{68}Ga-elution yield, low ^{68}Ge

breakthrough, high radioactive concentration of the ^{68}Ga solution and adequate purity of the ^{68}Ga for preparation of radiopharmaceuticals, has been demonstrated and evaluated.

4.2 Materials

Reagents such as hydrochloric acid, ammonium hydroxide, etc. were of analytical grade and were procured from S.D. Fine Chemicals, India. High performance liquid chromatography (HPLC) grade water and zirconyl chloride ($ZrOCl_2.8H_2O$, +99.9%) were purchased from E. Merck, Germany. Cerium (III) nitrate (+99.9%) was obtained from BDH, India. Analytical grade (+99.999%) GeO_2 was procured from Aldrich, England. DOTA-TATE (DOTA-D-Phe^1-Tyr^3-octreotate, DOTA=1,4,7,10-tetraazacyclo dodecane-1,4,7,10-tetraacetic acid) was obtained from Pi Chem, Austria. Paper chromatography (PC) strips (3 MM, 20 mm width) were purchased from Whatman International Limited, England. ^{68}Ge in HCl medium was obtained from Atom Hightech Company Limited, China, through an IAEA coordinated research project.

HPGe detector coupled with a multichannel analyzer (MCA) (Canberra Eurisys, France) with a 1.5 keV resolution at 1333 keV and range from 1.8 keV to 2 MeV was used for analysis of ^{68}Ga. The efficiency of this instrument was estimated using a standard ^{152}Eu source. Gamma activity of ^{68}Ga was routinely assayed using a NaI (Tl) scintillation counter (400-600 keV). The chemical analysis for the determination of trace level of metal contaminations was done using Inductively Coupled Plasma-Atomic Emission Spectroscopy (ICP-ES JY-238, Emission Horiba Group, France). The UV-Visible spectrometry of the ^{68}Ga samples were carried out using JASCO V-530, UV/Vis Spectrophotometer. The complexation yields of ^{68}Ga labeled compounds were studied using HPLC technique. The HPLC instrument (JASCO PU 1580, Japan) was equipped with a NaI (Tl) detector as well as a UV-Visible spectrometer.

4.3 Separation of ^{68}Ga from ^{68}Ge

4.3.1 Synthesis of t-ZrO_2 and CeO_2-PAN composite

The synthesis of t-ZrO_2 and CeO_2-PAN was carried out as per the procedure described in Chapter 2. Owing to the simple and reliable synthesis procedure using commercially available chemicals, large scale preparation of these sorbents could be achieved in the laboratory. It was therefore considered worthy to establish the suitability of these materials for the preparation of ^{68}Ge/^{68}Ga generators. The materials synthesized were porous with sufficiently large surface area and hence, could be used as a solid phase support in column chromatography operation. The materials demonstrated high resistance toward chemical attack and precluded the presence of Zr and Ce ion impurities in the eluate that could possibly interfere in complexation chemistry of Ga^{3+} ions. Subsequent investigations were directed towards optimization of experimental conditions necessary for the effective separation of ^{68}Ga from ^{68}Ge.

4.3.2 Determination of the distribution ratios (K_d) of the ^{68}Ge and ^{68}Ga ions

In order to explore the potential of t-ZrO_2 and CeO_2-PAN for the separation of ^{68}Ga from ^{68}Ge, distribution ratios (K_d) of Ge and Ga ions were determined at different concentrations of HCl solutions. The K_d values of the Ge and Ga ions were determined by batch equilibration method. A stoppered conical flask containing 200 mg of the respective sorbents, immersed in 20 mL of HCl solution spiked with 37 kBq of the ^{68}Ge/^{68}Ga radiotracer, was shaken for 1 h at room temperature (25 $^{\circ}$C). Subsequently, the supernatant solution was filtered through Whatman filter paper (No. 50). Since ^{68}Ge decays solely by electron capture to ^{68}Ga, the activity of ^{68}Ge could not be directly estimated by γ-ray spectrometry. For determination of the activity of ^{68}Ge, the filtrate was allowed to decay for 24 h, so that all the ^{68}Ga activity would decay except the amount which grows from and is in equilibrium with the ^{68}Ge. This ^{68}Ga activity would correspond to the ^{68}Ge activity and hence

measured in a well type NaI (Tl) counter using appropriate window settings (400-600 keV). On the other hand, for quantification of ^{68}Ga, it was measured immediately after filtration. The K_d values were calculated by using the following expression:

$$K_d = \frac{(A_i - A_{eq})V}{A_{eq}\, m}$$

where, A_i is the initial total radioactivity of 1 mL the solution, A_{eq} is the unadsorbed activity in 1 mL of the solution at equilibrium, V is the solution volume (mL) and m is the mass (g) of the adsorbent. All equilibration experiments were carried out in triplicate. The results obtained with t-ZrO_2 and CeO_2-PAN are summarized in **Table 4.2** and **Table 4.3** respectively.

Table 4.2: Distribution ratios (K_d) of ^{68}Ge and ^{68}Ga ions in t-ZrO_2

Conc. of HCl (M)	K_d	
	^{68}Ge	^{68}Ga
0.001	12598 ± 120	8 ± 2
0.01	12743 ± 88	0.10 ± 0.05
0.05	6645 ± 46	0.2 ± 0.1
0.1	6333 ± 52	0.10 ± 0.06
0.5	2131 ± 100	0.5 ± 0.1
1	1204 ± 84	0.7 ± 0.2
2	931 ± 50	0.6 ± 0.1
3	907 ± 53	0.4 ± 0.2
4	614 ± 45	0.4 ± 0.1
5	412 ± 61	0.6 ± 0.2

(n = 3, '±' indicates standard deviation)

Table 4.3: Distribution ratios (K_d) of ^{68}Ge and ^{68}Ga ions in CeO_2-PAN

Conc. of HCl (M)	K_d	
	^{68}Ge	^{68}Ga
0.001	5233 ± 144	113 ± 8
0.01	5152 ± 119	0.12 ± 0.07
0.05	4766 ± 68	0.2 ± 0.1
0.1	3033 ± 162	0.3 ± 0.1
0.5	2109 ± 113	0.5 ± 0.2
1	1654 ± 121	0.6 ± 0.2
2	1636 ± 111	0.7 ± 0.1
3	837 ± 56	0.6 ± 0.3
4	414 ± 59	0.7 ± 0.2
5	342 ± 77	0.7 ± 0.1

(n = 3, '±' indicates standard deviation)

It can be seen from the tables that for both the sorbents, under all examined concentrations, Ge ions had significantly high K_d values compared to Ga ions. Further, it can be noticed that the K_d values for Ge ions decreased gradually with increase in concentration of HCl. On the other hand, $^{68}Ga^{3+}$ ions had distinctly lower K_d values under acidic conditions and could thus be effectively separated from ^{68}Ge. Owing to the very high K_d values of Ge ions in 0.01 M HCl and very low K_d values of Ga^{3+} under the same conditions, it was decided to use 0.01 M HCl solution for elution of Ga^{3+}. Quantitative retention of ^{68}Ge was achieved and ^{68}Ga could be easily eluted out using 0.01 M HCl solution.

Nano zirconia and nano ceria particles can be considered to consist of discrete metal oxide clusters covered by surface hydroxyl groups. The interaction of nanosized metal oxide particles with aqueous solutions results in the hydroxylation of surface sites and this imparts a

pH-dependent surface charge which is primarily responsible for the uptake of metal ions. This phenomenon was studied by determination of the zeta potential of these materials at different pH environments. The zeta potential of t-ZrO_2 (**Fig. 2.12**) was positive up to pH 4, while in case of CeO_2-PAN (**Fig. 2.16**), the zeta potential values were positive up to pH 6. On further increase in pH, the zeta potential of these nanomaterials became zero (IEP) and subsequently became increasingly negative with further rise in pH. In dilute acid solutions (pH 2-3), the principal germanium compounds probably are $[GeO(OH)_3]^-$, $[GeO_2(OH)_2]^{2-}$ and $[[Ge(OH)_4]_8(OH)_3]^{3-}$ which are negatively charged [186,187]. The strong affinity of the sorbents for ^{68}Ge ions at pH ~2 is probably due to the electrostatic attraction of negatively charged germanium ions for the positively charged surface of the t-ZrO_2 and CeO_2-PAN. In the same medium, Ga exists as Ga^{3+} ions and hence a nearly complete elution could be achieved due to electrostatic repulsion of the positively charged Ga^{3+} ion from the positively charged surface of the nanomaterials.

However, on increasing the acidity of the solution, the K_d values of Ga ions increased, slightly. This might be due to the tendency of formation of negatively charged $[GaCl_4]^-$ complex at higher acidity which is probably retained on the positively charged surface of the nanomaterials. Therefore, 0.01 N HCl solution was chosen for elution of ^{68}Ga in all subsequent experiments.

4.3.3 Determination of the time of equilibration

In order to study the time dependence of sorption of ^{68}Ge onto t-ZrO_2 and CeO_2-PAN, the K_d of ^{68}Ge ions was determined in 0.01 M HCl as a function of time. The attainment of equilibrium was indicated by the constant K_d value after a certain period of time and the results for t-ZrO_2 and CeO_2-PAN are shown in **Fig. 4.2** and **Fig. 4.3,** respectively. It could be inferred from the figures that the equilibrium was attained within 50-60 minutes, when t-ZrO_2

was used as the sorbent and within 25-30 minutes when CeO_2-PAN was used. Therefore, this contact period was maintained in all subsequent batch equilibration experiments.

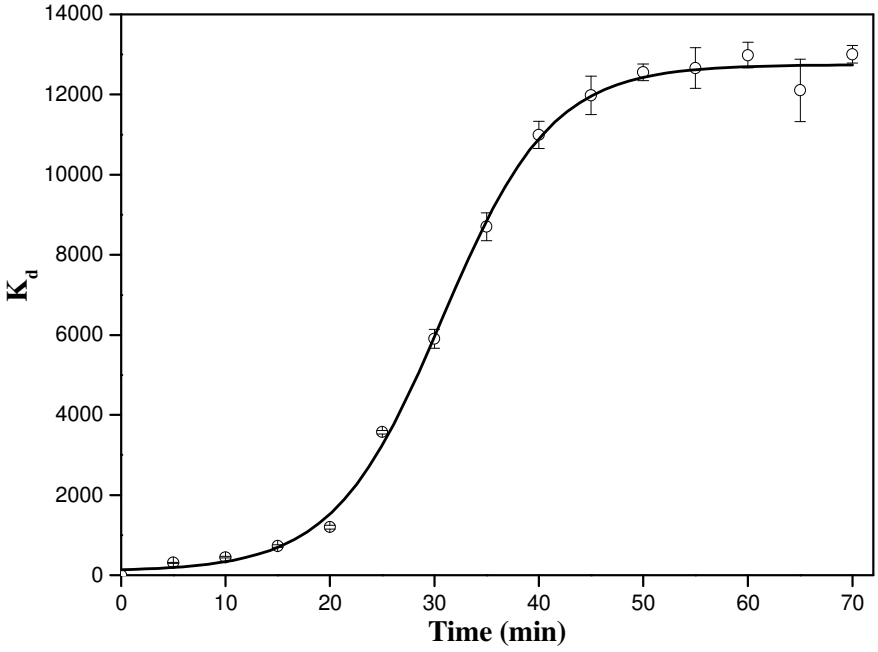

Fig. 4.2: Variation in K_d values of ^{68}Ge ions with time using t-ZrO_2 as sorbent

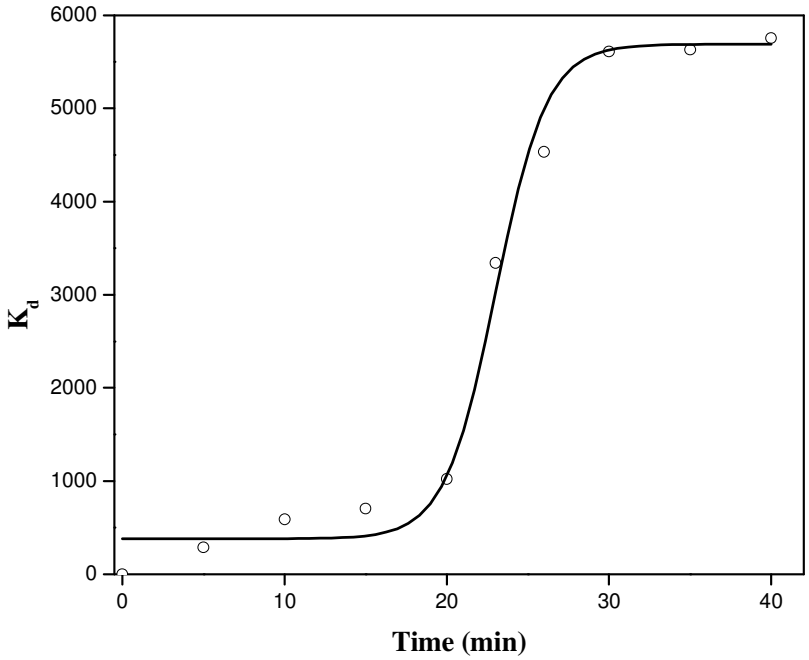

Fig. 4.3: Variation in K_d values of ^{68}Ge ions with time using CeO_2-PAN as sorbent

4.3.4 Determination of the sorption capacity of t-ZrO_2 and CeO_2-PAN

The sorption capacity of the sorbents were evaluated both under static as well as dynamic conditions. The solution of non-radioactive Ge(IV) was prepared by dissolving GeO_2 in 0.1 N sodium hydroxide. The concentration and the initial pH of the Ge solution were adjusted with 0.1 N HCl. HPGe detector coupled with a multichannel analyzer was used for analysis of ^{68}Ga and ^{68}Ge and also for their quantitative determination.

4.3.4.1 Static sorption capacity

The static sorption capacities of t-ZrO_2 and CeO_2-PAN for Ge ions were determined by batch equilibration method. An accurately weighed amount of sorbent (~200 mg) was taken in a stoppered glass conical flask and equilibrated with 20 mL of the Ge solution (5 mg of Ge mL^{-1}) spiked with ~370 kBq (10 μCi) of ^{68}Ge, for 1 h at pH 2. Subsequently, the contents were filtered and the filtrate was allowed to decay for 24 h. The activity of the decayed ^{68}Ge solution was measured using a NaI(Tl) detector and compared with that of the standard ^{68}Ge solution. The sorption capacity was calculated using the following expression:

$$\text{Capacity} = \frac{(A_o - A_e)V.C_o}{A_o\, m}$$

where A_o and A_e represented the radioactivity of ^{68}Ge in 1 mL of supernatant solution before and after sorption, respectively, C_o was the total Ge content (5 mg) in 1 mL of solution before sorption, V was the volume of solution and m was the mass (g) of the sorbent. The batch equilibration studies indicated that the static sorption capacities of t-ZrO_2 and CeO_2-PAN were 135 ± 10 mg Ge g^{-1} and 40 ± 5 mg g^{-1}, respectively, in 0.01 M HCl solution (n = 10).

4.3.4.2 Determination of breakthrough pattern and dynamic sorption capacity

In order to evaluate the sorption capacity of the nanomaterials for Ge under dynamic conditions, a borosilicate glass column of dimension 8 cm × 0.6 cm (i.d.) with a sintered disc (G_0) at the bottom was packed with a known amount of the respective sorbent. After the column was conditioned with 0.01 M HCl, Ge solution (5 mg Ge mL^{-1}), spiked with

^{68}Ge/^{68}Ga radiotracer, was allowed to pass through the column at a flow-rate of ~0.25 mL min^{-1}. 1 mL of this solution was kept as reference. The effluent was collected in fractions of 1 mL aliquots and allowed to decay for 1 day. The ^{68}Ge activity in the reference (C_o) and effluent fractions (C) were determined by measuring the 511 keV γ-ray peak in a HPGe detector. The ratio of the count rate 'C' of each 1 mL effluent fraction to the count rate 'C_o' of 1 mL of the original feed Ge solution was taken as the parameter to follow the sorption pattern. The breakthrough curves developed for t-ZrO_2 and CeO_2-PAN are illustrated in **Fig. 4.4** and **Fig. 4.5**, respectively. It can be seen from **Fig. 4.4** that for t-ZrO_2, the breakthrough point was reached after (76±3) mg of Ge (n=10), was quantitatively retained by 1 g of the sorbent in the column.

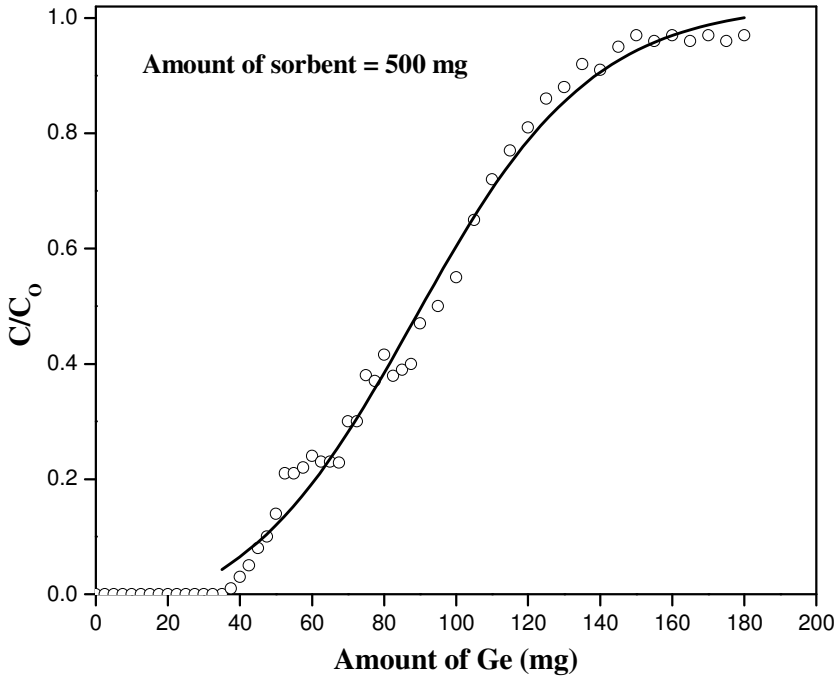

Fig. 4.4: Breakthrough profile of Ge ions on passing Ge (5 mg Ge mL^{-1}) solution through a 500 mg t-ZrO_2 column at a flow rate of 0.25 mL min^{-1}

Fig. 4.5 shows that the breakthrough capacity of CeO_2-PAN was (20±2) mg of Ge per g of the sorbent (n = 10). These results reflect that even a small column containing 200 mg of t-ZrO_2 or CeO_2-PAN is adequate for the preparation of a 37 GBq (1 Ci) ^{68}Ge/^{68}Ga generator.

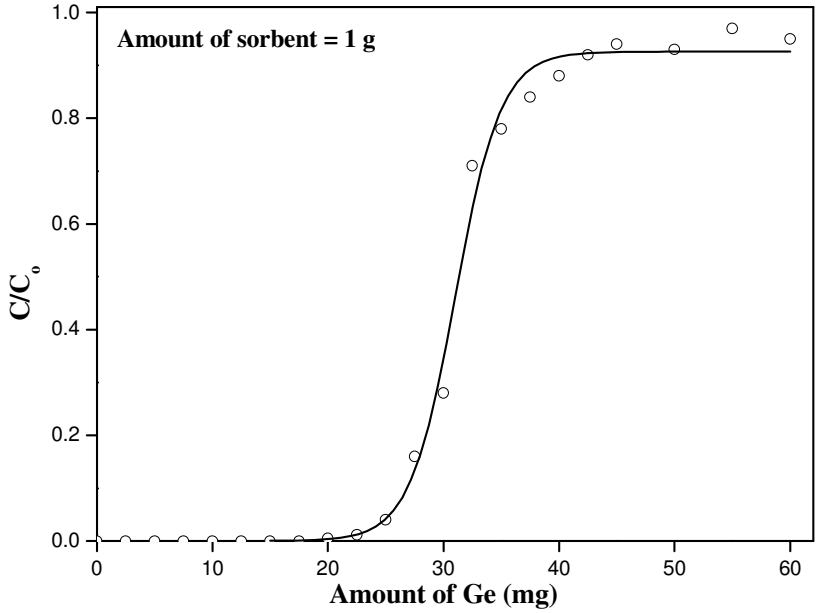

Fig. 4.5: Breakthrough profile of Ge ions on passing Ge (5 mg Ge mL^{-1}) solution through a 1 g CeO_2-PAN column at a flow rate of 0.25 mL min^{-1}

It must be mentioned here that the concentration of Ge ions (5 mg Ge mL^{-1}) used in these experiments, are far higher than the 'real' generator situation. However, it still serves the purpose and provides information on the sorption capacities of both the sorbent materials for Ge ions, which are appreciably high. This concentration of Ge ions was chosen to indicate the excellent capacity of the sorbent, much more than adequate to adsorb Ge ions expected to be present in a clinical scale ^{68}Ge/^{68}Ga generator. Since ^{68}Ge is available in no-carrier added form, the amount of Ge present in 37 GBq (1 Ci) of ^{68}Ge solution is only 0.14 mg. On passing Ge solutions, containing 0.14 mg of Ge (equivalent to 37 GBq of ^{68}Ge) through two columns, each containing only 200 mg of t-ZrO_2 or CeO_2-PAN, it was found that Ge ions were quantitatively taken up by the respective sorbents.

4.4 Development of $^{68}Ge/^{68}Ga$ generators

The separation processes could be demonstrated by developing two 740 MBq (20 mCi) $^{68}Ge/^{68}Ga$ generators using t-ZrO_2 and CeO_2-PAN as sorbent matrices, respectively. For the preparation of each generator, a borosilicate glass column of dimension 8 cm × 0.6 cm (i.d.) with a sintered disc (G_0) at the bottom was packed with 1 g of the respective sorbent and kept in a lead shielded container. It was pre-conditioned with 0.01 M HCl solution. A schematic diagram of the $^{68}Ge/^{68}Ga$ generator system is shown in **Fig. 4.6**. All the operations were carried out in the closed cyclic system using connecting tubes. Input/output connections were made with standard teflon tubings of 1 mm inner diameter and connectors. The generator column, connectors and connection tubings were integrated within a small portable lead shielded unit throughout experimental use for radioprotection purpose. Only the elution vial and output vial were accessible externally. A disposable 0.22 μm membrane filter was attached to the generator column output by teflon tubing.

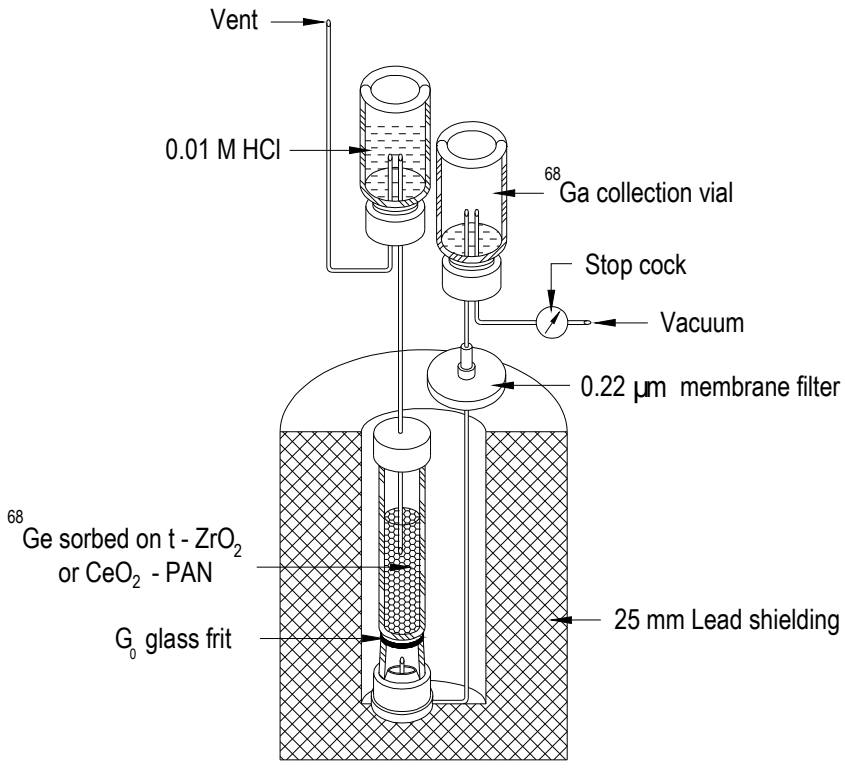

Fig. 4.6: Schematic diagram of the $^{68}Ge/^{68}Ga$ generator system

The $^{68}Ge/^{68}Ga$ solution containing 740 MBq (20 mCi) of ^{68}Ge at pH 2 was percolated into each column maintaining a flow rate of 0.25 mL min^{-1}. In case of both t-ZrO_2 as well as CeO_2-PAN based generators, about 740 MBq (20 mCi) of ^{68}Ge activity at pH 2, were quantitatively retained by the sorbents. The ^{68}Ge-loaded generator columns were then washed with 100 mL of 0.01 M HCl solution. On washing with 0.01 N HCl solution, only <0.5% of ^{68}Ge came out, from each generator column.

4.5 Choice of the eluent for the elution of ^{68}Ga from the $^{68}Ge/^{68}Ga$ generators

For the success of a $^{68}Ge/^{68}Ga$ generator in clinical PET, it is essential to obtain ^{68}Ga in an uncomplexed chemical form, maximize the elution yield of ^{68}Ga, minimize the ^{68}Ge breakthrough and keep the elution volume to a minimum. These requirements place severe constraints on the eluent that can be used, and the choice is rather limited. Gallium exists exclusively in +3 oxidation state in aqueous acidic solutions. It hydrolyzes nearly completely at neutral pH [188,189] and readily forms highly insoluble amorphous $Ga(OH)_3$, while Ga ions at hydrochloric acid concentrations >5.5 M form the negatively charged $[GaCl_4]^-$ complex [185]. In view of these limitations, it was decided to work under acidic conditions and use 0.01 M HCl as eluent, based on effectiveness of this solution in desorbing $^{68}Ga^{3+}$ from the sorbents while maintaining the level of ^{68}Ge impurity in the eluate to a permissible level. The decay of ^{68}Ge to ^{68}Ga is not accompanied by any serious disruption of chemical bonds. As these ^{68}Ge ions start transforming into ^{68}Ga ions, which do not form negative complexes at 0.01 M HCl, they are not retained by the sorbent matrices and hence an easy displacement of $^{68}Ga^{3+}$ ions is expected.

4.6 Elution profiles of $^{68}Ge/^{68}Ga$ generators

In order to optimize the minimum volume of eluent required for the elution of ^{68}Ga with maximum yield and radioactive concentration, the elution profiles of the generators were studied by collecting the ^{68}Ga eluates as 0.5 mL aliquots, and the activity of each

fraction was determined by measuring the 511 keV γ-ray peak in a HPGe detector. The ^{68}Ga-elution profiles of t-ZrO_2 and CeO_2-PAN based generators are illustrated in **Fig. 4.7** and **Fig. 4.8**, respectively.

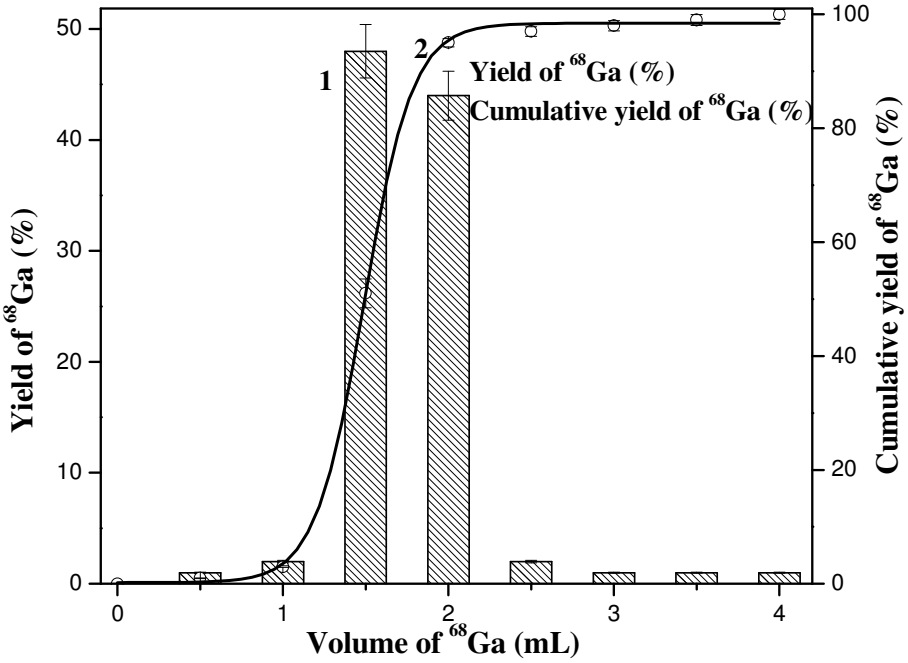

Fig. 4.7: Elution profile of the t-ZrO_2 based ^{68}Ge/^{68}Ga generator

It can be seen from the figures that the elution profiles of both the generators are quite sharp in nature. In the case of t-ZrO_2 based generator, <2% of the ^{68}Ga was eluted in the first 1 mL fraction and >90% of the ^{68}Ga activity was eluted in the subsequent 2 mL of eluate. Therefore, for the regular elutions of the t-ZrO_2 based generator, the first 1 mL fraction containing negligible amount of ^{68}Ga was discarded and the majority of ^{68}Ga was available in 2 mL of 0.01 N HCl solution with appreciable radioactive concentration. Similarly, in the case of the CeO_2-PAN based ^{68}Ge/^{68}Ga generator, <3% of the ^{68}Ga was eluted in the first 1.5 mL fractions and >90% of the ^{68}Ga activity was obtained in the subsequent 2 mL of eluent. Therefore, for the regular elutions of the CeO_2-PAN based generator, the first 1.5 mL fraction containing negligible amount of ^{68}Ga was discarded and the majority of ^{68}Ga in the

subsequent in 2 mL of 0.01 N HCl solution was used for the preparation of radiopharmaceuticals.

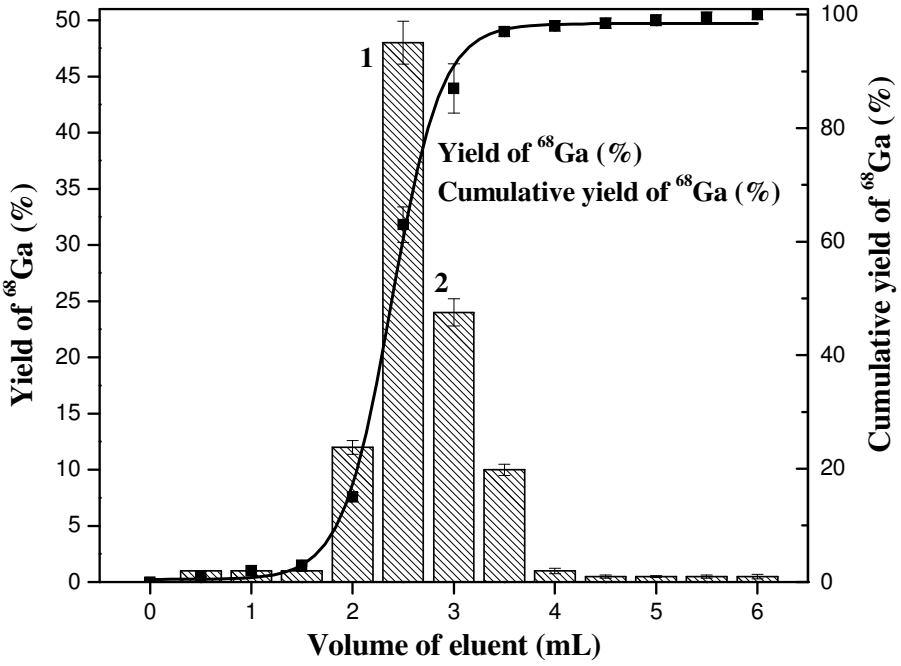

Fig. 4.8: Elution profile of the CeO_2-PAN based ^{68}Ge/^{68}Ga generator

4.7 Quality control of ^{68}Ga eluate

4.7.1 Radionuclidic purity

In order to utilize ^{68}Ga obtained from ^{68}Ge/^{68}Ga generators for clinical applications, special attention is necessary to ensure that the level of ^{68}Ge radionuclidic impurity present in ^{68}Ga is always below the permissible limit. This is important since, with the passage of time, even trace amounts of the long-lived ^{68}Ge impurity would reach appreciable proportions as a radionuclidic impurity. When small quantities (MBq/mCi levels) of radiopharmaceuticals labeled with short-lived ^{68}Ga are administered to patients for diagnostic purposes, even fractional percentages of the long-lived parent (^{68}Ge), if present, will add to the radiation dose to the patients and are therefore undesirable. The radionuclidic purity of the ^{68}Ga eluted from both the generators was assessed by measuring the half-life of ^{68}Ga and by γ-ray spectrometry

of the decayed ^{68}Ga samples using a calibrated HPGe detector coupled to a multi-channel analyzer.

4.7.1.1 Decay pattern of ^{68}Ga

The decay pattern of ^{68}Ga was monitored by following the half-life of ^{68}Ga using a NaI (Tl) counter (window 400-600 keV). The decay was followed for nearly 6 h (~6 half-lives of ^{68}Ga). The decay profile of a typical ^{68}Ga sample is shown in **Fig. 4.9**. The absence of any deviation at the lower end of the straight line decay curve confirmed that the ^{68}Ga samples were pure and contained negligible quantities of long-lived ^{68}Ge. The results were almost similar in case of both the generators. The half-life of ^{68}Ga as calculated using the decay profile was (66.7 ± 0.5) min (n =5) which was close to the 67.71 min half-life reported for ^{68}Ga.

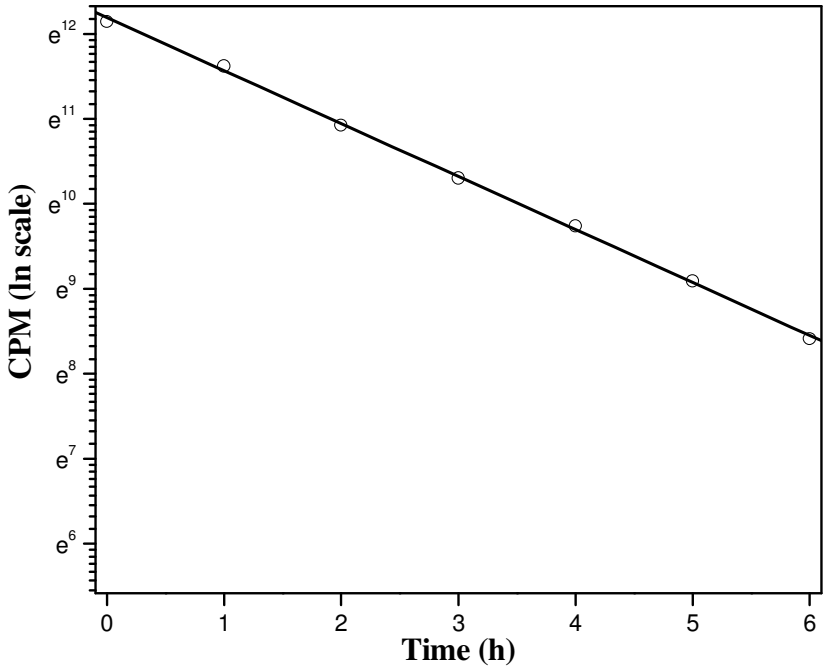

Fig 4.9: Decay profile of ^{68}Ga

4.7.1.2 γ-ray spectrometry

Since ^{68}Ge decays solely by electron capture to ^{68}Ga, the amount of ^{68}Ge contamin-

ation in ^{68}Ga eluate could not be directly estimated by γ-ray spectrometry. The ^{68}Ge contamination level in ^{68}Ga was quantified by allowing the separated ^{68}Ga samples to decay for 24 h and then measuring the 511 keV γ-ray peak, corresponding to emission from ^{68}Ga daughter. This in turn corresponds to the level of ^{68}Ge contaminant, which exists in secular equilibrium with ^{68}Ga. The amount of ^{68}Ge impurities in ^{68}Ga eluates from both the generators were always <20 Bq (<10^{-5}% of the total ^{68}Ga activity) in all the elutions over the period of 1 year.

The radionuclidic purities of ^{68}Ga obtained from the t-ZrO_2 and CeO_2-PAN based generators were comparable to that obtained from commercial generators [19,166,167]. However, it must be noted that the eluate (^{68}Ga) from commercial generators were subjected to multiple purification steps [2,166,167,183] to obtain clinical grade ^{68}Ga, whereas, the ^{68}Ge/^{68}Ga generators described here provided ^{68}Ga of similar purity in a single step**.** This proved that ^{68}Ga was availed from the nanomaterials based generators with high radionuclidic purity and was hence suitable for radiopharmaceutical applications.

4.7.2 Chemical purity

The ^{68}Ga eluted from the generators might be associated with other metal ions (like Zr, Ce, Cu, Pb, Co, Cr, Cd, Ni, Fe, Mn and Zn ions) as chemical impurities [19,167]. The presence of Zr and Ce ions in the ^{68}Ga eluates could be a possibility due to dissolution of t-ZrO_2 and CeO_2-PAN in HCl medium, respectively. The other metal ion impurities like Cu, Pb, Co, Cr, Cd, Ni, Fe, Mn ions could be introduced through the raw materials used and are noted to be occasionally present in the ^{68}Ge solution [19,167]. Additionally, ^{68}Ge may contain significant amounts of Zn ions as a decay product of ^{68}Ga. [19,167]. These metal ions might be eluted along with ^{68}Ga in HCl medium. The presence of these chemical impurities in ^{68}Ga might interfere in the complexation of ^{68}Ga with various ligands and biomolecules. Thus it is necessary to estimate the concentrations of these metal ions in the ^{68}Ga as a quality assurance

step. In order to determine the presence of chemical impurities in the ^{68}Ga eluate, the ^{68}Ga samples were allowed to decay for 7 days. The trace levels of the metal ion contamination in the decayed samples were determined by ICP-AES analysis. The calibration curves for these ions were obtained by using standard solutions having known concentration of these ions.

The level of Zr ions in the ^{68}Ga eluate from the t-ZrO_2 based ^{68}Ge/^{68}Ga generator, as analyzed by ICP-AES analysis, was found to be as low as (0.05±0.01) ppm [(0.05±0.01) µg mL^{-1}] (n =5). Similarly, in the ^{68}Ga eluate from the CeO_2-PAN based ^{68}Ge/^{68}Ga generator, the level of Ce ions was (0.08 ± 0.03) ppm [(0.08±0.03) µg mL^{-1}] (n = 5) The level of Zr and Ce ions impurity in the ^{68}Ga eluates were analyzed by random selection of ^{68}Ga samples over a period of 1 year. It was found that the level of Zr and Ce ions in the ^{68}Ga eluates from the respective generators was consistently low over this prolonged period of time. It is clear from the result that both t-ZrO_2 and CeO_2-PAN are stable to both radiation as well as chemical degradation on repeated elution over a prolonged period of 1 year and do not lead to the dissolution of the column matrices, unlike the conventional sorbents [19,166,167].

In the ^{68}Ga eluted from both the generators, Pb and Cr ions were below the detectable limits of the ICP-AES system used and the amounts of Co, Cu, Cd, Ni, Fe ions etc. were <5 ng mL^{-1}. Owing to the unavailability of instrumental facility to analyze radioactive samples, elemental analysis of Zn in the freshly eluted ^{68}Ga samples could not be carried out. The presence of Zn ions below appreciable amounts which could interfere in the complexation chemistry of ^{68}Ga could be indirectly tested by investigating the labeling efficacy of ^{68}Ga, described in the next section.

It was also essential to scrutinize the ^{68}Ga eluate from the CeO_2-PAN based ^{68}Ge/^{68}Ga generator for the presence of organic residues, possibly due to the radiolytic degradation of the polyacrylonitrile matrix. Trace amounts organic residue from the polyacrylonitrile binding matrix was assayed by UV-Visible spectrometry using the decayed ^{68}Ga samples. It

is reported that PAN shows weak absorption at λ_{max} of 278 nm in the UV-Visible spectra, which corresponds to the n–π* transition of nitrile-groups [190]. From the UV-Visible spectra of the decayed ^{68}Ga samples it could be inferred that PAN residue was not present in the ^{68}Ga eluate as no absorption was observed at this wavelength.

4.8 Labeling efficacy of ^{68}Ga

In order to evaluate the suitability of ^{68}Ga for biomedical applications, it was used for the preparation of ^{68}Ga-DOTA-TATE. This is also an indirect test to ascertain the chemical purity, as high chemical purity is essential to achieve a good complexation yield of the radiolabeled agent. For radiolabeling of DOTA-TATE with ^{68}Ga, 20 µL of DOTA-TATE solution (1 µg µL^{-1}) in HPLC grade water was mixed with 980 µL of 0.01 M ammonium acetate buffer (pH ~5) and 1 mL of ^{68}Ga eluate (~296 MBq, 8 mCi in 0.01 N HCl medium) was added to it. The pH of the resulting mixture was found to be ~4-4.5, and was carefully adjusted to ~4 (if required) by addition of 0.1 N HCl. The resulting mixture was incubated at 90 °C for 15 min. The extent of complexation achieved was determined by paper chromatography (PC) using 50% acetonitrile in water (v/v) as the eluting solvent as well as by high performance liquid chromatography (HPLC). HPLC was carried out using a dual-pump HPLC unit with a C-18 reversed phase HiQ-Sil (5 µm, 25 × 0.46 cm) column. The elution was monitored by measuring the 511 keV γ-ray of ^{68}Ga using NaI (Tl) detector (window 400-600 keV). The mobile phase consisted of water (A) and acetonitrile (B) mixtures with 0.1% trifluoroacetic acid and the following gradient elution technique was adopted for the separation: 0-4 min 95% A, 4-15 min 95% to 5% A, 15-20 min 5% A, 20-25 min 5% A to 95% A, 25-30 min 95% A. The flow rate was maintained at 1 mL min^{-1}. The paper chromatography (PC) patterns of the ^{68}Ga-DOTA-TATE and uncomplexed $^{68}Ga^{3+}$ as $^{68}GaCl_3$ are shown in **Fig. 4.10.**

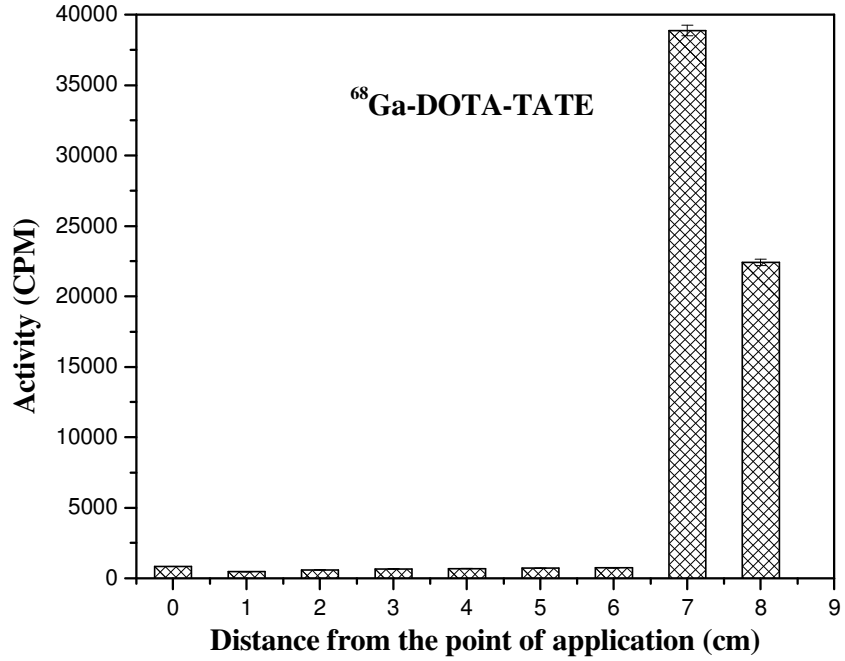

(a)

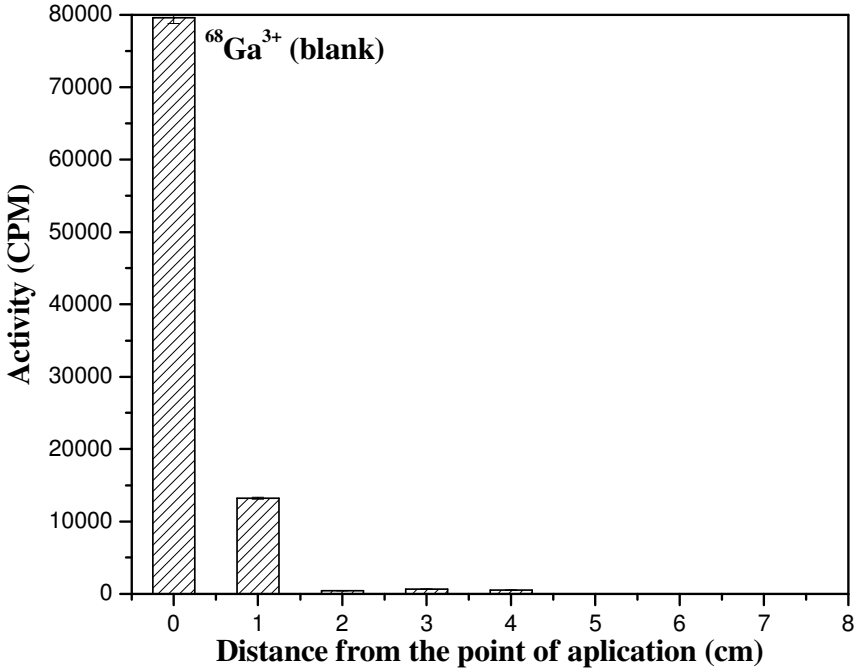

(b)

Fig. 4.10: Paper chromatographic patterns of (a) ^{68}Ga-DOTA-TATE and (b) $^{68}GaCl_3$ in 50% acetonitrile in water

From the PC pattern, it can be seen that ^{68}Ga-DOTA-TATE moved towards the solvent front (R_f = 0.8-0.9) (**Fig 4.10a**), while under identical conditions unlabeled $^{68}Ga^{3+}$ remained at the point of application (R_f = 0) (**Fig. 4.10b**). Further, it was observed that as low as 20 µg of DOTA-TATE (13.9 nmol) was sufficient for labeling ~296 MBq (8 mCi) of ^{68}Ga with >99% complexation yield. The complexation yield of ^{68}Ga-DOTA-TATE was validated by HPLC studies. A typical HPLC pattern of ^{68}Ga-DOTA-TATE is shown in **Fig. 4.11**.

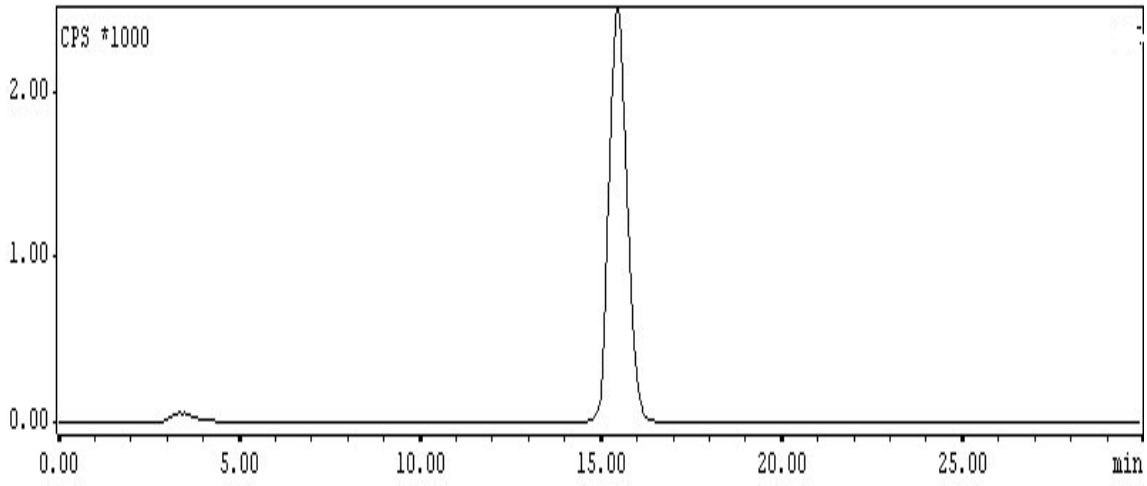

Fig. 4.11: HPLC pattern of ^{68}Ga-DOTA-TATE

The specific activity of ^{68}Ga-DOTA-TATE was ~21.3 MBq nmol^{-1} and it was obtained with >99% radiochemical purity. The high radiochemical purity of ^{68}Ga-DOTA-TATE was comparable to that of ^{68}Ga-DOTA-peptides prepared by the reported methods, adopting multiple purification steps [19,166,167,185]. The present findings amply suggest that traces of Zn ions, if present, in the eluate do not interfere significantly in the complexation chemistry of ^{68}Ga. The small volume of the ^{68}Ga eluate from the t-ZrO_2 and CeO_2-PAN based ^{68}Ge/^{68}Ga generators, with appropriate radioactive concentration and the availability of $^{68}Ga^{3+}$ ions in an uncomplexed and highly pure form, facilitate the direct use of ^{68}Ga for labeling of biomolecules without the inclusion of post-elution processing procedures.

4.9 Elution performance of the generators over a period of 1 year

The ^{68}Ge/^{68}Ga generators were eluted on every working day over a period of 1 year.

Over this period of time, the generators were eluted for more than 260 times. The performance of the t-ZrO_2 and CeO_2-PAN based generators with respect to the radiochemical yield of ^{68}Ga and the ^{68}Ge breakthrough is illustrated in **Fig. 4.12** and **Fig. 4.13,** respectively. The figures show that for the both the generators, the radiochemical yield of ^{68}Ga was always >80% and the level of ^{68}Ge impurity present in ^{68}Ga was $<10^{-5}$% over this period of 1 year.

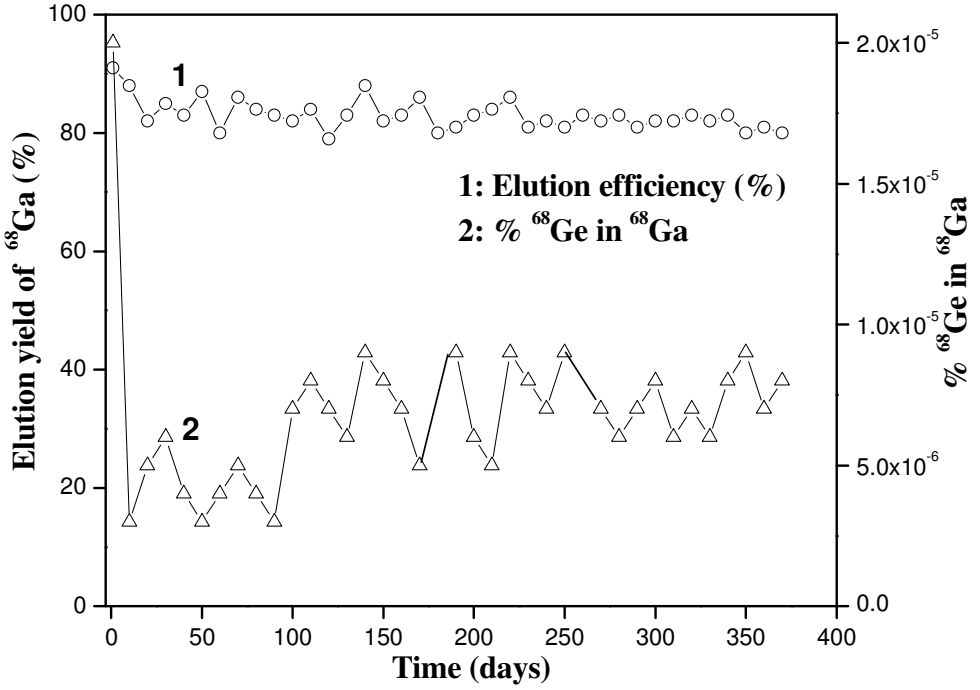

Fig. 4.12: Performance of the t-ZrO_2 based ^{68}Ge/^{68}Ga generator over a period of 1 y, data points shown at 10 d intervals

A major advantage of the t-ZrO_2 and CeO_2-PAN based ^{68}Ge/^{68}Ga generators is the consistency in their performance which is far superior to that of the widely used SnO_2 and TiO_2 based ^{68}Ge/^{68}Ga generators, which have been reported to show degrading performance on repeated elution, over a prolonged period of time [19,166,170]. It is reported by Asti et al [166], that the amount of ^{68}Ge breakthrough increased with time (~15% increase per month), ranging from 1.1×10^{-2}% to 2.6×10^{-2}% of the ^{68}Ga activity within the 7 months of evaluation.

Moreover, the elution yields of ^{68}Ga from these generators decreased from 82% to 69% on repeated elution (100 times) over the period of 7 months [166].

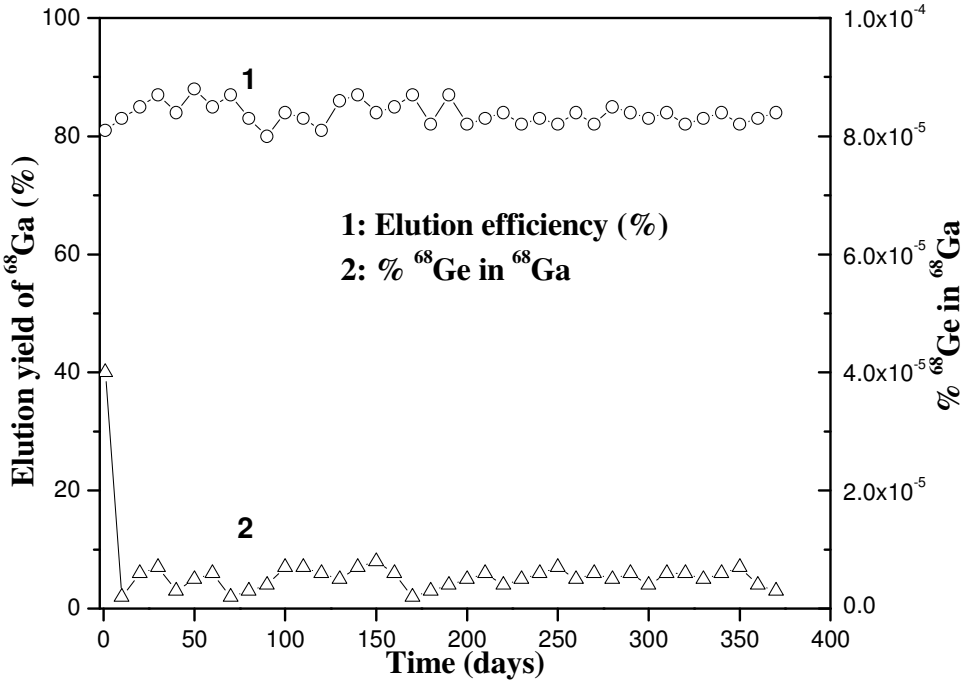

Fig. 4.13: Performance of the CeO_2-PAN based ^{68}Ge/^{68}Ga generator over a period of 1 y, data points shown at 10 d intervals

Though the consistency of the elution yield (>80%) and purity of ^{68}Ga are good indications of the radiation stability of the sorbents, the effect of radiation on the performance of t-ZrO_2 and CeO_2-PAN loaded with clinically useful amount of ^{68}Ge (~1.85 GBq or 50 mCi) is yet to be demonstrated. However, it is well reported that nanocrystalline metal oxides exhibit enhanced radiation stability compared to the bulk materials [68]. For both the generators, the sorbent matrices were stable to radiation, over a prolonged period of time, and did not lead to bleeding of Zr or Ce ions in the ^{68}Ga eluate, unlike the commercially available TiO_2 or SnO_2 based ^{68}Ge/^{68}Ga generators [19,166,167,183]. However, this needs to be ascertained by preparing generators of much higher activity.

4.10 Simulated study for the separation of Ga from a Ge carrier-added solution, equivalent to ~3.7 GBq (100 mCi) of ^{68}Ge

The performance of t-ZrO_2 and CeO_2-PAN as column matrices for ^{68}Ge/^{68}Ga generators of higher level of activity, was investigated by using inactive Ge carrier-added solution simulated to represent ~3.7 GBq (100 mCi) of ^{68}Ge. The simulated solution was prepared by dissolving 21 µg of GeO_2 (equivalent to 3.7 GBq of no-carrier-added ^{68}Ge) in 0.1 M NaOH. The resultant solution was evaporated to dryness and then reconstituted with 0.01 M HCl solution. The above solution was spiked with an equilibrium mixture of ^{68}Ge/^{68}Ga containing 185 MBq (5 mCi) of ^{68}Ge. The pH of the solution was adjusted to ~2 by adding 1 N HCl. The mixture was loaded in a borosilicate glass column [8 cm × 0.6 cm (i.d.)] containing 1 g of the respective sorbent, adopting the procedure outlined above. ^{68}Ga was eluted with 3 mL of 0.01 N HCl solution under the same conditions as in the previous studies. The efficiency of ^{68}Ga elution and the ^{68}Ge breakthrough were determined, for the generators developed using t-ZrO_2 and CeO_2-PAN sorbents. For both the sorbent materials, the recovery of ^{68}Ga from Ge/Ga mixture simulated to represent 3.7 GBq (100 mCi) of ^{68}Ge, was as good when lower amounts of ^{68}Ge were used. The overall yields of ^{68}Ga in the simulated experiments were always >80% and the ^{68}Ge breakthrough was $<10^{-5}$%. It must be mentioned here that although the simulated experiments gives a fair idea about the sorption capacity and separation efficacy of both the sorbents at higher level of activity, the effect of radiation dose over a prolonged period of time on the performance of the material is yet to be demonstrated.

4.11 Advantages of t-ZrO_2 and CeO_2-PAN based ^{68}Ge/^{68}Ga generators

The present study clearly suggests that both t-ZrO_2 and CeO_2-PAN are very effective sorbents for the preparation of ^{68}Ge/^{68}Ga generator for clinical applications. The major benefits in the use of these nanomaterial based sorbents in the preparation of ^{68}Ge/^{68}Ga generators are: (1) high capacity of the sorbents owing to small size and high specific surface

area (2) rapid packing due to the high density of the sorbents that settles in a few minutes, (3) rigidity which allows the use of high flow rates, (4) enhanced chromatographic efficiency due to large surface to volume ratio and (5) negligible ^{68}Ge bleeding due to the stable chemical link of the ^{68}Ge species to the matrix and (6) chemical and radiation stability of the sorbent matrices (7) direct usability of the ^{68}Ga eluate for the preparation of radiopharmaceuticals.

Several modifications can be incorporated in these new generator systems developed and reported here. This includes scaling up to higher activity level (up to 3.7 GBq, 100 mCi), use of extremely high purity reagents to avoid metal ion contamination, elution of ^{68}Ga under sterile conditions and automation of the entire process. It is my goal to carry out all these developments in near future to improve this generator into an easily adaptable system for hospital radiopharmacies.

4.12 Conclusions

In the present study, a rapid, simple, reliable and chemically efficient chromatography method has been established using t-ZrO_2 and CeO_2-PAN as sorbent matrices, to avail ^{68}Ga with acceptable radioactive concentration, yield and purity from ^{68}Ge. The efficacy of these new generation sorbent materials could be demonstrated by developing two 740 MBq (20 mCi) ^{68}Ge/^{68}Ga generators, which are still giving consistently good performance after repeated elutions over a period of 1 year. ^{68}Ga could be regularly eluted from the generator with acceptable radioactive concentration with substantially high yield and purity. The efficacy of ^{68}Ga for the preparation of radiopharmaceuticals for PET imaging could be confirmed by radiolabeling DOTA-TATE with very high complexation yield. The results presented here are promising and the generator systems are amenable for automation. These generators may be very useful for countries where commercial sources of PET radioisotopes are not readily available or too expensive.

CHAPTER 5

DEVELOPMENT OF $^{90}Sr/^{90}Y$ GENERATOR

"The significant problems we face cannot be solved at the same level of thinking we were when we created them."

ALBERT EINSTEIN

5.1 Introduction

5.1.1 Yttrium-90 (^{90}Y) – an important therapeutic radionuclide

^{90}Y is a therapeutic radioisotope of enormous interest and radiopharmaceuticals based on ^{90}Y are widely used for radiolabeling various targeting molecules for the treatment of cancer as well as in radiation synoviorthesis [191-200]. The broad interest in the use of ^{90}Y in therapeutic Nuclear Medicine is due to its suitable nuclear characteristics [15] ($t_{½}$ = 64.1 h, β^-_{max} 2.28 MeV, no γ-emission) and favorable chemistry. Particulate-based radiopharmaceuticals used for treatment of liver carcinoma as well as radiosynoviorthesis can be prepared by using ^{90}Y produced by neutron activation of ^{89}Y in a nuclear reactor [201-203]. As yttrium is mononuclidic, there is no need for enriched isotopes for irradiation. The radionuclidic purity of this directly (n,γ) activated product is generally very high. However, depending on the epithermal flux in the reactor, detectable levels of strontium-89 (^{89}Sr) could be present owing to the (n,p) reaction. Moreover, (n,γ)^{90}Y produced in a reactor, is of low specific activity due to the small neutron absorption cross-section (0.001 b) of ^{89}Y [15]. No-carrier-added (NCA) ^{90}Y of near theoretical specific activity is required for the preparation of labeled antibodies and peptides used for targeted therapy [203].

5.1.2 Availability of NCA ^{90}Y from ^{90}Sr

A radionuclide generator system based on the secular equilibrium of strontium-90 (^{90}Sr) decaying to ^{90}Y is a convenient method for the production of high specific activity ^{90}Y [59,204]. The simplified decay scheme of ^{90}Sr is shown in **Fig. 5.1**. There is an unlimited potential for availing NCA ^{90}Y, as ^{90}Sr is one of the major fission products and the annual world production of ^{90}Sr in the nuclear reactors amounts to several hundred megacuries [205]. Currently, spent reactor fuel is reprocessed in 5–6 countries, and these countries have the capability to develop the process chemistry required for large-scale isolation of ^{90}Sr from fission product waste.

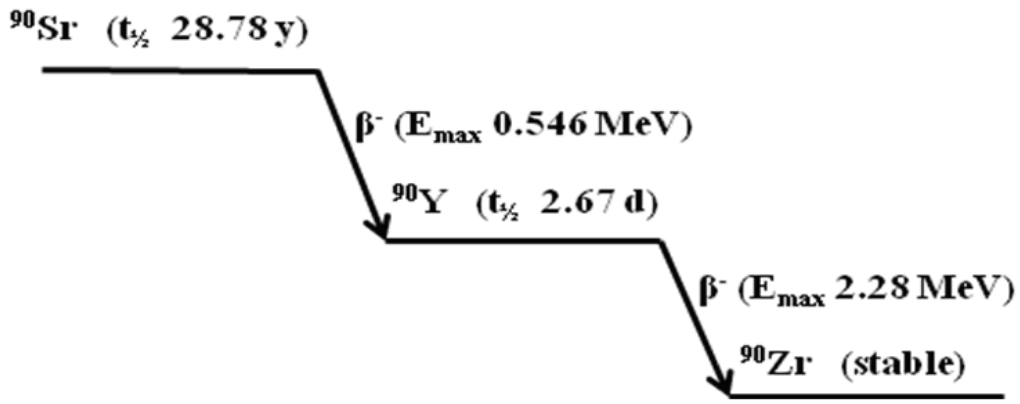

Fig. 5.1: Simplified decay scheme of ^{90}Sr (energy levels not drawn to scale)

There is an industrial level facility for recovery of ^{90}Sr (and other fission products) at Mayak, Russia [206]. A facility for the recovery of 55500 GBq (1500 Ci) of pure ^{90}Sr was set up at the Pacific Northwest National Laboratory, Washington, DC, USA, and the process chemistry used in that plant is documented [205]. At the Bhabha Atomic Research Centre, separation of ^{90}Sr from the high level PUREX waste usable for ^{90}Sr/^{90}Y generator has been developed [207]. ^{90}Sr/^{90}Y is one of the typical examples of a secular equilibrium with a very long-lived parent ($t_{½}$ 28.8 y) and a short-lived daughter ($t_{½}$ 64.1 h). By adapting suitable separation techniques, a few thousand Curies of usable high purity ^{90}Y can be isolated from a 37 GBq (1 Ci) stock of ^{90}Sr.

5.1.3 Separation of ^{90}Y from ^{90}Sr

Owing to the long half-life of ^{90}Sr, the technology required for fabrication of ^{90}Sr/^{90}Y generators is considerably different from that used for other generators such as the ^{99}Mo/^{99m}Tc and ^{188}W/^{188}Re generator systems [203]. The ^{90}Sr cannot be left in the column matrix any longer than necessary, because of denaturation of the sorbent resulting from energy deposition of the high energy β^- particles from decay of the ^{90}Sr and ^{90}Y [203]. This often results in the lowering of ^{90}Y yield and breakthrough of ^{90}Sr in the eluate [203]. The availability of ^{90}Y with very low levels of ^{90}Sr contamination is essential for therapeutic

applications, as ^{90}Sr localizes in the skeleton and, owing to its long half-life, has a very low maximum permissible body burden of 74 kBq (2 μCi) [208].

During the last two decades, several separation technologies have been developed for the separation of ^{90}Y from ^{90}Sr [59,204,209-221]. Most of the current separation techniques involve multiple steps such as solvent extraction, ion exchange or extraction chromatography either alone or in combination. A number of internationally valid patents have also been issued [222-225]. Bray et al. [222], used 'purified' HEDP to remove the ^{90}Y into the organic layer, followed by several steps of scrubbing, stripping, purification by ion exchange chromatography etc. The method was further modified using ^{90}Sr specific resins and a fresh patent was taken in 2006 [223]. This reported method is cumbersome, needing the manipulation of large quantities of ^{90}Sr activity in small volumes in several steps. The method described in the above patents also use a large amount of reagents such as acids, ion exchangers etc. thereby giving the possibility of introduction of metallic as well as organic impurities. The generation of radioactive waste is also very high in this technique. In the patent by Horwitz et al. [224], precipitation of ^{90}Sr and separation of the crystalline $^{90}Sr(NO_3)_2$ by centrifugation followed by filtering is done to remove the bulk quantity of ^{90}Sr. This is followed by purification of ^{90}Y by ion-specific resin. This procedure results in the production of high active ^{90}Sr waste, both, solid and liquid as well as the loss of ^{90}Sr. Moreover, the process is cumbersome and ^{90}Y availed might be associated with ^{90}Sr impurity. The patent by Betenekoy et al. [225] describes a method for purification of ^{90}Sr, followed by extraction of ^{90}Y by ion exchange. This method based on ion exchange using thermoxide type of adsorbents could possibly be used as an industrial scale process, but is not expected to be superior to the other reported methods.

Though a large number of separation technologies have been developed, none of them are amenable for regular use in a hospital radiopharmacy. The feasibility of installation of a

$^{90}Sr/^{90}Y$ generator system for operation in a Nuclear Medicine department is still an unrealistic proposition. Currently, ^{90}Y is separated by industrial manufacturers and supplied as a radiochemical in inorganic form to the radiopharmacies. The cost of ^{90}Y is high (US \$15–20 per mCi of ^{90}Y as compared to <\$1 per mCi of ^{131}I, a widely used well established therapeutic radioisotope) and the availability is limited due to the transportation logistics [226]. Hence, the benefits of targeted therapy using ^{90}Y radiopharmaceuticals are currently available only to a small number of patients in a few developed countries [203].

The development of a $^{90}Sr/^{90}Y$ generator that can be operated in a central pharmacy could increase the availability of ^{90}Y. In smaller countries, such generators could also be located in national radiopharmaceutical production centers. However, for developing such a generator, the possibility of unacceptable levels of ^{90}Sr breakthrough and the lack of proper analytical methods for estimation of ^{90}Sr in the eluted ^{90}Y, are some of the issues which need to be resolved. Also, the production of long-lived wastes that require careful handling and storage is encountered with the use of such generators. In addition, the security of ^{90}Sr in nuclear pharmacies and the potential hazards in case of its misuse in public domain have to be also kept in perspective. Since ^{90}Sr is a highly toxic radionuclide, it is very essential that the ^{90}Sr inventory is strictly maintained. ^{90}Sr should be handled in a well-established, controlled laboratory by trained personnel with strict inventory maintenance.

5.1.4 The present work

Reischl et al. [126] had demonstrated the separation of pure ^{86}Y, a PET radionuclide, from milligram quantities of irradiated ^{86}Sr by a simple electrochemical method. Later, Yoo et al. reported the use of the above electrochemical separation technique for the preparation of ^{86}Y for patient specific dosimetry studies prior to the administration of ^{90}Y based radiopharmaceuticals [127]. Both the experiments used milligram amounts (50-150 mg) of enriched ^{86}Sr and the researchers were able to isolate pure ^{90}Y in usable quantities (>100

mCi). The method used by them was simple, with minimum processing steps, low waste generation, recovery of unused ^{86}Sr enriched target and above all, the radionuclidic purity of the resultant ^{86}Y was acceptable for clinical work. The system developed by them is amenable for automation and can be operated in a Nuclear Medicine department based PET radiochemistry laboratory. The electrochemical method as a procedure for separating $^{90}Y^{3+}$ from $^{90}Sr^{2+}$ was reported, as early as 1957-58 by Lange et al. [227] and by Hamaguchi et al [228]. However, it was never utilized for the separation of clinical grade ^{90}Y from ^{90}Sr. This chapter describes the use of the electrochemical separation system for the development of a $^{90}Sr/^{90}Y$ generator. The feasibility of the method, both in terms of yield and the purity of the ^{90}Y for preparation of radiopharmaceuticals, has been demonstrated and evaluated, in the studies reported here.

5.2 Materials

^{90}Sr in equilibrium with ^{90}Y in 2 M HNO_3 was available in the Radiopharmaceuticals Division of the Bhabha Atomic Research Centre. $^{85+89}Sr(NO_3)_2$ is a regular product of the Radiopharmaceuticals Division, BARC for commercial supply. Nitric acid, ammonium hydroxide, acetone, ethyl alcohol and other reagents and chemicals were of analytical grade and were procured from S.D. Fine Chemicals, Mumbai, India. Platinum metal plates of high purity (+99.9%, provided with material testing certificate) were procured from M/s Hindustan Platinum, Mumbai, India. Paper chromatography strips were purchased from M/s Whatman, Kent, UK.

Gamma activity of $^{85+89}Sr$ was assayed using a NaI (Tl) scintillation counter (500–700 keV). ^{90}Y and ^{90}Sr activities when present in MBq (mCi) levels were measured in an ionization chamber. A NaI (Tl) scintillation counter was used in most counting experiments to measure the Bremmstrahlung radiations (50–500 keV) of ^{90}Y and ^{90}Sr when present in kBq (μCi) levels. A liquid scintillation counter (Model: Tricarb 2100TR, Packard Instrument,

Minnesota, USA) was used for the final measurement of Bq levels of ^{90}Sr activity in ^{90}Y. A HPGe multichannel analyzer, coaxial photon detector system (ORTEC, Oakridge, TN, USA) with a 0.5 keV resolution and 1.8 keV to 2 MeV range was used for identification of $^{85+89}Sr$, in the presence of ^{90}Y. The chemical analysis for the determination of trace levels of metal contaminations, were carried out using Inductively Coupled Plasma-Atomic Emission Spectroscopy (ICP-ES JY-238, Emission Horiba Group, France). A potentiostat unit with 100 V compliance, a maximum current of 2 A with 1.2 nA current resolution, $>10^{13}$ Ω input impedance, <5 pF capacitance and 10 μHz to 1 MHz built-in analyzer for impedance, was used in the electrochemical studies, for maintaining the potential between the electrodes. The apparatus for the electrochemical studies was prepared based on the reports of Reischl et al. [126] and Yoo et al. [127].

5.3 The electrochemical separation of ^{90}Y from ^{90}Sr

5.3.1 Principle of separation of Y from a mixture of Sr and Y

The separation of Y from a mixture of Sr and Y is based on the selective electrodeposition of Y on a platinum electrode. This is attributed to the difference in standard electrode potential of Sr^{2+} and Y^{3+} ions in acidic media. The electrochemical reactions involved and their standard reduction potentials are as follows [131]:

$$Sr^{2+} + 2e \rightarrow Sr \quad E^o = -2.89 \text{ V}$$

$$Y^{3+} + 3e \rightarrow Y \quad E^o = -2.27 \text{ V}$$

Though there is a very small difference in the standard electrode potentials of Sr^{2+} and Y^{3+} ions, Y^{3+} can be selectively electrodeposited on the cathode by controlled application of applied potential. When the electrolysis is carried out in aqueous medium using platinum electrodes, two possible background processes are also involved [229].

At cathode (negative electrode):

$$2H^+ + 2e \rightarrow H_2 \text{ (gas)}$$

At anode (positive electrode):

$$2H_2O \rightarrow O_2\ (gas) + 4H^+ + 4e$$

The hydrogen overpotential on platinum is practically negligible. When platinum electrodes are used, hydrogen is evolved at essentially the theoretical limit ($E^o = 0$ V).

For the electrodeposition of Y, the potential applied is far more negative than the threshold requirement of potential for the evolution of hydrogen gas at the platinum cathode. Consequently, brisk hydrogen gas evolution takes place at the platinum cathode and the pH of the electrolyte becomes alkaline near the vicinity of the cathode, due to the deficiency of H^+ ions [229,230]. Owing to the electrostatic attraction, both Sr^{2+} and Y^{3+} ions, which are positively charged, migrate towards the negatively charged cathode. At the surface of the electrode these metal ions react with water in alkaline environment to form their respective hydroxides. The separation of carrier-free ^{90}Y activity from an alkaline ^{90}Sr-solution was suggested in the classic text book by Friedlander et al. [231]. The difference in the solubility product of $Y(OH)_3$ (1×10^{-22}) and $Sr(OH)_2$ (3.2×10^{-4}) [232] allows selective deposition of Y on the surface of the cathode. The $Sr(OH)_2$ which is practically soluble in water goes to the bulk of the electrolyte, where the pH remains essentially acidic. The electrochemical deposition of yttrium has been extensively studied [230,233,234] in both aqueous as well as non-aqueous media. It is reported that yttrium is electrodeposited as a mixture of its oxide and hydroxides on the surface of metallic electrode when aqueous electrolytes are used [230]. The use of organic electrolytes for the electrochemical separation of ^{90}Y from ^{90}Sr was avoided, as the radiolytic damage to the electrolyte may be a deterrent to the efficiency of the separation. Moreover, the radiolytic products may contaminate the ^{90}Y and render it unsuitable for radiolabeling molecules for use in radiopharmaceuticals.

5.3.2 The electrochemical set-up

A schematic diagram of the electrochemical cell is shown in **Fig. 5.2.** For electrolysis,

the anode and cathode used were high purity platinum plates and a saturated calomel electrode (SCE) was used as the reference electrode. The electrochemical cell consisted of an open end quartz cylinder of 50 mL capacity fitted with an acrylic cap.

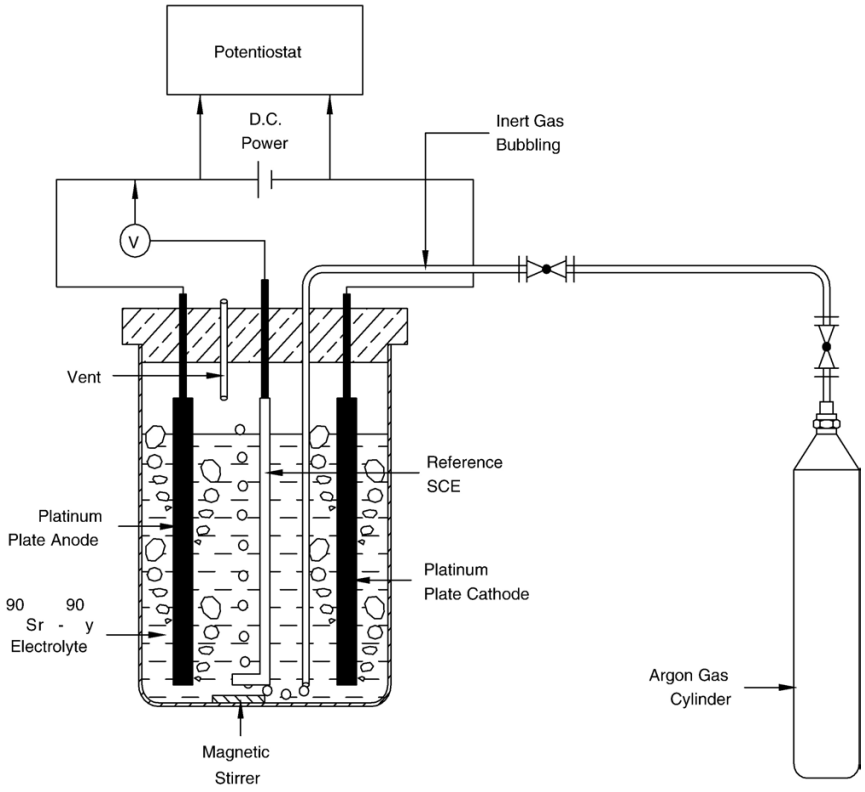

Fig 5.2: Schematic diagram of the electrochemical $^{90}Sr/^{90}Y$ generator

The electrodes were fabricated by spot welding platinum plates of size 75 (l)×10 (b)×0.5 mm (thickness) to a platinum rod. The electrodes were fitted 5 mm apart on the acrylic cap, which, along with the electrodes, fitted on the mouth of the quartz cylinder. The acrylic cap was used to vertically raise and lower the electrodes. The platinum electrodes were adjusted parallel to each other and then connected to the power supply using small screws which were embedded into the acrylic cap and touched the rod. A provision for passing gas through an acrylic tube, which dipped into the electrolysis solution, was given. A small outlet (~2.5 mm) was provided in the acrylic cap for venting the gases.

5.3.3 Optimization of the parameters of electrolysis for the separation of ^{90}Y from ^{90}Sr

5.3.3.1 Effect of the applied potential

Initially, to optimize the voltage to be applied for selective deposition of ^{90}Y, the effect of applied potential on deposition was studied by measuring the percentage deposition of ^{90}Y as a function of voltage when electrochemical deposition was performed at pH 2.5–3.0 at room temperature. The effects of applied potential on ^{90}Y deposition are summarized in **Table 5.1**.

Table 5.1: Effect of applied potential on electrodeposition of ^{90}Y from ^{90}Sr solution

Applied potential (V) (w.r.t. SCE)	Electrodeposition yield of ^{90}Y (%)
-1.0	4±2
-1.5	53±3
-2.0	80±3
-2.5	97±2
-3.0	>99

n=3, '±' indicates standard deviation

The results confirm the need for carrying out the electrodeposition experiment at -2.5 V with respect to SCE. The percentage of ^{90}Y deposited was observed to increase with increasing potential and attained maximum value at -2.5 V. Although the yield of ^{90}Y was >99% at -3.0 V, there was a possibility of co-deposition of ^{90}Sr at this voltage. Since the aim of the experiment was preferential separation of Y from Sr, the potential applied in subsequent experiments were maintained at -2.5 V with respect to SCE.

5.3.3.2 Effect of pH of the electrolyte

The pH of the electrolyte is critical for successful electrochemical deposition. Reischl et al. [126] had reported near-complete deposition (97±2%) of ^{90}Y at pH 2.5–3.0, and the same was adapted for these experiments. However, in order to examine if there are pH

changes during electrolysis and also to ensure that this pH range is the most optimum, one set of experiments were carried out to estimate the ^{90}Y deposition as a function of pH. As expected, in these experiments, ^{90}Y deposition was best in the range of pH 2–3 (**Fig. 5.3**), confirming the reports by Reischl et al. [126].

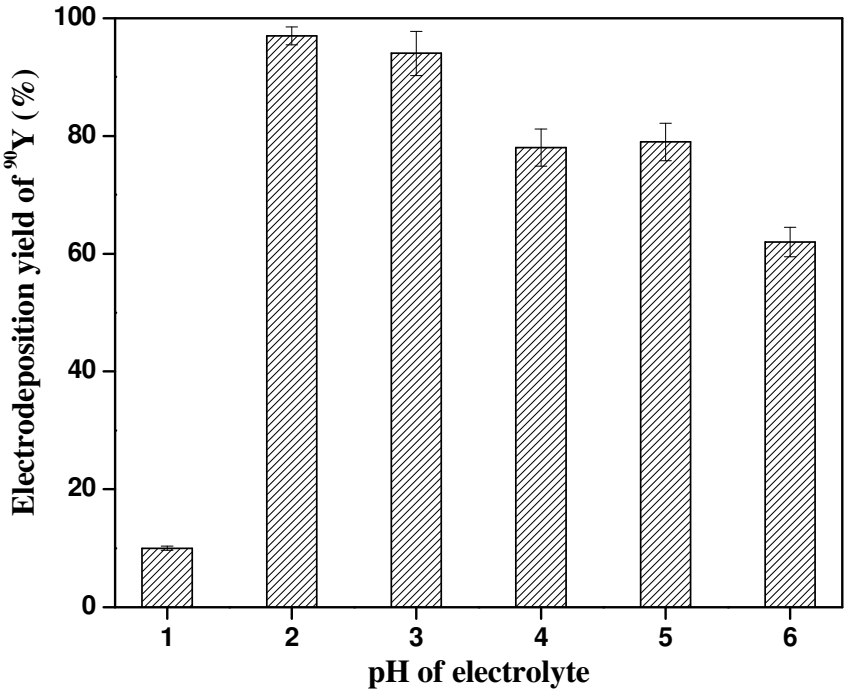

Fig. 5.3: Electrodeposition yield of ^{90}Y studied as a function of pH of the electrolyte

Although the pH of the electrolysis solution tends to increase slowly during electrolysis, the reduction in electrodeposition yield of ^{90}Y was not very significant, due to this shift in pH. Hence, there was no need to adjust the pH during electrochemical deposition. In all further experiments, electrolysis was carried out at pH 2.5–3.0 at a potential of −2.5 V with respect to SCE.

5.3.3.3 Effect of the time of electrodeposition

After optimization of the applied potential and pH of the electrolyte, experiments were carried out to estimate the minimum time required for quantitative electrodeposition of

Y at the optimum pH and potential. The electrodeposition yield of Y as a function of time is illustrated in **Fig. 5.4**, which shows the need to run the electrodeposition for at least 90 min.

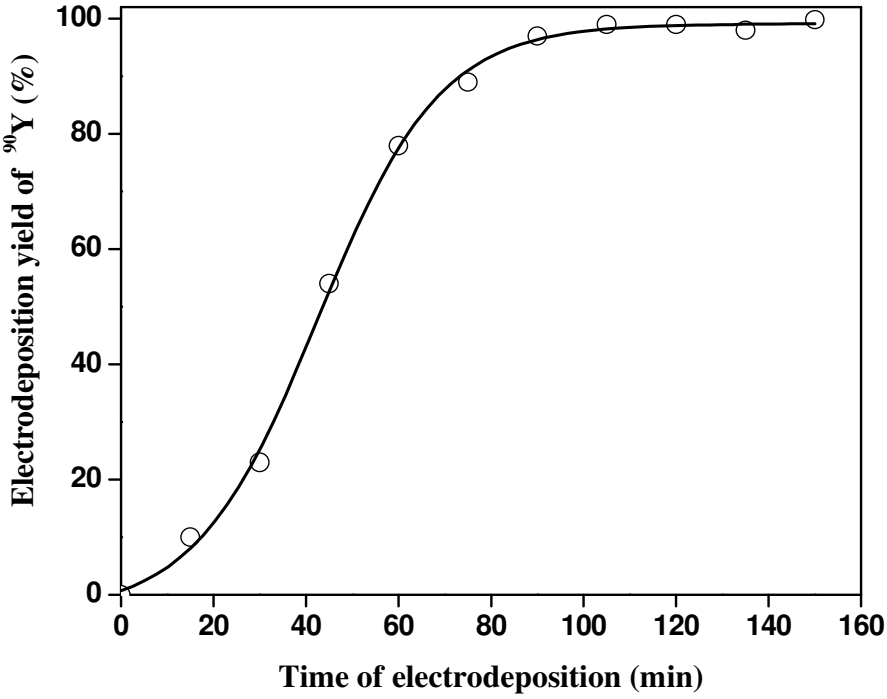

Fig. 5.4: Effect of time on the electrodeposition yield of ^{90}Y

5.3.3.4 Bubbling of argon gas during the course of electrolysis

Bubbling of an inert gas through the solution before and during electrolysis was essential to vent the gases produced during electrolysis as well as to keep the solution in dynamic form. It was observed that when electrodeposition was carried out without purging gas, the yield of ^{90}Y decreased drastically to <60%. This might be due to presence of dissolved oxygen in the electrolyte which interferes in the electroreduction of ^{90}Y. The use of nitrogen, helium and argon as inert gases, for the above purpose were evaluated and the results are summarized in **Table 5.2**. It is clear from the Table, that out of the three gases, helium and argon were found to be more suitable, than nitrogen. Argon gas was chosen for purging in all subsequent electrodeposition experiments, owing to ease of availability of this gas in our laboratory.

Table 5.2: Choice of gas purged during the course of electrodeposition of ^{90}Y

Gas purged	Electrodeposition yield of ^{90}Y (%)
Nitrogen	62 ± 3
Helium	96 ± 2
Argon	97 ± 1

n=3, '±' indicates standard deviation

5.4 Process Demonstration: Development of $^{90}Sr/^{90}Y$ generator

The method described by Reischl et al. [126] and Yoo et al. [127] was adapted for the separation of ^{90}Y from radioactive ^{90}Sr in equilibrium with ^{90}Y, containing zirconium-90 (^{90}Zr), the non-radioactive daughter product of ^{90}Y with a vital modification. This modification was carried out to avoid any co-deposition of ^{90}Sr along with ^{90}Y. It was observed that when the method proposed by Yoo et al. was followed, in which electrolysis was performed galvanostatically, the ^{90}Sr contamination in ^{90}Y was much more than the acceptable limit. So the electrolysis was carried out potentiostatically by applying a definite potential (−2.5 V with respect to SCE), at which only selective electrodeposition of ^{90}Y took place and the amount of ^{90}Sr co-deposited was well below the specified limits [208]. The electrochemical separation process involved two electrolysis cycles — the first cycle for separation and the second cycle for purification of ^{90}Y. The process adopted is described below.

Step 1: First electrolysis: The separation step

^{90}Sr was obtained as $^{90}Sr(NO_3)_2$ in 2 M HNO_3. 1.85 GBq (50 mCi) of this solution was placed in a 50 mL beaker and 37 MBq (1 mCi) of $^{85+89}Sr$ as $Sr(NO_3)_2$ was added as tracer to track the deposition of Sr in the electrode. The $^{90}Sr/^{90}Y$ equilibrium solution was evaporated to dryness and dissolved in 30 mL of 0.001 M HNO_3, which resulted in a clear solution. This ^{90}Sr solution was then transferred to the quartz electrochemical cell. The pH of

the electrolyte was adjusted to 2.5–3.0, if necessary, by drop-wise addition of 3% ammonium hydroxide. The electrolysis cell was then covered with the acrylic cap together with the two platinum electrodes. The electrodes were adjusted to be fully immersed in solution facing each other. Argon gas was gently bubbled through the solution for 10–15 min prior to applying current and the electrolysis was performed potentiostatically at −2.5 V with respect to SCE for 90 min. The electrodeposition yield after initial electrolysis was in the range of 97–98%. Removal of the electrodes from the electrolytic cell under voltage was recommended in previous work, the need for which was confirmed by these experiments. When the electrodes were removed after switching off the power supply, it was observed that the majority of the deposited ^{90}Y dissolved back into the electrolyte solution. This is not unexpected since ^{90}Y in hydroxide form is in extremely small quantities (ng-μg levels) and is thinly spread over the electrode surface which would be quickly dissolved by the acidic electrolyte solution in the absence of the potential. During the first electrolysis, the current initially applied was 200 mV which reduced to 100 mV at the end of the first electrolysis indicating the sharp decline in transport of ions, which in turn could be interpreted as the completion of Y^{3+} ion transport to the cathode.

Step 2: Second electrolysis: The purification step

At the end of initial electrolysis, the acrylic cap along with the electrodes was removed from the cell while maintaining the voltage. After switching off the current, the cathode plate was removed from the acrylic cell and washed with 10 mL of acetone in order to remove any free ^{90}Sr adsorbed on the surface of the electrode. After washing, the electrode was fitted to another acrylic cap into which a cylindrical platinum electrode of dimension 2.5 (ϕ)×75(l)×0.5 mm (thickness) was attached. A fresh quartz cell was filled with 50 mL of 0.003 M nitric acid, the pH of which was confirmed to be in the range 2.5–3 and carefully adjusted, if necessary. The acrylic cap containing the electrodes was fitted to the quartz cell,

and Argon gas was bubbled through the solution for 10–15 min. The cylindrical electrode was connected as the cathode, and the original platinum plate containing ^{90}Y was connected as the anode. Electrolysis was performed for 45 min at a constant potential of −2.5 V and 100 mA current, while Argon gas was continuously bubbled through the solution. During this process, ^{90}Y was leached from the platinum plate and was deposited onto the cylindrical platinum electrode. At the end of electrolysis, the acrylic cap was removed from the solution while maintaining the voltage. During the second electrolysis, the 100 mA current applied decreased by 20–30 mA by the end of the run. The cylindrical platinum electrode with the deposited ^{90}Y was washed with 10 mL of acetone, followed by leaching of ^{90}Y with 500 μL of acetate buffer at pH 4.75 into a separate glass tube. Rinsing the cylindrical platinum cathode with acetone removed whatever trace levels of ^{90}Sr loosely bound on the surface of the electrode. This step removed ~2% of the deposited ^{90}Y activity also. Most of the ^{90}Y activity (>95%) could be leached with 500 μL of 0.2 M acetate buffer at pH 4.75. The deposited ^{90}Y could be reconstituted in acetate, chloride or nitrate form. The use of 0.2 M acetate buffer at pH 4.75 was preferred, as the solution could be directly used for radiolabeling of biomolecules such as proteins and peptides. In the method proposed by Reischl et al. and Yoo et al., ^{86}Y was dissolved using 0.5–1.0 N HCl or 0.3–0.6 N HNO_3 and 2.8 M HNO_3/EtOH (3:1) [126,127], which would need further processing before radiolabeling the biomolecules. By appropriately adjusting the volume of the solution used for final dissolution, it was possible to obtain ^{90}Y at very high radioactivity concentrations. The time required for a complete run was about 3–4 h. The overall yield of ^{90}Y achieved was >90%.

Over a period of 2 years, the above experiments were repeated several times with 1.85 GBq (50 mCi) of ^{90}Sr, using the same feed solution in order to ascertain the consistency in the performance of the generator. The pH of the solution was checked and adjusted, if

needed, prior to each run. **Table 5.3** shows the results obtained in 10 typical batches. The performance of the $^{90}Sr/^{90}Y$ generator was consistently good in all the batches, over the period of 2 years.

Table 5.3: Performance of the electrochemical $^{90}Sr/^{90}Y$ generator

Batch No.	^{90}Sr in the electrolyte GBq (mCi) (Calculated)	^{90}Y growth period (Days)	Expected ^{90}Y activity GBq (mCi) (Calculated)	^{90}Y recovered GBq (mCi)	^{90}Y recovered (%)
1	1.850 (50.00)	15	1.81 (48.93)	1.68 (45.51)	92.9
2	1.848 (49.95)	09	1.67 (45.09)	1.57 (42.50)	94.3
3	1.847 (49.92)	33	1.84 (49.80)	1.68 (45.61)	91.6
4	1.843 (49.81)	16	1.81 (48.97)	1.69 (45.71)	93.4
5	1.841 (49.76)	13	1.77 (48.01)	1.68 (45.60)	95.1
6	1.840 (49.72)	20	1.83 (49.37)	1.71 (46.10)	93.3
7	1.837(49.65)	95	1.83 (49.33)	1.66 (44.98)	91.2
8	1.825 (49.34)	62	1.82 (49.13)	1.65 (44.56)	90.7
9	1.818 (49.13)	30	1.81 (49.01)	1.64 (44.32)	90.4
10	1.814 (49.03)	16	1.78 (48.20)	1.64 (44.34)	92.0

5.5 Maintenance of the ^{90}Sr feed solution and the electrodes after each typical batch

After each batch, in order to make the electrodes ready for subsequent experiments, they were washed with 3 M HNO_3. The platinum cathodes used in the above experiments were electrochemically cleaned by placing them in a 100 mL glass beaker containing 50 mL of 0.1 N HNO_3 solution. A new Cu electrode was also dipped in the solution and the polarity of the Pt cathode was reversed. A high voltage (10 V) was applied for 15 min and both the

electrodes were taken out from the solution after switching off the current. The platinum electrodes were then washed with water followed by washing with acetone.

The feed solution in the first electrolytic cell was also preserved since it retains most of the ^{90}Sr activity loaded in the cell. This solution was then allowed to stand for growth of ^{90}Y. The activity of the electrolyte in the second cell was monitored, since it was expected to contain traces of ^{90}Sr and ^{90}Y. It was then carefully transferred into a waste container. The acetone solutions obtained from washing the electrodes were also pooled and added to this solution, which was the only radioactive waste generated in this process. The total liquid waste generated in one typical operation contained only ~1 MBq (27 μCi) of ^{90}Sr. This essentially proves that the use of the electrochemical technique is also very advantageous from waste management point of view as it generates very small amount of radioactive waste in each typical batch.

5.6 Quality control of ^{90}Y

5.6.1 Radionuclidic purity of ^{90}Y

The extremely high toxicity of ^{90}Sr, limits its levels in the ^{90}Y used and also necessitates its absolute quantification before administering the ^{90}Y radiopharmaceutical to the patient. $^{90}Sr^{2+}$, being analogous to Ca^{2+}, gets accumulated in the bone. Owing to the bone seeking nature and the very long life of 28.8 y, the maximum permissible body burden (MPBB) for ^{90}Sr is as low as 74 kBq (2 μCi). This translates to limits of ^{90}Sr to 74 kBq in 37 GBq of ^{90}Y, assuming that a patient may be administered with a maximum of 37 GBq of ^{90}Y in his entire life time. This necessitates that ^{90}Y should be carefully analyzed to ensure that the levels of ^{90}Sr are well below the limits of 74 kBq per 37 GBq of ^{90}Y. Generally, radionuclidic purity estimation is performed by γ-spectrometry since many radionuclides used in Nuclear Medicine have γ-emission along with β^- emission, such as ^{188}W and ^{188}Re [203]. However, in the case of the $^{90}Sr/^{90}Y$ pair, both the parent and daughter are pure β^-

emitters and no γ-emissions are available to permit γ-analysis. Additionally, β-spectra of these two radioisotopes overlap to certain extent [59]. So in the case of ^{90}Sr/^{90}Y, β^- counting has to be done after separating them unambiguously.

Several methods have been described in literature for determination of ^{90}Sr contamination in the ^{90}Y availed from ^{90}Sr/^{90}Y generators [57-59,231,235,236]. For instance, a classical method available in literature describes the separation of ^{90}Sr and ^{90}Y under alkaline conditions on a filter paper [231]. However, the utility of this method for quantifying very low amounts of ^{90}Sr in ^{90}Y is not yet proven and needs to be fully validated before it can be used. Some authors have recently described a non-destructive assay method for determination of ^{90}Y and ^{90}Sr [235]. This method is used to quantify ^{90}Y based on counting of a very small fraction (34×10^{-6}) of positron branching taking place in ^{90}Y using a HPGe detector for several hours. However, this method would be impractical for regular use in a production laboratory or a radiopharmacy, wherein it is essential that the radiopharmaceutical is prepared and dispatched in a span of a few hours. These authors have also mentioned that this procedure requires sophisticated equipment which would be difficult to find in a radiopharmacy setup.

In this case, the purity of ^{90}Y was estimated by measurement of the half-life of ^{90}Y as well as by estimation of ^{90}Sr levels. ^{90}Sr levels were estimated either by measuring $^{85+89}$Sr activity used as tracers, using HPGe-based gamma ray spectroscopy and paper electrophoresis or by counting the ^{90}Sr present in the sample after allowing the ^{90}Y to decay for a very long period (~11.5 half lives of ^{90}Y). The extraction paper chromatography (EPC) technique recently reported by Pandey et al., allows estimation of the ppm levels of ^{90}Sr present in ^{90}Y [57]. The results were further validated by the inductively coupled plasma atomic emission spectroscopy (ICP-AES) analysis of the decayed ^{90}Y samples. The technical details of these techniques and the results obtained are described below.

5.6.1.1 Decay pattern of ^{90}Y

The decay pattern of ^{90}Y was monitored by following the half-life of ^{90}Y using a liquid scintillation counter. The decay was followed for nearly 700 h (~11.5 half-lives of ^{90}Y) and is illustrated in **Fig. 5.5**.The decay pattern conformed to the reported 64.1 h half-life of ^{90}Y. The absence of any deviation at the lower end of the straight line decay curve confirmed that the ^{90}Y fraction is pure and contains negligible quantities of ^{90}Sr.

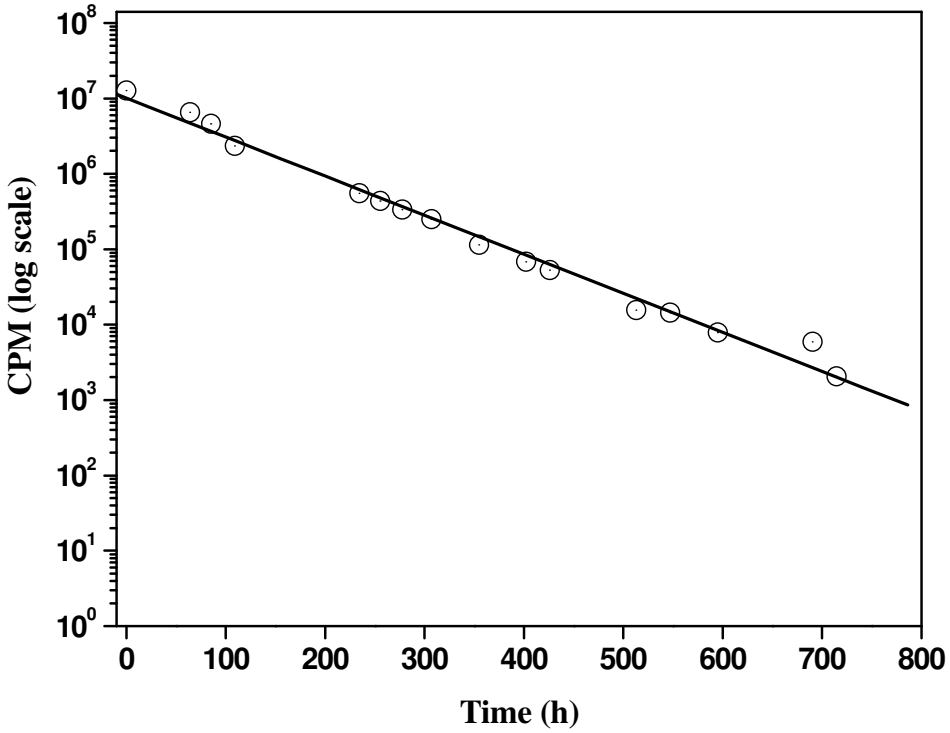

Fig. 5.5: Decay profile of ^{90}Y

5.6.1.2 Paper electrophoresis

The level of ^{90}Sr in ^{90}Y was also estimated by paper electrophoresis technique [236]. ^{90}Y in acetate form was applied at the centre of a Whatmann chromatographic paper (35 × 1 cm). Paper electrophoresis was carried out using 0.15 g L^{-1} sodium citrate in 0.03 M sodium chloride solution as the electrolyte. A potential of 500 V was applied for 2 h. At the end of electrolysis, the paper was dried, cut into 1 cm segments and counted in NaI (Tl) scintillation

counter. In the paper electrophoresis, ^{90}Sr and ^{90}Y were expected to move towards the cathode and anode, respectively [236]. While ^{90}Y moved towards the anode as expected, the studies did not show any detectable quantities of ^{90}Sr in the cathodic region (**Fig. 5.6**).

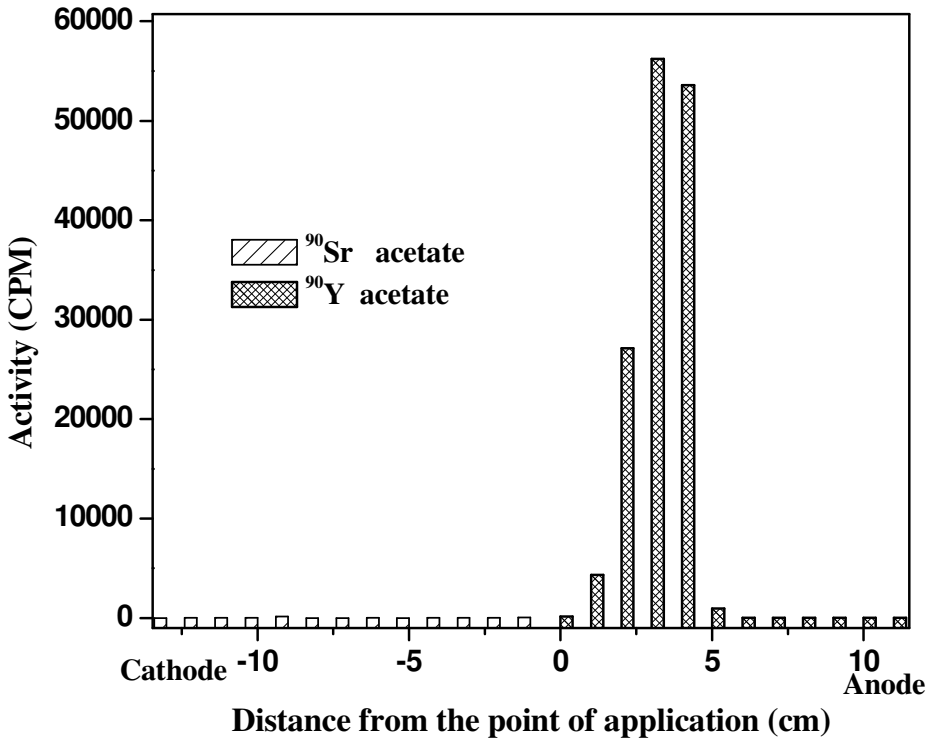

Fig. 5.6: Paper electrophoresis pattern of ^{90}Y

5.6.1.3 γ-ray spectrometry

In the initial experiments carried with $^{90}Sr/^{90}Y$ spiked with $^{85+89}Sr$, the ^{90}Y isolated was checked in an HPGe detector coupled to a MCA to evaluate the photon peaks due to the γ-rays corresponding to $^{85+89}Sr$ gamma activity. The spectrum did not show the presence of any of the peaks of ^{85}Sr, thereby indirectly confirming the absence of ^{90}Sr in the recovered ^{90}Y.

5.6.1.4 Extraction Paper Chromatography

The trace level of ^{90}Sr impurity present in ^{90}Y was detected and estimated by the novel, user friendly Extraction Paper Chromatographic (EPC) technique reported by Pandey

et al [57]. The procedure is based on the selective retention of ^{90}Y by 2-ethyl hexyl-2-ethyl hexyl phosphonic acid, a chelate impregnated at the point of application of the paper chromatography strip (Whatman 12×1 cm). A 5 μL acetate test solution containing 0.185 MBq (5 μCi) of ^{90}Y was applied on the paper which was developed in 0.9% NaCl solution. The paper strip was dried, cut into 1 cm segments, placed in scintillation vials which contained 10 mL of cocktail and counted by liquid scintillation counter. The ^{90}Sr activity present at the solvent front was then compared to the total applied activity to obtain the radionuclidic impurity levels. EPC pattern of the ^{90}Y solution isolated by this novel method is given in **Fig. 5.7**.

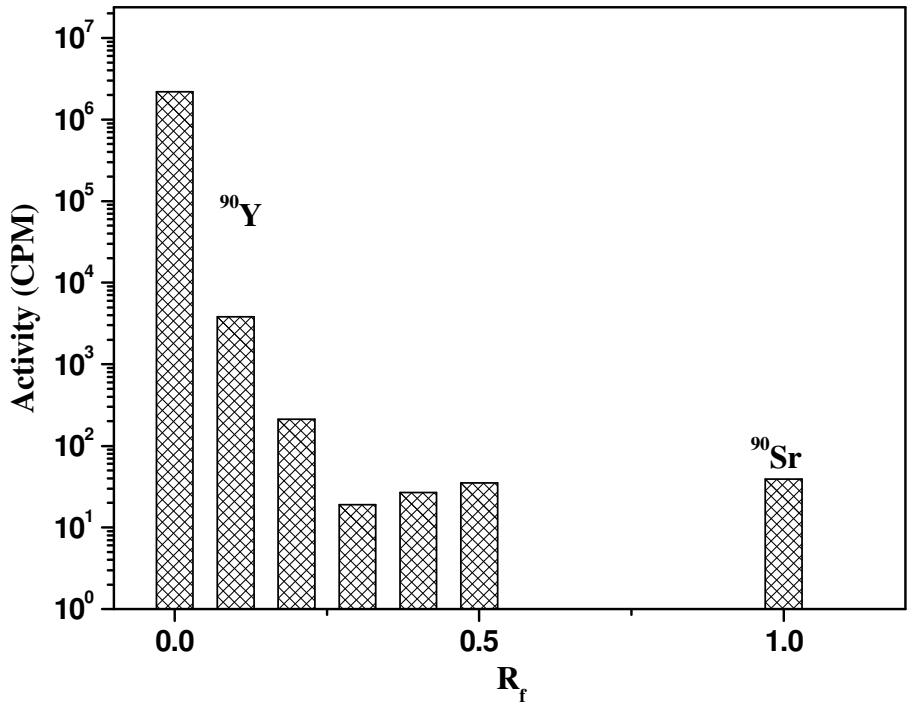

Fig 5.7: Extraction paper chromatography pattern of ^{90}Y

Estimation of the amount of ^{90}Sr by this method, in several batches gave the value as 30.2±15.2 kBq (817±411 nCi) of ^{90}Sr per 37 GBq (1 Ci) of ^{90}Y, corresponding to (0.817±0.411 ppm) of ^{90}Sr which is well within acceptable limits.

5.6.1.5 ICP-AES analysis of the decayed ^{90}Y samples

The level of ^{90}Sr impurity in ^{90}Y obtained from the generator could be further validated by ICP-AES analysis of the ^{90}Y samples. The ^{90}Y samples were allowed to decay for 2 months before subjecting them to ICP-AES analysis. The calibration curve for Sr ions was obtained by using standard solutions having known concentrations of these ions. The concentration of ^{90}Sr ions in decayed ^{90}Y samples were found to be <0.01 ppm, in 10 different batches.

5.6.2 Chemical purity of ^{90}Y

It is reported that the ^{90}Sr solution may be associated with chemical impurities like Cu^{2+}, Fe^{3+} and Zn^{2+} ions and also may contain significant amount of ZrO^{2+} ions as a decay product of ^{90}Y [215]. These metal ions may co-exist with ^{90}Y during its separation from ^{90}Sr and could affect the complexation chemistry of ^{90}Y. The possibility of such metal ion impurities can be avoided by the use of high purity chemicals. The level of Zr ions builds up in the ^{90}Sr solution with time and is a continuous process. However, it is expected that the ZrO^{2+} ions may be removed by electrodeposition along with ^{90}Y in the first few electrolysis and ^{90}Y availed from subsequent electrolysis will have negligible levels of these ions. This is attributed to the standard electrode potentials of ZrO^{2+} ions.

$$ZrO^{2+} + 2H^{+} + 4e \rightarrow Zr + H_2O \quad E^{o} = -1.5 \text{ V [131]}$$

The reduction of ZrO^{2+} is favored compared to that of Y^{3+} ions, whose standard reduction potential is -2.37 V. Consequently, when the ^{90}Sr solution is left unused for a long time (>2 months), it might be necessary to carry out one electrolysis in which ^{90}Zr is quantitatively co-deposited along with ^{90}Y. The ^{90}Y obtained from this electrolysis could be discarded and the ^{90}Y obtained from the subsequent electrolysis contained negligible amount of Zr ion impurity.

The trace levels of the metal ion contamination in the decayed ^{90}Y samples were

determined by ICP-AES analysis. The calibration curves for these ions were obtained by using standard solutions having known concentration of these ions. In the ^{90}Y samples, Cu^{2+} and Zn^{2+} ions were not detected. The level of Fe^{3+} impurities present was found to be (0.23±0.05) ppm and that of Zr ions was <0.01 ppm. It is clear from these results that ^{90}Y obtained from this generator is adequately free from metal ion impurities and is suitable for the preparation of radiopharmaceuticals. Further, the interference of trace amount of Fe and Zr ions in the complexation chemistry of ^{90}Y could be indirectly tested by investigating the labeling efficacy of ^{90}Y.

5.7 Labeling efficacy of ^{90}Y

The suitability of ^{90}Y for biomedical applications was evaluated by labeling a peptide (DOTA-TATE) with the radionuclide. This is also an indirect test to ascertain the chemical purity, as high chemical purity is essential to achieve a good complexation yield of the radiolabeled agent. In brief, 25 µL of DOTA-TATE solution (1 µg μL^{-1}) in HPLC grade water was mixed with 475 µL of ^{90}Y solution (~370 MBq in acetate buffer). The pH of the resulting mixture was found to be ~5. The mixture was incubated at 95 °C for 30 min. The extent of complexation achieved was determined by paper chromatography (PC) using 50% acetonitrile in water as the eluting solvent. The paper chromatographic patterns of unlabeled $^{90}Y^{3+}$ (in the form of $^{90}Y(CH_3COO)_3$) and that of ^{90}Y-DOTA-TATE are shown in **Fig. 5.8**. It can be seen from the Figure that ^{90}Y-DOTA-TATE moved towards the solvent front (R_f = 0.8-0.9) (**Fig. 5.8a)** while under identical conditions unlabeled $^{90}Y^{3+}$ remained at the point of application (R_f = 0) (**Fig. 5.8 b**). It was observed that as low as 25 µg of DOTA-TATE (17.4 nmol) was sufficient for labeling ~370 MBq (10 mCi) of ^{90}Y with >99% complexation yield. The present findings amply suggest that traces of Zr and Fe ions present in the ^{90}Y do not interfere significantly in the complexation chemistry of ^{90}Y.

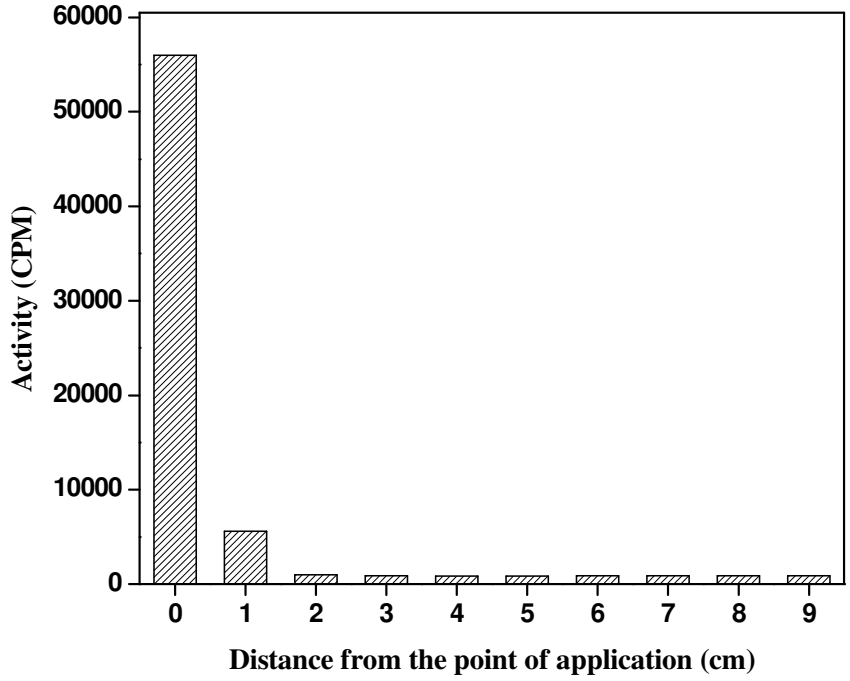

(a)

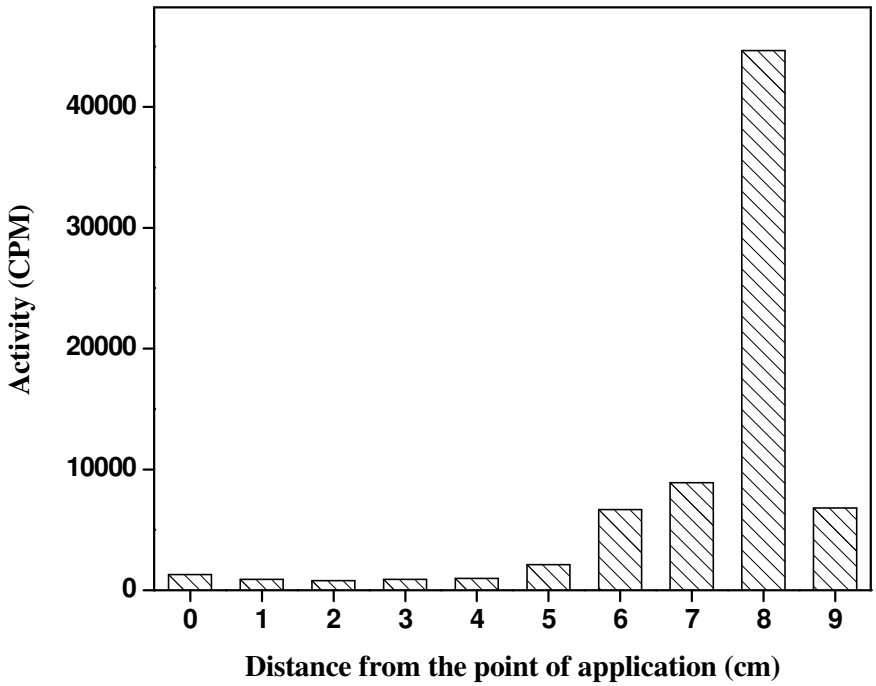

(b)

Fig. 5.8: Paper chromatographic patterns of (a) $^{90}Y(CH_3COO)_3$ and (b) ^{90}Y-DOTA-TATE in 50% acetonitrile in water (v/v)

5.8 Simulated study for recovery of ^{90}Y from Sr carrier-added ^{90}Sr solution, equivalent to 37 GBq (1 Ci) of ^{90}Sr

The effects of macroscopic amounts of strontium on the electrochemical separation of ^{90}Y was investigated by conducting the experiments by using a Sr/Y mixture prepared with inactive Sr and Y carrier and spiking it with ^{90}Sr and ^{90}Y. A solution simulated to represent equilibrium mixture of 37 GBq each of ^{90}Sr and ^{90}Y was prepared by dissolving 22.5 mg of anhydrous strontium carbonate and 2.32 μg of yttrium oxide in 2 M HNO_3. To this an equilibrium mixture of ^{90}Sr/^{90}Y containing 3.7 MBq (100 μCi) of ^{90}Sr as well as 3.7 MBq (100 μCi) of $^{85+89}$Sr was added. ^{90}Y was then separated by electrolysis as per the method outlined above. The activity content of the recovered ^{90}Y was measured to see the electrochemical deposition yield. The recovery of ^{90}Y when the feed was simulated to represent 37 GBq (1 Ci) of ^{90}Sr was also found to be as good as at lower strengths of ^{90}Sr. On analysis of the ^{90}Y product, no peak corresponding to $^{85+89}$Sr was observed in the HPGe detector confirming the purity of the product. Yields of 97–98% of ^{90}Y deposition were observed after the initial electrolysis step as well as the second electrolysis step. The higher yield after the second step observed in this case is perhaps due to the larger amounts of Y deposited on the electrode, wherein the loss during the acetone washing step is expected to be a smaller percentage of the total Y deposited.

5.9 Advantages of the electrochemical ^{90}Sr/^{90}Y generator

The electrochemical method offers several advantages, for use in a radionuclide generator system. The use of the same ^{90}Sr feed solution for electrolysis without further modification, except pH adjustment, is a prime significant advantage. A ^{90}Sr/^{90}Y generator of 37 GBq (1 Ci) ^{90}Sr capacity, can yield 16.6–18.5 GBq (450–500 mCi) of ^{90}Y twice a week, with insignificant loss of ^{90}Sr activity except by natural decay. Supplementing the activity by adding about 10% (3.7 GBq or 100 mCi) of ^{90}Sr once in every 4–5 years will be adequate to

keep the ^{90}Y supply constant. The entire separation procedure employs simple electrochemistry and is amenable for automation. The electrodes used are reusable after proper cleaning. Minimal amounts of chemicals are used for the whole process, and hence there is very little possibility of additional introduction of metal contamination. ^{90}Y is obtained in acetate buffer medium (pH 5) with appreciably high radioactive concentration and is directly suitable for radiolabeling biomolecules without any further chemical modifications. The waste generated is expected to contain only trace levels of ^{90}Sr. The waste generated can be monitored, classified and disposed as per regulatory requirements, and there is almost no solid waste coming out of the entire process.

Several modifications can be incorporated into this new method developed during the course of this work. These include scaling up, improving the electrolysis setup, use of extremely high purity reagents to avoid metal ion contamination, removal of accumulated Zr from the ^{90}Sr feed solution before its first use, incorporating a final step of ^{90}Y purification with ^{90}Sr-specific resin (if needed) and automation of the entire process. The method developed, if set up in a central radiopharmacy, will significantly reduce the cost of targeted therapy. The method could find further applications such as recovery of ^{90}Sr from waste solution and its purification for making it as a radiopharmaceutical raw material. Suitable modification of the electrochemical parameters needs to be developed depending on the specific application.

5.10 Conclusions

An electrochemical separation procedure has been successfully demonstrated for separation of ^{90}Y from ^{90}Sr, in high radiochemical yield and purity. The method has practical application and can be further developed to suit a well-established/regulated central radiopharmacy. The operational cost of such a generator will be reasonable for availing a long term supply of ^{90}Y suitable for therapeutic applications. The method developed is

superior to all the techniques thus far described in the literature and used by the commercial manufacturers for making ^{90}Y. It is believed that this electrochemical generator technology can be perfected and it has the potential to be widely used resulting in substantial benefit to the patients. Unlike other radionuclide generators used in the Nuclear Medicine departments, a ^{90}Sr/^{90}Y generator will not need frequent replacement, since very little of the radioactivity of ^{90}Sr is lost by decay. A 10% supplementation of the ^{90}Sr source every 4–5 years will ensure near constant output from the generator. This ^{90}Sr/^{90}Y generator has been named as "^{90}Y-Kamadhenu", based on the mythical cow "Kamadhenu", which yields unlimited supply of milk.

CHAPTER 6

DEVELOPMENT OF $^{188}W/^{188}Re$ GENERATORS

"A scientist in his laboratory is not a mere technician; he is also a child confronting natural phenomena that impress him as though they were fairy tales"

MARIE CURIE

6.1 Introduction

6.1.1 Rhenium-188 (^{188}Re): An important therapeutic radioisotope

^{188}Re is an attractive therapeutic radionuclide due to its reasonable half life ($t_{½}$ = 16.9 h), high-energy beta radiation ($E_{\beta max}$ = 2.118 MeV), low abundance (15.8%) of 155 keV photons and convenient availability from ^{188}W/^{188}Re generator with high specific activity [15,237]. The low energy (155 keV) gamma emission enables imaging for monitoring in-vivo localization and dosimetric calculations [237,238]. The chemistry of Re is similar to Tc, which is an additional advantage for working with molecules that have shown promising results as ^{99m}Tc-radiopharmaceuticals. ^{188}Re can be conveniently attached to antibodies, peptides and other molecules such as lipiodol and DMSA [239]. Currently, ^{188}Re is used for various medical applications including radioimmunotherapy, radionuclide synovectomy and bone pain palliation [240-247]. ^{188}Re has also been utilized for the preparation of radioactive stents for prevention of restonosis [248].

6.1.2 Availability of ^{188}Re from ^{188}W/^{188}Re generator

^{188}Re of modest specific activity can be produced by direct neutron activation of enriched ^{187}Re in a nuclear reactor. However, since high specific activity ^{188}Re is essential for therapeutic applications, the production method of choice is by the decay of the long-lived parent ^{188}W ($t_{½}$ = 69.4 d) via ^{188}W/^{188}Re generator. This method also provides logistic advantage for the supply of short-lived ^{188}Re to distant user sites. The simplified decay scheme of ^{188}W is shown in **Fig. 6.1**. The attractive physical properties of ^{188}Re and its production from ^{188}W/^{188}Re generator with adequate shelf-life, makes it an interesting option for clinical use. However, ^{188}W can only be produced by double neutron capture with low neutron absorption cross-sections [^{186}W(n,γ)^{187}W (σ = 37.9±0.6 b); ^{187}W(n,γ)^{188}W (σ = 64±10 b)]. Further, owing to rather long half-life of ^{188}W, relatively long irradiation periods are required even for the production of ^{188}W of modest specific activity [249]. Consequently,

^{188}W from the high flux reactors (ϕ ~10^{15} n cm^{-2} s^{-1}) such as the HFIR in Oak Ridge National Laboratory, USA or SM Reactor in Dmitrovgrad, Russian Federation can alone be used to make ^{188}W/^{188}Re generators to obtain no-carrier-added (NCA) ^{188}Re. The specific activity of ^{188}W, produced in the high flux reactors, ranges from 150-190 GBq g^{-1} of W [250].

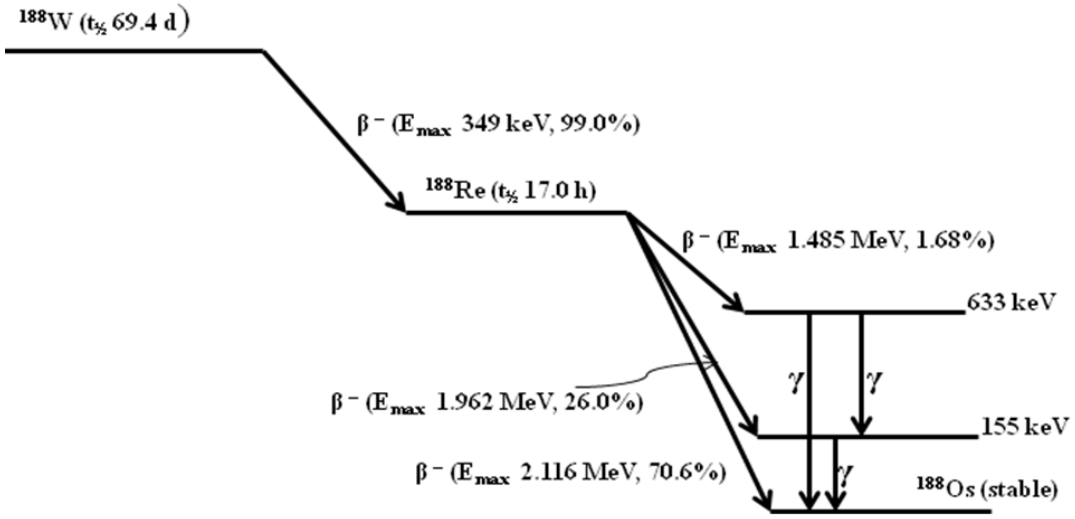

Fig. 6.1: Simplified decay scheme of ^{188}W (energy levels not drawn to scale)

Most of the commercially available ^{188}W/^{188}Re generators are akin to the ^{99}Mo/^{99m}Tc generators using alumina columns, where ^{188}W is retained on the alumina column and ^{188}Re is eluted with 0.9% NaCl solution [251-256]. Perego et al [251] examined the tungsten sorption capacity of a variety of alumina powders and reported that the maximum achievable sorption capacity was 80 mg W g^{-1} of alumina. Owing to the limited sorption capacity of alumina, ^{188}Re availed from alumina based ^{188}W/^{188}Re generators is of low radioactivity concentration, even while using ^{188}W produced in the high flux reactors. Often post-elution concentration of the ^{188}Re eluate is required [250,257-260] resulting in a fairly complex system, addition of chemical impurities, high dose rates and low reliability. Recently, automated systems for the concentration of ^{188}Re eluate have also been developed [259,261]. However, the high cost involved in the operation of the complex automation systems, escalates the production cost of ^{188}Re and renders it cost-ineffective.

The shortage in the suppliers producing $^{188}W/^{188}Re$ generator, primarily due to the non-availability of or inaccessibility to high flux reactors and the cost-ineffective process involved in obtaining ^{188}Re of appropriate radioactive concentration, might adversely affect the widespread application of this excellent radioisotope. To increase the availability of clinically useful ^{188}Re for radiotherapeutic applications, the development of $^{188}W/^{188}Re$ generators utilizing lower specific activity ^{188}W producible in medium neutron flux (~10^{14} n cm^{-2} s^{-1}) research reactors operational in many countries is worth pursuing. This in turn requires the development of alternate separation routes wherein ^{188}Re of adequate purity and radioactive concentration can be obtained from low specific activity ^{188}W. Several alternate sorbents like hydroxyapatite, the hydrous oxides of zirconium, titanium, manganese, tin (IV), and cerium, silica gel, the AG 1-X12 and AG 50 W-X12 ion-exchange resins and activated charcoal have been studied to determine their suitability for the preparation of $^{188}W/^{188}Re$ generators [262-266]. Unfortunately, none of these materials exhibited an improved W-sorption capacity compared to alumina. The other options such as $^{188}W/^{188}Re$ gel generators based on matrices such as zirconium or titanium tungstate [53,267,268] have also been explored with limited success. Though these matrices could retain higher W-content than alumina, the ^{188}Re elution performance from these matrices was inferior compared to the alumina based systems. In the last few years, several alternative sorbents with higher capacity for W such as gel-metal oxide composite, synthetic alumina, polymeric titanium oxychloride and polymeric zirconium compound (PZC), have been developed and exploited for the preparation of $^{188}W/^{188}Re$ generators [266,269-274]. However, these recent techniques have yet to be proven for their suitability for routine clinical applications and have not merited commercial exploitation.

6.1.3 The present work

This chapter describes the development of two novel approaches for the preparation

of $^{188}W/^{188}Re$ generators suitable for biomedical applications. The first approach is based on the selective electrodeposition of ^{188}Re from a feed solution of ^{188}W by controlled application of electrode potential and recovery of the ^{188}Re in high radioactive concentration, suitable for labeling studies. In the second approach, nanomaterial based sorbents (TiP and nano-ZrO_2) were utilized for the preparation of the $^{188}W/^{188}Re$ generators. Additionally, in order to concentrate ^{188}Re obtained from the conventional alumina based $^{188}W/^{188}Re$ generator, a simple electrochemical approach for the post-elution concentration of ^{188}Re has been developed. In this chapter, the overall process concept, scientific basis, experimental results, process validation and the possible challenges of using these novel approaches have been discussed. The feasibility of these separation methods, both in terms of yield and the purity of the ^{188}Re for radiopharmaceuticals applications, has been amply demonstrated and evaluated.

6.2 Development of an electrochemical $^{188}W/^{188}Re$ generator

The potential of the electrochemical approach for the development of $^{99}Mo/^{99m}Tc$ and $^{90}Sr/^{90}Y$ generators has been demonstrated in the earlier chapters. In this chapter, the possibility of developing an electrochemical $^{188}W/^{188}Re$ generator, wherein low specific activity ^{188}W can be used to obtain ^{188}Re with appreciably high radioactive concentration, has been explored. The radionuclidic and radiochemical purity of ^{188}Re has been determined and its suitability for the preparation of radiopharmaceuticals has been evaluated.

6.2.1 Materials

Tungsten-188 (specific activity 159 GBq g^{-1}) as sodium (^{188}W) tungstate was procured from the State Scientific Centre of Russia Research Institute of Atomic Reactors (PSUE) in Dmitrovgrad, Russia, through an IAEA Coordinated Research Project. Reagents such as hydrochloric acid, oxalic acid, ammonium hydroxide, etc. were of analytical grade and were procured from S.D. Fine Chemicals, Mumbai, India. Al_2O_3 (90 active acidic-I for column chromatography, 70-230 mesh ASTM) was obtained from Fluka. Stannous chloride, hydroxyethylidene diphosphonate (HEDP) and dimercaptosuccinic acid (DMSA) were obtained from Sigma Chemical Company, USA. Platinum metal wires of high purity (+99.9%) were procured from M/s Hindustan Platinum Ltd, Mumbai. Paper chromatography strips were purchased from M/s. Whatman, UK. Flexible silica gel plates (coating thickness 0.25 mm) were from J.T. Baker Chemical Company, USA.

The activity of ^{188}Re was measured using a NaI(Tl) scintillation counter (150-250 keV). HPGe detector coupled with a multichannel analyzer (MCA) (Canberra Eurisys, France) with a 1.5 keV resolution at 1333 keV and range from 1.8 keV to 2 MeV was used for analysis of ^{188}W in the presence of ^{188}Re and also for quantitative estimation. The radioisotope levels were determined by quantification of the 155 keV (15%) γ-ray peak of ^{188}Re and 291 keV (0.4%) γ-ray peak of ^{188}W. A D.C. power supply with 100 V compliance,

a maximum current of 2 A, 1.2 nA current resolution and >10^{13} Ohms input impedance was used for electrochemical studies.

6.2.2 Electrochemical separation of ^{188}Re from ^{188}W

6.2.2.1 Principle of electrochemical separation of ^{188}Re from ^{188}W/^{188}Re mixture

Separation of ^{188}Re from ^{188}W/^{188}Re mixture involves selective electrodeposition of ^{188}Re on a platinum cathode. This is based on the difference in standard reduction electrode potential of tungsten and rhenium ions in acidic solutions.

$$WO_3 + 6H^+ + 6e \rightarrow W + 3\ H_2O \qquad E^\circ = -0.090\ V\ [131]$$

$$ReO_4^- + 8H^+ + 7e \rightarrow Re + 4\ H_2O \qquad E^\circ = +0.362V\ [131]$$

Though the standard electrode potential of W is close to zero, it cannot be electrodeposited from its aqueous solutions [132]. This is because of the low hydrogen overvoltage and high discharge overpotential of ions of W, in aqueous medium [132]. Therefore, tungsten deposition is possible only from its molten salts [132]. However, the electrodeposition of very thin film of tungsten from an aqueous alkaline solution has been reported [132]. Therefore, acidic medium must be chosen to inhibit the electrodeposition of W on the electrode. On the other hand, Re can easily be electrodeposited from its aqueous solution and this phenomenon has been extensively studied [248,275-278]. The feasibility of electrodeposition of Re from an aqueous acidic medium wherein the electrodeposition of W could be precluded was exploited for the electrochemical separation of ^{188}Re from ^{188}W. Since ^{188}Re is continuously produced in the electrolyte as a result of the radioactive decay of ^{188}W, repeated electrodeposition of ^{188}Re from the same ^{188}W feed solution is a reasonable means to avail no-carrier-added (NCA) ^{188}Re.

6.2.2.2 The electrochemical set-up

A schematic diagram of the electrochemical cell is given in **Fig. 6.2**. The electrochemical system used was similar to the one used for the separation of ^{99m}Tc from

^{99}Mo, as described in Chapter 3. The electrodes used were made of high purity platinum wires. The electrochemical cell consisted of a glass vial (24 × 40 mm, 20 mm ID) and a teflon cap. The electrodes (length 50 mm and diameter 1.5 mm) were fitted 5 mm apart on the teflon cap. The teflon cap and the electrodes were fitted on the mouth of the glass vial. Vertical raising or lowering of the electrodes was carried out along with the teflon cap. The platinum electrodes were adjusted parallel to each other, connected to the power supply using small screws embedded into the teflon cap which were in contact with the electrode. A provision was provided for passing gas through a glass tube, dipped into the electrolysis solution. A small hole (~2.5 mm) was provided in the teflon cap for venting off gases, that might be formed.

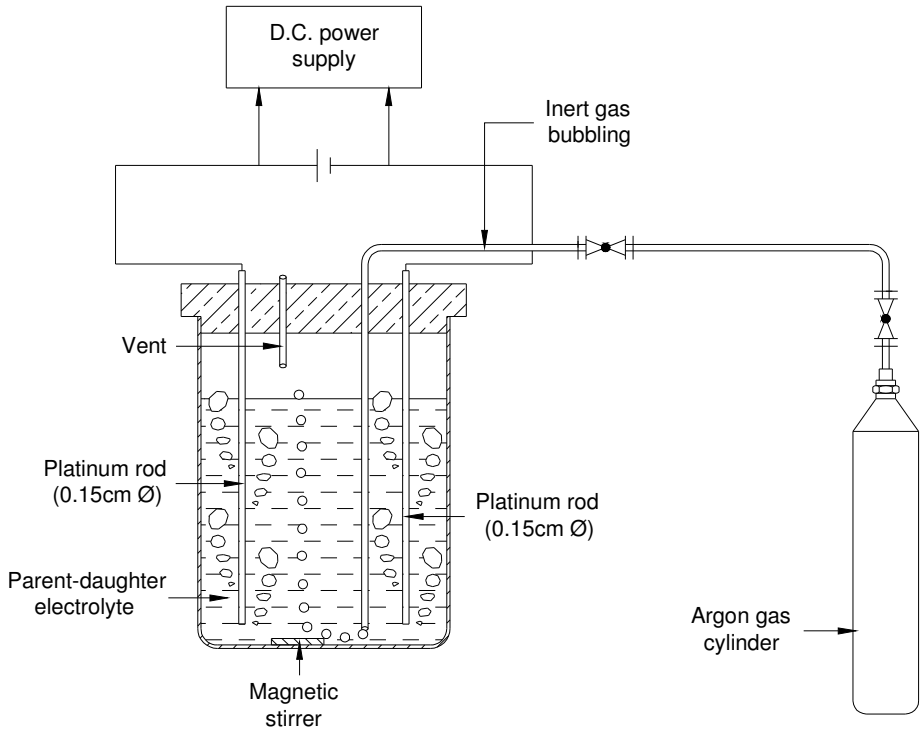

Fig. 6.2: Schematic diagram of the electrochemical ^{188}W/^{188}Re generator

6.2.2.3 Optimization of parameters for the electrochemical separation of ^{188}Re from ^{188}W

In order to achieve an effective electrochemical separation of ^{188}Re from ^{188}W, several experiments were carried out to choose a suitable electrolyte and to optimize the electrolysis

parameters such as the applied potential, pH of the electrolyte, time of electrodeposition, etc. All these experiments were conducted using ~37 MBq (1 mCi) of ^{188}W. In all the cases, before applying the potential on the electrodes, the electrolyte was heated to ~80°C while gently purging argon gas through the solution for 10 minutes.

6.2.2.3.1 Choice of the electrolyte

Szabo and Bakos reported the electro-reduction of rhenium from perrhenate solutions in sulphuric acid medium [276]. Based on their observation, an attempt to separate ^{188}Re from ^{188}W, using 0.1 M H_2SO_4 as electrolyte was made. However, it was observed that the yield of ^{188}Re deposited was low (~55%) and the amount of ^{188}W contamination due to co-deposition of W was significantly high. Use of other mineral acids such as HCl and HNO_3 as electrolyte also resulted in similar poor electrodeposition yield of ^{188}Re, despite reasonable operation time. Therefore separation of Re from W using mineral acids as electrolytes was not further pursued.

It is reported that oxalate and citrate ions facilitate reduction of ReO_4^- ions through formation of 1:1 complex in a weakly acidic medium. [133]. Oxalic acid was chosen in these studies to avoid the presence of organic residues in ^{188}Re, as these could potentially affect the preparation of ^{188}Re-based radiopharmaceuticals. All subsequent electrodeposition experiments were carried out using an oxalic acid bath.

6.2.2.3.2 Effect of applied potential

The applied potential is an important factor that influences the electrochemical separation of Re from W. The effect of applied potential on electrodeposition of ^{188}Re was studied by measuring the percentage electrodeposition of ^{188}Re as a function of potential, when electrolysis was carried out at pH 1-2. The results are shown in **Table 6.1**. The percentage of ^{188}Re deposited increased with increasing potential and it attained a nearly maximum value at ~7 V. When electrodeposition was carried out at higher applied potentials,

it was difficult to leach the ^{188}Re deposit from the electrode surface and therefore, the activity of ^{188}Re that could be recovered from the electrode was less than at lower voltages. In order to utilize the ^{188}Re deposited on the electrode for further studies, it is essential that the activity can be removed from the electrode surface easily. Therefore, the applied potential was maintained at 7 V in all the subsequent experiments.

Table 6.1: Effect of applied potential on the electrodeposition yield of ^{188}Re

Applied potential (V)	^{188}Re obtained (%)
3	27±6
5	49±4
7	81±3
9	77±10
11	75±9

n=3 '±' indicates standard deviation

6.2.2.3.3 Effect of the pH of the electrolyte

The pH of the electrolytic solution plays a crucial role in any electrodeposition experiment. In order to ensure the most optimum pH range, electrodeposition of ^{188}Re was studied as a function of pH at the optimal potential and the results are illustrated in **Fig. 6.3**. It is seen clearly from the figure that acidic pH was preferable. At pH between 1 and 2, maximum deposition (84±5%) occurred. Although the pH of the electrolytic solution tends to increase slowly during electrolysis, the reduction in electrodeposition yield due to this increase in pH was not very significant. Hence, there was no need to adjust the pH of the electrolyte during the process of electrodeposition.

6.2.2.3.4 Effect of the time of electrodeposition

Experiments were performed to ascertain the minimum time required for quantitative electrodeposition of ^{188}Re at optimum pH and applied potential. The electrodeposition yield

of ^{188}Re as a function of time is illustrated in **Fig. 6.4**, which showed the need to have at least 60 min electrodeposition period. It was found that during 60 min of electrolysis at applied potential of 7 V, current dropped from about 200 mA to 10 mA. Bubbling of argon as an inert gas through the solution before and during electrolysis was essential to vent the gases during electrolysis as well as to keep the solution in dynamic form.

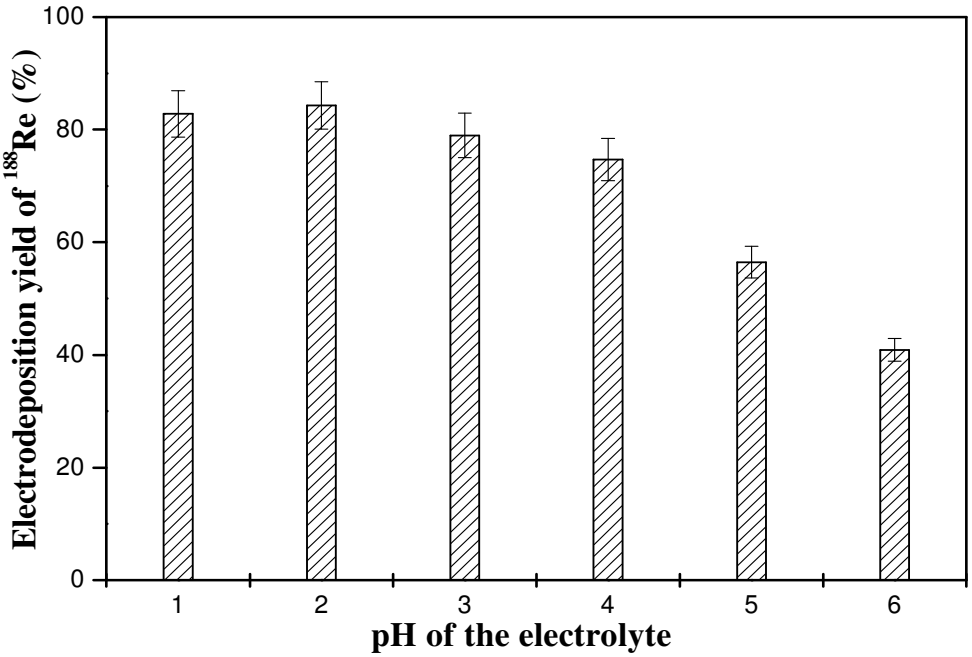

Fig. 6.3: Electrodeposition yield of ^{188}Re as a function of pH of the ^{188}W/^{188}Re solution

It was also essential to heat the electrobath to 80^{o}C concurrent with argon gas bubbling for 15 min prior to each run, to remove any dissolved O_2 gas and free radicals generated as a result of radiolysis of the electrolyte. The presence of these species reduces the electrodeposition of ^{188}Re on the electrode surface. It has been experimentally observed that absence of this operation leads to poor electrodeposition yield (30-40%). Removal of the electrodes from the electrolytic cell under applied potential is necessary, because 30-40% of the deposited ^{188}Re dissolves back into the electrolyte solution, when the electrodes are removed after switching off the power supply. This is not unexpected since ^{188}Re in its oxide

and metal form (72% ReO_2 and 28% Re^0 [278]) is in extremely small quantities (ng-μg levels) and is thinly spread over the electrode surface, and would quickly dissolve into the acidic electrolyte solution, if not held on through a potential difference.

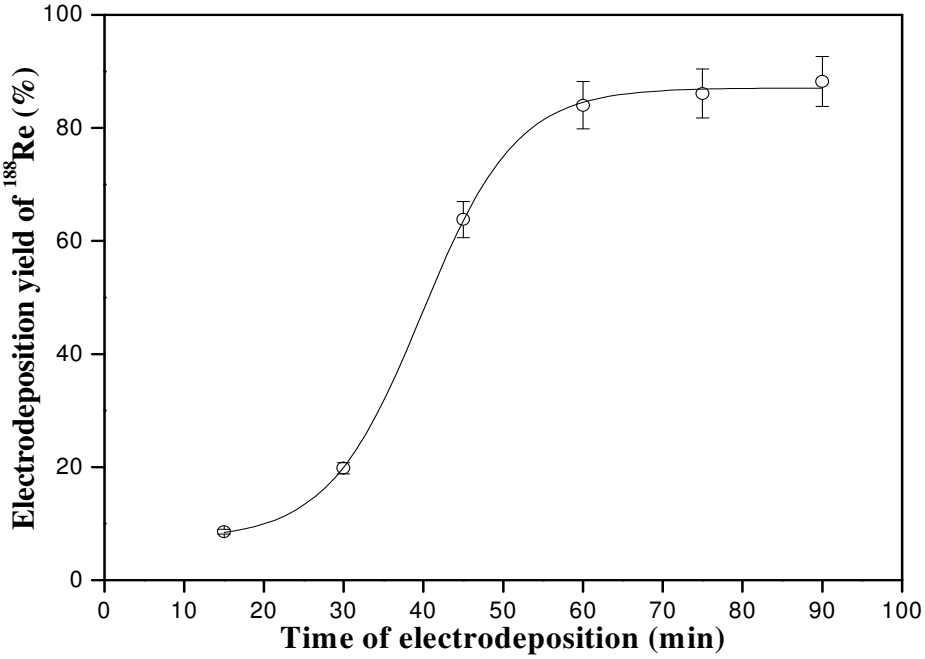

Fig.6.4: Effect of time on the electrodeposition yield of ^{188}Re from ^{188}W/^{188}Re solution

6.2.3 Process demonstration: Development of ^{188}W/^{188}Re generator

After optimization of the experimental parameters, the electrochemical separation process was demonstrated by developing a 1.11 GBq (30 mCi) ^{188}W/^{188}Re generator. For this, 1.11 GBq (30 mCi) of an equilibrium mixture of ^{188}W/^{188}Re as sodium (^{188}W) tungstate in 2 M NaOH was taken in a 10 mL vial, evaporated to dryness and reconstituted in 5 mL of 0.1 M oxalic acid, resulting in a clear solution. The pH of this solution was adjusted to 1-2 (if required) by drop-wise addition of 3% ammonium hydroxide. Thereafter it was transferred to the electrochemical cell which was then covered with the teflon cap together with the two platinum electrodes fully dipped into the solution. Electrolysis was performed by applying a constant potential of 7 V (current 200 mA, current density 328 mA cm^{-2}), for 60 min. After

the electrolysis, the electrodes were removed from the cell while maintaining the potential. The applied potential was turned off after removal of the electrodes from the solution. The cathode containing the electrodeposited ^{188}Re was then placed in a narrow test tube (0.5 cm diameter) containing 500 µL of warm (~60 ^{o}C) 0.1 M HCl to yield perrhenic acid. The electrode was removed after 5 min and the ^{188}Re solution was neutralized by addition of 500 µL of 0.1 M NaOH. The yield of ^{188}Re after the first electrolysis step was 86±3%, but the product was associated with trace amounts of ^{188}W contamination (0.05-0.1%), which was removed by a purification step. This was perhaps due to the adherence of the electrolytic solution to the electrode, rather than electrodeposition of ^{188}Re. After electrolysis, the $^{188}ReO_4^-$ was subjected to purification by passing through a small column (10 mm × 2 mm) containing 200 mg of alumina, preconditioned with normal 0.9% saline solution. This eliminated trace amounts of ^{188}W as well as 5-8% of ^{188}Re activity that might be present in any form other than perrhenate. **Table 6.2** summarizes the results of the studies to evaluate the performance of the generator over time and illustrates that 70-86% ^{188}Re could be recovered in ten out of the thirteen attempts from the same ^{188}W stock solution.

The yields were significantly lower on three occasions, when the stock solution was not subjected to electrolytic separation for an extended period of time (>7 days). One reason for this observation could be the preferential electrodeposition of ^{188}Os (the stable decay product of ^{188}Re) over ^{188}Re. The standard reduction electrode potential (E°) of Os is +0.85 V and the electrochemical reaction is:

$$OsO_4 + 8H^+ + 8e^- \rightarrow Os + 4H_2O \text{ [131]}$$

Since the standard reduction electrode potential value for Os is more positive than that for Re, its electrodeposition is more favored. Therefore, the electrochemical separation procedure must be carried out frequently, at least once in 5 days. Since ^{188}W/^{188}Re generator is expected to be used at least once in three days for effective and economical use, this may not be a

problem. However, when there is a prolonged gap of >7 days, it may be necessary to carry out one electrolysis with low yields, which can be discarded, followed by another in adequate yields that can be used.

Table 6.2: Performance of the electrochemical $^{188}W/^{188}Re$ generator

^{188}W in the electrolyte GBq (mCi)	^{188}Re growth period (days)	Expected ^{188}Re activity GBq (mCi)	^{188}Re recovered GBq (mCi)	^{188}Re recovered (%)
1.10 (29.8)	3	1.03 (27.8)	0.81 (21.8)	78.6
1.07 (28.9)	2.6	0.97 (26.2)	0.68 (18.3)	70.1
1.04 (28.1)	2	0.89 (24.1)	0.65 (17.5)	73.0
1.02 (27.5)	5	0.96 (26.1)	0.68 (18.5)	70.8
0.97 (26.1)	11	0.87 (23.6)	0.33 (9.0)	37.9[@]
0.86 (23.3)	3	0.76 (20.5)	0.62 (16.8)	81.5
0.84 (22.6)	4	0.79 (21.5)	0.62 (16.7)	78.5
0.80 (21.7)	16	0.67 (18.2)	0.26 (0.70)	38.8[@]
0.68 (18.5)	2	0.58 (15.7)	0.50 (13.7)	86.2
0.67 (18.1)	3	0.62 (16.8)	0.46 (12.4)	74.2
0.65 (17.6)	3	0.60 (16.3)	0.46 (12.5)	76.7
0.63 (17.1)	7	0.59 (16.1)	0.24 (6.5)	40.6[@]
0.59 (15.9)	4	0.56 (15.1)	0.45 (12.2)	80.3

[@] *The ^{188}W stock electrolyte solution remained unused for long period prior to these separations.*

6.2.4 Maintenance of ^{188}W feed solution and the electrodes after each batch

The inventory of ^{188}W was carefully maintained during the shelf-life of the $^{188}W/^{188}Re$ generator. After each experiment, a lead cap with acrylic lining but without electrodes was placed on the electrolysis cell containing ^{188}W, for radiation shielding. The entire assembly

was housed in a lead shielded container similar to the one used for the $^{99}Mo/^{99m}Tc$ generator **(Fig. 3.2)**. At the end of each batch, the electrodes were cleaned as per the procedure described in Chapters 3 and 4.

6.2.5. Quality control of ^{188}Re

6.2.5.1 Radionuclidic purity

The radionuclidic purity of ^{188}Re was ascertained by several means. The principal radionuclidic impurity that can be expected in the ^{188}Re product is ^{188}W. The decay of ^{188}Re was followed for 1 week by measuring the activity in a NaI(Tl) counter. The decay profile of ^{188}Re is shown in **Fig. 6.5**. The absence of any deviation at the lower end of the straight line decay curve confirmed that the ^{188}Re samples were pure and contained negligible quantities of long-lived ^{188}W. The half-life of ^{188}Re as calculated from the decay profile was (16.7 ± 0.2) h (n =5), which is close to the 16.9 h half-life reported for ^{188}Re.

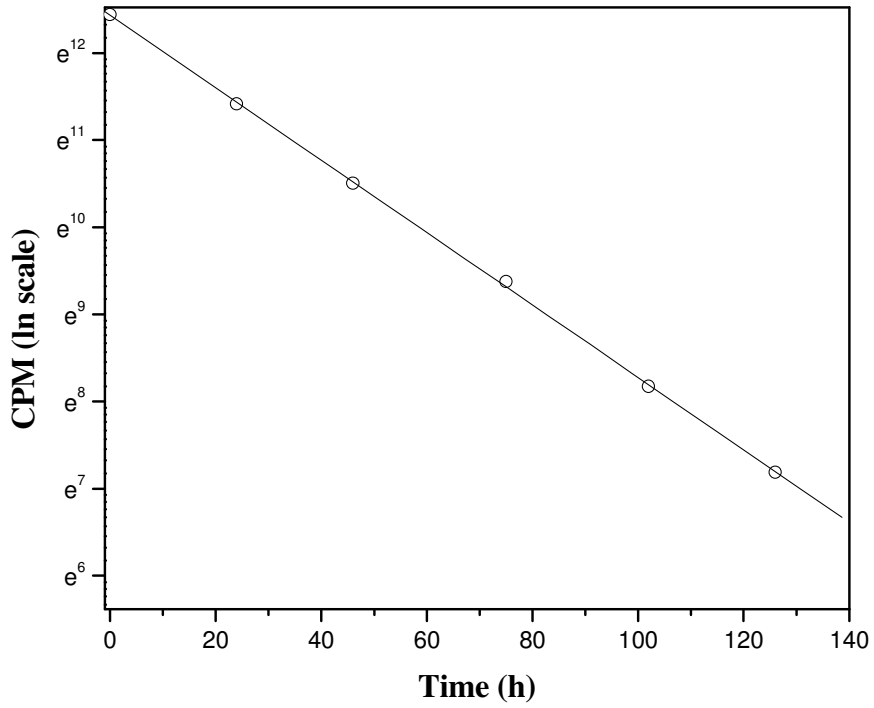

Fig. 6.5: Decay profile of ^{188}Re

Radionuclidic purity measurements were also made using a calibrated HPGe detector coupled with multichannel analyzer. The γ-ray spectrum of the freshly eluted ^{188}Re samples is illustrated in **Fig. 6.6**. The γ-ray spectrum of ^{188}Re did not show the presence of peaks corresponding to those of ^{188}W (227 keV and 291 keV). The ^{188}W contamination level in ^{188}Re was quantified by allowing the separated ^{188}Re samples to decay for 15 days and then measuring the 155 keV γ-ray peak of ^{188}Re in a HPGe detector. During this period of time, the ^{188}W impurity present in ^{188}Re decays and forms a ^{188}W/^{188}Re equilibrium mixture, which can be quantified by measuring the ^{188}Re present. The results were further confirmed by counting the decayed samples for a long time (6 h) and measuring the 291 keV γ-ray peak of ^{188}W. The levels of ^{188}W impurity present in ^{188}Re after passing through the alumina column were $<10^{-4}$ % in all the batches, which were well within the stipulated limit of 10^{-3}% as per the pharmacopoeias [135].

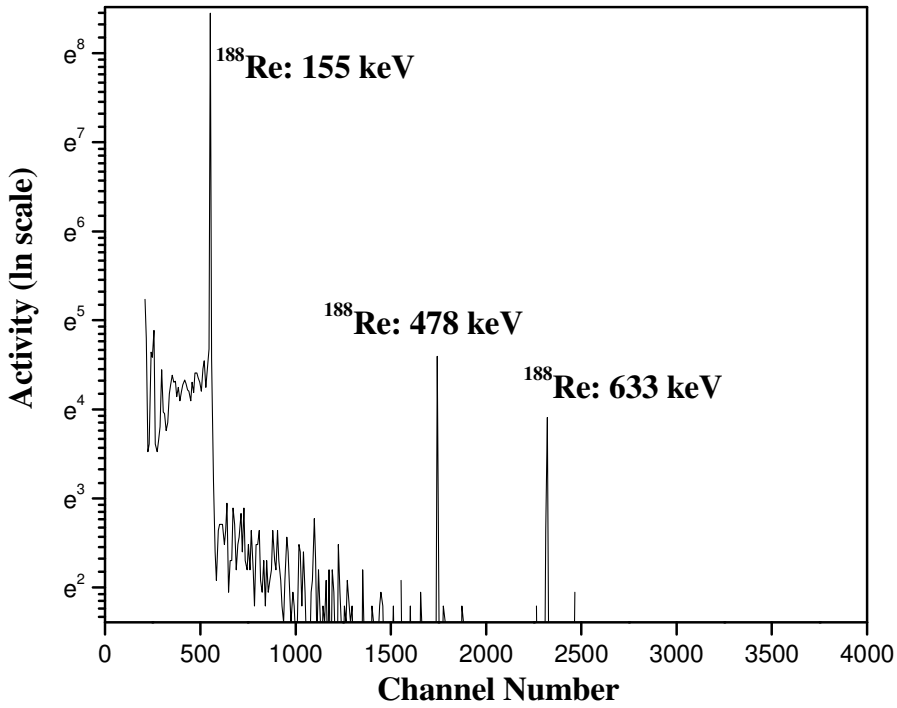

Fig. 6.6: Gamma spectrum of ^{188}Re

6.2.5.2 Radiochemical purity

To evaluate the radiochemical purity of $^{188}ReO_4^-$, 5 µL of the activity was applied on a paper chromatographic strip (Whatman 12 cm ×1 cm) at 1.5 cm from the lower end. The strip was developed in 0.9% NaCl solution. After the chromatography, the paper strip was dried, cut in to 1 cm segments, placed in test tubes and counted in a NaI (Tl) scintillation counter. The paper chromatographic pattern of ^{188}Re is shown in **Fig. 6.7**. The radiochemical purity of ^{188}Re as perrhenate was >99%, which was within the prescribed limits of ≥95% as per the pharmacopoeias [135].

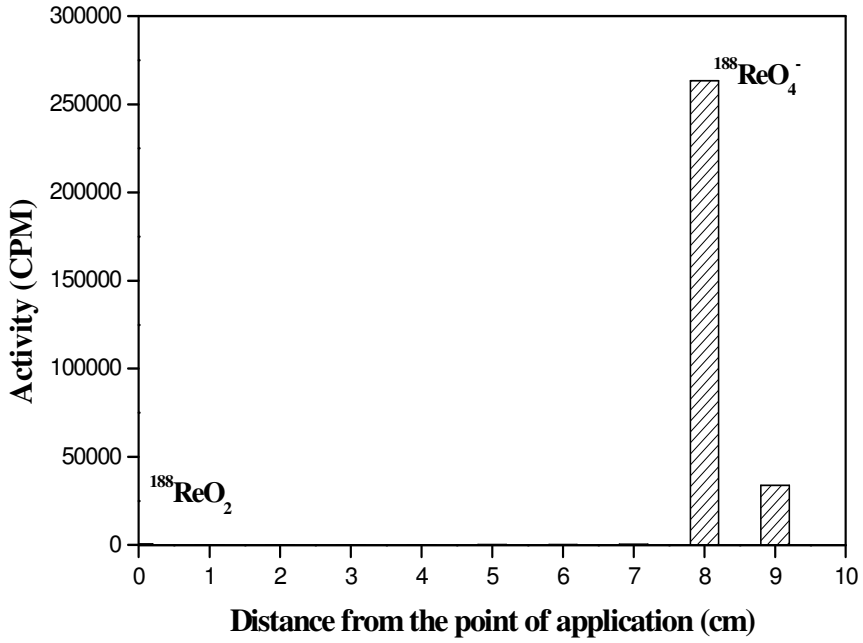

Fig. 6.7: Paper chromatographic pattern of $^{188}ReO_4^-$ in 0.9% NaCl solution

6.2.6 Labeling efficacy of ^{188}Re

Radiolabeling studies are important as they provide information about the suitability of the separated radiotracer for the preparation of radiopharmaceuticals. ^{188}Re availed from the electrochemical generator was used to prepare complexes of dimercaptosuccinic acid

(DMSA) and hydroxyethylidene diphosphonate (HEDP) as per the reported procedures [279-282] described briefly below.

6.2.6.1 Preparation of ^{188}Re-DMSA

DMSA (2 mg, 11 μM) was dissolved in 0.1 mL of bicarbonate buffer (0.5 M, pH 9) in a 10 mL vial. To this solution, 0.4 mL of $^{188}ReO_4^-$ obtained from the generator was added and the resultant volume was made up to 1 mL by adding 0.5 mL of normal saline (0.9% NaCl) solution. For the reduction of $^{188}ReO_4^-$ ions, 0.02 mL of stannous chloride solution (20 mg mL^{-1}) was added and the reaction mixture was purged with nitrogen gas. The mixture was heated in a boiling water bath for 30 min and allowed to cool to room temperature. The pH of the reaction mixture was adjusted between 1 and 2 before subsequent experiments.

6.2.6.2 Preparation of ^{188}Re-HEDP

HEDP (50 mg, 335 μM) was dissolved in 0.2 mL of bicarbonate buffer (0.5 M, pH 9) in a 10 mL vial. To this solution, 0.20 mL of $^{188}ReO_4^-$ obtained from the generator was added, followed by addition of 0.2 mL (100 μg, 0.54 μM Re) NH_4ReO_4 solution. The resultant volume was made up to 1 mL by adding 0.4 mL of normal saline (0.9% NaCl) solution. The pH of the reaction mixture adjusted to ~2 after addition of 0.04 mL of stannous chloride solution (250 mg mL^{-1}). The reaction mixture was purged with nitrogen and heated in a boiling water bath for 30 min and allowed to cool to room temperature.

In order to characterize the ^{188}Re-DMSA and ^{188}Re-HEDP complexes, thin layer chromatography (TLC) was performed using flexible silica gel plates. 5 μL portions of the test solution were applied at a distance of 1.5 cm from the lower end of the two TLC plates (12 cm × 1 cm). The strips were developed in saline and acetone, respectively. The strips were dried, cut into 1 cm fragments, and the radioactivity was measured. In TLC using acetone as solvent, the complex remained at the point of application (**Fig. 6.8 a**). Under identical conditions, $^{188}ReO_4^-$ moved towards the solvent front.

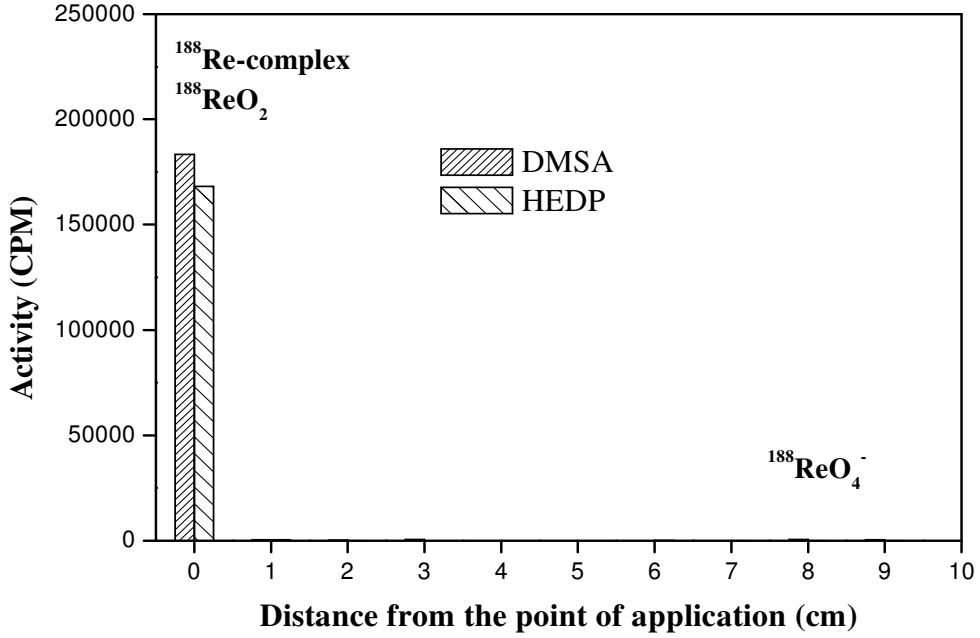

(a)

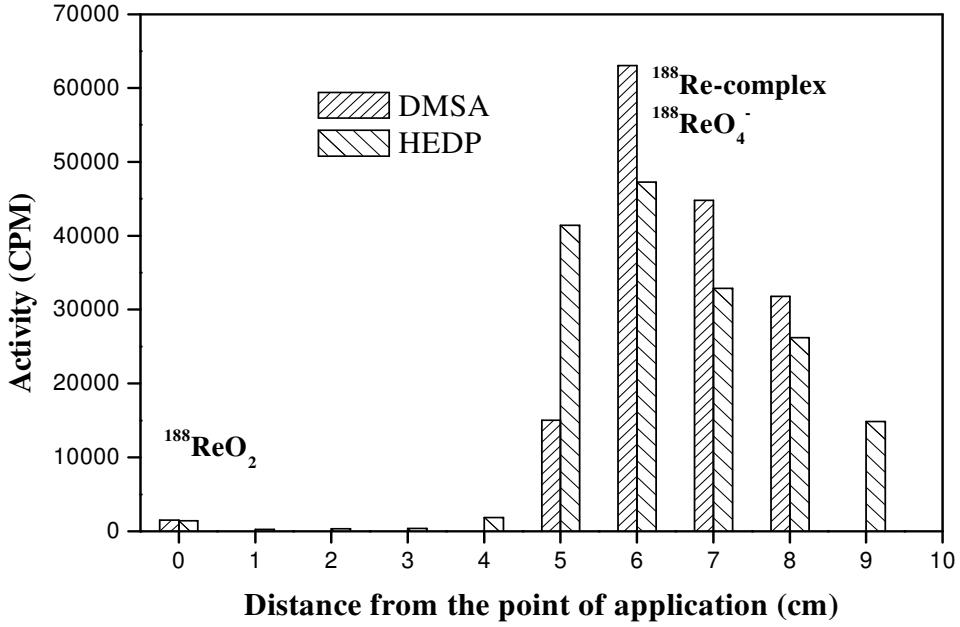

(b)

Fig. 6.8: Paper chromatographic patterns of ^{188}Re-DMSA and ^{188}Re-HEDP complexes in (a) acetone medium and (b) saline medium

However, if hydrolyzed rhenium ($^{188}ReO_2$) is present, it will also remain at the origin and hence an additional quality control procedure was essential to estimate this radiochemical impurity in the complex. The TLC pattern, using 0.9% NaCl solution as solvent is shown in **Fig. 6.8 b**, illustrating that the free $^{188}ReO_4^-$ as well as the complexes migrated with the solvent front, whereas hydrolyzed rhenium remained at the origin. By combining the results of both the TLCs, the complexation yield was estimated to be >98% in both the cases, which ascertained the suitability of ^{188}Re for the preparation of radiopharmaceuticals.

6.2.7 Simulated study for the separation of Re from carrier-added W solution, equivalent to ~37 GBq (1 Ci) of $^{188}W/^{188}Re$

The effects of macroscopic amounts of tungsten on the electrochemical separation of no-carrier-added ^{188}Re were investigated by conducting experiments using W/Re mixtures containing inactive W and Re carrier equivalent to ~37 GBq (1 Ci) ^{188}W in equilibrium with ^{188}Re. The mixture was spiked with an equilibrium mixture of $^{188}W/^{188}Re$ containing 37 MBq (1 mCi) of ^{188}Re. This simulated solution was prepared by dissolving 292 mg of WO_3 (equivalent to 37 GBq (1 Ci) of ^{188}W at 159 GBq g^{-1} of ^{188}W specific activity) and 1.45 μg (equivalent to 37 GBq of ^{188}Re) of ammonium perrhenate in 2 M NaOH. The resultant solution was evaporated to dryness and then reconstituted with 0.1 M oxalic acid solution. ^{188}Re was separated by electrolysis as described above and the radioactivity of the recovered ^{188}Re was measured. The recovery of ^{188}Re from W/Re mixture simulated to represent 37 GBq (1 Ci) of ^{188}W, was equally good as when lower amounts of ^{188}W were used. The overall yields of ^{188}Re in the simulated experiments were 85±2% and the amount of ^{188}W impurity present in it was $<10^{-4}$%.

6.2.8 Advantages of the electrochemical $^{188}W/^{188}Re$ generator

The electrochemical $^{188}W/^{188}Re$ generator system is inexpensive, efficient, simple to operate and can be easily scaled up. This method offers a scope to use low specific activity

^{188}W obtained from the medium flux reactors for preparation of $^{188}W/^{188}Re$ generators suitable for biomedical applications. $^{188}ReO_4^-$ can be availed from the generator with appreciably high radioactive concentration and purity and hence can directly be used for the preparation of radiopharmaceuticals. Additionally, the system produces very little radioactive waste and the entire process is amenable for automation. The adaptation of this technique can extend the useful shelf-life of the generator. Another important feature is that, at the end of the generator life after a reasonable decay period, it would be possible to recover the enriched ^{186}W target from the solution for fabrication of new targets for irradiation.

6.2.9 Conclusions

The potential utility of electrochemical separation procedure to isolate carrier free ^{188}Re from ^{188}W has been demonstrated. The procedure yielded ^{188}Re of high radionuclidic and radiochemical purity, in the form of $^{188}ReO_4^-$ suitable for preparation of radiopharmaceuticals. The method is promising for the separation of no-carrier-added ^{188}Re from ^{188}W produced in medium flux reactors. The results presented in this study are quite encouraging and further development of this method into a usable system with up to 37 GBq (1 Ci) of ^{188}W is warranted.

6.3 Post-elution concentration of ^{188}Re by an electrochemical method

The column chromatographic generator using a bed of alumina remains the most popular procedure for accessing ^{188}Re for radiopharmaceutical applications. However, owing to the limited sorption capacity of alumina (80 mg W g^{-1} of alumina) [251], large amount of alumina (>9 g) is required to bind ^{188}W (14-27 GBq) for the preparation of clinical-scale ^{188}W/^{188}Re generators [250]. The large size of the alumina column, in turn, results in large eluate volumes (>20 mL) with low radioactive concentration of $^{188}ReO_4^-$, which is unacceptable for radiopharmaceutical applications. The specific volume activity of ^{188}Re bolus from a typical 18.5 GBq ^{188}W/^{188}Re generator can be as low as 0.74 GBq mL^{-1} [250]. Therefore, post-elution concentration of $^{188}ReO_4^-$ solution to increase its radioactive concentration is required. The post-elution concentration step also extends the useful shelf-life of ^{188}W/^{188}Re generators.

Concentration using ion-exchange columns is the most commonly used approach for post-elution concentration of ^{188}Re solution [250,257-260]. The reported methods take advantage of the very low amounts of no-carrier added (NCA) ^{188}Re in the generator eluates which is trapped on a tiny column of a suitable anion exchanger, from which it can be re-eluted in a small volume. This section describes the results of the studies on an electrochemical approach to concentrate $Na^{188}ReO_4$ obtained from alumina based ^{188}W/^{188}Re generator and demonstrate its utility for radiolabeling studies.

6.3.1 Materials

Tungsten-188 (specific activity 159 GBq g^{-1}) as sodium (^{188}W) tungstate ($Na_2{}^{188}WO_4$) was procured from the State Scientific Centre of Russia Research Institute of Atomic Reactors (PSUE) in Dmitrovgrad, Russia, through an IAEA Coordinated Research Project (CRP). Reagents such as hydrochloric acid, oxalic acid, ammonium hydroxide, etc. were of A.R. grade and procured from S.D. Fine Chemicals, India. Al_2O_3 (90 active acidic I for

column chromatography, 70-230 mesh ASTM) was obtained from Fluka. Stannous chloride and dimercaptosuccinic acid (DMSA) were obtained from Sigma Chemical Company, USA. Na_2H_2HEDP was obtained from Sigma Chemical Company, St. Louis (USA). Platinum metal wires of high purity (+99.9%) were procured from M/s Hindustan Platinum Ltd, Mumbai, India. Paper chromatography strips were purchased from M/s. Whatman, UK. Flexible silica-gel plates (coating thickness 0.25 mm) were from J.T. Baker Chemical Company, USA.

A HPGe Multichannel analyzer, coaxial photon detector system, Canberra Eurisys, France with 0.5 keV resolution and range from 1.8 keV to 2 MeV was used for analysis of ^{188}W, in the presence of ^{188}Re and also for their quantitative estimation. The radioactivities of ^{188}Re and ^{188}W were determined by quantification of the 155 keV (15%) and 291 keV (0.4%) photo peaks, respectively. A D.C. power supply with 100 V compliance, a maximum current of 2 A, 1.2 nA current resolution and $>10^{13}$ Ohms input impedance was used for electrochemical studies.

6.3.2 Development of alumina based $^{188}W/^{188}Re$ generator

The alumina based $^{188}W/^{188}Re$ generator was developed as per the reported procedure [254]. A borosilicate glass column of dimension 15 cm × 0.4 cm (i.d.) with sintered disc (G_2) at the bottom was placed in a lead shield and packed with 4 g of acidic alumina. It was then preconditioned to pH 3 with 0.001 N nitric acid solution. The column was loaded by passing 10 mL of $Na_2[^{188}WO_4]$ (1.85 GBq of ^{188}W) solution through the column at a flow rate of 0.25 mL min^{-1}. The column was then washed with 100 mL of saline (0.9% NaCl) solution. ^{188}Re was eluted from this generator using 0.9% NaCl solution as the eluent.

6.3.3 Post-elution concentration of ^{188}Re

6.3.3.1 Principle of electrochemical concentration of ^{188}Re

Concentration of ^{188}Re involves electrodeposition of ^{188}Re on a platinum cathode as per the reaction:

$$ReO_4^- + 8H^+ + 7e \rightarrow Re + 4H_2O \qquad E^o = +0.362V \text{ [131]}$$

Subsequently, the electrodeposited ^{188}Re could be dissolved in a small volume of saline (0.9% NaCl) solution.

6.3.3.2 The electrochemical set up

The electrochemical assembly used for the concentration of ^{188}Re was similar to the one described for the electrochemical $^{188}W/^{188}Re$ generator (Section 6.2.2.2).

6.3.3.3 Optimization of the electrochemical parameters for the deposition of ^{188}Re

The parameters for electrodeposition of ^{188}Re from a solution containing ^{188}W were optimized for the preparation of the $^{188}W/^{188}Re$ generator (Section 6.2.2.3). In this study, the parameters for electrolysis were again verified in the absence of ^{188}W and in presence of chloride ions in the solution. The electrolysis parameters such as the applied potential, pH of the electrolyte, time of electrodeposition, etc., were optimized by using 37 MBq (1 mCi) of ^{188}Re. The pH of the $^{188}ReO_4^-$ solution was adjusted by addition of 1 N oxalic acid solution before transferring it to the electrochemical cell.

6.3.3.3.1 Effect of applied potential

The effect of the applied potential on the electrodeposition of ^{188}Re at pH 1-2 at room temperature is shown in **Table 6.3**. The reported values in the table shows the yields of ^{188}Re recovered in 0.1 N HCl solutions. The percentage of ^{188}Re deposited was observed to increase with increasing potential and reached a maximum value of 91±3 % at ~7 V. On further increase of potential, the ^{188}Re deposit became adherent to the electrode surface and was not fully recoverable. Hence, all subsequent experiments were carried out at a potential of 7 V. Though the standard reduction electrode potential of ReO_4^-/Re is only +0.362 V [131], maximum electrodeposition could be achieved only at 7 V, which was ~20 times higher than the standard reduction potential. Due to this high over-voltage, Re was not deposited purely as a metal, but as a mixture of its oxide and metal form [278].

Table 6.3: Effect of applied potential on the electrodeposition yield of ^{188}Re from saline solution

Applied potential (V)	Electrodeposition of ^{188}Re (%)
3	27±6
5	49±4
7	91±3
9	87±8
11	85±9

(n = 3, '±' indicates standard deviation)

6.3.3.3.2 Effect of the pH of the electrolyte

The electrodeposition yield of ^{188}Re was studied as a function of the pH of the electrolyte. **Fig. 6.9** shows the results of the studies on effect of pH of the electrolyte on electrodeposition. It is seen that maximum deposition (~87 %) of ^{188}Re took place at pH 2. The pH of the electrolysis solution tends to increase slowly during electrolysis, but this increase in pH does not necessitate pH adjustment.

6.3.3.3.3 Effect of the time of electrodeposition

In order to optimize the time required to obtain maximum electrodeposition, the electrodeposition yield of ^{188}Re was studied as a function of time at the optimum applied potential and pH. The results are shown in **Fig. 6.10**, which shows the need to carry out the electrodeposition for 45 min. It was found that during 45 minutes of electrolysis at applied potential of 7 V, current dropped from about 350 mA to 100 mA. The drop in current might be due to the decrease in the conductance of the electrolyte with time owing to the electrodeposition of Re.

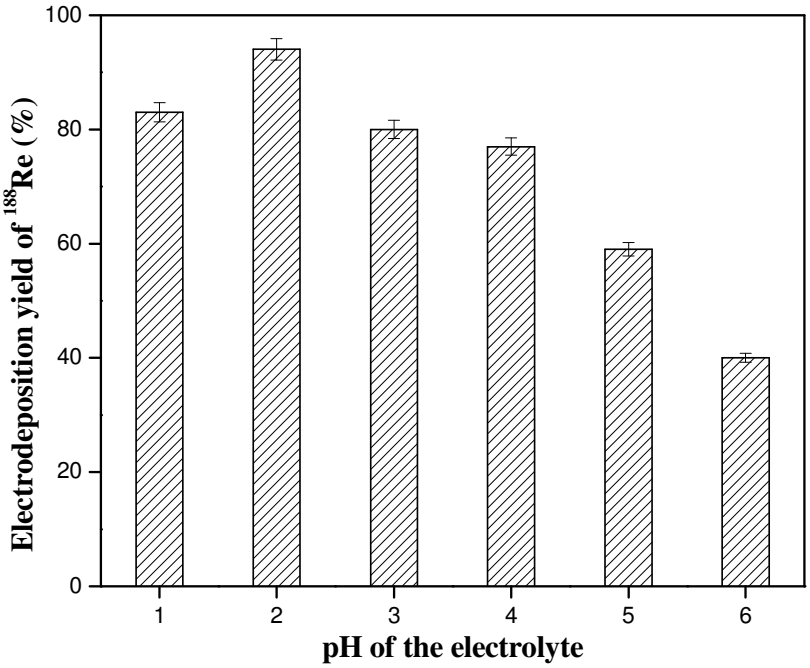

Fig. 6.9: Effect of pH of saline solution on the electrodeposition yield of ^{188}Re

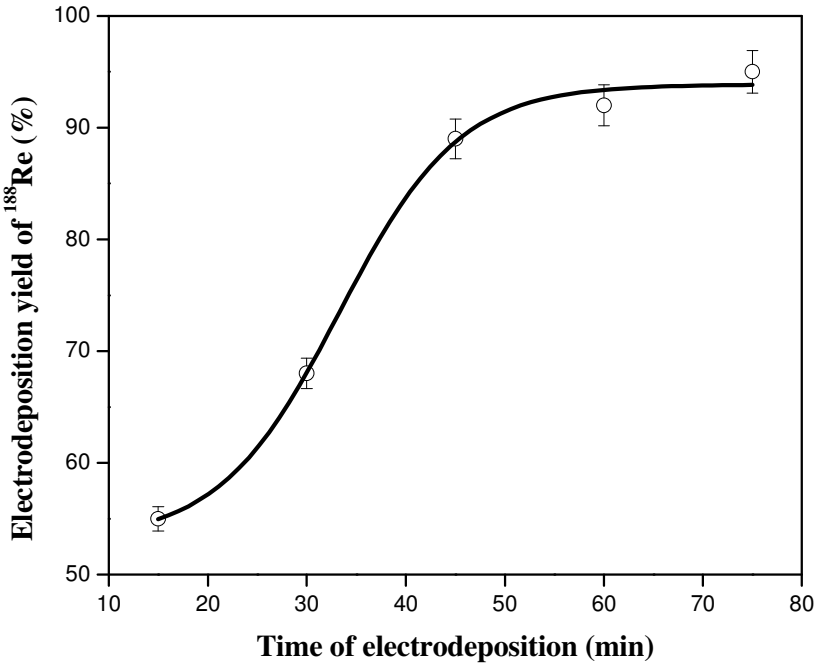

Fig. 6.10: Effect of time on the electrodeposition yield of ^{188}Re from saline solution

6.3.4 Process demonstration: Concentration of $^{188}ReO_4^-$ solution

The $^{188}W/^{188}Re$ generator was eluted with 15 mL of saline solution. The ^{188}Re eluate was transferred to the electrolysis cell and the cell was then covered with the teflon cap together with the two platinum electrodes which were fully dipped into the solution. Prior to electrolysis, argon gas was gently purged through the solution for 10 minutes. Electrolysis was performed by applying a constant potential of 7 V (current 350 mA, current density 574 mA cm^{-2}) for 45 minutes. After the electrolysis, the electrodes were removed and the current was turned off. The electrodeposited ^{188}Re could be brought into saline (0.9% NaCl) solution by placing the electrode in a narrow (1 mL) glass vial (0.5 cm diameter) containing 500 μL of saline solution. A new Pt electrode was also dipped in the solution and the polarity of the cathode was reversed. A high voltage (10 V) was applied for ~20 s and both the electrodes were taken out from the solution after switching off the current. Thus, the ^{188}Re deposit was electrochemically dissolved in saline solution. The radioactivity in the solution was measured and it was observed that ^{188}Re could be concentrated to ~500 μL with an average yield of 85-90%.

In order to study the effect of volume of ^{188}Re solution on the electrodeposition process, the volume of the ^{188}Re eluate was varied by addition of saline solution. **Table 6.4** summarizes the results of the studies to evaluate the performance of the method at varying electrolyte volume at optimum pH, applied potential and time. 37 MBq (1 mCi) of ^{188}Re was used in all the experiments. It is observed that although the radioactive concentration of ^{188}Re in the electrolyte decreases with increasing volume, the efficiency of electrodeposition of ^{188}Re is nearly the same irrespective of the differing ^{188}Re concentration. Dilution of the electrolyte with 0.9% NaCl solution increased the number of Na^+ and Cl^- ions in the electrolyte, but the results demonstrated that the presence of these ions does not influence the efficiency of electrodeposition of ^{188}Re. The results of this study suggest that this technique

can be successfully used for concentrating solution having very low radioactive concentration of ^{188}Re in 0.9% NaCl medium.

Table 6.4: Effect of volume of the electrolyte on the electrodeposition yield of ^{188}Re

Volume of electrolyte (mL)	% Deposition of ^{188}Re
5	88±4
10	89±5
20	83±2
30	90±4
40	89±5
50	87±6

n = 3, '±' indicates standard deviation; Activity of ^{188}Re used = 37 MBq (1 mCi)

It was observed that ^{188}Re could be concentrated to ~100 folds with an average of 85-90% yields. The average practical yield (corrected for decay loss) of >85% is comparable to the yield of 80-90% from the conventional ion-exchange based concentration systems. The experiments were repeated using a simulated solution of ReO_4^- with a Re content equivalent to 37 GBq (1 Ci), prepared by dissolving ~1.6 µg of NH_4ReO_4. The simulated solution of ^{188}Re contained 37 MBq (1 mCi) of ^{188}Re as tracer. It was observed that the results of the simulated experiments were similar to the ones with lower content of Re atoms, with an overall yields of 88±2% (n = 5).

6.3.5 Quality control of ^{188}Re

The suitability of ^{188}Re obtained after post-elution concentration, for preparation of radiopharmaceuticals was determined by adopting the quality control procedures described earlier. The level of ^{188}W impurity in ^{188}Re was determined to be $<10^{-5}$%. It is likely that ^{188}Re eluate from old ^{188}W/^{188}Re generators may have above permissible levels of ^{188}W, due to damage of the column matrix under the intense radiation environment. ^{188}W will remain in

the solution under the electrochemical conditions employed by us as ^{188}W cannot be deposited in aqueous medium [132]. Thus, this approach not only fulfills the most important concentration role but also increases in the radionuclidic purity of ^{188}Re. The radiochemical purity of $^{188}ReO_4^-$ recovered after electrolysis was >99% of the total ^{188}Re activity, which is within the prescribed limits of ≥95% as per the pharmacopoeias [135].

6.3.6 Labeling efficacy of ^{188}Re

^{188}Re was used to label dimercaptosuccinic acid (DMSA) and hydroxyethylidene diphosphonate (HEDP) as per the procedure described earlier (Section 6.2.6). The complexation yield of ^{188}Re with DMSA and HEDP was >98%, thereby demonstrating the suitability of the concentrated ^{188}Re for the preparation of radiopharmaceuticals.

6.3.7 Advantages of the electrochemical concentration procedure

The main advantage of this procedure is the simplicity of the electrochemical method, which might be an alternative to the existing multi-step chromatographic processes to provide clinical grade ^{188}Re. The electrochemical method is effective for the concentration of ^{188}Re solution, irrespective of the extent of dilution. Additionally, unlike the conventional approaches, the electrochemical concentration procedure does not lead to the addition of chemical impurities in ^{188}Re which may interfere in the preparation of ^{188}Re-based radiopharmaceuticals.

6.3.8 Conclusions

A simple electrochemical method to enhance the radioactive concentration of ^{188}Re was successfully demonstrated. This procedure can concentrate ^{188}Re solution of very low radioactive concentration to volume appropriate for the preparation of radiopharmaceuticals. Therefore, this strategy can be effectively utilized for the concentration of ^{188}Re availed from a ‘jumbo’ alumina column based $^{188}W/^{188}Re$ generator, prepared using low specific activity

^{188}W. Further development of this technique into a user-friendly system suitable for adaptation in hospital radiopharmacies would be interesting and worthwhile.

6.4 Development of $^{188}W/^{188}Re$ generators using nanomaterials as sorbents

The present study was aimed at exploring the potential advantages of using TiP and nano-ZrO_2 as alternative sorbents for the preparation of $^{188}W/^{188}Re$ generators. The potential of nanomaterial based sorbents in the preparation of $^{99}Mo/^{99m}Tc$ and $^{68}Ge/^{68}Ga$ generators has been demonstrated in the earlier chapters. This section describes the development of two $^{188}W/^{188}Re$ generators using this novel class of sorbents. The performance of the generators was evaluated to ascertain that the features necessary for preparation of radiopharmaceuticals such as, high yield of ^{188}Re, low ^{188}W breakthrough and high radioactive concentration and adequate purity of the ^{188}Re solution are complied with.

6.4.1 Materials

Reagents such as hydrochloric acid, ammonium hydroxide, etc. were of analytical grade and were procured from S.D. Fine Chemicals, Mumbai. Zirconyl chloride ($ZrOCl_2.8H_2O$), titanium tetrachloride ($TiCl_4$) and isopropyl alcohol (A.R. grade) were obtained from E. Merck, Mumbai, India. Stannous chloride, hydroxyethylidene diphosphonate (HEDP) and dimercaptosuccinic acid (DMSA) were obtained from Sigma Chemical Company, USA. Paper chromatography strips were purchased from M/s. Whatman, UK. Flexible silica plates (coating thickness 0.25 mm) were from J.T. Baker Chemical Company, USA. Tungsten-188 (specific activity 159 GBq g^{-1}) as sodium (^{188}W) tungstate was procured from the State Scientific Centre of Russia Research Institute of Atomic Reactors (PSUE) in Dmitrovgrad, Russia, through an IAEA Coordinated Research Project.

A HPGe detector coupled with a multichannel analyzer (Canberra Eurisys, France) with 0.5 keV resolution and range from 1.8 keV to 2 MeV was used for analysis of ^{188}W, in the presence of ^{188}Re and also for their quantitative estimation. The radionuclide amounts were determined by quantification of the 155 keV (15%) and 291 keV (0.4%) photo peaks of ^{188}Re and ^{188}W, respectively.

6.4.2 Separation of ^{188}Re from ^{188}W

6.4.2.1 Synthesis of TiP and nano-ZrO_2

The synthesis of TiP and nano-ZrO_2 sorbents was carried out as per the procedure described in Chapter 2. The synthesis processes are inexpensive, simple, carried out at ambient conditions and amenable for large-scale production. The materials were synthesized in several batches and the product obtained in all the batches was granular with adequate mechanical strength. The excellent flow characteristics, chemical stability and attrition resistance exhibited by these sorbents proved their suitability for fixed-bed column operations.

6.4.2.2 Determination of distribution ratio (K_d) of ^{188}W and ^{188}Re ions

The pH of the solution plays an important role with respect to the sorption of ^{188}W and ^{188}Re ions on the nano metal oxide surface. The effect of pH of the solution on the K_d values of ^{188}W and ^{188}Re ions was studied to optimize the experimental conditions necessary for satisfactory loading of ^{188}W in the column as well as easy elution of ^{188}Re. In order to determine the K_d values, 200 mg of sorbent was suspended in 20 mL solution containing $^{188}WO_4^{2-}$ or $^{188}ReO_4^-$ ions as radiotracer, in a 50 mL stoppered conical flask. The solution was shaken for 1 h at 25 °C using a wrist arm mechanical shaker and then filtered. The activities of the solution before and after equilibration were measured in a well type NaI(Tl) counter using appropriate window ranges (100-200 keV for ^{188}Re and 250-350 keV for ^{188}W). The distribution ratios were calculated using the following expression:

$$K_d = \frac{(A_i - A_{eq})V}{A_{eq}\, m}$$

where, A_i is the initial radioactivity of 1 mL the solution, A_{eq} is the unadsorbed activity in 1 mL of the solution at equilibrium, V is the solution volume (mL) and m is the mass (g) of the sorbent. The distribution ratio (K_d) results for ^{188}W and ^{188}Re ions in TiP and nano-ZrO_2 are summarized in **Table 6.5** and **Table 6.6**, respectively.

Table 6.5: Distribution ratios (K_d) of $^{188}WO_4^{2-}$ and $^{188}ReO_4^-$ ions in TiP

Medium	K_d	
	^{188}W	^{188}Re
pH 1	191±4	23±3
pH 2	244±6	61±6
pH 3	235±3	83±2
pH 4	195±7	56±2
pH 5	189±2	38±1
pH 6	175±8	46±4
pH 7	34±1	15±1
pH 8	22±2	3±1
0.9% NaCl	90±1	0.7±0.3

(n = 3; '±' represent the standard deviation)

Table 6.6: Distribution ratios (K_d) of $^{188}WO_4^{2-}$ and $^{188}ReO_4^-$ ions in nano-ZrO_2

Medium	K_d	
	^{188}W	^{188}Re
pH 1	143±4	6±3
pH 2	469±10	31±5
pH 3	616±12	61±8
pH 4	315±14	24±12
pH 5	133±7	<0.01
pH 6	122±8	<0.01
pH 7	23±3	<0.01
pH 8	10±2	<0.01
0.9% NaCl	188±9	0.2±0.1

(n = 3; '±' represent the standard deviation)

The results indicate that under all examined experimental conditions both TiP and nano-ZrO_2 adsorb tungstate ions better than perrhenate ions. In both the sorbents, the K_d values for tungsten and rhenium ions are higher under acidic conditions, reaching a maximum at around pH 2-3. As these sorbents showed far lower affinity for ^{188}Re compared to ^{188}W in 0.9% NaCl solution, ^{188}Re formed from the decay of ^{188}W could be easily eluted with 0.9% NaCl solution.

In conjunction with this work that deals with the sorption of ^{188}W on the nanomaterials based sorbents, attempts were made to correlate the K_d values with the zeta potential of these sorbents at different pH environments. The effect of pH on zeta potential of TiP and nano-ZrO_2 in aqueous solution were shown in **Fig. 2.4** and **Fig. 2.8,** respectively. Owing to the positive zeta potential of the sorbents under acidic conditions, they can be expected to enhance the removal of negatively charged tungstate polyanions from the aqueous solution at acidic pH. The variation of zeta potential and K_d with pH of the solution show a similar trend. These results give an indication that the electrostatic force is primarily responsible for the sorption of ^{188}W in the present study.

Though the sorption process of the nano metal oxide sorbents has been considered a surface phenomenon, the possibility of specific chemical interactions between polytungstate anions $[HW_6O_{21}]^{5-}$ [283] and the sorbent could also be possible. The selective uptake of negatively charged polytungstate ions may be considered to take place by two steps. The first one may be due to electrostatic attraction of negatively charged anion on the positively charged surface of the sorbent. Subsequently, it may form a stable complex of the type $[MW_6O_{24}]^{8-}$ (M = Ti or Zr) at this pH range, similar to that reported with alumina [141]. However, in order to predict the exact mechanism of ^{188}W uptake, further studies are warranted which are outside the scope of this thesis. Optimum retention of ^{188}W was obtained when the pH of the ^{188}W feed solution was adjusted in the range of 2-3. The decay of ^{188}W to

^{188}Re is not accompanied by any serious disruption of chemical bonds. ^{188}W is expected to be retained strongly on the sorbent matrix as polymeric tungstate ions. As these tungstate ions start transforming into perrhenate ion ($^{188}ReO_4^-$), which has only -1 charge, the binding would get weaker and an easy displacement of $^{188}ReO_4^-$ is expected. Moreover, the pH of 0.9% NaCl solution is ~7 and the zeta-potentials of both these sorbents are negative at this pH. Therefore, due to electrostatic repulsion $^{188}ReO_4^-$ gets eluted easily with normal 0.9% NaCl solution.

6.4.2.3 Determination of the time of equilibration

In order to study the time dependence of sorption of ^{188}W onto TiP and nano-ZrO_2, distribution ratio (K_d) values of ^{188}W ions in 0.001 M HNO_3 solution was determined at different time intervals, as described above. The K_d values (mean of three experiments) were used to monitor the progress of the sorption process. The time when K_d remained unchanged, was taken as the indication of the attainment of equilibrium. The plots of K_d versus time for TiP and nano-ZrO_2, are shown in **Fig. 6.11** and **Fig. 6.12**, respectively. As inferred from the curves, contact times of 45 min for TiP and 15 min for nano-ZrO_2 respectively were maintained in order to attain sorption equilibrium in the batch processes.

6.4.2.4 Determination of sorption capacity of TiP and nano-ZrO_2

The sorption capacity, indicative of the ability of the sorbent to retain ^{188}W, depends on the number of available sorption sites within the matrix. The sorption capacities of the sorbents were determined both under static and dynamic conditions.

6.4.2.4.1 Static sorption capacity

The static sorption capacity of the sorbent for W ions was determined by batch equilibration method. For this, 0.5 g of accurately weighed sorbent was taken in a glass stoppered conical flask and equilibrated with 50 mL of sodium tungstate solution of

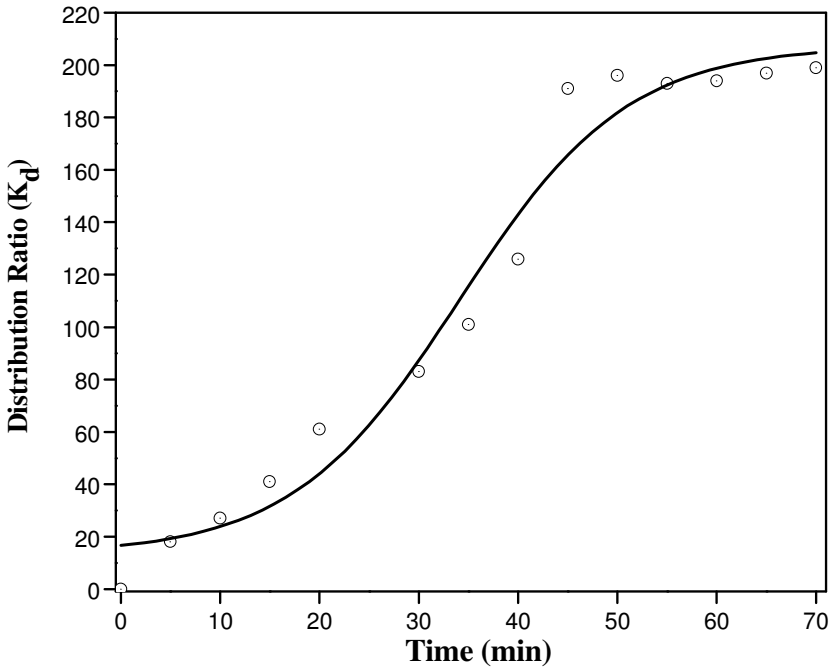

Fig. 6.11: Variation in K_d values of $^{188}WO_4^{2-}$ ions with time using TiP as sorbent

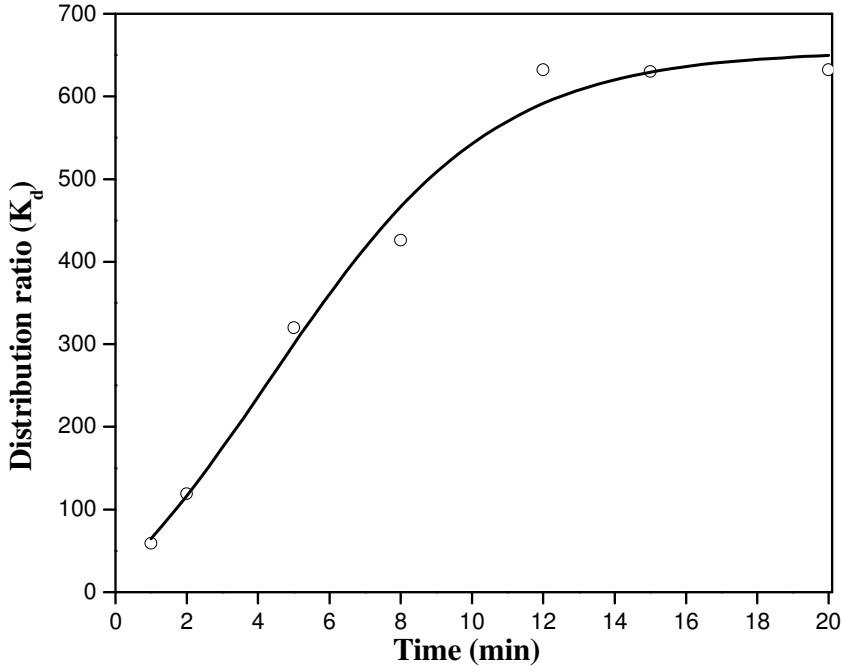

Fig. 6.12: Variation in K_d values of $^{188}WO_4^{2-}$ ions with time using nano-ZrO_2 as sorbent

concentration 10 mg W mL^{-1}, spiked with ~100 μCi (3.7 MBq) of ^{188}W, for 1 h at room temperature. The pH of the solution was adjusted to ~3. At the end, the contents were filtered through a Whatman filter paper (No. 542). The activities of ^{188}W in the solution before and after sorption were estimated by using HPGe detector coupled to a multichannel analyzer, by measuring the counts at 291 keV peak corresponding to ^{188}W in 1 mL aliquots. All measurements were carried out at 25° C in triplicate. The sorption capacity was calculated using the following expression:

$$\text{Capacity} = \frac{(A_o - A_e)V.C_o}{A_o\, m}$$

where A_o and A_e represented the radioactivity of ^{188}W in 1 mL of supernatant solution before and after sorption, respectively, C_o was the total W content (10 mg) in 1 mL of solution before sorption, V was the volume of solution and m was the mass (g) of the sorbent. The static sorption capacity of TiP was (320 ± 5) mg W g^{-1} while that of nano-ZrO_2 was (312 ± 9) mg W g^{-1}. These results suggest that the W-sorption capacities of TiP and nano-ZrO_2 are much higher than that of alumina, which has a maximum sorption capacity of ~80 mg W g^{-1} [251].

6.4.2.4.2 Determination of breakthrough pattern and dynamic sorption capacity

In order to estimate the W sorption capacity under dynamic conditions, a borosilicate glass column of dimension 15 cm × 0.4 cm (i.d.) with a sintered disc (G_2) at the bottom was packed with 0.5 g of the respective sorbent. After the column was conditioned with 0.01 M HNO_3, sodium tungstate solution (10 mg W mL^{-1}), spiked with ^{188}W tracer (37 kBq mL^{-1}) was allowed to pass through the column at a rate of 0.25 mL min^{-1}. 1 mL of this solution was kept as reference. The effluent was collected in fractions of 1 mL aliquots. The ^{188}W activity in the reference (C_o) and effluent fractions (C) were determined by measuring the 291 keV γ-ray peak of ^{188}W in a HPGe detector. The ratio of the count rate 'C' of each 1 mL effluent to

the count rate 'C_o' of 1 mL of the original feed W solution was taken as the parameter to follow the sorption pattern. The breakthrough profiles for TiP and nano-ZrO_2 are depicted in **Fig. 6.13** and **Fig. 6.14**, respectively.

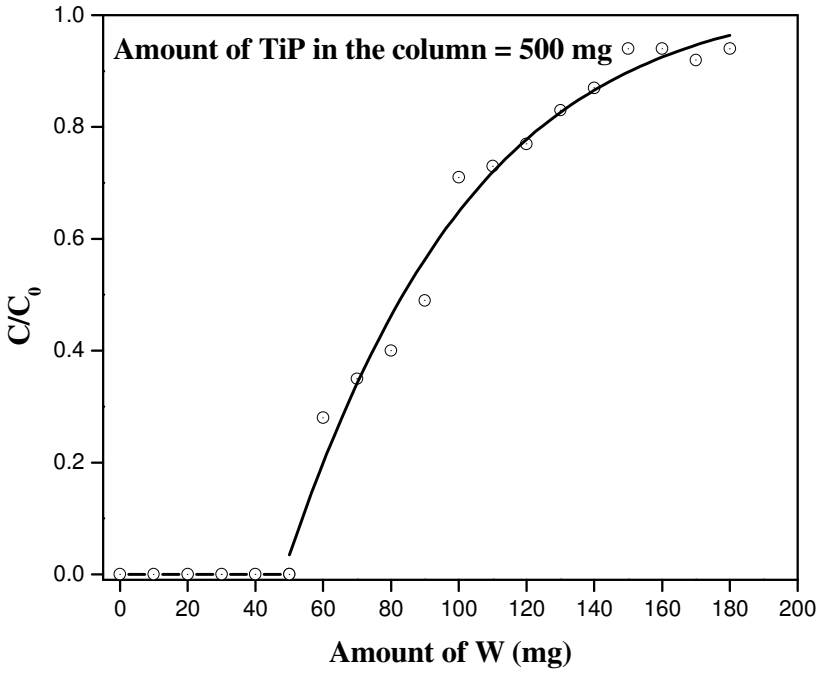

Fig. 6.13: Breakthrough profile of WO_4^{2-} ions on passing W (10 mg W mL^{-1}) solution through a 500 mg TiP column at a flow rate of 0.25 mL min^{-1}

The breakthrough profile portrays the sorption behavior of ^{188}W in a generator column bed containing the sorbent. In case of TiP, the breakthrough point was reached after (102 ± 5) mg of W (n = 5) was quantitatively retained by 1 g of TiP in the column. Similarly, in case of nano-ZrO_2, it was observed that the breakthrough point was reached after (120 ± 7) mg of W (n = 5) was quantitatively retained by 1 g of sorbent in the column. The breakthrough capacities of these sorbents (>100 mg W g^{-1}) were much higher than that of alumina (~48 mg W g^{-1}) [284]. Further, it can be seen from the figures, the saturation capacity of these sorbents (at $C/C_0 = 0.9$) was ~300 mg W g^{-1}.

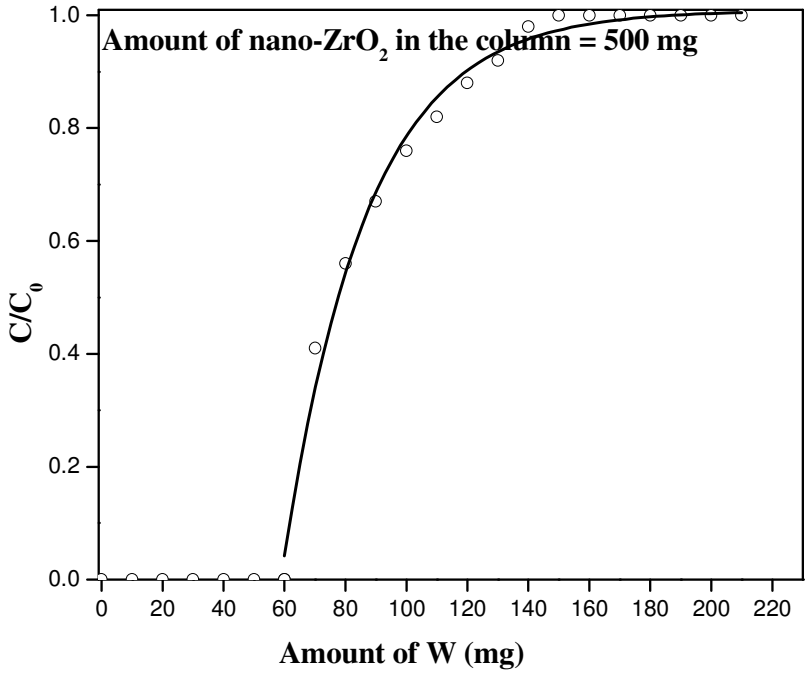

Fig. 6.14: Breakthrough profile of WO_4^{2-} ions on passing W (10 mg W mL^{-1}) solution through a 500 mg nano-ZrO_2 column at a flow rate of 0.25 mL min^{-1}

Also it is observed that the breakthrough capacities of both the sorbents were much less than their static sorption capacities. This was probably due to the mass transfer limitations such as incomplete external film diffusion and/or to intraparticle transfer. However, the protocol for preparing chromatographic column generator using sorbent matrix preloaded with ^{188}W under static conditions is not recommended owing to difficulties in handling of radioactive material. This will not only cause associated radioactive contamination problem but also increase the radiation exposure to the personnel involved. Furthermore, even if the generator is prepared, the operating performance is likely to deteriorate when the activity loaded is high. Therefore, post loading of ^{188}W activity protocol, was followed despite the lower sorption capacity that could be achieved.

6.4.3 Development of $^{188}W/^{188}Re$ generators

In order to integrate the experimental findings and to establish the utility of the

sorbents in radiation environments, it was necessary to carry out process demonstration runs to evaluate the behavior of the sorbents in the presence of intense radiation environment with the radiolytic products generated due to ^{188}W. This could be accomplished by developing two $^{188}W/^{188}Re$ generators of 1.85 GBq (50 mCi) each, using TiP and nano-ZrO_2 as sorbents. For the preparation of each generator, a borosilicate glass column of dimension 10 cm (l) × 0.8 cm (i.d.) with sintered disc (G_0) at the bottom was packed with 2 g of sorbent. A schematic diagram of the $^{188}W/^{188}Re$ generator system is shown in **Fig. 6.15**. All the operations were carried out in the closed cyclic system using connecting tubes. Input/output connections were made with standard teflon tubings of 1 mm inner diameter and connectors.

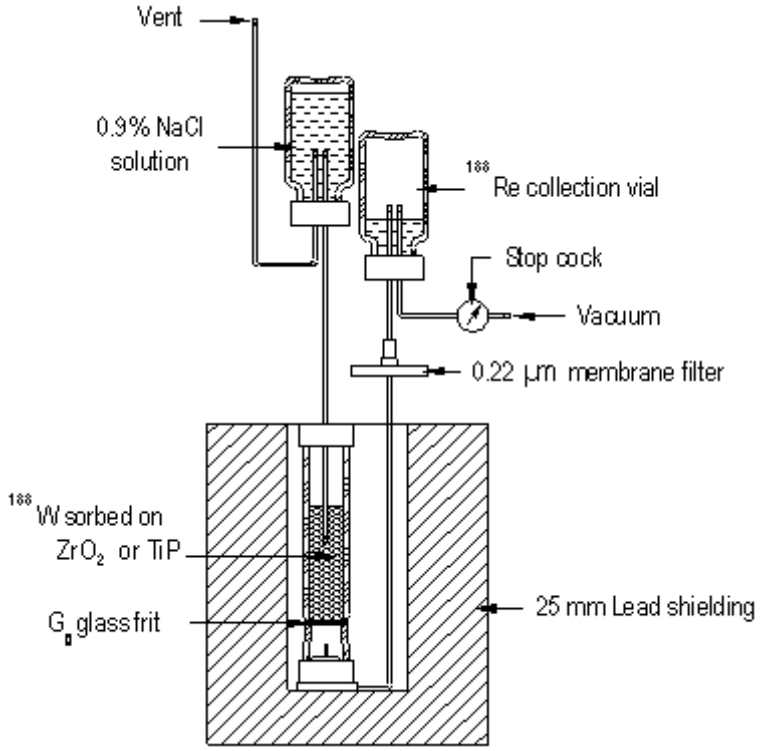

Fig. 6.15: Schematic diagram of $^{188}W/^{188}Re$ generator system

The generator column, connectors and connection tubings were integrated within a small portable lead shielded unit throughout experimentation for radioprotection purpose. Only the elution vial and output vial were accessible externally. A disposable 0.22 µm membrane filter was attached to the generator column output by teflon tubing. The generator column was

preconditioned with 0.001 N nitric acid solution at pH 3. The column was then loaded by passing of $Na_2{}^{188}WO_4$ solution maintained at pH 3 through the column at a flow rate of 0.25 mL min^{-1}, by applying suction using a peristaltic pump. Each of the columns was then washed with 100 mL of 0.9% NaCl solution. In case of both the sorbents, >99% of ^{188}W was retained in the respective columns and on washing with 0.9% NaCl solution, <0.5% of ^{188}W was eluted out. The generators were regularly eluted with 4 mL of 0.9% NaCl solution for 6 months.

6.4.4 Elution profiles of the $^{188}W/^{188}Re$ generators

In order to optimize the minimum volume of eluent required for elution of ^{188}Re with maximum yield, the elution profile of the generators were studied. This study also gives an idea on the practical utility and separation capability of the sorbents. In order to examine the elution profile, the $^{188}W/^{188}Re$ generators were eluted with 0.9% NaCl solution at a flow rate of 0.5 mL min^{-1}. All runs were performed at room temperature. The eluate was collected as 1 mL aliquots and each fraction was counted for gamma activity. The elution profiles of the TiP and nano-ZrO_2 based generators are illustrated in **Fig. 6.16** and **Fig. 6.17**, respectively. It can be seen from the figures that in both the cases, ~90% of $^{188}ReO_4^-$ available in the generator was eluted within the first 4 mL volume of eluent with appreciable radioactive concentration and by eliminating the fractions with lower activity, one could get the product in very high radioactive concentration.

6.4.5 Quality control of ^{188}Re

The suitability of ^{188}Re obtained from TiP and nano-ZrO_2 based $^{188}W/^{188}Re$ generators were determined by adopting the quality control procedures described for the electrochemical $^{188}W/^{188}Re$ generator (Section 6.2.3). The levels of ^{188}W impurity, as determined by the γ-ray spectrometry of the decayed ^{188}Re samples, were $<10^{-4}$% of the ^{188}Re activity.

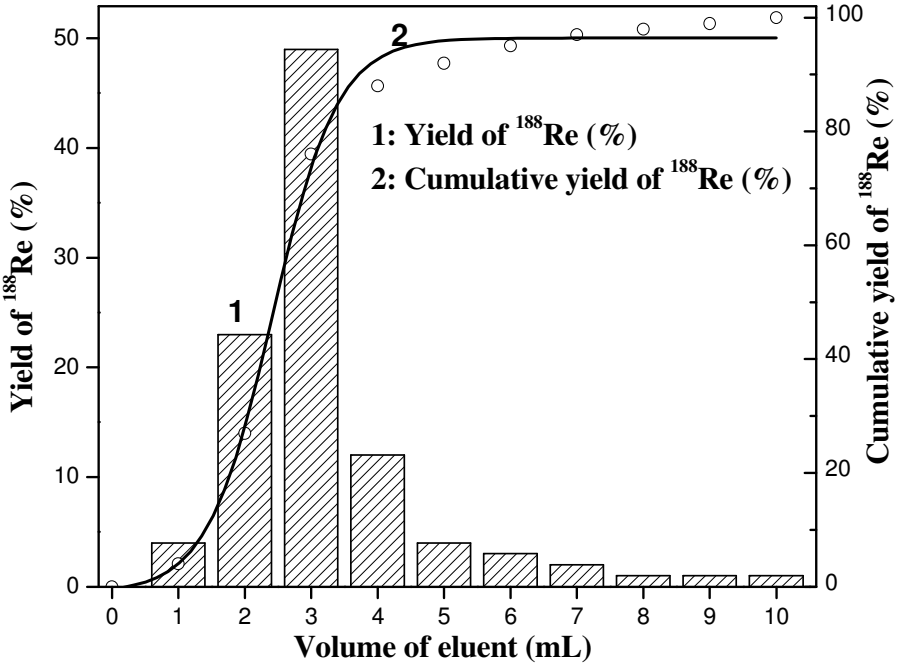

Fig. 6.16: Elution profile of the TiP based ^{188}W/^{188}Re generator

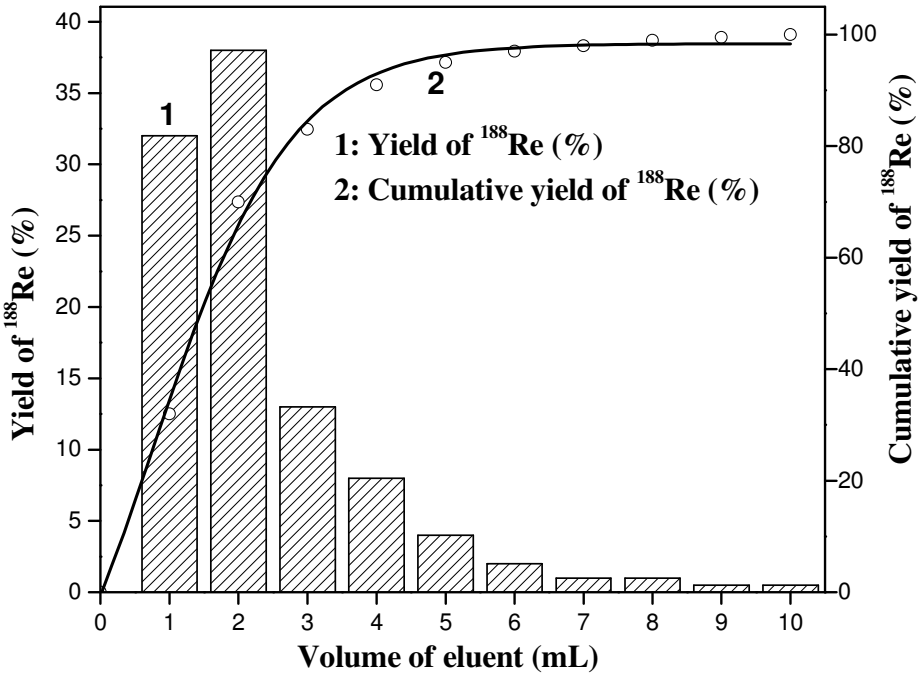

Fig. 6.17: Elution profile of the nano-ZrO_2 based ^{188}W/^{188}Re generator

The radiochemical purity of $^{188}ReO_4^-$ was >99%. The levels of Ti and Zr ions in the ^{188}Re eluate, as determined by ICP-AES analysis of the decayed ^{188}Re samples were <0.1 ppm. The levels of radionuclidic, radiochemical and chemical impurities in ^{188}Re obtained from both the generators were well within the acceptable limits prescribed in the pharmacopoeias [135].

6.4.6 Labeling efficacy of ^{188}Re

In order to examine the suitability of $^{188}ReO_4^-$ obtained from the generators for radiolabeling studies, it was complexed with DMSA and HEDP, as per the procedure described earlier (Section 6.2.6). The complexation yields of ^{188}Re-DMSA and ^{188}Re-HEDP were always >98%, demonstrating the suitability of ^{188}Re obtained from the TiP and nano-ZrO_2 based generators for biomedical applications.

6.4.7 Elution performance of $^{188}W/^{188}Re$ generators over a period of 6 months

The $^{188}W/^{188}Re$ generators were evaluated for their performance for a period of 6 months. The generators were eluted regularly with 4 mL of 0.9% NaCl solution. Over this period of time, the generators were eluted for >50 times. The performance of the TiP and t-ZrO_2 based $^{188}W/^{188}Re$ generators with respect to the radiochemical yield of ^{188}Re and the ^{188}W breakthrough are illustrated in **Fig. 6.18** and **Fig. 6.19,** respectively. The figures show that for the both the generators the radiochemical yield of ^{188}Re was always >75% and the level of ^{188}W impurity present in ^{188}Re was $<10^{-3}$% over the extended period of 6 months.

6.4.8 Simulated study for the separation of Re from a W carrier-added solution equivalent to ~37 GBq (1 Ci) of ^{188}W

The effects of macroscopic amounts of tungsten on the efficiency of chromatographic separation of ^{188}Re from ^{188}W, using TiP and nano-ZrO_2 sorbents were investigated by using W/Re mixture containing inactive W and Re carriers equivalent to ~ 37 GBq (1 Ci) of ^{188}W.

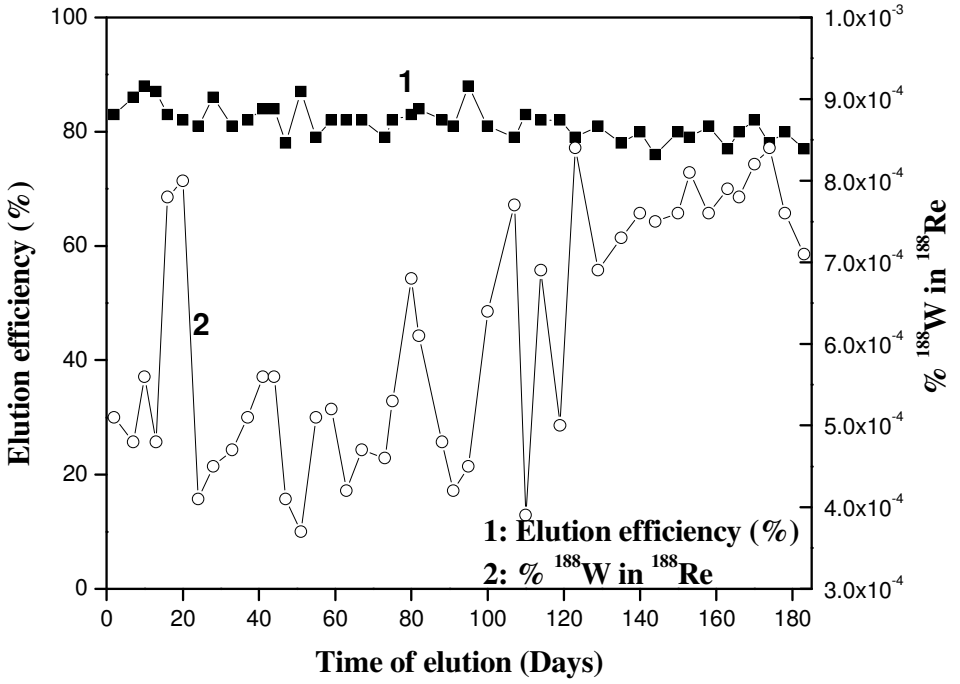

Fig. 6.18 Elution performance of the TiP based $^{188}W/^{188}Re$ generator over a period of 6 months

The mixture was spiked with an equilibrium mixture of $^{188}W/^{188}Re$ containing 37 MBq (1 mCi) of ^{188}W and ^{188}Re. This simulated solution was prepared by dissolving 292 mg of WO_3 (equivalent to 37 GBq of ^{188}W at 159 GBq g^{-1} of W specific activity) and 1.45 µg (equivalent to 37 GBq of ^{188}Re) of ammonium perrhenate in 2 M NaOH. The resultant solution was evaporated to dryness and then reconstituted with 0.001 M HNO_3 solution and the pH of the solution was adjusted to ~3. The mixture was loaded in a borosilicate glass column [15 cm × 0.4 cm (i.d.)] containing 2.5 g of the sorbent adopting the procedure described above. ^{188}Re was eluted with 4 mL of 0.9% NaCl solution under the same conditions as in the previous studies. The efficiency of ^{188}Re elution and the ^{188}W breakthrough were determined. It was observed that, while using TiP or nano-ZrO_2 as column matrices, the recovery of ^{188}Re from W/Re mixture simulated to represent 37 GBq (1 Ci) of ^{188}W, was as good as when lower amounts of ^{188}W were used. The overall yields of ^{188}Re in the simulated experiments were

~80% and the ^{188}W breakthrough was $<10^{-3}$%. However, in order to utilize these sorbents for the preparation of clinical-scale 37 GBq (1 Ci) $^{188}W/^{188}Re$ generators, the effect of radiation at higher level of activity on the performance of the sorbent materials needs to be demonstrated.

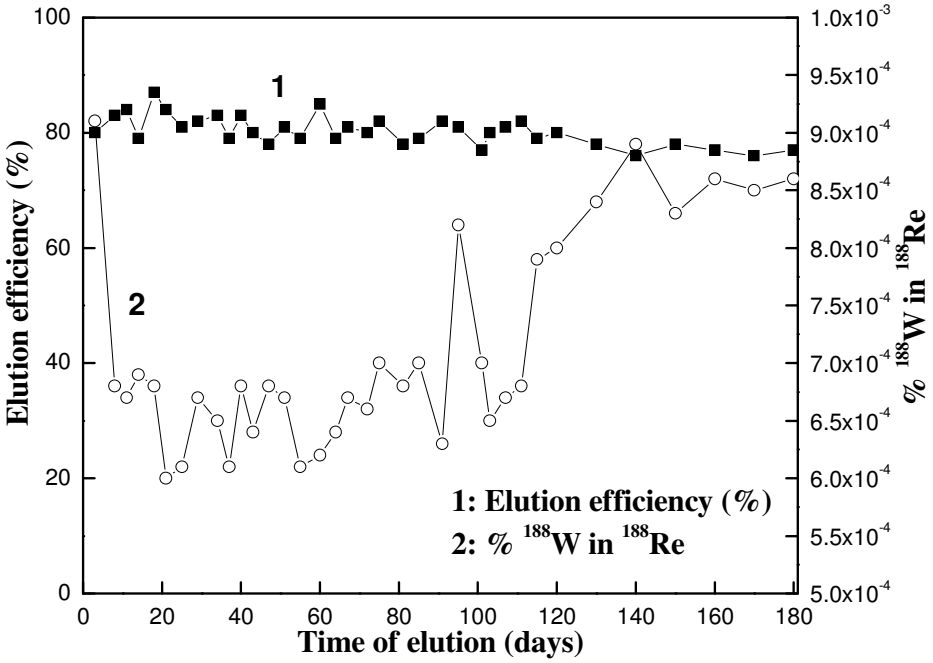

Fig. 6.19 Elution performance of the nano-ZrO_2 based $^{188}W/^{188}Re$ generator over a period of 6 months

6.4.9 Recovery of enriched ^{186}W from the spent generator columns

Since enriched ^{186}W is very expensive, this process would be economically viable if the ^{186}W sorbed in the generator column could be recovered after the expiry of the shelf-life of the generator and reused. Moreover, the exhausted generator columns cannot be directly discarded without removing the sorbed ^{188}W from the column. Therefore, this also is an important step from waste management point of view. Hence, attempts were made to remove ^{186}W along with ^{188}W from the used columns prior to disposal. The spent generator columns were washed with 100 mL of saline solution. Washing of the spent generator with saline

solution before W was eluted, resulted in the depolymerization of tungstate ions adsorbed on the sorbent surface and thus facilitated desorption of ^{186}W + ^{188}W. Tungsten was desorbed from the columns by passing 5 M NaOH solution containing H_2O_2 (15 mL of 5 M NaOH solution + 1 mL of 30% H_2O_2) through the column as per the method adopted for alumina [285]. The flow rate of the eluent was ~0.5 mL min^{-1}. The eluate was collected as 1 mL aliquots throughout the elution, and each sample was counted for gamma activity. Then, all the fractions were pooled together and the total activity of ^{188}W eluted was determined in HPGe detector. The elution behavior of W from the TiP and nano-ZrO_2 columns is illustrated in **Fig. 6.20** and **Fig. 6.21**, respectively. It is seen from the figures that from both the generator columns, the recovery of W is quite fast, and nearly all the ^{186}W could be eluted out in the first 4-5 mL of the eluent.

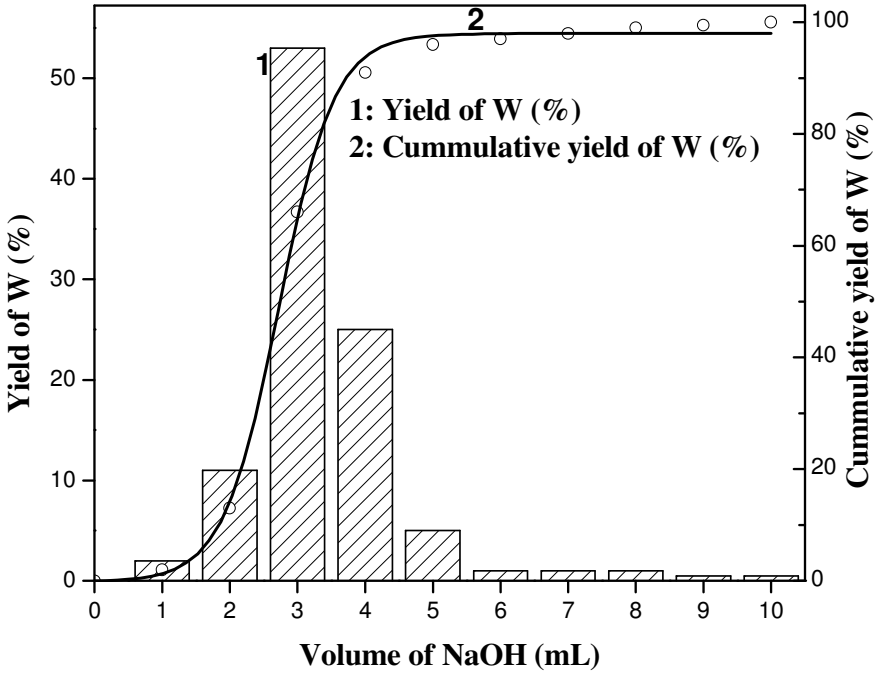

Fig. 6.20: Recovery of W from the used TiP column by passing NaOH-H_2O_2 solution at a flow rate of 0.5 mL min^{-1}

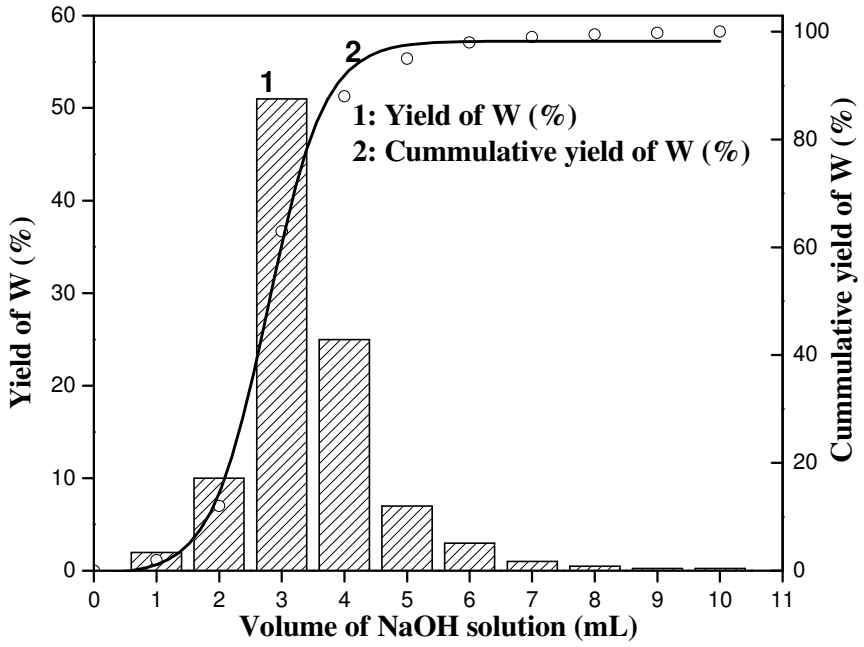

Fig. 6.21: Recovery of W from the used nano-ZrO_2 column by passing NaOH-H_2O_2 solution at a flow rate of 0.5 mL min^{-1}

The mechanism of desorption from the TiP and nano-ZrO_2 columns could be explained as follows. The zeta-potential of TiP and nano-ZrO_2 are negative under alkaline conditions. As the pH of the external solution rises, depolymerisation of polytungstate anionic species sorbed in the column takes place and they exist as WO_4^{2-} under alkaline conditions. Owing to electrostatic repulsion, the negatively charged WO_4^{2-} ions get desorbed from the column by passing NaOH solution. As a result of radiation and chemical changes caused by the ionizing radiation, W ions might be sorbed on the nanocrystalline materials in a reduced state. Addition of H_2O_2 to the NaOH solution promotes the oxidation of the W ions to form WO_4^{2-} ions and thus facilitates their elution.

6.4.10 Advantages of the TiP and nano-ZrO_2 based $^{188}W/^{188}Re$ generators

Development of chromatographic $^{188}W/^{188}Re$ generators containing nanomaterial based sorbents possessing high sorption capacities has the potential for utilizing ^{188}W produced from semi-enriched ^{186}W, in medium flux (~10^{14} n cm^{-2} s^{-1}) research reactors.

Owing to their operational simplicity and excellent performance, these new generator systems based on relatively inexpensive sorbent materials can easily be adapted by many Nuclear Medicine departments. Unlike the conventional alumina based systems, ^{188}Re can be availed from these generators with appreciably high radioactive concentration and can directly be used for the preparation of radiopharmaceuticals.

However, the specific activity of ^{188}W from irradiation in medium flux (~10^{14} n cm^{-2} s^{-1}) reactors would be far lesser than the product from high flux reactors (~10^{15} n cm^{-2} s^{-1}). This would then have an influence on the amount of sorbent and hence the size of the column to be used. For example, assuming the specific activity of ~150 GBq g^{-1} from high flux reactors, a 4 g column could hold up to 400 mg of W corresponding to ~60 GBq ^{188}W (~1.6 Ci). Here, a generator of 37 GBq (1 Ci) can easily be prepared using 3-4 g of the nanomaterial sorbent. In case of low specific activity ^{188}W expected from medium flux reactors, say 10 folds lesser at 15 GBq g^{-1}, a 5 g column would be able to hold ~7.5 GBq (~200 mCi) of ^{188}W, adequate for R&D work. If a therapeutic grade generator is desired using ^{188}W from medium flux reactors, a far larger column will have to be used and the ^{188}Re eluted, which would be dilute, will need to be concentrated. These issues were not studied, since for preparation of therapeutic radiopharmaceuticals at the hospitals, it would perhaps be economical to procure ^{188}W from the few manufacturers with access to high flux reactors, rather than use low specific activity ^{188}W from medium flux reactors. However, for research purposes, lower strength generator using low specific activity ^{188}W from medium flux reactors would be a good option.

The other benefits of these sorbent materials are (1) rapid packing due to the high density of the sorbent which settles in a few minutes, (2) rigidity which allows the use of high flow rates without increase in pressure or shrinking or swelling of the sorbent and (3)

negligible ^{188}W bleeding due to the stable chemical link of the ^{188}W species to the matrix and (4) the radiation and chemical stability of the sorbents over a prolonged period of time.

6.4.11 Conclusions

The results of this study demonstrate that TiP and nano-ZrO_2 with significantly high sorption capacities are promising sorbent materials for the preparation of $^{188}W/^{188}Re$ radionuclide generator. These sorbents exhibited high affinity for ^{188}W in comparison to ^{188}Re, and hence was suitable for the separation of ^{188}Re from ^{188}W. The $^{188}W/^{188}Re$ generators prepared using these sorbents provide carrier-free ^{188}Re (as $^{188}ReO_4^-$) on elution with 0.9% NaCl solution, with >80% yield. ^{188}Re could be availed from the generators with acceptable radionuclidic, radiochemical and chemical purity for clinical application. The $^{188}W/^{188}Re$ generators developed using these sorbents performed consistently well over the period of 6 months. Additionally, it was possible to recover the adsorbed $^{186}W + ^{188}W$ from the spent generator prior to disposal, leading to economic advantage. Taking these into account, it is opined that TiP and nano-ZrO_2 can be used as alternative sorbents for the preparation of clinical grade $^{188}W/^{188}Re$ chromatographic generators.

REFERENCES

[1] Ramamoorthy N. Discovery of artificial radioactivity by I. Curie and F. Joliot. In: Tomar BS, editor. Nobel Prize winning discoveries in nuclear sciences. IANCAS Bulletin 2007; 5: 59-67.

[2] Venkatesh M. Frontiers in radioisotope applications. In: Proceedings of the Nuclear and Radiochemistry Symposium (NUCAR-97); 1997, p 45-57

[3] Rayudu GVS. Production of radionuclides for medicine. Sem Nucl Med 1990; 20: 100-110.

[4] Brucer M. A chronology of nuclear medicine. (Buntaine RR, editor). Heritage Publications, St. Louis, Missourie; 1990.

[5] Friedlander G, Kennedy JW, Macias ES, Miller JM. Sources of nuclear bombarding particles. In: Nuclear and Radiochemistry. 3rd edition, John Wiley and Sons, New York; 1981, p 552-597.

[6] Mc Cready R. Milestones in nuclear medicine. Eur J Nucl Med 2000; 27: S49-S79.

[7] Smithers DW. Some varied applications of radioactive isotopes to the localization and treatment of tumors. Acta Radiol 1951; 35: 49-61.

[8] Venkatesh M. Rosalyn Sussman Yalow. In: Tomar BS, editor. Nobel Prize winning discoveries in nuclear sciences. IANCAS Bulletin 2007; 5: 81-90.

[9] Jones AG. Technetium in nuclear medicine. Radiochim Acta 1995; 71: 289-297.

[10] Early PJ. Use of diagnostic radionuclides in medicine. Health Phys 1995; 69: 649-661.

[11] Richards P, Tucker WD, Srivastava SC. Technetium-99m: An historical perspective. Int J Appl Radiat Isot 1982; 33: 793-799.

[12] Eckelman WC. Unparalleled contribution of technetium-99m to medicine over 5 decades. J Am Coll Cardiol Img 2009; 2: 364-368.

[13] Saha GB. Radiopharmaceuticals and methods of radiolabeling. In: Fundamentals of nuclear pharmacy. 3rd Edition, Springer-Verlag, New York; 2000, p 80-108.

[14] Qaim SM. Nuclear data relevant to the production and application of diagnostic radionuclides. Radiochim Acta 2001; 89: 223-231.

[15] Firestone R. Table of isotopes (Shirley VS, editor). 8th edition, John Wiley and Sons Inc, New York; 1996.

[16] Lauridsen B. Table of exposure rate constants and dose equivalent rate constants. Riso National Laboratory, Rosklide, Denmark; 1982.

[17] Coenen HH, Elsinga PH, Iwata R, Kilbourn MR, Pillai MRA, Rajan MGR, Wagner Jr. HN, Zaknun JJ. Fluorine-18 radiopharmaceuticals beyond [^{18}F]FDG for use in oncology and neurosciences. Nucl Med Biol 2010; 37: 727-740.

[18] Nabi HA, Zubeldia JM. Clinical applications of ^{18}F-FDG in oncology. J Nucl Med Technol 2002; 30: 3-9.

[19] Roesch F, Riss PJ. The renaissance of the ^{68}Ge/^{68}Ga radionuclide generator initiates new developments in ^{68}Ga radiopharmaceutical chemistry. Curr Top Med Chem 2010; 10: 1633-1668.

[20] Qaim SM. Therapeutic radionuclides and nuclear data. Radiochim Acta 2001; 89: 297-302.

[21] Volkert WA, Goeckeler WF, Ehrhardt GJ, Ketring AR. Therapeutic radionuclides: Production and decay properties considerations. J Nucl Med 1991; 32: 174-185.

[22] Wessels BW, Rogus RD. Radionuclide selection and model absorbed dose calculations for radiolabeled tumor associated antibodies. Med Phys 1984; 11: 638-645.

[23] Adelstein SJ, Manning FJ (editors) Isotopes for Medicine and the Life Sciences. National Academies Press, Washington D.C.; 1995.

[24] Lambrecht RM. Radionuclide generators. Radiochim Acta 1983; 34: 9-24.

[25] Knapp Jr FF, Mirzadeh S. The continuing important role of radionuclide generator systems for nuclear medicine. Eur J Nucl Med 1994; 21: 1151-1165.

[26] Mirzadeh S, Knapp Jr FF. Biomedical radioisotope generator systems. J Radioanal Nucl Chem 1996; 203: 471-488.

[27] Vaalburg W, Van Herk G, Paans AMJ, Woldring MG. Cyclotron production of radioisotopes for use in nuclear medicine. J Radioanal Nucl Chem 1977; 35: 31-35.

[28] Saha GB. Production of radionuclides. In: Fundamentals of Nuclear Pharmacy. 3rd Edition, Springer-Verlag, New York; 2000, p 46-64.

[29] Pinajian JJ. ORNL 86-in. cyclotron. In: Andrews GA, editor. Radioactive pharmaceuticals. U.S. A.E.C. Symposium Series, Oak-Ridge, Tennessee, USA; 1965, p 143-154.

[30] Friedlander G, Kennedy JW, Macias ES, Miller JM. Nuclear Reaction. In: Nuclear and Radiochemistry. 3rd edition, John Wiley and Sons, New York; 1981, p 110-190.

[31] Baker PS. Reactor produced radionuclides. In: Andrews GA, editor. Radioactive pharmaceuticals. U.S. A.E.C. Symposium Series, Oak-Ridge, Tennessee, USA; 1965, p 129-142.

[32] Mushtaq A. Reactors are indispensible for radioisotope production. Ann Nucl Med 2010; 24: 759-760.

[33] Richards P. Radionuclide generators. In: Andrews GA, editor. Radioactive pharmaceuticals. U.S. A.E.C. Symposium Series, Oak-Ridge, Tennessee, USA; 1965, p 155-163.

[34] Padmanabhan S, Ramamoorthy N. Technetium-99m generators: Principles and features. In: Ramamoorthy N, Shivarudrappa V, Bhelose AA, editors.

Radiopharmaceuticals and hospital radiopharmacy practices. Department of Atomic Energy, Government of India, Mumbai, India; 2000, p 1-10.

[35] Knapp Jr FF, Butler TA (editors). Radionuclide generators: New systems for nuclear medicine applications. ACS Symposium Series, American Chemical Society, USA; 1984.

[36] Rosch F, Knapp Jr FF. Radionuclide generators. In: Vertes A, Nagy S, Klenscar Z, editors. Radiochemistry and radiopharmaceutical chemistry in life sciences: Handbook of Nuclear Chemistry. Kluwer Academic Publisher, Dordrecht, The Netherlands; 2003, p 81-118.

[37] Failla G.: US Patents 1-553-794 and 1-609-614 (1920).

[38] Winsche WE, Stang Jr LG, Tucker WD. Production of Iodine-132. Nucleonics 1951; 8: 14-18.

[39] Friedlander G, Kennedy JW, Macias ES, Miller JM. Equations of radioactive decay and growth. In: Nuclear and Radiochemistry. 3rd edition, John Wiley and Sons, New York; 1981, p 191-205.

[40] Boyd RE. Technetium-99m generators-The available options. Int J Appl Radiat Isot 1982; 33: 801-809.

[41] Boyd RE. Molybdenum-99: Technetium-99m generator. Radiochim Acta 1982; 30: 123-145.

[42] Molinsky VJ. A review of ^{99m}Tc generator technology. Int J Appl Radiat Isot 1982; 33: 811-819.

[43] Boyd RE. Technetium generators: Status and prospects. Radiochim Acta 1987; 41: 59-63.

[44] Boyd RE. The gel generator: a viable alternative source of ^{99m}Tc for nuclear medicine. Appl Radiat Isot 1997; 48: 1027-1033.

[45] Mushtaq A. Inorganic ion-exchangers: Their role in chromatographic radionuclide generators for the decade 1993-2002. J Radioanal Nucl Chem 2004; 262: 797-810.

[46] Samuelson O. Ion exchange separations in analytical chemistry. John Wiley and Sons Inc., New York; 1963.

[47] Taskaev E, Taskaeva M, Nikolov P. Extraction generator for [^{99m}Tc]sodium pertechnetate production. Appl Radiat Isot 1995; 46: 13-16.

[48] Svoboda K. Survey of solvent extraction ^{99m}Tc-generator technologies. Radiochim Acta 1987; 41: 83-89.

[49] Morrison GH, Freiser H. Solvent extraction in analytical chemistry. John Wiley and Sons, Inc., New York; 1962.

[50] Zsinka L. ^{99m}Tc sublimation generators. Radiochim Acta 1987; 41: 91-96.

[51] Evans JV, Moore PW, Shying ME, Sodeau JM. Zirconium molybdate gel as a generator for technetium-99m - I. The concept and its evaluation. Appl Radiat Isot 1987; 38: 19-23.

[52] Moore PW, Shying ME, Sodeau JM, Evans JV, Maddalena DJ, Farrington, KH. Zirconium molybdate gel as a generator for technetium-99m - II. High activity generators. Appl Radiat Isot 1987; 38**:** 25-29.

[53] Dadachov MS, So LV, Lambrecht RM, Dadachova E. Development of titanium tungstate-based ^{188}W/^{188}Re gel generator using tungsten of natural isotope abundance. Appl Radiat Isot 2002; 57: 641-646.

[54] Monroy-Guzman F, Romero OC, Velazquez HD. Titanium molybdate gels as matrix of ^{99}Mo/^{99m}Tc generators. J Nucl Radiochem Sci 2007; 8: 11-19.

[55] Monroy-Guzman F, Diaz-Archundia LV, Ramirez AC. Effect of the Zr : Mo ratio on ^{99m}Tc generator performance based on zirconium molybdate gels. Appl Radiat Isot 2003; 59: 27-34.

[56] Saha GB. Quality control of radiopharmaceuticals. In: Fundamentals of nuclear pharmacy. 3rd Edition, Springer-Verlag, New York; 2000, p 143-167.

[57] Pandey U, Dhami PS, Jagesia P, Venkatesh M, Pillai MRA. A novel extraction paper chromatography (EPC) technique for the radionuclidic purity evaluation of ^{90}Y for clinical use. Anal Chem 2008; 80: 801-807.

[58] Bonardi ML, Martano L, Groppi F, Chinol M. Rapid determination of ^{90}Sr impurities in freshly ‘‘generator eluted’’ ^{90}Y for radiopharmaceutical preparation. Appl Radiat Isot 2009; 67: 1874–1877.

[59] Skraba WJ, Arino H, Kramer HH. A new ^{90}Sr/^{90}Y radioisotope generator. Int J Appl Radiat Isot 1978; 29: 91-96.

[60] Lingane JJ. Controlled potential separation of metals prior to other determinative methods. In: Electroanalytical Chemistry. 2nd Edition. Interscience Publishers, Inc., New York; 1966, p 416-433.

[61] Pradeep T. Nano: The essentials Understanding Nanoscience and Nanotechnology. 1st edition. Tata McGraw Hill Publishing Company Limited, New Delhi, India; 2008.

[62] Poole Jr CP, Owens FJ. Introduction to Nanotechnology. 1st Edition. Wiley India Pvt. Ltd., New Delhi, India; 2007.

[63] Feynman RP. There's plenty of room at the bottom. In: Gilbert HD, editor. Miniaturization**.** Reinhold Publishing Corporation, New York; 1961, p 282-296.

[64] Andrievski RA. Modern Nanoparticle Research in Russia. J Nanopart Res 2003; 5: 415-418.

[65] Cao G. Nanostructures & Nanomaterials: Synthesis, Properties & Applications. 1st Edition. Imperial College Press, London, UK; 2004.

[66] Herring C, Galt JK. Elastic and plastic properties of very small metal specimens**.** Phys Rev 1952; 85: 1060–1061.

[67] Rose M, Balogh AG, Hahn H. Instability of irradiation induced defects in nanostructured materials. Nucl Instrum Methods Phys Res Sect B 1997; 119: 127-128.

[68] Bai XM, Voter AF, Hoagland RG, Nastasi M, Uberuaga BP. Efficient annealing of radiation damage near grain boundaries via interstitial emission. Science 2010; 327: 1631-1634.

[69] Cumbal L, Greenleaf J, Leun D, Sengupta AK. Polymer supported inorganic nanoparticles: characterization and environmental applications. React Funct Polym 2003; 54: 167–180.

[70] Okuyama K, Lenggoro IW. Preparation of nanoparticles via spray route. Chem Eng Sci 2003; 8: 537–547.

[71] Rao CNR, Vivekchand SR, Biswas K, Govindaraj A. Synthesis of inorganic nanomaterials. Dalton Trans 2007; 3728–3749

[72] Rao CNR, Thomas PJ, Kulkarni GU. Nanocrystals: Synthesis, properties and applications. Springer series on material science, Volume 95, Hong Kong; 2007.

[73] Rao CNR, Muller A, Cheetham AK (editors) The chemistry of nanomaterials: Synthesis, properties and applications. 1st Edition. Wiley-VCH Verlag, Weinheim, Germany; 2004.

[74] Rao CNR, Muller A, Cheetham AK (editors) Nanomaterials Chemistry: Recent developments and new directions. 1st Edition. Wiley-VCH-Verlag, Weinheim, Germany; 2007.

[75] LaMer VK, Dinegar RH. Theory, production and mechanism of formation of monodispersed hydrosols. J Am Chem Soc 1950; 72: 4847-4848.

[76] Leofanti G, Padovan M, Tozzola G, Venturelli B. Surface area and pore structure of catalysts. Catal Today 1998; 41: 207-219.

[77] Banwell CN, McCash EM. Infrared Spectroscopy. In: Fundamentals of Molecular Spectroscopy. 4th Edition. Tata McGraw-Hill Publishing Company Ltd., New Delhi, India; 2006, p 55-99.

[78] West AR. X-Ray Diffraction. In: Solid State Chemistry and its Applications. 1st Edition. John Wiley and Sons, Singapore; 2005, p 115-186.

[79] Necula BS, Apachitei I, Fratila- Apachitei LE, Teodosiu C, Duszcyk J. Stability of nano/microsized particles in deionized water and electroless nickel solutions. J Colloid Inferf Sci 2007; 314: 514-522.

[80] Berg JM, Romoser A, Banerjee N, Zebda R, Sayes CM. The relationship between pH and zeta potential of ~30 nm metal oxide nanoparticle suspensions relevant to in vitro toxicological evaluations. Nanotoxicology 2009; 3: 276–283.

[81] Xu R. Progress in nanoparticles characterization: Sizing and zeta potential measurement. Particuology 2008; 6: 112-115.

[82] Marquis BJ, Love SA, Braun KL, Haynes CL. Analytical methods to assess nanoparticle toxicity. Analyst 2009; 134: 425-439.

[83] Li Y, Nam CT, Ooi CP. Iron(III) and manganese(II) substituted hydroxyapatite nanoparticles: Characterization and cytotoxicity analysis. J Phys: Conf Ser 2009; 187: 1-8.

[84] Wu L, Qiu L, Shi C, Zhu J. A nanoparticle-based solution DNA sandwich assay using ICP-AES for readout. Biomacromolecules 2007; 8: 2795–2800.

[85] Fischer HC, Fournier-Bidoz S, Chan WCW, Pang KS. Quantitative detection of engineered nanoparticles in tissues and organs: An investigation of efficacy and linear dynamic ranges using ICP-AES. Nanobiotechnology 2007; 3: 46-54.

[86] Asilturk M, Sayılkan F, Erdemoglu S, Akarsu M, Sayılkan H, Erdemoğlu M, Arpac E. Characterization of the hydrothermally synthesized nano-TiO_2 crystallite and the photocatalytic degradation of Rhodamine B. J Hazard Mater 2006; 129: 164-170.

[87] Zhang H, Liu Y, Zhu K, Siu G, Xiong Y, Xiong C. Infrared spectra of nanometer granular zirconia. J Phys: Condens Matter 1999; 11: 2035-2042.

[88] Yin SF, Xu BQ. On the preparation of high-surface-area nano-zirconia by reflux-digestion of hydrous zirconia gel in basic solution. Chemphyschem 2003; 3: 277-281.

[89] Chuah GK, Jaenicke S, Cheong SA, Chan KS. The influence of preparation conditions on the surface area of zirconia. Appl Catal A: Gen. 1996; 145: 267-284.

[90] Guo GY, Chen YL. A nearly pure monoclinic nanocrystalline zirconia. J Solid State Chem 2005; 178: 1675-1682.

[91] Sebesta FJ. Composite sorbents of inorganic ion-exchangers and polyacrylonitrile binding matrix I. Methods of modification of properties of inorganic ion-exchangers for application in column packed beds. J Radioanal Nucl Chem 1997; 220: 77-88.

[92] Nilchi A, Khanchi A, Atashi H, Bagheri A, Nematollahi L. The application and properties of composite sorbents of inorganic ion exchangers and polyacrylonitrile binding matrix. J Hazard Mater 2006; A137: 1271-1276.

[93] Nilchi A, Atashi H, Javid AH, Saberi R. Preparations of PAN-based adsorbers for separation of cesium and cobalt from radioactive wastes. Appl Radiat Isot 2007; 65: 482-487.

[94] Xue TJ, McKinney A, Wilkie CA. The thermal degradation of polyacrylonitrile. Polym Degrad Stab 1997; 58: 193-202.

[95] Kim H, Lee C, Shul Y, Moon J, Lee E. Evaluation of PAN–TiO_2 composite adsorbent for removal of Pb(II) ion in aqueous solution. Sep Sci Technol 2003; 38: 695-713.

[96] Liang CY, Krimm S. Infrared spectra of high polymers VII. Polyacrylonitrile. J Polym Sci 1958; 31: 513-522.

[97] Takahashi H, Shimazu H, HirataY, Sameshima S. Interaction between ultrafine ceria particles and glycine. J Ceram Process Res 2004; 5: 25-29.

[98] Dong X, Hong G, Yu D, Yu D. Synthesis and properties of cerium oxide nanometer powders by pyrolysis of amorphous citrate. J Mater Sci Technol 1997; 13:113-116.

[99] Bremer KH, Aktiengesellschaft H. Large scale production and distribution of Tc-99m generators for medical use. Radiochim Acta 1987; 41: 73-81.

[100] Cecchin D, Zucchetta P, Faggin P, Bolla E, Bui F. ^{99}Mo/^{99m}Tc generator shortage. J Nucl Med 2010; 51: 14N-15N.

[101] Gould P. Medical isotope shortage reaches crisis level. Nature 2009; 460: 312-313.

[102] Perkins AC, Vivian G. Molybdenum supplies and nuclear medicine services. Nucl Med Commun 2009; 30: 657-659.

[103] Webster P. North America's medical isotope crisis. Lancet 2009; 374: 103.

[104] Ballinger JR. ^{99}Mo shortage in nuclear medicine: crisis or challenge? J Label Compds Radiopharm 2010; 53: 167-168.

[105] Pillai MRA, Knapp Jr FF. Overcoming the ^{99m}Tc shortage: Are options being overlooked? J Nucl Med 2011; 52: 15N-28N.

[106] Gould P. Medical isotopes: time to secure supplies? Lancet Oncol 2008; 9: 1027.

[107] Homogeneous Aqueous Solution Nuclear Reactors for the Production of ^{99}Mo and other Short Lived Radioisotopes. IAEA-TECDOC-1601, IAEA, Vienna, 2008.

[108] Ruth T. Accelerating production of medical isotopes. Nature 2009; 457: 536–537.

[109] Ali SA, Ache HJ. Production techniques of fission molybdenum-99. Radiochim Acta 1987; 41: 65-72.

[110] Walt TNV, Coetzee PP. The isolation of ^{99}Mo from fission material for use in the ^{99}Mo/^{99m}Tc generator for medical use. Radiochim Acta 2004; 92: 251-257.

[111] Baker RJ. A system for the routine production of concentrated technetium-99m by solvent-extraction of molybdenum-99. Int J Appl Radiat Isot 1971; 22: 483-485.

[112] Arino H, Kramer HH. Fission product ^{99m}Tc generator. Int J Appl Radiat Isot 1975; 26: 301-303.

[113] Chattopadhyay S, Das SS, Barua L. A simple and rapid technique for recovery of ^{99m}Tc from low specific activity (n,γ)^{99}Mo based on solvent extraction and column chromatography. Appl Radiat Isot 2010; 68: 1-4.

[114] Chattopadhyay S, Das SS, Barua L. A simple and rapid technique for recovery of ^{99m}Tc from low specific activity (n,γ)^{99}Mo based on solid–liquid extraction and column chromatography methodologies. Nucl Med Biol 2010; 37: 17-20.

[115] Chattopadhyay S, Das SS, Barua L, Goomer NC. Recovery of ^{99m}Tc from $Na_2[^{99}Mo]MoO_4$ solution obtained from reactor-produced (n,γ)^{99}Mo using a tiny Dowex-1 column in tandem with a small alumina column. Appl Radiat Isot 2008; 66: 1814-1817.

[116] Blower PJ. Extending the life of a Tc-99m generator: a simple and convenient method for concentrating generator eluate for clinical use. Nucl Med Commun 1993; 14: 995–997.

[117] Guhlke S, Beets AL, Oetjin K. Convenient concentration of rhenium-188 and technetium-99m eluates from tungsten-188/rhenium-188 or (n,γ)-produced molybdenum-99/technetium-99m generators to high specific volumes. J Label Compd Radiopharm 1998; 40: 294–297.

[118] Gomez JS, Correa FG. ^{99m}Tc generator with hydrated MnO_2 as adsorbent of ^{99}Mo. J Radioanal Nucl Chem 2002; 254: 625-628.

[119] Mushtaq A, Mansoor MS, Karim HM, Khan MA. Hydrated titanium dioxide as an adsorbent for ^{99}Mo-^{99m}Tc generator. J Radioanal Nucl Chem 1991; 147: 257-261.

[120] Masakazu T, Katsuyoshi T, Koji I, Kiyoyuki K, Mizuka N, Yoshi, H. A ^{99m}Tc generator using a new inorganic polymer adsorbent for (n,γ) ^{99}Mo. Appl Radiat Isot 1997; 48: 607-611.

[121] Hasegawa K, Shirokawa Y, Aoshimia A, Sano Y. Electrochemical separation of actinides and lanthanides in the aqueous solution. J Nucl Sci Technol 2002; S3: 343-346.

[122] Khan J, Tripathi BP, Saxena A, Shahi VK. Electrochemical membrane reactor: In situ separation and recovery of chromic acid and metal ions. Electrochim Acta 2007; 52: 6719-6727.

[123] Economou A, Clark AK, Fielden PR. Determination of Co(II) by chemiluminescence after in situ electrochemical pre-separation on a flow-through mercury film electrode. The Analyst 2001; 126:109-113.

[124] Rosíkova K, John J, Sebesta F. Separation of radionuclides from chemical and electrochemical decontamination wastes. J Radioanal Nucl Chem 2003; 255: 397-402.

[125] Eichler B, Kratz JV. Electrochemical deposition of carrier-free radionuclides. Radiochim Acta 2000; 88: 475-482.

[126] Reischl G, Roesch F, Machulla HJ. Electrochemical separation and purification of yttrium-86. Radiochim Acta 2002; 90: 225-228.

[127] Yoo J, Tang L, Perkins TA, Rowland DJ, Laforest R, Lewis JS, Welsch MJ, Preparation of high specific activity ^{86}Y using a small biomedical cyclotron. Nucl Med Biol 2005; 32: 891-897.

[128] George H. Method of removal of technetium from radio-contaminated metal. US Patent No. 5458745 (1995).

[129] Masson M, Lecomte M, Masslennikov A, Peretroukhine V. Method of separating technetium from a nitric acid solution. US Patent No. 6179981 (2001).

[130] Boyd GE, Larson QV, Motta EE. Isolation of milligram quantities of long-lived technetium from neutron irradiated molybdenum**.** J Am Chem Soc 1960; 82: 809-815.

[131] Khomutov NE.: Table of molal standard electrode potentials and their temperature coefficients in aqueous solutions at 25 ºC. In: Khomutov NE, editor. Electrochemistry: Electrodeposition of metals and alloys. Achievements in Science: Chemistry Series. Referativnyi Zhurnal Khimiya, Moscow; 1969, p. 2-27.

[132] Mickhailov NJ, Melnikova MM, Lukashina ND. Electrodeposition of rare earth metals and alloys. In: Khomutov NE, editor. Electrochemistry: Electrodeposition of metals and alloys. Achievements in Science: Chemistry Series. Referativnyi Zhurnal Khimiya, Moscow; 1969, p. 175.

[133] Vajo JJ, Aikens DA, Ashley L, Poeltl DE, Bailey RA, Clark HM, Bunce SC. Facile electroreduction of perrhenate in weakly acidic citrate and oxalate media. Inorg Chem 1981; 20: 3328-3333.

[134] Engelmann MD, Metz LA, Delmore JE, Engelhard M, Ballou NE. Electrodeposition of technetium on platinum for thermal ionization mass spectrometry (TIMS). J Radioanal Nucl Chem 2008; 276:493-498.

[135] British Pharmacopoeia Commission, British Pharmacopoeia, 2008, The Stationery Office, Norwich, U.K. (www.pharmacopoeia.org.uk)

[136] Richards P, O'Brien MJ. Rapid determination of ^{99}Mo in separated ^{99m}Tc. J Nucl Med 1969; 10: 517.

[137] Sarkar S, Cara PW, Mcneff CV, Subramanian A. Characterization and optimization of a chromatographic process based on ethylenediamine-N,N,N',N'-tetra

(methylphosphonic) acid-modified zirconia particles. J Chromatogr B 2003; 790: 143-152.

[138] Ragai J, Selim ST. Ion exchange and surface properties of titania gels from Ti-III solutions. J Colloid Interface Sci 1987; 115: 139-146.

[139] Parks GA. Aqueous surface chemistry of oxides and complex oxide minerals. Adv Chem Ser 1967; 67: 121–160

[140] Spanos N, Lycourghiotis A. Molybdenum-oxo species deposited on alumina by adsorption: III. Advances in the mechanism of Mo(VI) deposition. J Catal 1994; 147: 57-71.

[141] Steigman J. Chemistry of the alumina column. Int J Appl Radiat Isot 1982; 33: 829-834.

[142] Fani M, Andre JP, Maecke HR. ^{68}Ga-PET: A powerful generator-based alternative to cyclotron-based PET radiopharmaceuticals. Contrast Media Mol Imaging 2008; 3: 53-63.

[143] Breeman WAP, Verbruggen AM. The ^{68}Ge/^{68}Ga generator has high potential, but when can we use ^{68}Ga-labelled tracers in clinical routine? Eur J Nucl Med Mol Imaging 2007; 34: 978–981.

[144] Pagou M, Zerizer I, Al-Nahhas A. Can gallium-68 compounds partly replace ^{18}F-FDG in PET molecular imaging? Hellenic J Nucl Med 2009; 12: 102-105.

[145] Ambrosini V, Campana D, Tomassetti P, Grassetto G, Rubello D, Fanti S. PET/CT with 68Gallium-DOTA-peptides in NET: An overview. Eur J Radiol 2011 *(In press).*

[146] Fellner M, Baum RP, Kubícek V, Hermann P, Lukes I, Prasad V, Rosch F. PET/CT imaging of osteoblastic bone metastases with ^{68}Ga bisphosphonates: First human study. Eur J Nucl Med Mol Imaging 2010; 37: 834.

[147] Shetty D, Lee YS, Jeong JM. ^{68}Ga-labeled radiopharmaceuticals for positron emission tomography. Nucl Med Mol Imaging 2010; 44: 233-240.

[148] Banerjee SR, Pullambhatla M, Byun Y, Nimmagadda S, Green G, Fox JJ, Horti A, Pomper MG. ^{68}Ga-labeled inhibitors of prostate-specific membrane antigen (PSMA) for imaging prostate cancer. J Med Chem 2010; 53: 5333-5341.

[149] Kratochwil C, Giesel FL, Lopez-Benítez R, Schimpfky N, Kunze K, Eisenhut M, Kauczor HU, Haberkorn U. Intra individual comparison of selective arterial versus venous ^{68}Ga-DOTATOC PET/CT in patients with gastroenteropancreatic neuroendocrine tumors. Clin Cancer Res 2010; 16: 2899-2905.

[150] Ferreira CL, Lamsa E, Woods M, Duan Y, Fernando P, Bensimon C, Kordos M, Kiefer GE. Evaluation of bifunctional chelates for the development of gallium-based radiopharmaceuticals. Bioconjugate Chem 2010; 21: 531-536.

[151] Rominger A, Saam T, Vogl E, Übleis C, Fougère CL, Förster S, Haug A, Hacker M. In vivo imaging of macrophage activity in the coronary arteries using ^{68}Ga-DOTATATE PET/CT: Correlation with coronary calcium burden and risk factors. J Nucl Med 2010; 51: 193-197.

[152] Gabriel M, Decristoforo C, Kendler D, Dobrozemsky G, Heute D, Uprimny C. ^{68}Ga-DOTA-Tyr3-octreotide PET in neuroendocrine tumors: comparison with somatostatin receptor scintigraphy and CT. J Nucl Med 2007; 48: 508–518.

[153] Kowalski J, Henze M, Schuhmacher J, Macke HR, Hoffmann M, Haberkom U. Evaluation of positron emission tomography imaging using [^{68}Ga]-DOTA-D- Phe1-Tyr3-octreotide in comparison to [^{111}In]-DTPA-OC SPECT. First results in patients with neuroendocrine tumours. Mol Imaging Biol 2003; 5: 42–48.

[154] Rosch F, Knapp FF. Radionuclide generators. In: Vertes A, Nagy S, Klencsar Z, Rosch F, editors. Handbook of Nuclear Chemistry, Kluwer Academic Publishers; Dordrecht, The Netherlands; 2003, p. 81-118

[155] Cheng W, Jao Y, Lee C, Lo A. Preparation of a ^{68}Ge/^{68}Ga generator with a binary Ga/Ag electrodepositions as solid target. J Radioanal Nucl Chem 2000; 245: 25-30.

[156] Loc'h C, Maziere B, Comar D, Knipper R. A new preparation of germanium-68. Int J Appl Radiat Isot 1982; 33: 267-270.

[157] Porile NT, Tanaka S, Amano H, Furukawa M, Iwata S, Yagi M. Nuclear reactions of ^{69}Ga and ^{71}Ga with 13-56 MeV protons. Nucl Phys 1963; 43: 500-522.

[158] Mirzadeh S, Lambrecht RM. Radiochemistry of germanium. J Radioanal Nucl Chem 1996; 202: 7-102.

[159] Horiguchi T, Kunahora H, Inoue H, Yoshizawa Y. Excitation functions of Ge(p,xnyp) reactions and production of ^{68}Ge. Int J Appl Radiat Isot 1983; 34: 1531-1535.

[160] Karpeles VA. Herstellug eines ^{68}Ga-generator. Radiochim Acta 1969; 12: 22.

[161] Nagame Y, Unno M, Nakahara H, Murakami Y. Production of ^{67}Ga by alpha bombardment of natural zinc. Int J Appl Radiat Isot 1978; 29: 615-619.

[162] Nagame Y, Nakahara H, Furukawa M. Excitation function for α and ^{3}He particles induced reactions on zinc. Radiochim Acta 1989; 46: 5-8.

[163] Goldsmith SJ. Update on nuclear medicine imaging of neuroendocrine tumors. Future Oncology 2009; 5: 75-84.

[164] Smyth D, Al-Ejeh F, Tsopelas C, Brown M, Chatterton B. Molecular imaging with gallium-68 labelled biomolecules. ANZ Nucl Med 2009; 40: 1.

[165] Ocak M, Antretter M, Knopp R, Kunkel F, Petrik M, Bergisadi N. Full automation of ^{68}Ga labelling of DOTA-peptides including cation exchange pre purification. Appl Radiat Isot 2010; 68: 297-302.

[166] Asti M, De Pietri G, Fraternali A, Grassi E, Sghedoni R, Fioroni F. Validation of $^{68}Ge/^{68}Ga$ generator processing by chemical purification for routine clinical application of ^{68}Ga-DOTATOC. Nucl Med Biol 2008; 35: 721-724.

[167] Zhernosekov KP, Filosofov DV, Baum RP, Aschoff P, Bihl H, Razbash AA. Processing of generator-produced ^{68}Ga for medical application. J Nucl Med. 2007; 48: 1741-1748.

[168] Bartholoma MD, Louie AS, Valliant JF, Zubieta J. Technetium and gallium derived radiopharmaceuticals: Comparing and contrasting the chemistry of two important radiometals for the molecular imaging era. Chem Rev 2010; 110: 2903-2920.

[169] Aardaneh K, Van Der Walt TN. Ga_2O for target, solvent extraction for radiochemical separation and SnO_2 for the preparation of a $^{68}Ge/^{68}Ga$ generator. J Radioanal Nucl Chem 2006; 268: 25-32.

[170] McElvany KD, Hopkins KT, Welch MJ. Comparison of $^{68}Ge/^{68}Ga$ generator systems for radiopharmaceutical production. Int J Appl Radiat Isot 1984; 35: 521-524.

[171] Ehrhardt GJ, Welch MJ. A new Germanium-68/Gallium-68 generator. J Nucl Med 1978; 19: 925-929.

[172] Arino H, Skraba WJ, Kramer HH. A new $^{68}Ge/^{68}Ga$ radioisotope generator system. Int J Appl Radiat Isot 1978; 29: 117-120.

[173] Schuhmacher J, Maier-Borst W. A new $^{68}Ge/^{68}Ga$ radioisotope generator system for production of ^{68}Ga in dilute HCl. Int J Appl Radiat Isot 1981; 32: 31-36.

[174] Ambe S. Germanium-68-gallium-68 generator with alpha-ferric oxide support. Appl Radiat Isot 1988; 39: 49-51.

[175] Malyshev KV, Smirnov VV. Gallium-68 yield from hydrated zirconium oxide-based generators. Sov Radiochim 1975; 17: 137-140.

[176] Aardaneh K, van der Walt TN. Ga_2O for target, solvent extraction for radiochemical separation and SnO_2 for the preparation of a $^{68}Ge/^{68}Ga$ generator. J Radioanal Nucl Chem 2006; 268: 25-32.

[177] Bao B, Song M. A new $^{68}Ge/^{68}Ga$ generator based on CeO_2. J Radioanal Nucl Chem 1996; 213: 233-238.

[178] Egamediev SK, Khujaev S, Mamatkazina AK. Influence of the preliminary treatment of aluminium oxide on the ^{68}Ge-^{68}Ga radionuclide chain. J Radioanal Nucl Chem 2000; 246: 593-596.

[179] Benhong C, Zongquan L, Yongxian W. ^{68}Ge-^{68}Ga generator with alpha-ferric oxide support in trigonal structure. J Radioanal Nucl Chem 1998; 238: 175-177.

[180] Neirinckx RD, Davis MA. Potential column chromatography for ionic Ga-68. II: Organic ion exchangers as chromatographic supports. J Nucl Med 1980; 21: 81-83.

[181] Nakayama M, Haratake M, Koiso T, Ishibashi O, Harada K, Nakayama H, Sugii A, Yahara S, Arano Y. Separation of ^{68}Ga from ^{68}Ge using a macroporous organic polymer containing *N*-methylglucamine groups. Anal Chim Acta 2002; 453: 135–141.

[182] Nakayama M, Haratake M, Ono M, Koiso T, Harada K, Nakayama H, Yahara S, Ohmomo Y, Arano Y. A new $^{68}Ge/^{68}Ga$ generator system using an organic polymer containing N-methylglucamine groups as adsorbent for ^{68}Ge. Appl Radiat Isot 2003; 58: 9-14.

[183] de Blois E, Chan HS, Naidoo C, Sedres D, Krenning EP, Breeman WAP. Characteristics of SnO_2-based $^{68}Ge/^{68}Ga$ generator and aspects of radiolabelling DOTA-peptides. Appl Radiat Isot 2011; 69: 308-315.

[184] Velikyan I, Beye GJ, Langström B. Microwave-supported preparation of ^{68}Ga bioconjugates with high specific radioactivity. Bioconjugate Chem 2004; 15: 554-560.

[185] Meyer GJ, Maecke H, Schuhmacher J, Knapp WH, Hofmann M. ^{68}Ga-labelled DOTA-derivatised peptide ligands. Eur J Nucl Med Mol Imaging 2004; 31: 1097-1104.

[186] Neirinckx AD, Davis MA. Potential column chromatography generators for ionic Ga-68. I. Inorganic Substrates. J Nucl Med 1979; 20: 1075-1079.

[187] Everest DA, Salmon JE. Studies in the chemistry of quadrivalent germanium: Ion-exchange studies of solutions of germinates. J Chem Soc 1954; 2438–2443.

[188] Bernstein LR. Mechanisms of therapeutic activity for gallium. Pharmacol Rev 1998; 50: 665–682.

[189] Green MA, Welch MJ. Gallium radiopharmaceutical chemistry. Int J Rad Appl Instrum B 1989; 16: 435–448.

[190] Vega I, Morris W, D'Accorso N. PAN chemical modification: Synthesis and characterization of terpolymers with 1,2,4-oxadiazolic pendant groups. React Funct Polym 2006; 66: 1609-1618.

[191] Goldenberg DM. The role of radiolabeled antibodies in the treatment of non-Hodgkin's lymphoma: the coming of the age of radioimmunotherapy. Crit Rev Oncol Hematol 2001; 39:195–201.

[192] Grillo-Lopez AJ. Zevalin: the first radioimmunotherapy approved for the treatment of lymphoma. Expert Rev Anticancer Ther 2002; 2: 485–93.

[193] Davies AJ. Radioimmunotherapy for B-cell lymphoma: Y-90 ibritumomab tiuxetan and I-131 tositumomab. Oncogene 2007; 26: 3614–3628.

[194] Witzig TE, Molina A, Gordon LI, Emmanouilides C, Schilder RJ, Flinn IW, Darif M, Macklis R, Vo K, Wiseman GA. Long-term responses in patients with recurring or refractory B-cell non-Hodgkin lymphoma treated with yttrium 90 ibritumomab tiuxetan. Cancer 2007; 109: 1804–1810.

[195] Paganelli G, Bartolomei M, Grana C, Ferrari M, Rocca P, Chinol M. Radioimmunotherapy of brain tumour. Neurol Res 2006; 28: 518–522.

[196] Ferrari M, Cremonesi M, Bartolomei M, Bodei L, Chinol M, Fiorenza M, Tosi G, Pagneli G. Dosimetric model for locoregional treatment of brain tumours with ^{90}Y conjugates: clinical applications with ^{90}Y-DOTATOC. J Nucl Med 2006; 47: 105–112.

[197] Breeman WA, Kwekkeboom DJ, de Blois E, de Jong M, Visser TJ, Krenning EP. Radiolabelled regulatory peptides for imaging and therapy. Anticancer Agents Med Chem 2007; 7: 345–347.

[198] Kwekkeboom DJ, Mueller-Brand J, Paganelli G, Anthony LB, Pauwel S, Kvols LK, O'Dorisio TM, Valkema R, Bodei L, Chinol M, Maecke HR, Krenning EP. Overview of results of peptide receptor radionuclide therapy with three radiolabelled somatostatin analogs. J Nucl Med 2005; 46: 62S–66S.

[199] Gulec SA, Mesoloras G, Dezarn WA, McNeillie P, Kennedy AS. Safety and efficacy of Y-90 microsphere treatment in patients with primary and metastatic liver cancer: the tumor selectivity of the treatment as a function of tumor to liver flow ratio. J Transl Med 2007; 5: 15.

[200] Wong CY, Savin M, Sherpa KM, Qing F, Campbell J, Gates VL, Lewandowski RJ, Cheng V, Thie J, Fink-Bennett D, Nagle C, Salem R. Regional yttrium-90 microsphere treatment of surgically unresectable and chemotherapy-refractory metastatic liver carcinoma. Cancer Biother Radiopharm 2006; 21: 305–313.

[201] Ehrhardt GJ, Day DE. Therapeutic use of ^{90}Y microspheres. Nucl Med Biol 1987; 14: 233-242.

[202] Kawashita M, Shineha R, Kim HM, Kokubo T, Inoue Y, Araki N, Nagata Y, Hiroka M, Sawada Y. Preparation of ceramic microspheres for in-situ radiotherapy of deep-seated cancer. Biomaterials 2003; 24: 2955-2963.

[203] Therapeutic Radionuclide Generators: $^{90}Sr/^{90}Y$ and $^{188}W/^{188}Re$ generators. IAEA Technical Report Series No. 470 (2009).

[204] Chinol M, Hnatowich DJ. Generator-produced Yttrium-90 for radioimmunotherapy. J Nucl Med 1987; 28: 1465-1471.

[205] Wester DW, Steele RT, Rinehart DE, Des Chane JR, Carson KJ, Rapko BM, Tenforde TS. Large-scale purification of ^{90}Sr from nuclear waste materials for production of ^{90}Y, a therapeutic medical radioisotope. Appl Radiat Isot 2003; 59: 35–41.

[206] Report of first research coordination of the CRP on "Development of generator technologies for therapeutic radionuclides". IAEA, Vienna; 2005, p. 3-18.

[207] Ramanujam A, Dhami PS, Chitnis RR, Achuthan PV, Kannan R, Gopalakrishnan V, Balu K. Separation of strontium-90 from PUREX high level waste and development of $^{90}Sr/^{90}Y$ generator. BARC report 2000/E/009 (2000).

[208] Maximum permissible body burden and maximum permissible concentrations of radionuclides in air and water for occupational exposure. National Bureau of Standards Handbook. 69, U.S. Department of Commerce, AFP 160-67; 1959, p. 38.

[209] Salutsky ML, Kirby HW. Preparation and half-life of carrier-free yttrium-90. Anal Chem 1955; 27: 567–569.

[210] Wike JS, Guyer CE, Ramey DW, Phillips BP. Chemistry for commercial scale production of yttrium-90 for medical research. Appl Radiat Isot 1990; 41: 861–865.

[211] Lee TW, Ting G. Study on the separation of carrier free Yttrium-90 from Sr-90. Isotopenpraxis 1991; 27: 269–273.

[212] Dietz LM, Horwitz EP. Improved chemistry for production of yttrium-90 for medical applications. Appl Radiat Isot 1992; 43: 1093–1101.

[213] Hsieh BT, Ting G, Hsieh HT, Shen LH. Preparation of carrier-free yttrium-90 for medical applications by solvent extraction chromatography. Appl Radiat Isot 1993; 44: 1473–1480.

[214] Dash A, Bhattacharya PK. Preparation of a ^{90}Sr-^{90}Y generator using zirconium antimonate. Appl Radiat Isot 1994; 45: 415–417.

[215] Castillo AX, Pérez-Malo M, Isaac-Olivé K, Mukhallalati H, González EC, Berdeguez MT, Díaz NC. Production of large quantities of ^{90}Y by ion-exchange chromatography using an organic resin and a chelating agent. Nucl Med Biol 2010; 37: 935-942.

[216] Naik PW, Jagasia P, Dhami PS, Achuthan PV, Tripathi SC, Munshi SK, Dey PK, Venkatesh M. Separation of carrier-free ^{90}Y from ^{90}Sr by SLM technique using D2EHPA in N-dodecane as carrier. Sep Sci Technol 2010; 45: 554-561.

[217] Xiques Castillo A, Isaac Olivé K, Casanova González E, Beckford D, Leyva Montaña R, Montero Álvarez A, Olivé Álvarez E. An adapted purification procedure to improve the quality of ^{90}Y for clinical use. Radiochim Acta 2009; 97: 739-746.

[218] Shapovalov VV, Nerozin NA, Smetanin EY, Mel'Nichenko NA. A semicountercurrent extraction generator of ^{90}Y. Radiochemistry 2009; 51: 507-509.

[219] Lee JS, Park UJ, Son KJ, Han HS. One column operation for ^{90}Sr/^{90}Y separation by using a functionalized-silica. Appl Radiat Isot 2009; 67: 1332-1335.

[220] Dhara S, Sarkar S, Basu S, Chattopadhyay P. Separation of the ^{90}Sr-^{90}Y pair with cerium (IV) iodotungstate cation exchanger. Appl Radiat Isot 2009; 67: 530-534.

[221] Dhami PS, Naik PW, Dudwadkar NL, Kannan R, Achuthan PV, Moorthy AD, Jambunathan U, Pandey U, Venkatesh M. Studies on the development of a two stage

SLM system for the separation of carrier-free ^{90}Y using KSM-17 and CMPO as carriers. Sep Sci Technol 2007; 42: 1107-1121.

[222] Bray LA, Wester DW. Method of separation of yttrium-90 from strontium-90, US Patent 5, 512, 256 (1996).

[223] Bray LA. Method for separating and purifying Yttrium-90 from Strontium-90. WO/2006/025975. World Intellectual Property Organization, 2006.

[224] Horwitz EP, Hines JJ. A method for isolating and purifying ^{90}Y from ^{90}Sr in multi-curie quantities. WO 01/80251. World Intellectual Property Organization, 2001.

[225] Betenekov ND, Sharygin LM, Brown RW. Sr-90/Y-90 radionuclide generator for production of high quality Y-90 solution. WO/2006/046966. World Intellectual Property Organization, 2006.

[226] The world market for therapeutic radiopharmaceuticals. Biotech Report No. 230. http://www.biotechsystems.com/reports/230/default.asp.

[227] Lange G, Herrmann G, Strassmann F. Preparation of strontium-90 free yttrium-90 by electrolysis. J Inorg Nucl Chem 1957; 4: 146–154.

[228] Hamaguchi H, Ikeda N, Kawashima T. Isolation of carrier free yttrium from the radioactive strontium-yttrium system by electrochemical deposition. Bunseki Kagaku 1958; 7: 243–246.

[229] Muylder JV. Atlas of electrochemical equilibria in aqueous solutions. In: Pourbaix M, editor. National Association of Corrosion Engineers, Houston, TX; 1974.

[230] Zhitomirsky I, Petric A. Electrochemical deposition of yttrium oxide. J Mat Chem 2000; 10: 1215-1218.

[231] Friedlander G, Kennedy JW, Macias ES, Miller JM. Techniques in nuclear chemistry. In: Nuclear and Radiochemistry. 3rd edition, John Wiley and Sons, New York; 1981, p 287-337.

[232] Avila-Rodriguez MA, Nye JA, Nickles RJ. Production and separation of non-carrier-added ^{86}Y from enriched ^{86}Sr targets. Appl Radiat Isot 2008; 66: 9-13.

[233] Mohite UK, Gadave KM, Lokhande CD. Electrosynthesis of yttrium from non-aqueous bath. Indian J Eng Mater Sci 1995; 2: 93-94.

[234] Matsuda Y, Imahashi K, Yoshimoto N, Morita M. Formation of yttrium oxide by electrodeposition in organic electrolyte. J Alloy Compd 1993; 193: 277-279.

[235] Selwyn RG, Nickles RJ, Thomadsen BR, De Werd LA, Micka JA. A new internal pair production branching ratio of ^{90}Y: the development of a non-destructive assay for ^{90}Y and ^{90}Sr. Appl Radiat Isot 2007; 65: 318–327.

[236] Venkatesh M, Pandey U, Dhami PS, Kannan R, Achuthan PV, Chitnis RR, Gopalakrishnan V, Banerjee S, Samuel G, Pillai MRA, Ramanujam A. Complexation studies with ^{90}Y from a novel ^{90}Sr/^{90}Y generator. Radiochim Acta 2001; 89: 413–417.

[237] Knapp Jr FF. Rhenium-188—a generator-derived radioisotope for cancer therapy. Cancer Biother Radiopharm 1998; 13: 337-349.

[238] Jeong JM, Knapp Jr FF. Use of the Oak Ridge National Laboratory Tungsten-188/Rhenium-188 generator for preparation of the Rhenium-188 HDD/Lipiodol complex for trans-arterial liver cancer therapy. Semin Nucl Med 2008; 38: S19-S29.

[239] Abram U, Alberto R. Technetium and Rhenium - Coordination chemistry and nuclear medical applications. J Braz Chem Soc 2006; 17: 1486-1500.

[240] Savio E, Gaudiano J, Robles AM, Balter H, Paolino A, López A, Hermida JC, De Marco E, Martinez G, Osinaga E, Knapp FF Jr. Rhenium-188 HEDP: pharmacokinetic characterization, clinical and dosimetric evaluation in osseous metastatic patients with two levels of radiopharmaceutical dose. BMC Nucl Med 2001; 1: 2-10.

[241] Blower PJ, Kettle AG, O'Doherty MJ, Coakley AJ, Knapp Jr. FF. ^{99m}Tc(V)-DMSA quantitatively predicts ^{188}Re(V) DMSA distribution in patients with prostate cancer metastatic to bone. Eur J Nucl Med 2000; 9: 1405-1409.

[242] Liepe K, Hlises R, Kropp J, Gruning T, Runge R, Koch R, Knapp Jr. FF, Franke WG. Rhenium-188-HEDP in palliative treatment of bone metastases. Cancer Biother Radiopharm 2000; 15: 261-265.

[243] Palmedo H, Guhlke S, Bender H, Sartor J, Schoeneich G, Grunwald F, Knapp FF, Biersack HJ. Dose escalation study with rhenium-188 hydroxyethylidene diphosphonate in prostate cancer patients with osseous metastases. Eur J Nucl Med 2000; 27: 123-130.

[244] Knapp Jr FF, Spencer R, Kropp J. Intravascular radiation therapy with radioactive filled balloons for inhibition of restonosis after angioplasty: A new opportunity for nuclear medicine. J Nucl Med 2001; 42: 1384-1387.

[245] Weinberger J, Giedd KN, Simon AD, Marboe C, Knapp Jr. FF, Trichter F, Amols H. Radioactive beta-emitting solution filled balloon treatment prevents porcine coronary restonosis. Cardiovasc Rad Med 1999; 1: 252-256.

[246] Tzanopoulou S, Sagnou M, Paravatou-Petsotas M, Gourni E, Loudos G, Xanthopoulos S, Lafkas D, Pelecanou M. Evaluation of Re and ^{99m}Tc complexes of 2-(4′-aminophenyl) benzothiazole as potential breast cancer radiopharmaceuticals. J Med Chem 2010; 53: 4633-4641.

[247] Chen Y, Xiong QF, Yang XQ, He L, Huang ZW. Evaluation of ^{188}Re-DTPA-Deoxyglucose as a potential cancer radiopharmaceutical. Am J Roentgenol 2010; 194: 761-765.

[248] Hafeli UO, Warburton MC, Landau U. Electrodeposition of radioactive rhenium onto stents to prevent restonosis. Biomaterials 1998; 19: 925-933.

[249] Knapp Jr FF, Callahan AP, Beets AL, Mirzadeh S. Processing of reactor-produced ^{188}W for fabrication of clinical scale alumina based $^{188}W/^{188}Re$ Generators. Appl Radiat Isot 1994; 45: 1123-1128.

[250] Guhlke S, Beets AL, Oetjen K, Mirzadeh S, Biersack HJ, Knapp Jr. FF. Simple new method for effective concentration of ^{188}Re solution from an alumina based ^{188}W-^{188}Re generator. J Nucl Med 2000; 41: 1271-1278.

[251] Perego R, Wierczinski B, Zhernosekov K, Henkelmann R, Türler A, Nikula T, Buck O. Development of an improved 130 GBq $^{188}W/^{188}Re$ generator. Eur J Nucl Med Mol Imaging 2007; 34: S210.

[252] Dadachova E, Mirzadeh S, Lambrecht RM. Tungsten ion-alumina interaction in a ^{188}W-^{188}Re biomedical generator. J Phys Chem 1995; 99: 10976-10981.

[253] Kamioki H, Mirzadeh S, Lambrecht RM, Knapp Jr FF, Dadachova K. $^{188}W/^{188}Re$ generator for biomedical applications. Radiochim Acta 1994; 65: 39-46.

[254] Knapp Jr FF, Lisic EC, Mirzadeh S. Tungsten-188/carrier-free rhenium-188 perrhenic acid generator system. US patent 5, 275, 802 (1994).

[255] Coursey BM, Calhoun JM, Cessna JT, Hoppes DD, Schima FJ, Unterweger MP, Golas DB, Callahan AP, Mirzadeh S, Knapp Jr. FF. Assay of the eluent from alumina based Tungsten-188/Rhenium-188 generator. Radioact Radiochem 1990; 4: 38–49.

[256] Callahan AP, Rice DE, Knapp Jr. FF. Rhenium-188 from therapeutic application from an alumina based tungsten-188/rhenium-188 radionuclide generator. A radionuclide generator system based on sorption of ^{188}W sodium or potassium tungstate on alumina gives good yields of ^{188}Re for radiolabeling of therapeutic agents. Nuc Compact 1989; 20: 3-6.

[257] Sarkar SK, Venkatesh M, Ramamoorthy N. Evaluation of two methods of concentrating perrhenate (^{188}Re) eluates from ^{188}W-^{188}Re generator. Appl Radiat Isot 2009; 67: 234-239.

[258] Mansur MS, Mushtaq A, Jehangir M. Concentration of ^{99m}Tc-pertechnate and ^{188}Re-perrrhenate. Radiochim Acta 2006; 94: 107-111.

[259] Jackel B, Cripps R, Guntay S, Bruchertseifer H. Development of semi-automated system for the preparation of ^{188}Re aqueous solutions of high and reproducible activity concentrations. Appl Radiat Isot 2005; 63: 299-304.

[260] Mushtaq A. Concentration of $^{99m}TcO_4^-$/$^{188}ReO_4^-$ by a single, compact, anion exchange cartridge. Nucl Med Commun 2004; 25: 957-962.

[261] Luo TY, Lo AR, Hsieh BT, Lin WJ. A design for automatic preparation of highly concentrated (Re-188)-perrhenate solutions. Appl Radiat Isot 2007; 65: 21-25.

[262] Lewis RE. Production of 70-day Tungsten-188 and development of a 17 hour Rhenium-188 radioisotope generator. J Nucl Med 1966; 7: 804-805.

[263] Hayes RL. Rhenium-188 as a possible diagnostic agent. Oak Ridge Associated Universities. Medical Division Report ORAU 1966; 101: 74-77.

[264] Monroy-Guzman F, Badillo-Almaraz VE, Flores De La Torre JA, Cosgrove J, Knapp FF. Hydroxyapatite-Based Mo-99/Tc-99m and W-188/Re-188 Generator Systems. Proceeding of the International Symposium on Trends in Radiopharmaceuticals, ISTR-2005, IAEA, Vienna, Austria, Vol. 1, p 333–348 (2007).

[265] Knapp FF, Mirzadeh S. Reactor capabilities for production of Tungsten-188 for the Tungsten-188/Rhenium-188 generator system. Oak Ridge National Laboratories, Report ORNL/TM-12222; 1992, p 6-9.

[266] So LV, Nguyen CD, Pellegrini P, Bui VC. Polymeric titanium oxychloride sorbent for ^{188}W/^{188}Re nuclide pair separation. Sep Sci Technol 2009; 44: 1074-1098.

[267] Dadachov M, Lambrecht RM, Hetherington E. An improved tungsten-188/rhenium-188 gel generator based on zirconium tungstate. J Radioanal Nucl Chem 1994; 184: 267-278.

[268] Dadachov M, Lambrecht RM. ^{188}W-^{188}Re gel generators based on metal tungstates. J Radioanal Nucl Chem 1995; 200: 211-221.

[269] Iller E, Polkowska-Motrenko H, Wawszczak D, Konior M, Milczarek J. Synthesis and testing of a gel metal oxide composites as filling materials for ^{188}W-^{188}Re generator column. Annual Report, Radioisotope Centre POLATOM. 4, 102 (2007).

[270] Iller E, Deptula A, Brykala M, Sypula M, Konior M. Preliminary results of synthesis and investigations of new materials for packing of chromatographic columns of W-188/Re-188 generators**.** Eur J Nucl Med Mol I 2007; 34: S210.

[271] Monroy-Guzman F, Almaraz VEB, Gutierrez TR, Cohen LG, Cosgrove J, Knapp Jr. FF, Nava PR, Rosales CJ. Development of inorganic adsorbents as matrices of generators for therapeutic radionuclides. In: Therapeutic Radionuclide Generators: ^{90}Sr/^{90}Y and ^{188}W/^{188}Re Generators. IAEA-TRS-470 (2009).

[272] Matsuoka H, Hasimoto K, Hishinuma Y, Ishikawa K, Terunuma H, Tatenuma K. Application of PZC to ^{188}W/^{188}Re generator. J Nucl Radiochem Sci 2005; 6: 189-191

[273] Iller E, Polkowska-Motrenko H, Lada W, Wawszczak D, Sypula M, Doner K, Konior M, Milczarek J, Zoladek J, Ralis J. Studies of gel metal-oxide composite samples as filling materials for W-188/Re-188 generator column. J Radioanal Nucl Chem 2009; 281: 83–86.

[274] Lee JS, Lee JS, Park UJ, Son KJ, Han HS. Development of a high performance ^{188}W/^{188}Re generator by using a synthetic alumina. Appl Radiat Isot 2009; 67: 1162-1166.

[275] Szabo S, Bakos I. Rhenium deposition onto platinum surface by reduction of perrhenic acid with methanol in hydrochloric acid media. React Kinet Catal Lett 1998; 65: 259-263.

[276] Szabo S, Bakos I. Electro reduction of rhenium from sulphuric acid solutions of perrhenic acid. J Electroanal Chem 2000; 492: 103-111.

[277] Schrebler R, Cury P, Orellana M, Gomez H, Cordova R, Dalchiele EA. Electrochemical and nanoelectrogravimetric studies of the nucleation and growth mechanisms of rhenium on polycrystalline gold electrode. Electrochim Acta 2001; 46: 4309-4318.

[278] Hahn BP, May RA, Stevenson KJ. Electrochemical deposition and characterization of mixed valent rhenium oxide films prepared from a perrhenate solution. Langmuir 2007; 23: 10837-10845.

[279] Kothari K, Pillai MRA, Unni PR, Shimpi HH, Noronha OPD, Samuel AM. Preparation of [^{186}Re]Re-DMSA and its biodistribution studies. Appl Radiat Isot 1999; 51: 43-49.

[280] Blower PJ, Lam A, Knapp Jr. FF, O'Doherty MJ, Coakley AJ. Preparation, biodistribution and dosimetry of ^{188}Re(V)-DMSA in patients with disseminated bone metastases. Nucl Med Commun 1996; 17: 258-263.

[281] Kothari K, Pillai MRA, Unni PR, Shimpi HH, Noronha OPD, Samuel AM. Preparation, stability studies and pharmacological behavior of [^{186}Re]Re-HEDP. Appl Radiat Isot 1999; 51: 51-58.

[282] Lin WY, Hsieh JF, Lin CP, Hsieh BT, Ting G, Wang SJ, Knapp Jr. FF. Effect of reaction conditions on preparations of rhenium-188 hydroxyethylidene diphosphonate complexes. Nucl Med Biol 1999; 26: 455-459.

[283] Khalid M, Mushtaq A, Iqbal MZ. Sorption of tungsten (VI) and rhenium (VI) on various ion exchange materials. Sep Sci Technol 2001; 36: 283–294.

[284] Lukie DM, Vucina JL, Milonjie SK. Separation of tungsten and rhenium on alumina in dynamic conditions. J Radioanal Nucl Chem 2007; 273: 357-362.

[285] Mushtaq A. Recovery of enriched ^{186}W from spent $^{188}W/^{188}Re$ generators. Appl Radiat Isot 1996; 47: 727-729.

LIST OF PUBLICATIONS

International Journals (Full papers)

[1]. Development of an electrochemical ^{90}Sr-^{90}Y generator for the separation of ^{90}Y suitable for targeted therapy

Rubel Chakravarty, Usha Pandey, Remani B. Manolkar, Ashutosh Dash, Meera Venkatesh and M.R. Ambikalmajan Pillai

Nucl. Med. Biol. **2008**; 35: 245-252.

[2] Polymer embedded nanocrystalline titania sorbent for ^{99}Mo-^{99m}Tc generator

Rubel Chakravarty, Rakesh Shukla, Shyamla Gandhi, Ramu Ram, Ashutosh Dash, Meera Venkatesh and A.K. Tyagi

J. Nanosci. Nanotechnol. **2008**; 8: 4447-4452.

[3] A novel $^{188}W/^{188}Re$ electrochemical generator with potential for medical applications

Rubel Chakravarty, Ashutosh Dash, Kanchan Kothari, M.R. Ambikalmajan Pillai and Meera Venkatesh

Radiochim. Acta **2009**; 97: 309-317.

[4] Separation of clinical grade ^{188}Re from ^{188}W using polymer embedded nanocrystalline titania (TiP)

Rubel Chakravarty, Ashutosh Dash and Meera Venkatesh

Chromatographia **2009**; 69: 1363-1371.

[5] A novel electrochemical technique for the production of clinical grade ^{99m}Tc using (n, γ)^{99}Mo

Rubel Chakravarty, Ashutosh Dash and Meera Venkatesh

Nucl. Med. Biol. **2010**; 37: 421-428.

[6] Nanocrystalline zirconia: A novel sorbent for the preparation of $^{188}W/^{188}Re$ generator

Rubel Chakravarty, Rakesh Shukla, A.K. Tyagi, Ashutosh Dash and Meera Venkatesh.

Appl. Radiat. Isot. **2010**; 68: 229-238.

[7] Post-elution concentration of ^{188}Re by an electrochemical method

Rubel Chakravarty, Ashutosh Dash, M.R.A. Pillai and Meera Venkatesh.

Appl. Radiat. Isot. **2010**; 68: 2302-2305.

[8] Practicality of tetragonal nano-zirconia as a prospective sorbent in the preparation of ^{99}Mo/^{99m}Tc generator for biomedical applications

Rubel Chakravarty, Rakesh Shukla, Ramu Ram, A.K. Tyagi, Ashutosh Dash and Meera Venkatesh

Chromatographia **2010**; 72: 875-884.

[9] Nano-ceria-PAN composite based advanced sorbent material: A major step forward in the field of clinical grade ^{68}Ge/^{68}Ga generator

Rubel Chakravarty, Rakesh Shukla, Ramu Ram, Meera Venkatesh, Ashutosh Dash and A. K. Tyagi

ACS Appl. Mater. Interfaces **2010**; 2: 2069-2075.

[10] Development of nano-zirconia based ^{68}Ge/^{68}Ga generator for biomedical applications

Rubel Chakravarty, Rakesh Shukla, Ramu Ram, Avesh Kumar Tyagi, Ashutosh Dash and Meera Venkatesh

Nucl. Med. Biol. **2011**; 38: 575-583.

[11] A novel electrochemical ^{99}Mo/^{99m}Tc generator

Rubel Chakravarty, Meera Venkatesh and Ashutosh Dash

J. Radioanal. Nucl. Chem. **2011**; 72: 875-884.

International Journals (Abstracts)

[1] Development of $^{90}Sr/^{90}Y$ generators for radiotherapeutic applications

R. Chakravarty, P. Dhami, U. Pandey, P. Naik, A. Dash, M.R.A. Pillai and M. Venkatesh

J. Nucl. Med. **2008**; 49(S1): 45.

[2] An electrochemical ^{90}Sr-^{90}Y generator and estimation of the radionuclidic purity using extraction paper chromatography

U. Pandey, **R. Chakravarty**, P. S. Dhami, A. Dash, M. Venkatesh and M.R.A. Pillai

Q. J. Nucl. Med. Mol. Imaging **2008**; 52(S1): 78.

[3] Validation of 'BARC Technique' for estimation of the radionuclidic purity of ^{90}Y and measurement of ^{90}Sr in ^{90}Y prepared by different $^{90}Sr/^{90}Y$ generators

U. Pandey, **R. Chakravarty**, P. Dhami, M. Venkatesh and M.R.A. Pillai

J. Nucl. Med. **2008**; 49(S1): 93.

[4] A novel electrochemical approach for post-elution concentration of ^{188}Re

R. Chakravarty, A. Dash, M.R.A. Pillai, M. Venkatesh

J. Nucl. Med. **2008**; 49(S1): 296.

[5] Nanocrystalline zirconia: A novel sorbent for the preparation of $^{99}Mo/^{99m}Tc$ generator

R. Chakravarty, R. Shukla, R. Ram, A.K. Tyagi, A. Dash and M. Venkatesh

J. Labelled Compd. Rad. **2009**; 52(S1): 500.

International Atomic Energy Agency – Technical Report Series (IAEA-TRS)

[1] Development of $^{90}Sr/^{90}Y$ generator technologies and their evaluation in the preparation of therapeutic radiopharmaceuticals

Meera Venkatesh, Ashutosh Dash, Usha Pandey, P.S. Dhami, **Rubel Chakravarty**

IAEA Technical Report Series No. 470, 73-82 (**2009**).

[2] Development of $^{188}W/^{188}Re$ generators

Meera Venkatesh, Shishir Kumar Sarkar, **Rubel Chakravarty**, G. Arjun, Ashutosh Dash, P. Saraswati

IAEA Technical Report Series No. 470, 145-151 (**2009**).